NASA Contractor Report 4555

Admittance Model for the Shuttle Remote Manipulator System in Four Configurations

Loukas Papadopoulos and Robert H. Tolson
Joint Institute for Advancement of Flight Sciences
The George Washington University
Langley Research Center
Hampton, Virginia

Prepared for
Langley Research Center
under Cooperative Agreement NCC1-104

National Aeronautics and
Space Administration

Office of Management

Scientific and Technical
Information Program

1993

ABSTRACT

A possible scenario for robot task performance in space is to mount two small, dexterous arms to the end of the Shuttle Remote Manipulator System (SRMS). As these small robots perform tasks, the flexibility of the SRMS may cause unsuccessful task executions. In order to simulate the dynamic coupling between the SRMS and the arms, admittance models of the SRMS in four brakes locked configurations have been developed. The admittance model permits calculation of the SRMS end-effector response due to end-effector disturbing forces. The model will then be used in conjunction with a Stewart Platform, a vehicle emulation system.

An application of the admittance model has been shown by simulating the disturbing forces using two SRMS payloads, the Dextrous Orbital Servicing System (DOSS) manipulator and DOSS carrying a 1000 lb. cylinder. Mode by mode comparisons were conducted to determine the minimum number of modes required in the admittance model while retaining dynamic fidelity. It was determined that for all four SRMS configurations studied, between 4 and 6 modes of the SRMS structure (depending on the excitation loads) were sufficient to retain tolerances of 0.01 inches and 0.01°. These tolerances correspond to the DOSS manipulator carrying no object. When the DOSS carries the 1000 lb. cylinder, between 15 and 20 modes were sufficient, approximately three or four times as many modes as for the unloaded case.

TABLE OF CONTENTS

LIST OF FIGURES

LIST OF TABLES

NOMENCLATURE

Symbols	Meaning
a	Time of constant DOSS joint torque application, sec
α_r	First freeplay angular motion of SRMS joint r
A	State-space matrix representing the system dynamics
ASAD	All Singing, All Dancing
b	Time of zero DOSS joint torque application (i.e., coast, or drift time), sec
β_r	Second freeplay angular motion of SRMS joint r
B	State-space matrix characterizing the input
C	State-space measurement matrix
CBAR	NASTRAN bulk data deck card that defines a simple beam element (i.e., constant properties through out beam, no cross-sectional warping, neutral and shear center axes coincide)
CCTV	Closed circuit television
CELAS2	NASTRAN bulk data deck card that defines a scalar spring element (i.e., translational and/or rotational)
CONM2	NASTRAN bulk data deck card that defines a concentrated mass (and mass moments of inertia) at a grid point
CQUAD4	NASTRAN bulk data deck card that defines a quadrilateral shell, or plate element
CSDL	Charles Stark Draper Laboratory
D	State-space direct transmission matrix

DADS	Dynamic Analysis and Design System
DOSS	Dextrous Orbital Servicing System
DRS	Draper Remote Manipulator System Simulator
EI	Bending Stiffness of a beam, lb-in^2
ELP	Elbow Pitch joint
$\eta(t)$	Modal coordinate
$f_{j,j+1}$	Flexibility matrix of a section of an SRMS link, $\frac{1}{\text{lb}-\text{in}}$
$f_{link\,j}$	Total flexibility matrix of SRMS link j, $\frac{1}{\text{lb}-\text{in}}$
F_{rr}	Equivalent flexibility matrix of SRMS joint r due to the flexibility of the joint and link, $\frac{\text{rad}}{\text{lb}-\text{in}}$, in Abelow joint coordinates
$\bar{F}_{rr}$	Flexibility matrix of SRMS joint r due only to the flexibility of the joint, $\frac{\text{rad}}{\text{lb}-\text{in}}$, in Abelow joint coordinates
γ_r	Primary SRMS joint r angular motion
G_γ^r, G_u^r	Primary SRMS joint r drive axis torque
G_α^r	SRMS joint r first freeplay axis torque
G_β^r	SRMS joint r second freeplay axis torque
G_v^{ri}	Inboard SRMS joint r torque along the first freeplay axis
G_w^{ri}	Inboard SRMS joint r torque along the second freeplay axis

G_v^{ro}	Outboard SRMS joint r torque along the first freeplay axis
G_w^{ro}	Outboard SRMS joint r torque along the second freeplay axis
GENEL	NASTRAN bulk data deck card that defines a general element, or a 6 x 6 stiffness or flexibility (inverse of stiffness) matrix
GJ	Torsional Rigidity of a beam, lb-in^2
GRID	NASTRAN bulk data deck card that defines the location of a geometric point on a structure, and coordinate frame to output displacements and orientations
GWU	George Washington University
I	Identity matrix
K_{rr}	Torsional stiffness matrix of SRMS joint r in the GWU finite element model joint coordinates, $\frac{\text{lb}-\text{in}}{\text{rad}}$
$\tilde{K}_{rr}$	Torsional stiffness matrix of SRMS joint r in Abelow joint coordinates
K_u^r	SRMS joint stiffness along the primary joint drive axis
K_v^{ri}	SRMS inboard joint r stiffness along the first freeplay axis
K_w^{ri}	SRMS inboard joint r stiffness along the second freeplay axis
K_v^{ro}	SRMS outboard joint r stiffness along the first freeplay axis
K_w^{ro}	SRMS outboard joint r stiffness along the second freeplay axis
LCS	Load Cell Simulation

$\bar{M}$	Constant torque amplitude in the drive axis DOSS joint torque profile, lb-in
MAT1	NASTRAN bulk data deck card that defines the material properties for a linear, isotropic material
MATLAB	Matrix manipulation software
MSC/NASTRAN	Finite Element Code
ODU	Old Dominion University
OSR	Orbiter Structural Reference
PBAR	NASTRAN bulk data deck card that defines the geometrical properties of a CBAR beam element
Φ	Total SRMS system undamped mode shape matrix
Φ^*	Truncated, or reduced, SRMS end-effector undamped mode shape matrix
ϕ_i	i^{th} eigenvector of the total system undamped mode shape matrix
ϕ_i^*	i^{th} eigenvector of the truncated SRMS End-Effector undamped mode shape matrix
$\vec{r}$	Position vector from joint of interest to the SRMS payload center of mass, inches
$\vec{r}^*$	Position vector from DOSS base to the joint of interest, inches
R	Transformation from Abelow to GWU finite element model joint coordinate frame
$R^{r-1,r}$	Transformation matrix that transforms coordinates from body r to r - *1*
RBAR, or RBE2	NASTRAN bulk data deck cards that defines a rigid body element

RSS	Root Sum Square
SIMFAC	Remote Manipulator System Simulation Facility
SES	Systems Engineering Simulator
SHP	Shoulder Pitch joint
SHR	Shoulder Roll joint
SHY	Shoulder Yaw joint
slinch	English mass unit, equals 12 slugs
STARDYNE	Structural analysis computer code
SWO	Swing-out joint
SRMS	Shuttle Remote Manipulator System
SSF	Space Station Freedom
U^r	Primary SRMS joint r drive axis
u(t)	State-space input vector
V^r	First freeplay axis of SRMS joint r
ω_i	Natural frequency of mode i, $\frac{\text{rad}}{\text{sec}}$
$\vec{\omega}_{c.m.}$	Angular velocity of the SRMS payload center of mass, $\frac{\text{rad}}{\text{sec}}$
W^r	Second freeplay axis of SRMS joint r
$\theta_x(t)_{adm}$	x component of orientation for the SRMS end-effector using the admittance model in the transient analysis
$\theta_x(t)_{comp}$	x component of orientation for the SRMS end-effector using the compound model in the transient analysis

$\theta_y(t)_{adm}$	y component of orientation for the SRMS end-effector using the admittance model in the transient analysis
$\theta_y(t)_{comp}$	y component of orientation for the SRMS end-effector using the compound model in the transient analysis
$\theta_z(t)_{adm}$	z component of orientation for the SRMS end-effector using the admittance model in the transient analysis
$\theta_z(t)_{comp}$	z component of orientation for the SRMS end-effector using the compound model in the transient analysis
$\vec{W}_{admittance}$	Wrench applied to the SRMS end-effector using the admittance model in the transient analyses
$\vec{W}_{feedback}$	Feedback wrench applied to the SRMS end-effector due to SRMS payload motion
$\vec{W}_{c.m.}$	Wrench, at SRMS payload center of mass, required to produce SRMS payload center of mass motion
$\vec{W}_{compound}$	Wrench applied to the SRMS end-effector using the compound model in the transient analyses
WRP	Wrist Pitch joint
WRR	Wrist Roll joint
WRY	Wrist Yaw joint
x(t)	State-space state vector
$x_{adm}(t)$	x component of displacement for the SRMS end-effector using the admittance model in the transient analysis
$x_{comp}(t)$	x component of displacement for the SRMS end-effector using the compound model in the transient analysis
y(t)	State-space output vector

$y_{adm}(t)$	y component of displacement for the SRMS end-effector using the admittance model in the transient analysis
$y_{comp}(t)$	y component of displacement for the SRMS end-effector using the compound model in the transient analysis
$\overline{y}_{c.m.}$	SRMS payload center of mass translations, inches
$\overline{y}_{E.E.}$	SRMS End-Effector translations, inches
ζ_i	Modal damping factor of mode i
$z_{adm}(t)$	z component of displacement for the SRMS end-effector using the admittance model in the transient analysis
$z_{comp}(t)$	z component of displacement for the SRMS end-effector using the compound model in the transient analysis

I. INTRODUCTION

1.1 Motivation

"Robotic manipulators are widely used in manufacturing applications in which the manipulator base is fixed and the manipulator performs a repetitive task."[1] However, "with the emergence of outer space as a premier environment for commercial and scientific development"[2], new types of applications call for robotic manipulators to be mounted on non-stationary bases (i.e. bases floating in space). Such applications could involve the use of the Shuttle Remote Manipulator System (SRMS) carrying smaller robot arms to perform assembly or maintenance operations on satellites, or on the space station. Examples of compliant or non-stationary bases are given in Figure 1-1 where (a) depicts a manipulator mounted on a truck interacting with the vehicle's suspension system and compliant tires, and (b) depicts a maintenance robot performing certain tasks on a satellite. Such tasks can introduce disturbances on the satellite, and thus possibly affect satellite, or robot performance. In these situations, robot contact and inertial forces will cause reaction forces and moments at the base. These forces and moments will excite a response in the supporting structure which is compliant. The effects of this dynamic coupling may include loss of position accuracy, which could cause inability to perform the required task.

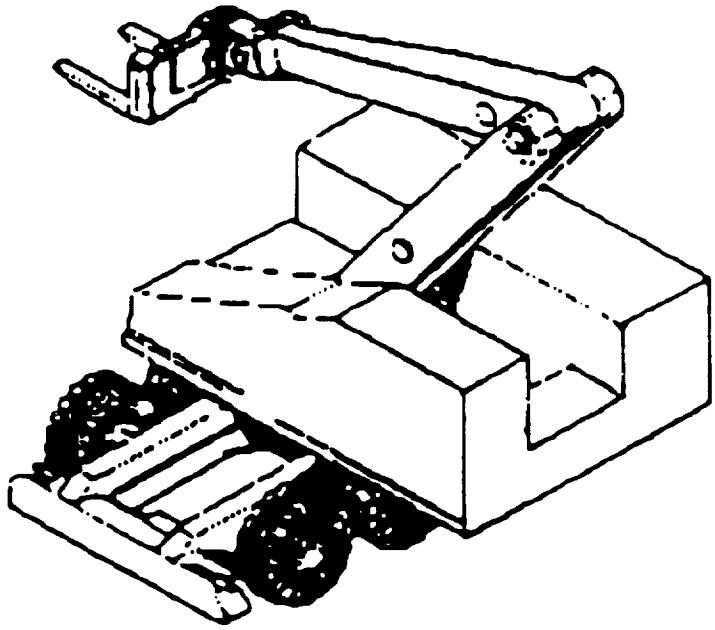

(a) An Earth-based Manipulator Mounted on a Truck.

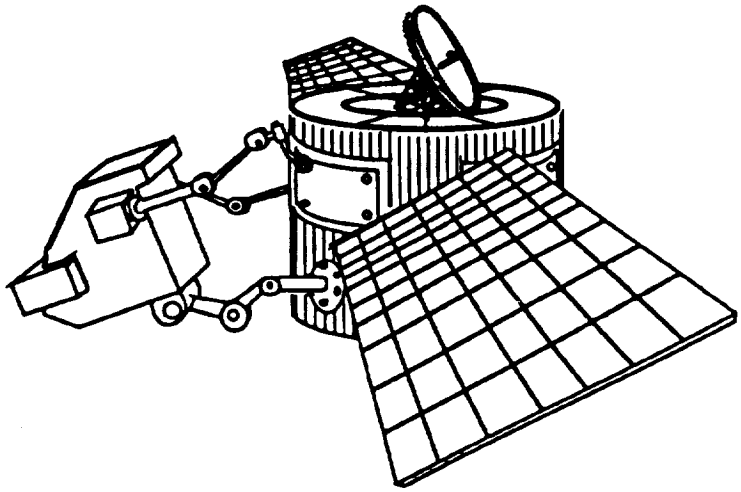

(b) A Space-based Manipulator Working on a Satellite.

Figure 1-1: Examples of Robotic Manipulators Mounted on (a) Compliant, and (b) Non-stationary Bases.[2]

1.2 Background

Several dynamic simulators for the SRMS exist. SPAR Aerospace of Canada developed two simulators. The first, known as the Remote Manipulator System Simulation Facility (SIMFAC), [3], was operational around 1977, and the second is All Singing, All Dancing (ASAD), [4], developed approximately the same time period as SIMFAC. SIMFAC is a real-time simulator based on a 23 degree-of-freedom mathematical model of the SRMS. ASAD is non real-time, but is a high fidelity simulator based on a 35 degree-of-freedom mathematical model of the SRMS. To ascertain whether the simplifications of the SIMFAC simulator were valid, it was compared with ASAD, and "although the ASAD results showed more frequent activity due to the higher frequency modes modeled, good correlation was shown at the lower frequencies, thus, the SIMFAC mathematical model was verified".[3]

A third SRMS dynamic simulator was developed by The Charles Stark Draper Laboratory, known as the Draper Remote Manipulator System Simulator (DRS) [5]. DRS is a high fidelity, non real-time, non-linear simulator which has been validated with flight data since 1985. This is considered to be the best SRMS simulator available; it includes the joint and link flexibilities, non-linear effects of the gear drives, plus the effects of the Shuttle control and safety systems. Recently, NASA-Johnson Space Center have also developed a real-time SRMS simulator, Systems Engineering Simulator (SES), and has validated it against flight data in 1992, [6,7].

1.3 Problem Statement

Conducting experiments in space is very expensive and time consuming, hence, potential dynamic interactions between manipulator motions and compliant base responses should first be studied on earth. However, one of the challenges of this endeavor is simulating a zero-gravity environment for these earth-based experiments. Baker [8] lists several approaches to emulating a microgravity environment. One of these is to mount the system on a spatial mechanism designed to emulate the motion which would be expected in outer space.

This spatial mechanism, known as a Stewart Platform, is a six degree-of-freedom, in-parallel, hydraulically actuated machine which can mimic the motion of a wide range of systems within its work space and bandwidth limitations. It permits the experimental study of dynamic interactions that may result between manipulators and their carrying vehicle. Figure 1-2 depicts the vehicle emulator concept, as well as the Stewart Platform.

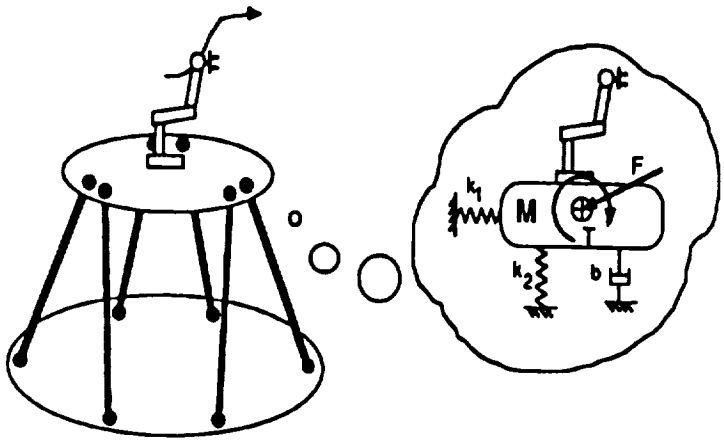

Figure 1-2: The Vehicle Emulator Concept.[1]

One proposed scenario is to mount the ground-based Dextrous Orbital Servicing System (DOSS) manipulator, shown in Figure 1-3, on the Stewart Platform.

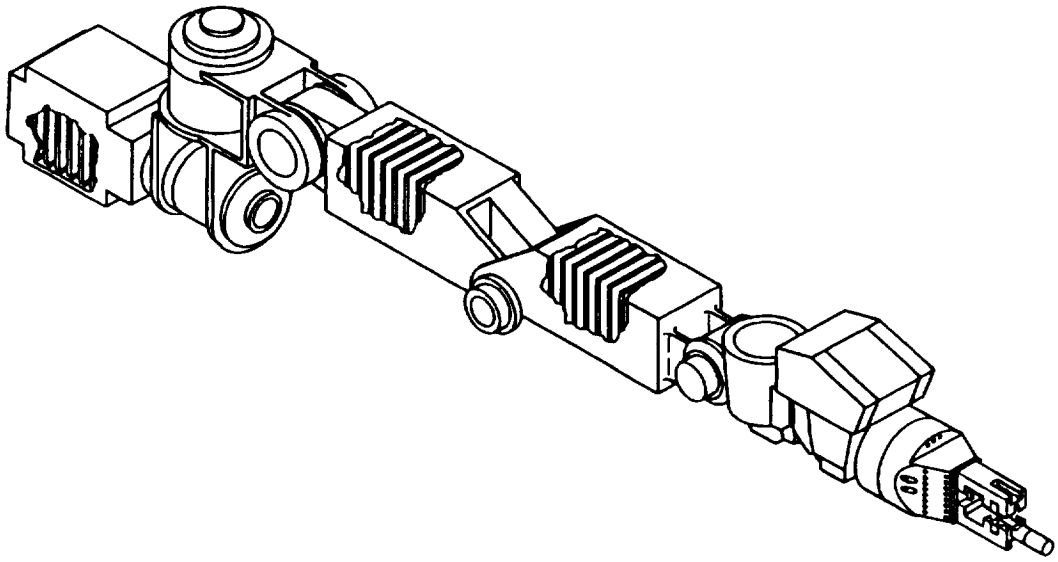

Figure 1-3: The Dextrous Orbital Servicing System (DOSS) Manipulator.

As the DOSS manipulator performs a specified maneuver, inertial and contact forces and moments (in three orthogonal directions which will be referred to as a *wrench*) will be generated at the base of the DOSS arm, which will be measured by a load cell located on the platform. The platform will then respond as the end-effector of the SRMS would in space, given the same applied disturbance, Figure 1-4. Hence, the dynamics that would be observed in space shown in the top picture of Figure 1-4 can be simulated on earth in the lab with the platform (bottom graph). The platform is able to behave as the SRMS end-effector through the control strategy known as admittance control (discussed in section 1.5). This control strategy uses an admittance model, which represents the equations of motion for that part of the dynamical system being emulated. It takes wrench as input and outputs the position and orientation of the modeled system. The platform then emulates this motion.

To develop an admittance model it is necessary to study the relationship between model complexity and fidelity, since the admittance model will be used in real-time calculations. Hence, the goal is to develop the simplest possible admittance model that would effectively simulate the dynamic behavior of the SRMS end-effector. In the context of this study, real-time means that all of the dynamic calculations are performed as fast or faster than the bandwidth of the platform.

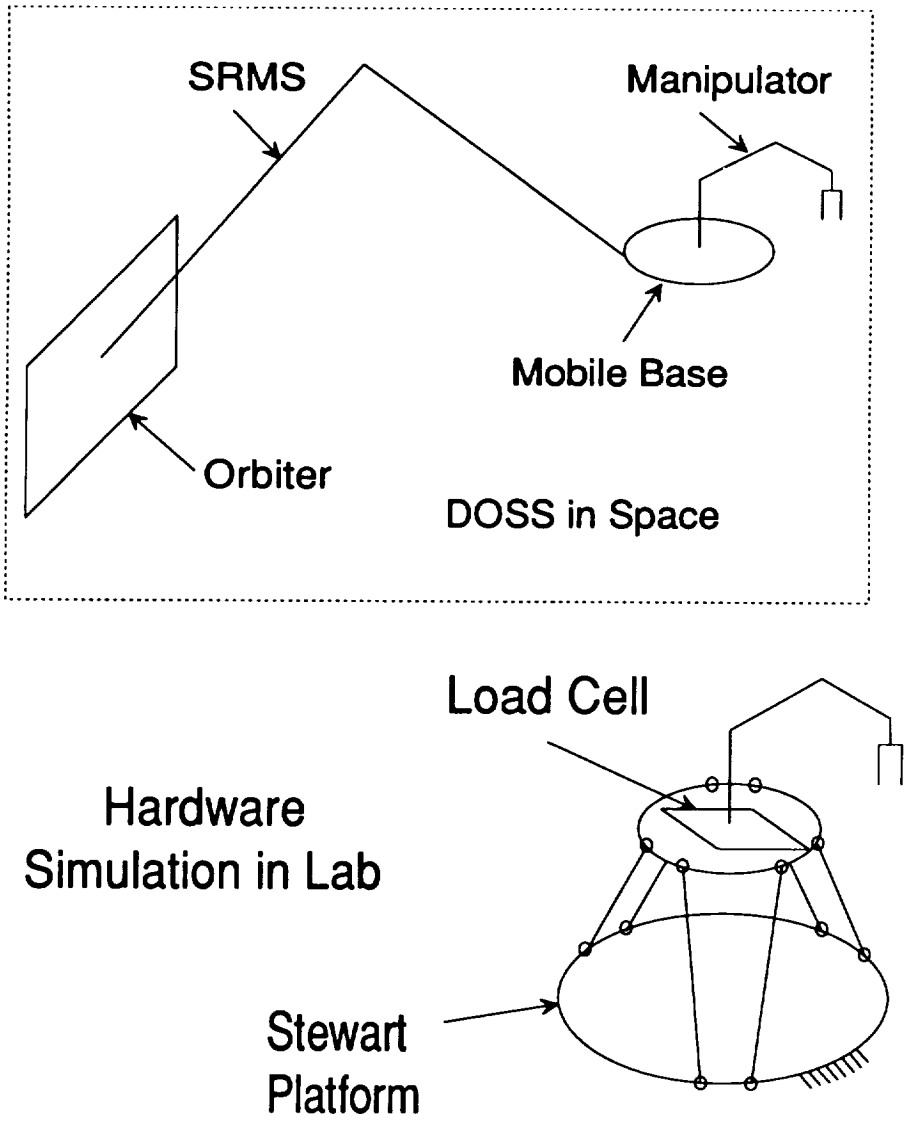

Figure 1-4: The Stewart Platform Emulating the SRMS End-Effector for Earth-based Experiments.

Since the Stewart Platform emulates motions in real-time, of the four SRMS simulators mentioned in section 1.2, only the SIMFAC and SES simulators can be used by the platform. However, because these simulators were unavailable and

undocumented, it was decided to develop an independent admittance model of the SRMS end-effector in four brakes locked configurations. This admittance model was based on a finite element model of the SRMS, which will be discussed in section 2.2. The procedure for developing the admittance model is as follows

a. Develop a finite element model of the SRMS in the four brakes locked configurations and perform a normal modes analysis using MSC/NASTRAN, a finite element code used at NASA-Langley Research Center.

b. Transform the equations of motion from physical to mode space using the results from the normal modes analysis

c. The admittance model is obtained from the frequencies and modal information at the SRMS end-effector (discussed in section 3.3).

The benefit of developing an independent admittance model is that it can be easily changed since the documentation is readily available.

The input wrench to the admittance model (i.e., admittance wrench) was required in order to perform the transient analyses. The admittance wrench was determined by rigidly attaching an SRMS payload (i.e., the DOSS manipulator, and the DOSS plus 1000 lb. cylinder) to the SRMS end-effector in the finite element model. Transient analyses were conducted on this modified finite element model, or compound finite element model, by determining a wrench from hypothetically slewing the DOSS manipulator (i.e., compound wrench). The accelerations of the SRMS end-effector will be used to obtain the accelerations of the SRMS payload center of mass. The Newton-Euler equations will determine the wrench required to cause the motion of the payload center of mass just

obtained. The sum of the hypothetical slew wrench and the wrench from the Newton-Euler equations will be the admittance wrench. The details of this procedure are discussed in section 6.3.

1.4 Assumptions and Limitations

The SRMS is an inherently non-linear, flexible system whose dynamic characteristics are configuration dependent. For the present study we will develop a linear dynamic model of the SRMS for four representative configurations. Therefore, only small angle motions of the SRMS end-effector will be assumed to take place. While the arm is in these configurations, the brakes on each joint are assumed to be locked. Therefore, the control system of the SRMS is suppressed for this study. Also, the Orbiter is assumed rigid and fixed in space, so the dynamics of the Orbiter is not considered.

1.5 Admittance Control

The Stewart Platform emulates the dynamics of the modeled system (i.e. manipulator base vehicle) through the control strategy known as *admittance control.* "The word *admittance* refers to the implementation of the modeled system as a transfer function from wrench as the input (effort) to position and orientation as the output (flow)."[1] Consider the example of a simple one degree-of-freedom system with mass m connected to a spring k and damper c acting in parallel, whose equation of motion is

$$m\ddot{x}(t) + c\dot{x}(t) + kx(t) = F(t) \qquad (1\text{-}1)$$

where $F(t)$ is the applied force, and $x(t)$ is the displacement of mass m.

Taking a Laplace transform with the initial conditions set to zero, we obtain the system transfer function as

$$\frac{x(s)}{F(s)} = \frac{1}{ms^2 + cs + k}$$

The above system transfer function would be the admittance model (in the Laplace domain) for mass m. In physical space, the admittance model is a set of differential equations that represent the dynamics of the vehicle emulated by the platform (for the above example, it would be equation (1-1)). For this simple one degree-of-freedom system, the admittance model is just the equation of motion. However, for multi degree-of-freedom systems, the admittance model would not be the equations of motion of the entire system, but of only that part of the system being emulated by the platform. Therefore, for this study, the admittance model does not represent the equations of motion of the SRMS, but only of the end-effector. Using the reciprocal of the system transfer function entails the other control strategy known as *impedance control.*

1.6 Organization of Study

The remainder of this study is organized as follows

Chapter II. Shuttle Remote Manipulator System (SRMS). Contains a description of the SRMS. Also discussed is the finite element model and the four configurations used to obtain the undamped mode shapes and natural frequencies of the SRMS in four brakes locked configurations. The section discussing the finite element model describes the joint stiffness development which simulates the brakes locked mode of the SRMS.

Chapter III. Implementation of Admittance Model. Contains a description of the Stewart Platform and how the admittance control for the platform works. Also discussed is the form of the admittance model used in the transient analyses.

Chapter IV. Finite Element Model Validation. Before any finite element model can be used it must be validated. This chapter contains the validation of the finite element model against three other finite element models of the SRMS. The configurations listed in this chapter are different from those in chapter II, and are used for validation purposes only.

Chapter V. SRMS Admittance Model. Contains the undamped mode shapes and natural frequencies of the SRMS, in the four brakes locked configurations, used to create the admittance model.

Chapter VI. Admittance Model Application Using Load Cell Simulation. Contains SRMS end-effector responses due to different applied wrenches and errors associated with using a lower order admittance model (a *small number* of modes) vs. a higher order one (a *large number* of modes). Also discussed is the method for calculating the input wrench to the admittance model of the SRMS end-effector.

Chapter VII. Concluding Remarks. Contains a summary of the study.

II. SHUTTLE REMOTE MANIPULATOR SYSTEM (SRMS)

2.1 Description

The Shuttle Remote Manipulator System (SRMS) is an anthropomorphic, teleoperated, flexible manipulator. The primary purpose of the SRMS is to deploy (up to 65,000 lbs.[9]) and retrieve payloads (up to 35,000 lbs.[9]), as well as vehicle berthing tasks in and around the Orbiter cargo bay. The manipulator is mounted to the port side longeron near the forward bulkhead of the Orbiter cargo bay, shown in Figure 2-1, by means of a manipulator positioning mechanism. The arm is rotated from its stowed to its operational position outside the cargo bay by a shoulder swing-out joint. The swing-out joint's purpose is to rotate and lock the arm 19.48° outboard from its stowed position. This is done to ensure adequate clearance when the arm is performing maneuvers.

The SRMS is approximately 50 ft. long from the shoulder pitch joint to the end-effector, and consists of six controllable joints: shoulder yaw and pitch, elbow pitch, wrist pitch, yaw, and roll joints. The rotational limits of each joint are given in Figure 2-2. For detailed information regarding construction and operation of these joints the reader is referred to References 10, 11, and 12. The SRMS weight is approximately 957 lbs., including elbow and wrist closed circuit television (CCTV) cameras. The elbow camera provides for general cargo bay, arm, and payload viewing, and the wrist camera assists the operator in maneuvering the end-effector to the payload grapple fixture.

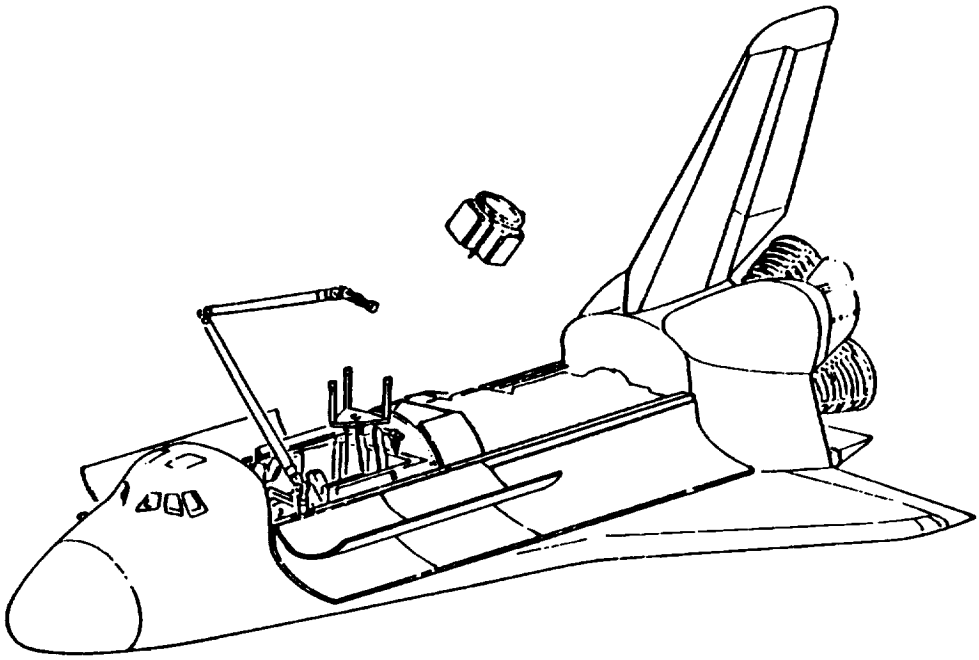

Figure 2-1: Orbiter and The Remote Manipulator System in a Deployed Configuration.[13]

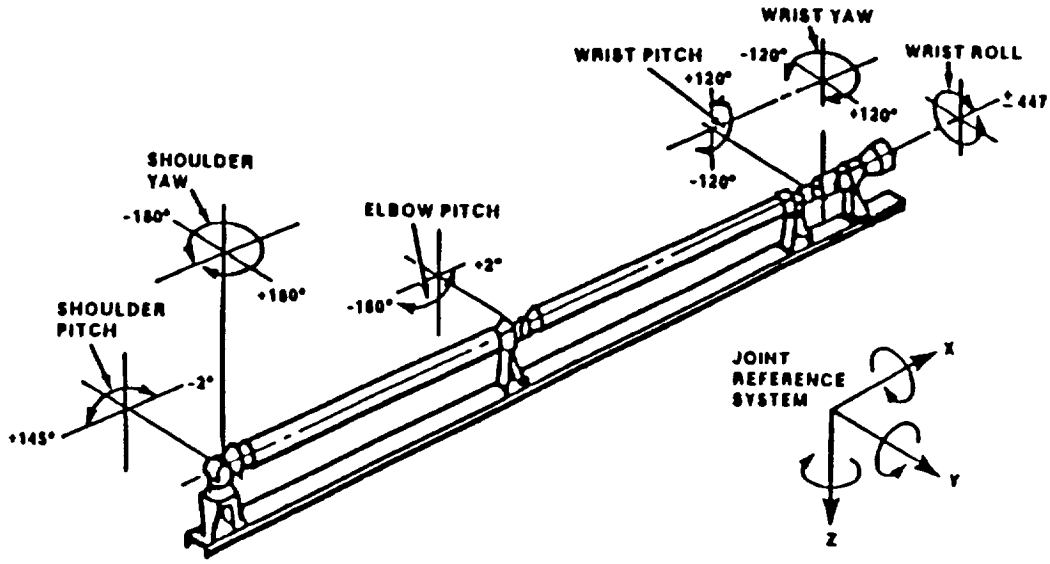

Figure 2-2: Rotational Limits of each Joint of the SRMS.[13]

The manipulator arm consists of seven links. Links 3 and 4 are the longest, 20.92 and 23.16 ft., more commonly known as the upper and lower arm booms, respectively. They consist of two thin-walled, circular cross sectioned booms manufactured from a graphite epoxy composite material. For detailed information regarding construction of the arm booms the reader is referred to References 10, 11, and 14. The entire SRMS mechanical assembly is illustrated in Figure 2-3. For a listing of geometric, mass, and structural properties of the SRMS, the reader is referred to Appendix A.

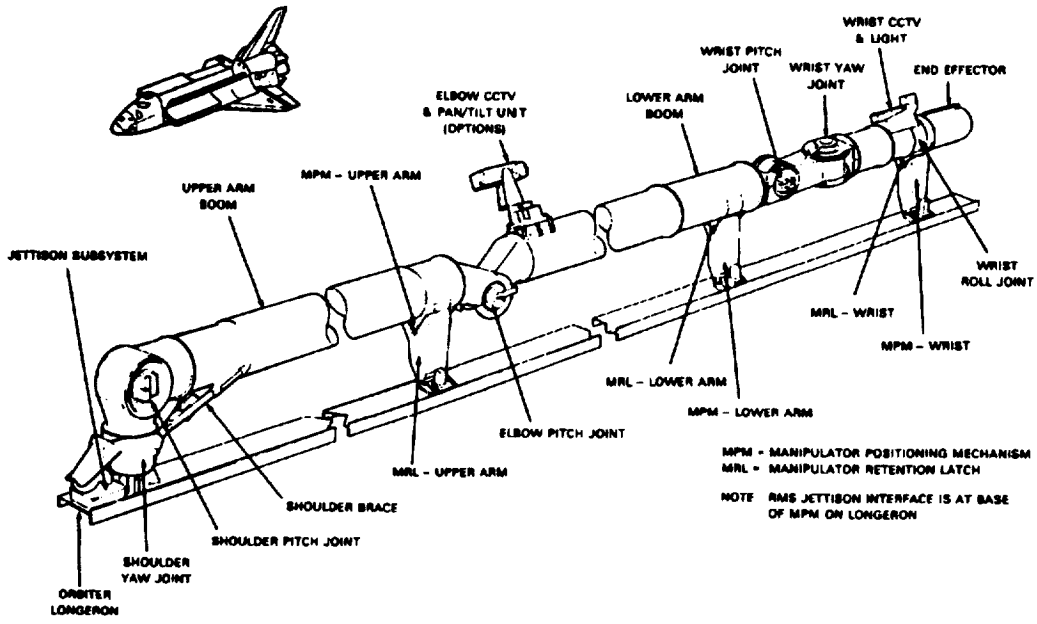

Figure 2-3: The Entire Mechanical Assembly of the SRMS.[15]

To effectively describe the motion of the SRMS, several coordinate frames are required:

1. Orbiter Structural Reference (OSR) frame
   - fixed to the orbiter
   - X-axis points toward the Orbiter's tail, Y-axis points out the starboard wing, and the Z-axis completes the right-handed triad
   - Orbiter nose coordinates: (236.0, 0.0, 400.0) inches

2. Swing-out joint frame
   - fixed to the swing-out joint
   - X-axis points toward the Orbiter's tail, Z-axis points along the centerline of link 1, and the Y-axis completes the right-handed triad (in stowed configuration)
   - The origin is located (679.5, -96.5, 412.25) inches in the OSR frame

3. Six joint frames
   - fixed to the outboard portion of each joint (rotates with each link)
   - X-axis points toward the Orbiter's tail, Y-axis points out the port wing, and the Z-axis completes the right-handed triad (arm in stowed configuration)

The OSR and swing-out frames are shown in Figure 2-4. Figure 2-5 shows the SRMS in the stowed configuration with all six joint frames labeled.

In order to conduct meaningful dynamic analyses, a common database of SRMS parameter values should be used for all simulation studies. For this reason, the most recent publication of SRMS data (July 1991) was used throughout this study [16]. There is one caveat that should be mentioned concerning this reference. Although it was published in 1991, basically all the properties of the SRMS in it were taken from a SPAR document published circa 1983, [17]. In other words, the properties reported in [16] are 10 years old.

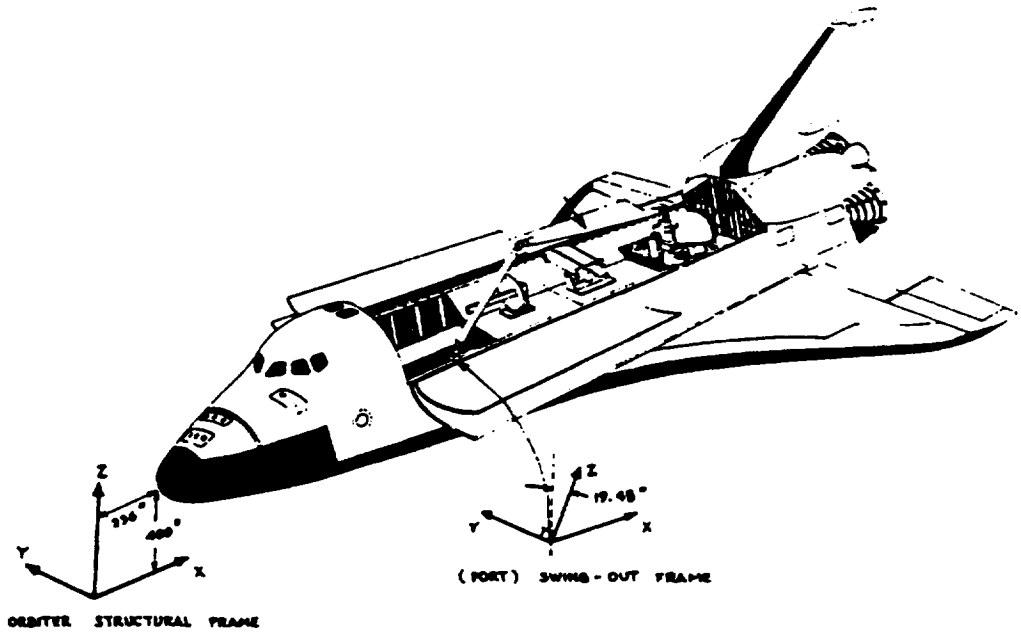

Figure 2-4: Orbiter Showing the OSR and Swing-out Frames.[16]

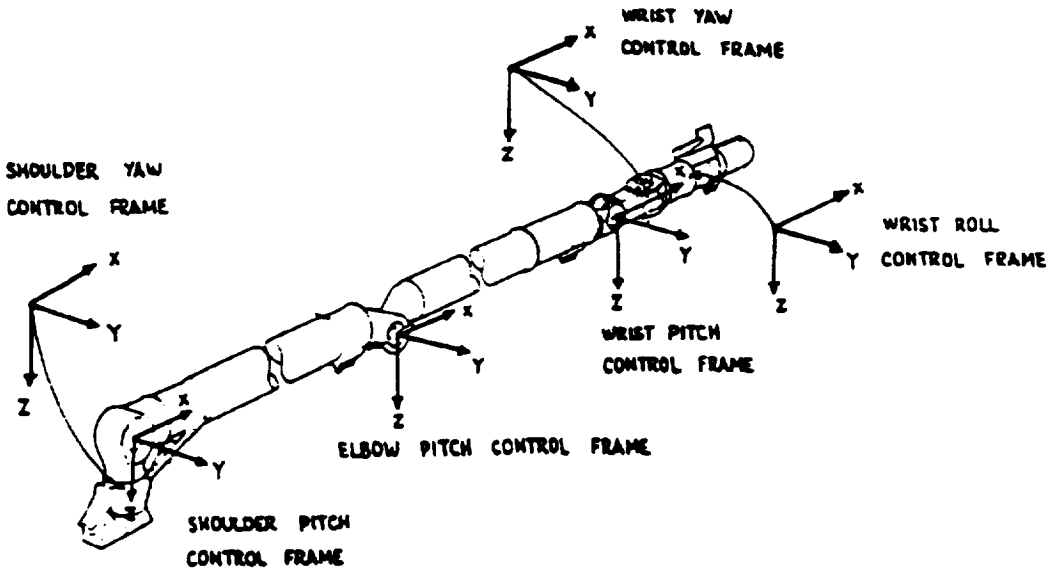

Figure 2-5: SRMS, in Stowed Configuration, Showing All Joint Coordinate Frames.[16]

2.2 Finite Element Model

Berthing is a possible method of mating the Space Station Freedom (SSF) and the Orbiter via the SRMS. This procedure may present potential dynamic interaction issues between the Orbiter, SSF, and the SRMS. Recently, both NASA-Johnson Space Center and the NASA-Langley Research Center have been involved in independently analyzing this berthing procedure.[18] To better understand the dynamics of the SRMS, a NASTRAN finite element model was developed, called the base model, and is described below.[9,18]

2.2.1 Description

The base finite element model was developed using the English System of Units, where length is measured in inches, mass in slinches (1 slinch = 12 slugs), time in seconds, and force in pounds. Readers not familiar with NASTRAN bulk data cards are referred to the Nomenclature for definitions of these cards. The base finite element model contains the following characteristics:

1. All joints rigidly fixed (i.e., RBE2 cards are included constraining all six degrees-of-freedom at every joint, except the swing-out joint).

2. The upper and lower arm booms (links 3 and 4) are represented as flexible bodies by discretizing them into 9 beam elements (CBAR elements) each; the other links (1, 2, 5, 6 and 7) are represented as rigid bodies by using RBE2 elements.

3. All the flexibility between the Orbiter port longeron and the arm/Orbiter interface, including the swing-out joint, is modeled by an equivalent spring (GENEL element) which represents both translational and torsional stiffness. It is assumed that the moment M_z will not exceed 13680 lb-in (Table A-5).

4. The Orbiter is assumed to be rigid and fixed in space. Its center of mass is rigidly attached to the arm attachment point with a rigid element (RBE2 element).

5. The masses of both booms are placed in the model using non-structural mass (assumed to be uniformly distributed) in the PBAR card.

6. Links are modeled as circular beam cross-sections.

7. Elbow offset is included.

This research expanded the base model to include

8. The rotational degree-of-freedom constraints (item 1.) were removed in order to add joint flexibility. This flexibility is represented by equivalent 3-D torsional springs (GENEL cards). Because links 1, 2, 5, 6 and 7 are modeled as rigid bodies, any flexibility that they may have is included in the joint stiffness matrices. The translational degree-of-freedom constraints were retained.

The modified base model, referred to herein as the GWU (George Washington University) model, consists of 132 degrees-of-freedom including the constraints, and is illustrated in Figure 2-6. The reader is referred to Appendix B for a listing of the GWU finite element model for all four brakes locked configurations. The geometrical and material properties of the CBAR elements are given in Tables 2-1 and 2-2, respectively.

A total of nine beam (CBAR) elements are used to model each boom. This discretization was adequate to provide a good approximation of the overall mass properties of each boom.[9] The rationale for modeling links 1, 2, 5, 6, and 7 as rigid bodies will be discussed in section 2.2.2.2.

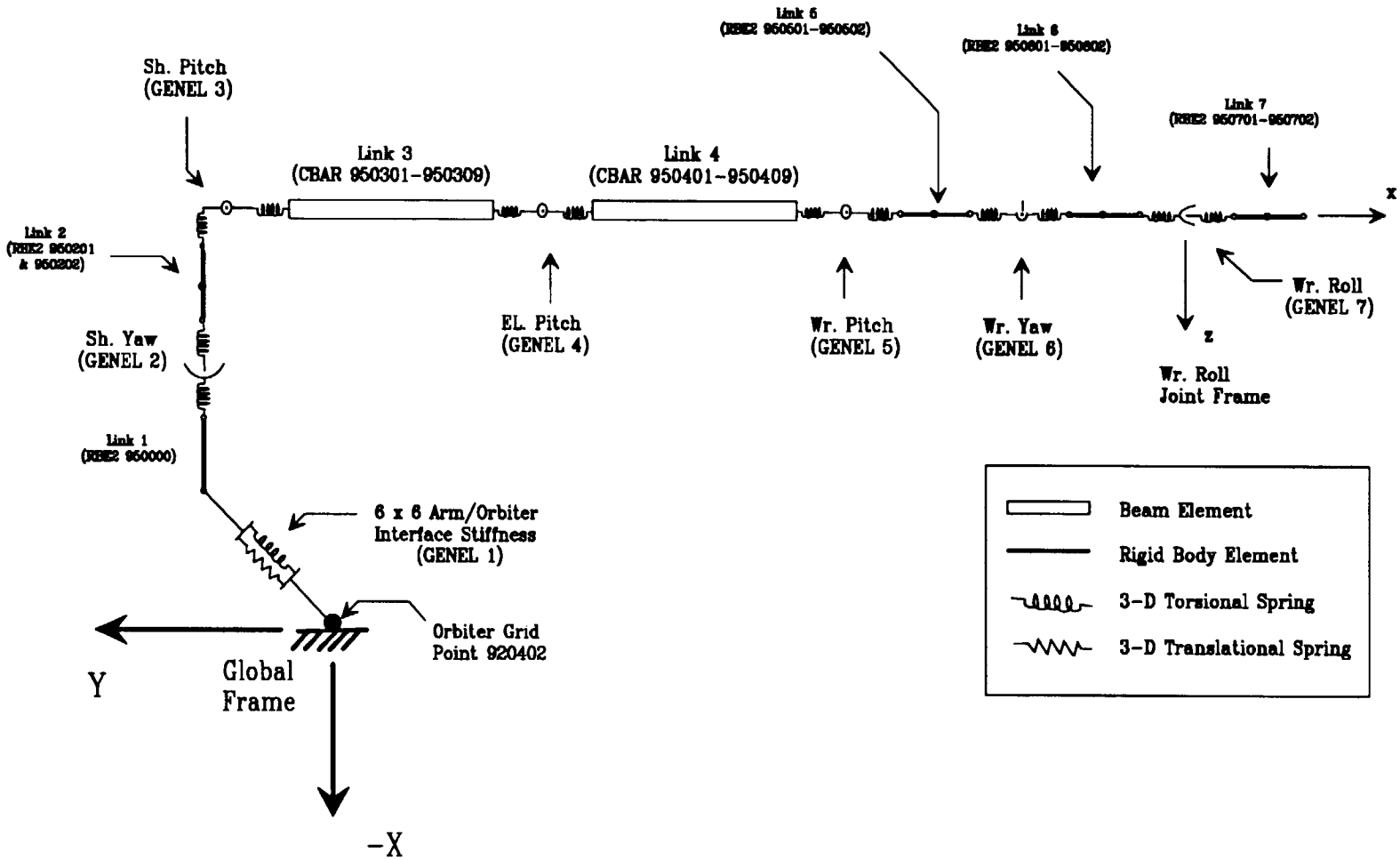

Figure 2-6: SRMS, in Stowed Configuration, as Modeled by the GWU Finite Element Model.

The values that were used for the link mass moment of inertias was from the ASAD model. Reference 16 lists other inertia values for the SRMS. The inertia properties for links 3 and 4 were entered using their respective PBAR cards. Since links 1, 2, 5, 6, and 7 were modeled as rigid bodies there are no associated PBAR cards, so their inertia, as well as their masses, were entered using CONM2 cards and placed at their respective geometric centers.

The CBAR beam element does not allow for explicit specification of axial mass moment of inertia. Therefore, CONM2 cards were added to each grid point of the booms to correct the deficiency. These axial moments of inertia are listed in Table 2-3. The inertias for links 1 and 2 in Table 2-3 correspond to I_{zz} in Table A-3 (ASAD model), and likewise for links 5, 6, and 7 to I_{xx}.

NASTRAN does not explicitly permit entering values of bending and torsional stiffness, EI and GJ, respectively, so these quantities must be entered individually. By estimating the moment of area, I, based on link diameter information, the modulus of elasticity, E, can be obtained. The same procedure was used to obtain the shear modulus, G. The finite element model, therefore, contains the same EI and GJ as listed in Reference 16 (i.e. the product is preserved).

Finally, the finite element programs are set up such that when a normal modes analysis is performed (NASTRAN solution sequence 103), the mode shapes of all the grid points are given with respect to the coordinate system in which they were defined in (i.e. local mode shapes).

Table 2-1: GWU Finite Element Geometric Properties for the Beam Elements.

Link	Section	Length (in.)	Cross-Sectional Area (in.^{2})	Moment of Area (in.^{4})		Polar Moment of Area, J (in.^{4})
				I_1	I_2	
1	---	11.0000	---	---	---	---
2	---	12.0000	---	---	---	---
3	$L_{3'4}$	28.4664	2.12160	46.712	43.091	56.010
	L_{34}	197.0836	3.24720	63.919	63.919	127.830
	$L_{34'}$	25.5000	2.12160	31.255	25.856	39.585
4	$L_{4'5}$	12.4998	1.15350	28.269	20.167	41.829
	L_{45}	225.9842	2.23680	43.699	43.699	87.303
	$L_{45'}$	39.4660	0.52546	11.893	10.112	15.388
5	---	18.0000	---	---	---	---
6	---	30.0000	---	---	---	---
7	---	26.0000	---	---	---	---

Table 2-2: GWU Finite Element Material Properties for the Beam Elements.

Link	Section	Non-Structural Mass (slinch/inch) $x\,10^{-3}$	Young's Modulus, E (psi) $x\,10^7$	Shear Modulus, G (psi) $x\,10^6$	Poisson's Ratio ν
3	$L_{3'4}$	3.1608	1.7405	6.6935	0.30
	L_{34}	3.1608	2.3003	5.7798	0.99
	$L_{34'}$	3.1608	1.7405	6.6935	0.30
4	$L_{4'5}$	1.7871	1.7405	6.6935	0.30
	L_{45}	1.7871	2.2495	5.9103	0.90
	$L_{45'}$	1.7871	1.7405	6.6935	0.30

Table 2-3: Axial Mass Moment of Inertia of the SRMS Links per Grid Point.

Link	Grid Point Number	Axial Mass Moment of Inertia (slug-ft^2)
1	920999	1.272
2	921202	0.6463
3	921301 to 921310	0.26848
4	921401 to 921410	0.17232
5	921502	0.1704
6	921602	0.9254
7	921702	0.9107

2.2.2 Joint Stiffness

2.2.2.1 Joint Flexibility

This section discusses how the joint stiffness values in the finite element model were obtained. This development parallels Abelow [19]. The following provides the rotation transformation matrices for each joint of the SRMS, which transform coordinates from body r to body $r-1$. The rotation angles γ_r are about the primary drive axis for each joint (i.e., all roll joints rotate about the local x-axis, all yaw joints rotate about the local z-axis, and all pitch joints rotate about the local y-axis). These transformations will be used in obtaining the stiffness matrix at a joint.

Shoulder Swing-out (r = 1) and Wrist Roll (r = 7) Joint:

$$R^{r-1,r} = \begin{bmatrix} 1 & 0 & 0 \\ 0 & \cos\gamma_r & -\sin\gamma_r \\ 0 & \sin\gamma_r & \cos\gamma_r \end{bmatrix} \tag{2-1}$$

Shoulder (r = 2) and Wrist (r = 6) Yaw Joints:

$$R^{r-1,r} = \begin{bmatrix} \cos\gamma_r & -\sin\gamma_r & 0 \\ \sin\gamma_r & \cos\gamma_r & 0 \\ 0 & 0 & 1 \end{bmatrix} \tag{2-2}$$

Shoulder (r = 3), Elbow (r = 4), and Wrist (r = 5) Pitch Joints:

$$R^{r-1,r} = \begin{bmatrix} \cos\gamma_r & 0 & \sin\gamma_r \\ 0 & 1 & 0 \\ -\sin\gamma_r & 0 & \cos\gamma_r \end{bmatrix} \tag{2-3}$$

The joints of the SRMS are composed of many parts (i.e., motor modules, motor transition pieces, gearboxes, sensors, etc.).[20] as shown in Figure 2-7 for the shoulder joint assembly. These various components of the joint contribute to its overall flexibility because they are all flexible to some degree. Therefore, in order to accurately determine the joint stiffness every component in the joint must be considered.

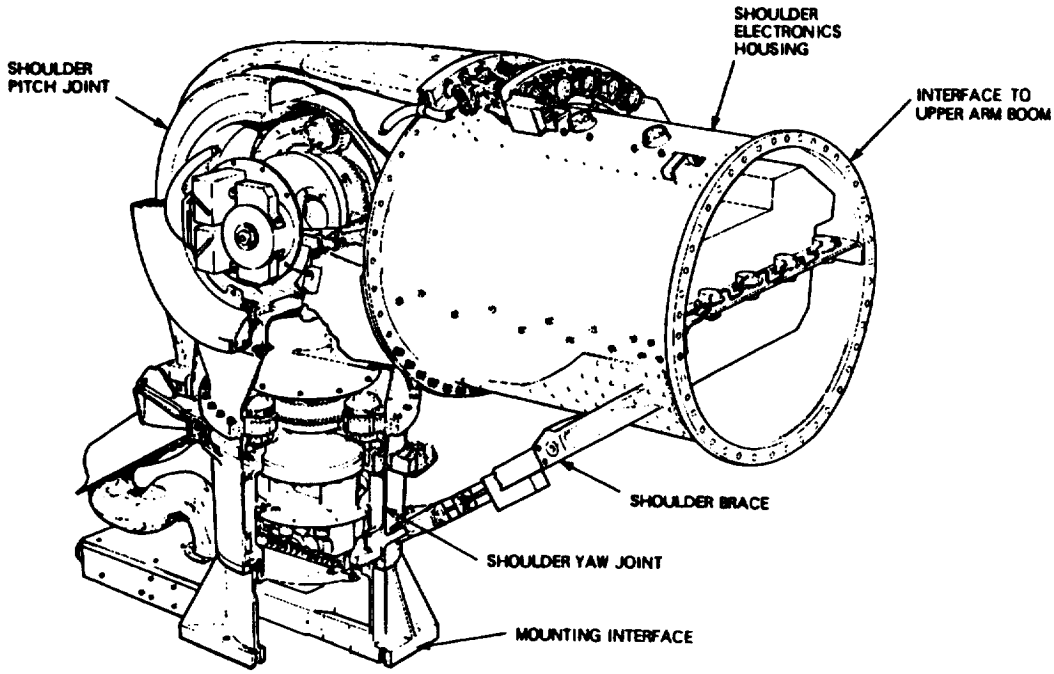

Figure 2-7: Shoulder Joint Assembly of the SRMS.[20]

The joints of the SRMS are also composed of two joint housings, or shafts.[20] The first shaft is fixed with respect to the primary joint rotation, and the second shaft rotates with the joint. The shaft that is fixed is known as the inner shaft, and the shaft that rotates is the outer shaft; this is true for every joint except the shoulder pitch joint which has the opposite definition. Associated with both these shafts are stiffnesses in each of the three orthogonal directions (see Figure 2-8). The inner shaft joint stiffnesses are known as the inboard stiffnesses, and likewise for the outer shaft as outboard stiffnesses. These inboard and outboard stiffnesses are provided in Table 2-4, and are given with respect to Abelow's joint coordinate system shown in Figure 2-9. This coordinate system can be described as follows: in the stowed configuration the local

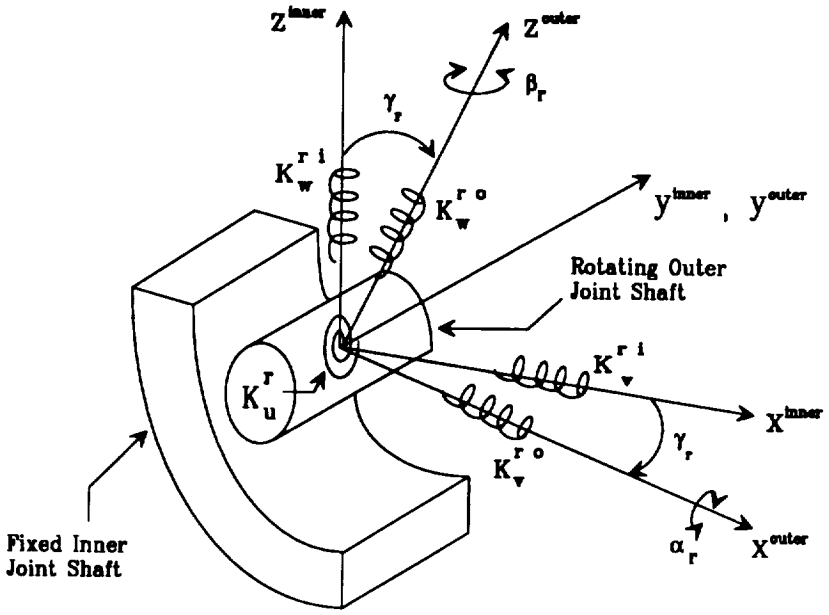

Figure 2-8: Inboard and Outboard Stiffness Representation of an SRMS Joint.

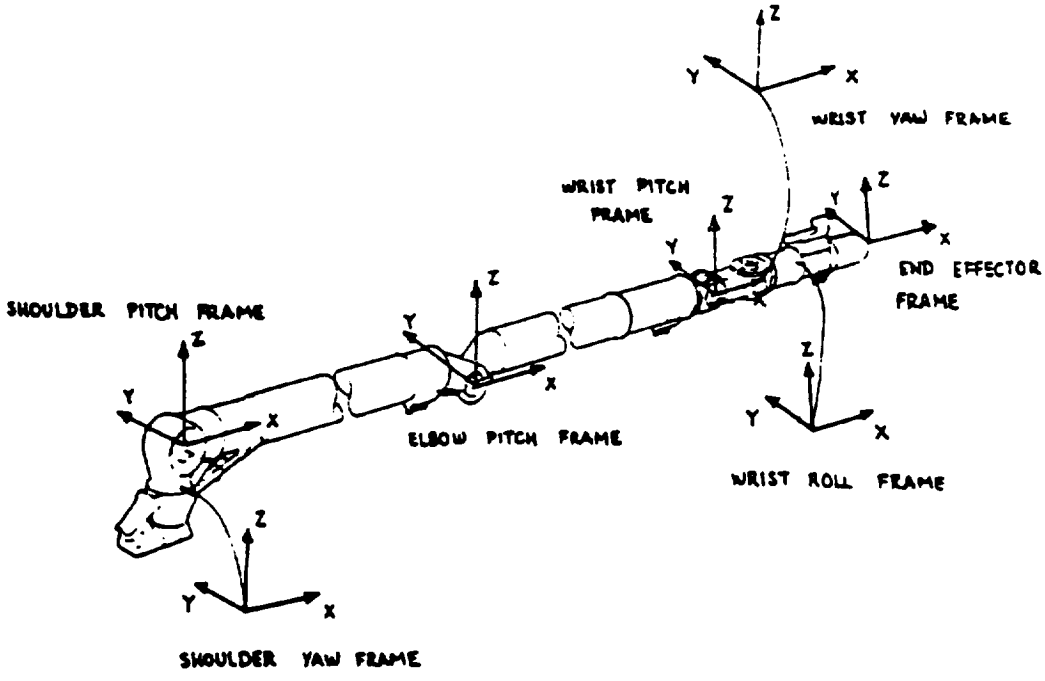

Figure 2-9: Abelow Joint Coordinate Frames.[16]

x-axes point toward the Orbiter's tail, the local y-axes point out the starboard wing, and the local z-axes complete the right-handed triad. Table 2-4 was obtained from [19] which represents the most recent publication available, circa 1980, for these stiffness values. Therefore, the method selected to model the joints[19] was to use torsional springs with the stiffnesses given in Table 2-4. Figure 2-8 illustrates this concept for an SRMS joint where the primary rotation is in the y-axis.

The three orthogonal directions in Figure 2-8 are known as the primary drive axis $(direction\ U^r)$, and the first $(direction\ V^r)$ and second $(direction\ W^r)$ freeplay axes, with angular motions γ_r, α_r, and β_r, respectively, where the superscript and subscript r denotes the joint number. The freeplay directions are mutually orthogonal to the primary drive axis, and can be thought of as *slop*, or undesirable motions of the joint as a result of the necessity of permitting primary rotation, in the joint.

The joint stiffness in the drive direction is K_u^r, K_v^{ri} and K_w^{ri} are the stiffnesses of the inboard portion of the joint in the two freeplay directions, and K_v^{ro} and K_w^{ro} are the stiffnesses of the outboard portion of the joint in the two freeplay directions. The superscripts i and o denote inboard and outboard, respectively, and the subscripts u, v, and w denote the primary drive axis, first and second freeplay axes, respectively. The inboard portion of the joint is independent of the joint angle. On the other hand, the outboard stiffness is dependent on the joint angle. It should also be mentioned that the joint drive stiffness K_u^r is considered part of the inboard portion of the joint, therefore the outboard portion only has two, rather than three stiffness values (allowing for a total

of five torsional springs at a joint).

Table 2-4: Inboard and Outboard Torsional Joint Stiffnesses of the Joints.

Joint Number r	Joint	Joint Axes	Joint Stiffness (lb-ft)/rad	
			Inboard $x 10^6$	Outboard $x 10^6$
2	Shoulder Yaw	x (V^2)	4.159	6.892
		y (W^2)	3.470	5.721
		z (U^2)	4.777	
3	Shoulder Pitch	x (W^3)	6.591	1.096
		y (U^3)	2.320	
		z (V^3)	3.822	2.193
4	Elbow Pitch	x (W^4)	0.866	1.867
		y (U^4)	1.153	
		z (V^4)	1.470	2.340
5	Wrist Pitch	x (W^5)	0.217	1.444
		y (U^5)	0.330	
		z (V^5)	3.713	1.444
6	Wrist Yaw	x (V^6)	1.350	0.774
		y (W^6)	1.350	0.419
		z (U^6)	0.336	
7	Wrist Roll	x (U^7)	0.404	
		y (V^7)	0.314	0.742
		z (W^7)	3.080	0.728

The stiffness matrix for a joint can be obtained by writing the potential energy for a system of torsional springs. This potential energy equation can be written in two parts, the first part represents the inboard, and the second term is the outboard. Using the fact that the outboard stiffnesses are dependent of joint rotation, and the inboard is not, both terms can be grouped to obtain the general flexibility matrix at a joint, $\bar{F}_{rr}$

$$\bar{F}_{rr} = \left[R^{r-1,r}\right]^T diag\left[0 \;,\; \frac{1}{K_v^{ro}} \;,\; \frac{1}{K_w^{ro}}\right]\left[R^{r-1,r}\right] + diag\left[\frac{1}{K_u^{r}} \;,\; \frac{1}{K_v^{ri}} \;,\; \frac{1}{K_w^{ri}}\right] \tag{2-4}$$

Equation (2-4) represents the flexibility of the joint itself, and the reader is referred to section C.1 of Appendix C for a more detailed discussion of its derivation as obtained from [19]. Equation (2-4) is used when the joint primary rotation is along the local x axis, thus, the primary joint stiffness K_u^r is in the (1,1) element of the inboard matrix If, however, the primary joint rotation was along the local y-axis, or z-axis, then it would be located in the (2,2), or (3,3) element, respectively. Taking this into account produces the joint flexibility matrices of the SRMS due to the flexibility of the joints themselves. The flexibility of the swing-out joint (r = 1) is not modeled using equation (2-4) because its flexibility is taken into account by the arm/Orbiter interface stiffness (Table A-5).

2.2.2.2 Link Flexibility

This section addresses the issue of whether or not a link of the SRMS should

be modeled as rigid, or flexible. Regardless of the outcome, all flexibility of the joint and links must be taken into account. If a link is modeled as flexible then the flexibility of the joint is due to itself only. However, if the link can be modeled as rigid, then the flexibility of that link should be lumped into the flexibility of the surrounding joint. The latter option does not increase the total number of degrees-of-freedom of the finite element model. Reference 19 discusses a method implementing the latter idea, and will be used in this study.

The question of whether to model the links of the SRMS as rigid, or flexible bodies can be answered by considering the fundamental frequency of each link. Table 2-5 lists the fundamental frequencies in two bending directions and in torsion for all seven links (obtained by representing each link as a clamped-free, Euler-Bernoulli beam).[21] In this table, links 1, 2, 5, 6, and 7 were assumed to have the same cross sectional area and polar moment of area (outer diameter = average of upper and lower boom outer diameters, and inner diameter = average of upper and lower boom inner diameters).

Table 2-5: SRMS Link Fundamental Bending and Torsional Natural Frequencies.

Link	Fundamental Frequency (Hz)			
	x-y Bending	x-z Bending	y-z Bending	Torsion
1	---	225.47	246.86	211.10
2	---	232.20	182.67	148.87
3	1.51	1.55	---	19.47
4	1.18	1.23	---	17.57
5	84.79	89.75	---	99.88
6	15.37	14.52	---	38.34
7	21.46	21.52	---	53.24

Table 2-5 indicates that links 1, 2, 5, 6, and 7 have bending and torsional fundamental frequencies greater than 10 Hz. The highest frequency of interest for the present analysis is 5-10 Hz (bandwidth of the Stewart Platform). Since these links have such high fundamental frequencies (i.e. greater than the bandwidth), the link vibrational motion would act as DC signals, i.e. static displacements. Hence, links 1, 2, 5, 6, and 7 can be modeled as rigid bodies in the finite element model. Links 3 and 4, however, have bending frequencies lower than the bandwidth, therefore, they should be modeled as flexible bodies in the finite element model.

The link flexibility can be determined by writing the bending equation of a simple cantilever beam, and comparing it to Hooke's Law for a torsional spring. Performing this comparison, one can determine the flexibility of a link section (since each link is composed of several sections)

Link's 1 (j = 1) and 2 (j = 2):

$$f_{j,j+1} = diag\left[\frac{l}{EI} \;,\; \frac{l}{EI} \;,\; \frac{l}{GJ}\right]_{j,j+1} \tag{2-5}$$

Link's 5 (j = 5), 6 (j = 6), and 7 (j = 7):

$$f_{j,j+1} = diag\left[\frac{l}{GJ} \;,\; \frac{l}{EI} \;,\; \frac{l}{EI}\right]_{j,j+1} \tag{2-6}$$

where EI and GJ represent the bending and torsional stiffnesses of a link. See section C.2 of Appendix C for a more detailed discussion of link flexibility.

Links 1 and 2 have their torsion axes in the local z-axis, hence the (3,3) term in equation (2-5). Likewise, links 5, 6, and 7 have torsion in the local x-axis, hence the (1,1) term in equation (2-6). Using equations (2-5) and (2-6) for each link section, and adding terms, produces the total link flexibility

$$f_{link\,1} = f_{12} \tag{2-7}$$

$$f_{link\,j} = f_{j',j+1} + f_{j,j+1} + f_{j,(j+1)'} \qquad j = 2,5,6 \tag{2-8}$$

$$f_{link\,7} = f_{7'8} + f_{78} \tag{2-9}$$

2.2.2.3 Equivalent Joint Flexibility

Combining the joint flexibility matrices at a point, equation (2-4) and the link flexibility matrices, equations (2-5) through (2-9), results in the total flexibility matrix of a joint.

Shoulder (r = 2) and Wrist (r = 6) Yaw Joints:

$$F_{rr} = \left[R^{r-1,r}\right]^T \left\{ diag\left[\frac{1}{K_v^{ro}} , \frac{1}{K_w^{ro}} , 0\right] + f_{link\,r-1} \right\} \left[R^{r-1,r}\right] + diag\left[\frac{1}{K_v^{ri}} , \frac{1}{K_w^{ri}} , \frac{1}{K_u^{r}}\right] \tag{2-10}$$

Shoulder Pitch Joint (r = 3):

$$F_{rr} = \left[R^{r-1,r}\right]^T \left\{ diag\left[\frac{1}{K_w^{ro}} , 0 , \frac{1}{K_v^{ro}}\right] + f_{link\,r-1} \right\} \left[R^{r-1,r}\right] + diag\left[\frac{1}{K_w^{ri}} , \frac{1}{K_u^{r}} , \frac{1}{K_v^{ri}}\right] \tag{2-11}$$

Elbow (r = 4) and Wrist (r = 5) Pitch Joints:

$$F_{rr} = \left[R^{r-1,r}\right]^T diag\left[\frac{1}{K_w^{ro}} , 0 , \frac{1}{K_v^{ro}}\right] \left[R^{r-1,r}\right] + diag\left[\frac{1}{K_w^{ri}} , \frac{1}{K_u^{r}} , \frac{1}{K_v^{ri}}\right] \tag{2-12}$$

Wrist Roll Joint (r = 7):

$$F_{rr} = [R^{r-1,r}]^T \left\{ diag\left[0 \ , \frac{1}{K_v^{ro}} \ , \frac{1}{K_w^{ro}}\right] + f_{link\,r-1} \right\} [R^{r-1,r}] + f_{link\,r} + diag\left[\frac{1}{K_u^{r}} \ , \frac{1}{K_v^{ri}} \ , \frac{1}{K_w^{ri}}\right] \tag{2-13}$$

The stiffness matrices for each joint are obtained by taking the inverse of the flexibility matrices

$$\tilde{K}_{rr} = F_{rr}^{-1} = \begin{bmatrix} k_{xx}^{rr} & k_{xy}^{rr} & k_{xz}^{rr} \\ k_{yx}^{rr} & k_{yy}^{rr} & k_{yz}^{rr} \\ k_{zx}^{rr} & k_{zy}^{rr} & k_{zz}^{rr} \end{bmatrix} \qquad r = 2, \ldots, 7$$

The joint stiffness matrices, $\tilde{K}_{rr}$, $r = 2, \ldots, 7$, are in Abelow's local joint reference frame shown in Figure 2-9. However, the joint stiffnesses are required in the GWU model coordinate system shown in Figure 2-5.

The Abelow stiffnesses can be converted to the GWU model frame by observing Figures 2-5 and 2-9. It can be seen that the GWU model coordinate frames can be obtained by performing a 180° rotation about Abelow's local x-axis in every joint except the swing-out joint. Therefore the rotation matrix $[R]$ transforming from Abelow to GWU model frames is

$$[R] = \begin{bmatrix} 1 & 0 & 0 \\ 0 & -1 & 0 \\ 0 & 0 & -1 \end{bmatrix}$$

The stiffness matrix transformation from one frame to the other is

$$K_{GWU} = [R]\, K_{Abelow}\, [R]^T \tag{2-14}$$

Carrying out the matrix multiplication of equation (2-14), results in simply adding negative signs to all the elements of the first row and first column (except the (1,1) element, which remains unchanged) of each Abelow joint stiffness matrix of the SRMS, $\bar{K}_{rr}$, $r = 2, \ldots, 7$. Therefore, the total SRMS joint stiffness matrices, K_{rr} , $r = 2, \ldots, 7$ in the GWU finite element model coordinate frames are

$$K_{rr} = \begin{bmatrix} k_{xx}^{rr} & -k_{xy}^{rr} & -k_{xz}^{rr} \\ -k_{yx}^{rr} & k_{yy}^{rr} & k_{yz}^{rr} \\ -k_{zx}^{rr} & k_{zy}^{rr} & k_{zz}^{rr} \end{bmatrix} \qquad r = 2, \ldots, 7 \tag{2-15}$$

Performing the algebra required by equations (2-10) through (2-13), and taking the inverse obtains $\bar{K}_{rr}$. Transforming $\bar{K}_{rr}$ to K_{rr} by equation (2-14) obtains the joint stiffness values as used in the GWU finite element model by the GENEL element. Section C.3 of Appendix C lists the joint stiffness values from equation (2-15) for the four SRMS configurations.

2.3 Four Configurations

Three typical SRMS configurations were selected for this study. They include an Unberth, Low Hover, and Deploy configuration of the SRMS. These configurations are shown in Figures 2-10 through 2-12, and are actual configurations used to deploy a satellite.[22] The figures provide four-view plots of the configurations. The upper-left and right-hand quadrants of these figures provide a front and side view of the Orbiter, respectively. The lower-left and right-hand quadrants provide a top and frontal oblique angle view of the Orbiter, respectively. The Unberth configuration has the SRMS reaching inside the cargo bay. The Low Hover configuration positions the SRMS over of the cargo bay, and the Deploy configuration releases the satellite.

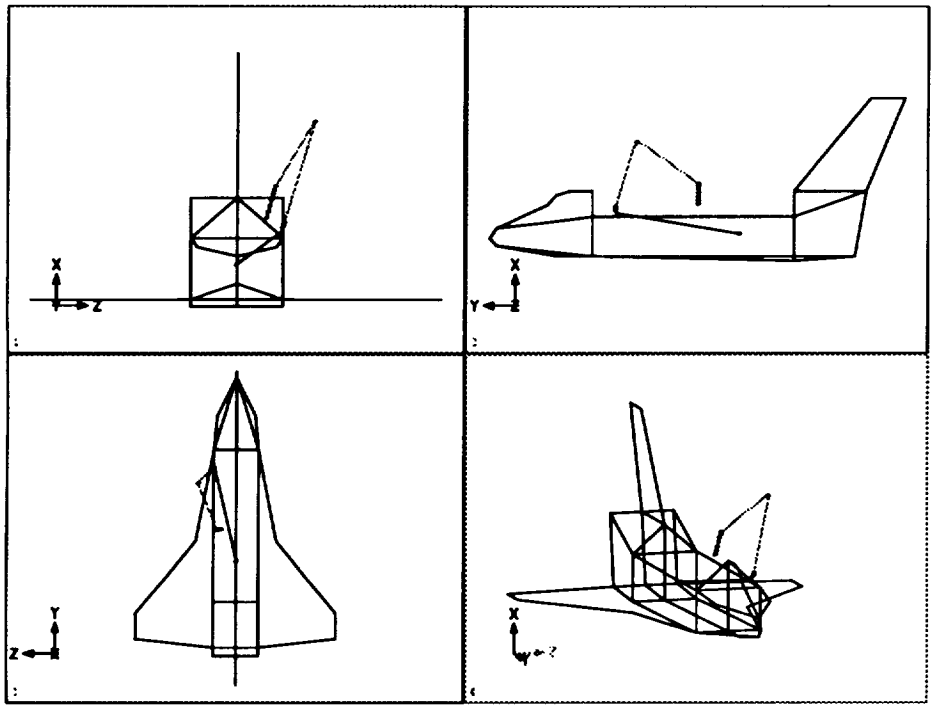

Figure 2-10: Unberth Configuration.

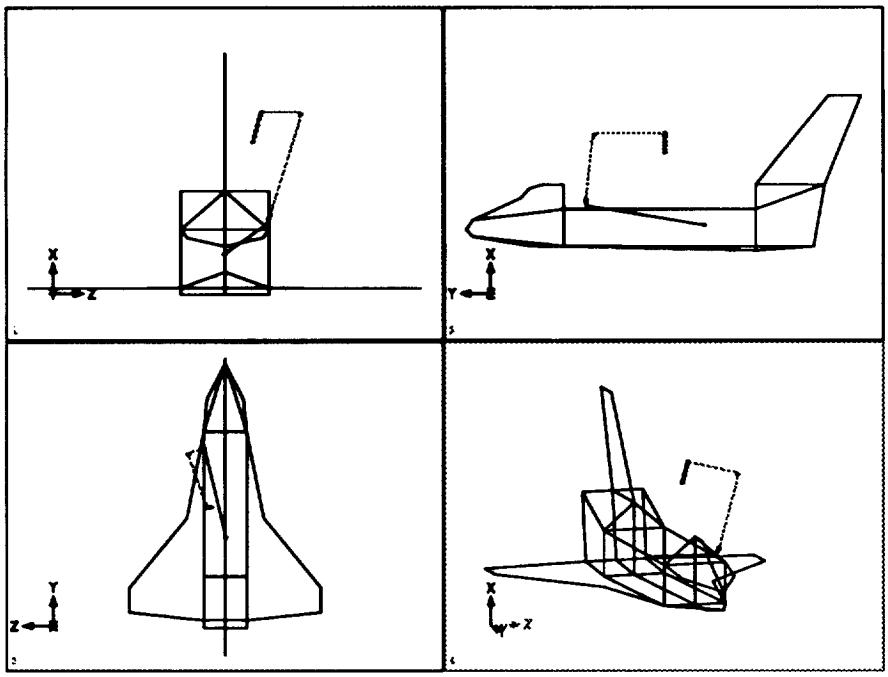

Figure 2-11: Low Hover Configuration.

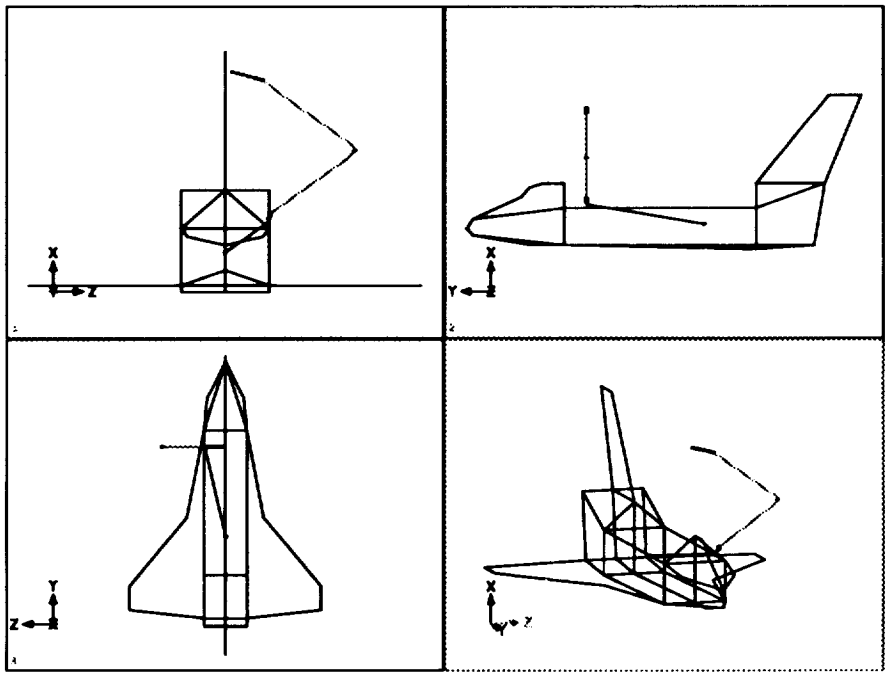

Figure 2-12: Deploy Configuration.

A fourth SRMS configuration was also selected representing a typical SSF capture configuration, shown in Figure 2-13. The SRMS may one day carry a servicing robot to the space station for repairs. This is a possible configuration for the arm when servicing the station, which is why it is also used in this study. The joint angles for the four configurations are listed in Table 2-6 (joint coordinate frames of Figure 2-5) and are given in the following order: shoulder swing-out, yaw, and pitch joints, elbow pitch, wrist pitch, yaw, and roll joints.

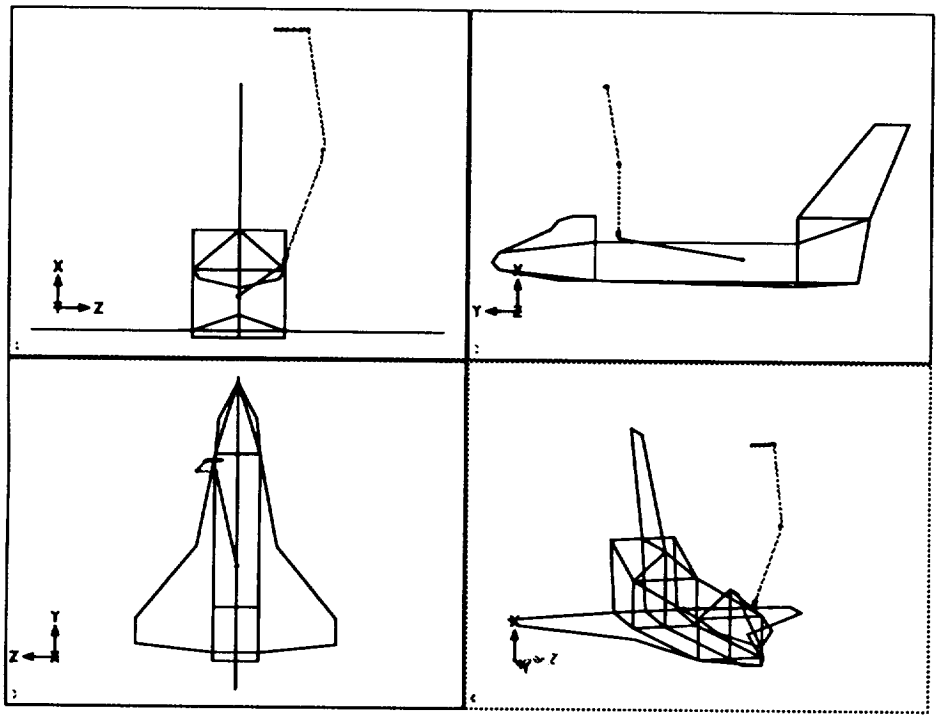

Figure 2-13: Capture Configuration.

Table 2-6: Joint Angles for the Four Study Configurations.

Configuration	Joint Angles (degrees)						
	SWO	SHY	SHP	ELP	WRP	WRY	WRR
Unberth	19.48	-8.96	73.90	-112.64	-51.96	4.43	28.99
Low Hover	19.48	-18.91	83.95	-90.55	-84.85	4.24	38.97
Deploy	19.48	-89.96	125.3	-108.61	-21.17	-0.04	110.0
Capture	19.48	-109.24	90.60	-30.35	-80.79	18.10	26.12

III. IMPLEMENTATION OF ADMITTANCE MODEL

This chapter describes how the admittance model would be implemented to simulate the SRMS end-effector (section 3.1). Section 3.2 describes the general admittance control concept for a manipulator mounted on the platform. Finally, the form of the admittance model used to perform the transient simulations is shown in section 3.3.

3.1 Stewart Platform

The Stewart Platform, or vehicle emulation system, consists of a six degree-of-freedom platform with six hydraulically actuated prismatic legs, in a parallel configuration, and a fixed base. A photograph of the mechanism is shown in Figure 3-1. The six prismatic actuators are each connected by a two degree-of-freedom universal joint to the fixed base and by a three degree-of-freedom spherical joint to the top plate of the platform. The base universal joints, connecting the legs to the platform base, lie on a circle of 52.77 inch radius and the top plate spherical joints, connecting the legs to the top plate, lie on a circle of 12 inch radius. These joints provide the top plate of the platform the capability to maneuver in six degrees-of-freedom. With this mechanism a wide range of three-dimensional motions can be emulated.

The motion of the platform is achieved by the extension and contraction of each

leg. The platform can perform ±30° rotations and ±12 inch translations.[23] The maximum bandwidth at which the platform can provide motion is projected to be between 5-10 Hz.

A six axis force/torque sensor, located on the platform top plate, measures the wrench that is produced by the manipulator mounted on the platform. The force/torque sensor has a vertical load capacity of 4000 lbs.[23] which accommodates the large forces generated by a fast slewing manipulator and large manipulator weight. A photograph of the force/torque sensor is shown in Figure 3-2. The sampling rate of the sensor is projected to be between 90-100 Hz. Therefore, the load cell is sampling approximately 10 times faster than the platform can perform motions.

3.2 Admittance Manipulator Compound Control

Figure 3-3 shows the admittance control concept for the Stewart Platform as applied to a compound manipulator. The load cell is mounted on the top plate of the platform, and the robot is mounted on top of the load cell. As the robot performs a specified task, the force/torque sensor measures the wrench $(F_x, F_y, F_z, M_\alpha, M_\beta, M_\gamma)$ generated at the robot base. This wrench is the input to the admittance model. The output is position (x, y, z) and orientation (α, β, γ) of the modeled system. This response is then used to drive the platform accordingly, by calculating the six leg lengths $(L_1, \ldots, L_6)$.

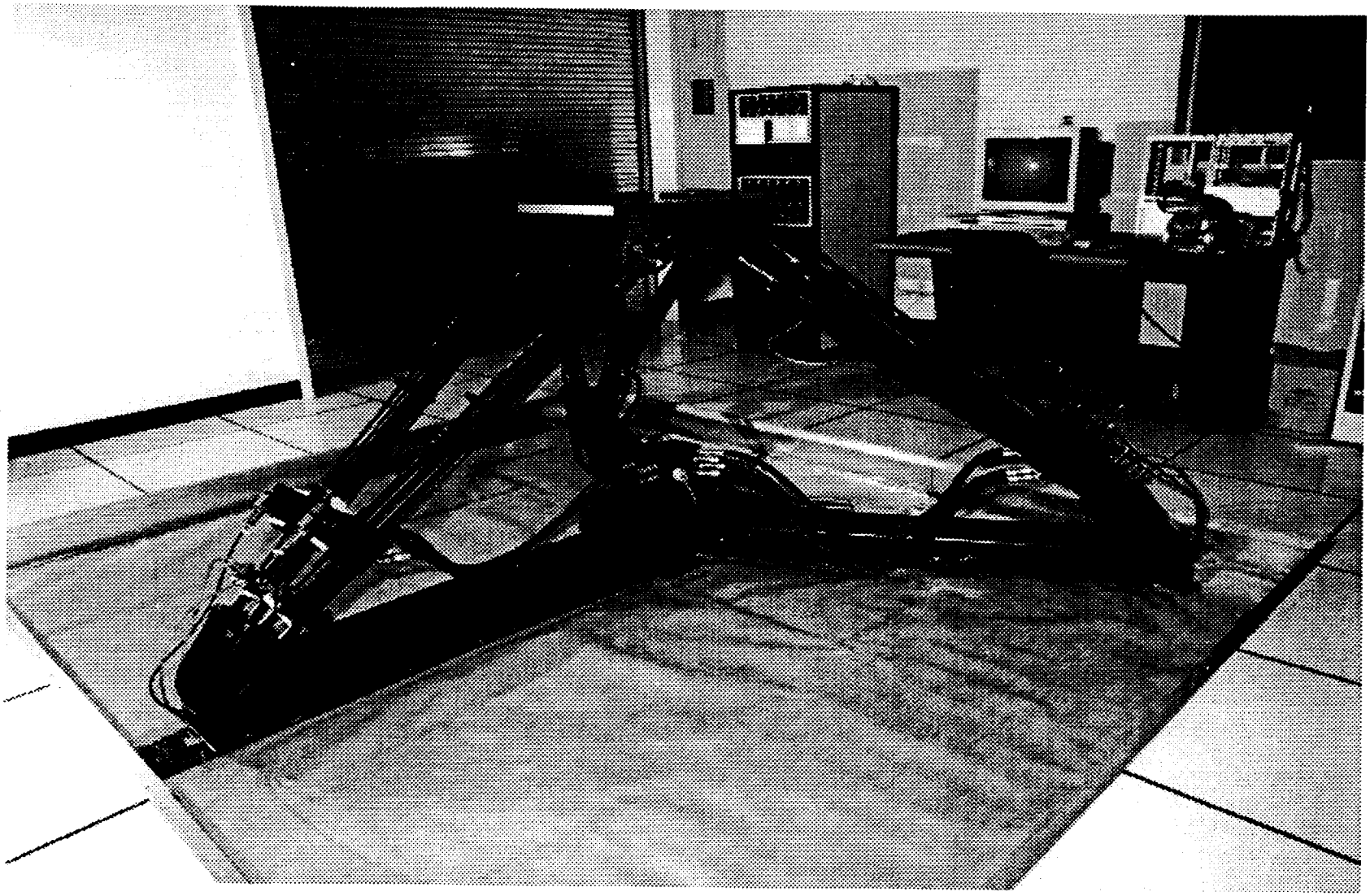

Figure 3-1: Photograph of the Stewart Platform in the Laboratory.

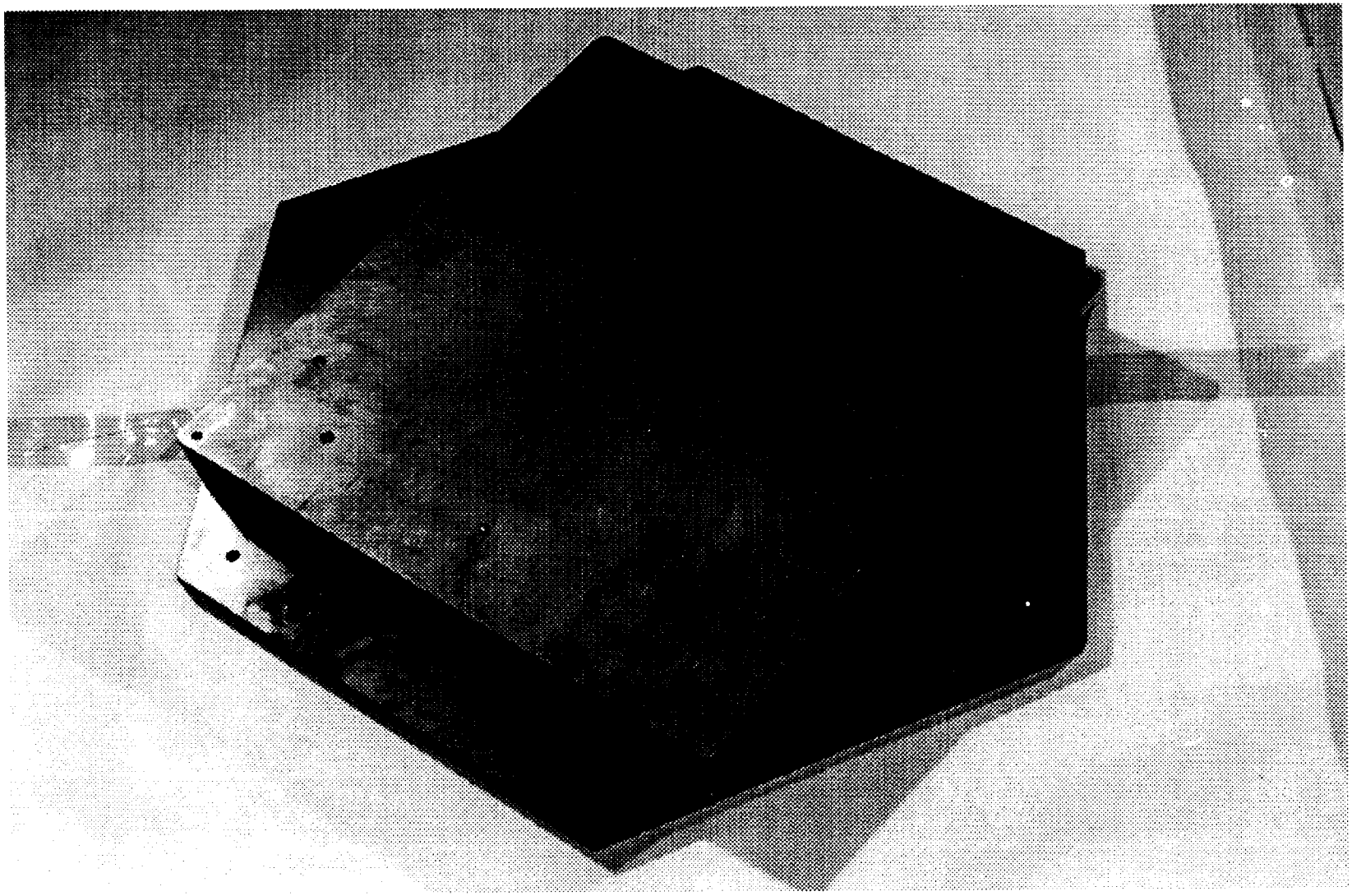

Figure 3-2: Photograph of the 6-axis Force/Torque Sensor.

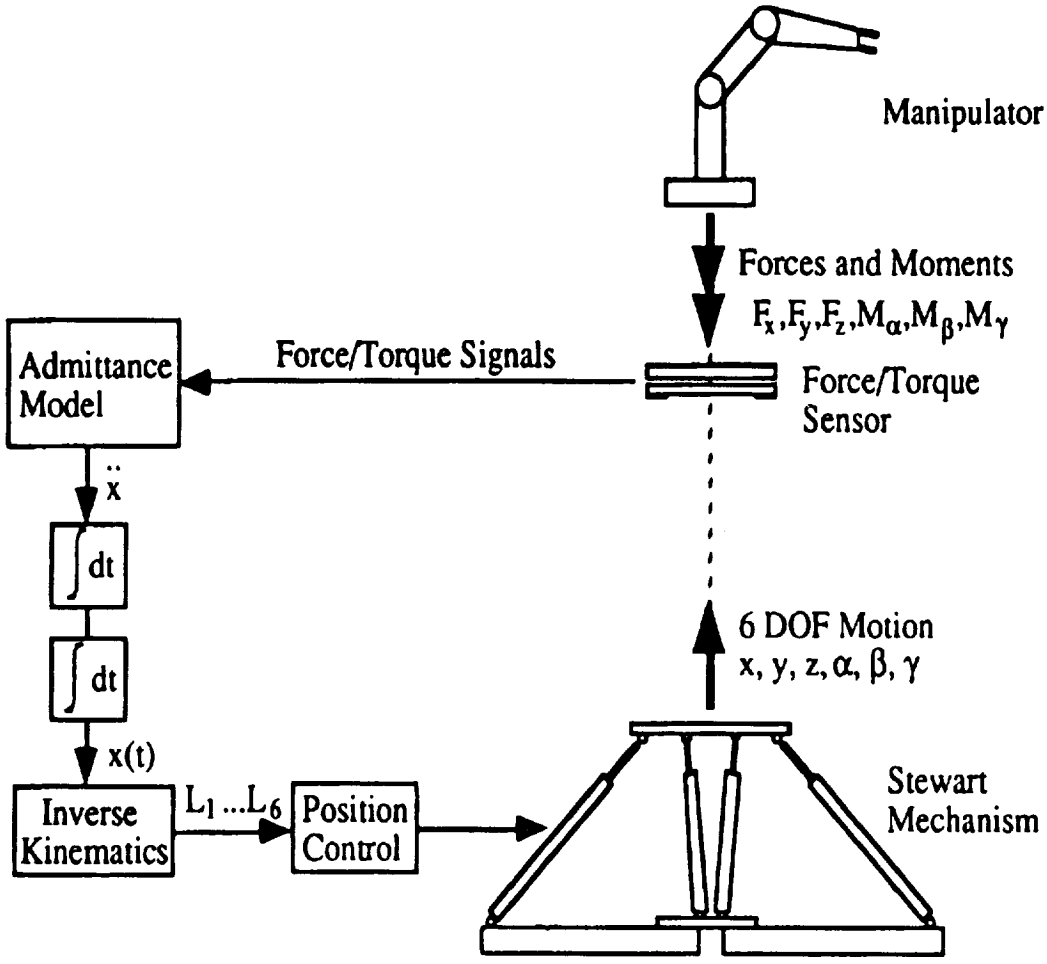

Figure 3-3: The Admittance Control Concept for the Stewart Platform.[2]

3.3 Admittance Model

The equation of motion of the SRMS with brakes locked can be written as

$$M\,\ddot{q}(t) + C\,\dot{q}(t) + K\,q(t) = F(t) \tag{3-1}$$

where matrices M, C, and K represent the mass, damping, and stiffness of the SRMS, respectively. F(t) is the wrench applied to the SRMS end-effector produced by the

SRMS payload, and q(t) represents the vector of generalized displacements. Equation (3-1) represents a set of linear, ordinary, **coupled**, second order differential equations written in physical space. One method of solving equation (3-1) is to use the concept of mode superposition. The basic premise behind this method is that the solution vector q(t) may be expressed as a linear combination of all n eigenvectors of the system, where n represents the total number of degrees-of-freedom. Therefore,

$$q(t) = \left[\{\phi_1\}\ \{\phi_2\}\ \cdots\ \{\phi_n\}\right]\eta(t) = [\Phi]\,\eta(t) \tag{3-2}$$

where the matrix Φ represents the system undamped mode shapes listed column-wise (of all the grid points and all the modes), and $\eta(t)$ corresponds to a vector of modal coordinates. Two points are made concerning equation (3-2). The first is that, since the input force in equation (3-1) is only at the SRMS end-effector, and the only desired displacements are at the end-effector, $q^*(t)$, then the only mode shape information required is at the end-effector. The second point is that the size of the mode shape matrix is usually large (i.e., mode wise), therefore, a modal truncation is performed to reduce the size, so

$$q^*(t) \approx \left[\{\phi_1^*\}\ \{\phi_2^*\}\ \cdots\ \{\phi_i^*\}\right]\eta(t) = [\Phi^*]\,\eta(t) \tag{3-3}$$

where $i < n$, and Φ^* is a truncated, or reduced end-effector mode shape matrix of i modes and is of size (6 x i).

If we make use of the transformation to mode space (equation (3-3)) in equation (3-1), and pre-multiply by the transpose of the mode shape matrix, the result yields a

set of linear, ordinary, **uncoupled**, second order differential equations

$$I\ddot{\eta}(t) + \begin{bmatrix} \backslash & \\ & 2\zeta_i\omega_i \\ & & \backslash \end{bmatrix}\dot{\eta}(t) + \begin{bmatrix} \backslash & \\ & \omega_i^2 \\ & & \backslash \end{bmatrix}\eta(t) = (\Phi^{\bullet})^T F(t) \qquad (3\text{-}4)$$

The modal mass matrix, I, is the identity matrix assuming the mode shapes are mass normalized. The modal damping matrix is a diagonal matrix where ζ_i and ω_i represent the modal damping factors and natural frequencies per mode number i. The modal stiffness matrix is a diagonal matrix of the square of the natural frequencies, and the symbol ^{T} denotes transpose.

To perform the simulations discussed in chapter 6, equations (3-4) were written in state-space format, or as a set of first order differential equations, given by

$$\begin{aligned} \dot{x}(t) &= Ax(t) + Bu(t) \\ y(t) &= Cx(t) + Du(t) \end{aligned} \qquad (3\text{-}5)$$

where matrix A represents the system dynamics (frequencies and modal damping terms), and matrix B characterizes the input u(t). The measurement matrix C selects the desired output from the state vector x(t) to form the measurement y(t), and D represents the direct transmission matrix.

Though not computationally efficient, one way of forming the state vector x(t) is to list all the modal coordinates first followed by the modal velocities, so

$$x(t) = \begin{Bmatrix} \eta_1(t) \\ \vdots \\ \eta_i(t) \\ \dot{\eta}_1(t) \\ \vdots \\ \dot{\eta}_i(t) \end{Bmatrix} \tag{3-6}$$

then,

$$A = \begin{bmatrix} \underline{0} & I \\ -diag(\omega_i^2) & -diag(2\zeta_i\omega_i) \end{bmatrix} \tag{3-7}$$

$$B = \begin{bmatrix} \underline{0} \\ (\Phi^*)^T \end{bmatrix} \tag{3-8}$$

$$C = \Phi^* L \tag{3-9}$$

where $L = [\, I \;\; \underline{0} \,]$, $[\, \underline{0} \;\; I \,]$, $\left[\, -diag(\omega_i^2) \;\; -diag(2\zeta_i\omega_i) \right]$, if position, velocity, or acceleration is the desired output, respectively. In the case of acceleration measurement, $D = \left[\Phi^*(\Phi^*)^T\right]$, otherwise it is zero. Matrix A is of size $2i \times 2i$, B is $2i \times N_i$, C is $N_o \times 2i$, and D is $N_o \times N_o$, where N_i and N_o are the number of inputs and outputs, respectively, and are both equal to 6 for this study.

IV. FINITE ELEMENT MODEL VALIDATION

4.1 Introduction

Due to the complexity of the SRMS, modeling simplifications of the manipulator arm dynamics must be made. These simplifications must be made carefully, since any alteration in the dynamics may render the results from that simulation useless. Thus, this chapter provides a validation of the GWU finite element model as compared with existing models of the SRMS [24,25].

Five SRMS brakes locked configurations (A, B, C, D, and S) are analyzed in this chapter. Table 4-1 provides a description of these configurations and Table 4-2 lists the joint angles in the GWU model joint coordinate frames (Figure 2-5). Figures 4-1 through 4-5 provide four-view plots of the configurations (shown in the same format as the configurations in section 2.3). These five configurations should not be confused with the ones shown in section 2.3. The four configurations in section 2.3 will be used to obtain the admittance model of the SRMS. The ones here are used only for validation of the GWU finite element model.

Table 4-1: Description of the Five SRMS Configurations used in Validating the GWU Finite Element Model.[24]

Configuration	Description
A	The arm is in a typical payload grappling configuration with the end effector positioned over the orbiter cockpit window.
B	The end-effector is in the symmetry plane of the orbiter, 17 feet above the point where the payload is placed in the cargo bay.
C	The end-effector is at the point where the payload is placed in the cargo bay.
D	The arm has been swung out from the stowed position.
S	The arm is straight up; the distance from the arm attachment point to the end-effector is maximum.

Table 4-2: Joint Angles for Configurations A, B, C, D and S.[24]

Joint	Configuration (degrees)				
	A	B	C	D	S
Shoulder Swing-out	19.48	19.48	19.48	19.48	19.48
Shoulder Yaw	-121.76	-19.378	-5.435	0.00	0.00
Shoulder Pitch	96.8	92.174	80.357	0.00	90.00
Elbow Pitch	-98.757	-91.317	-121.315	0.00	0.00
Wrist Pitch	75.366	-81.744	-46.42	0.00	0.00
Wrist Yaw	9.802	-24.241	-25.676	0.00	0.00
Wrist Roll	-119.743	-68.661	-83.967	0.00	0.00

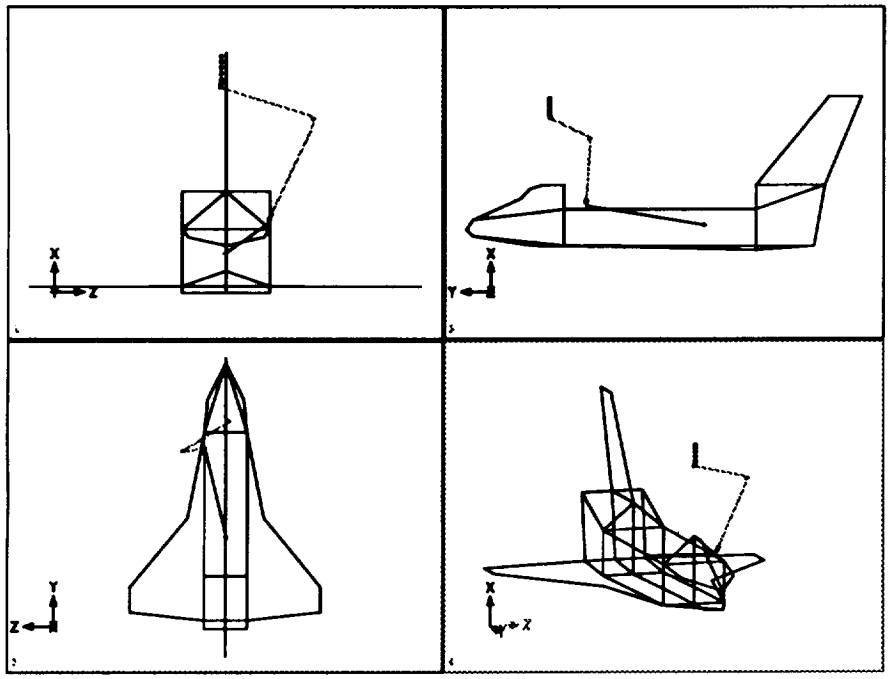

Figure 4-1: Configuration A.

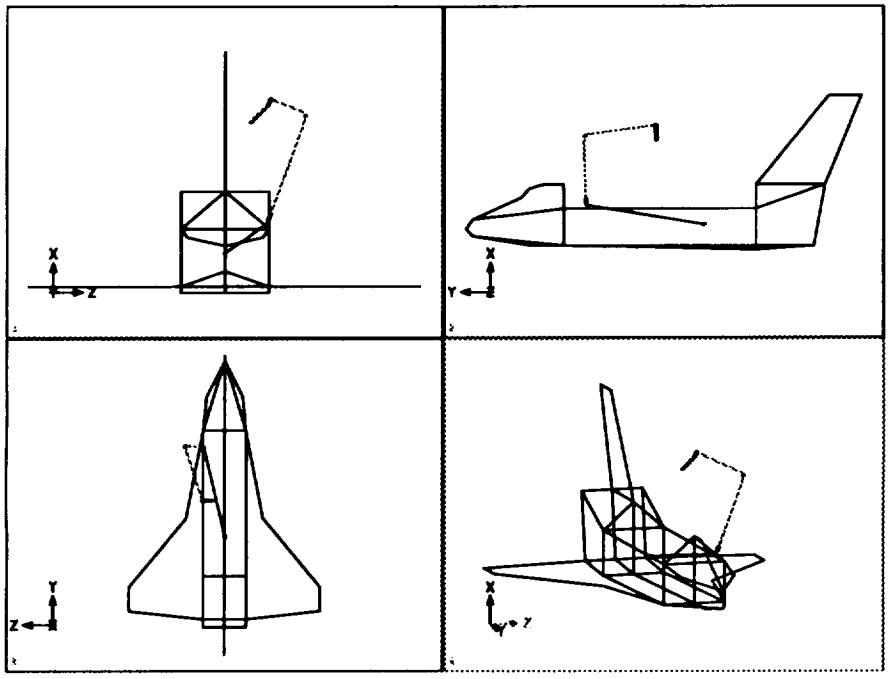

Figure 4-2: Configuration B.

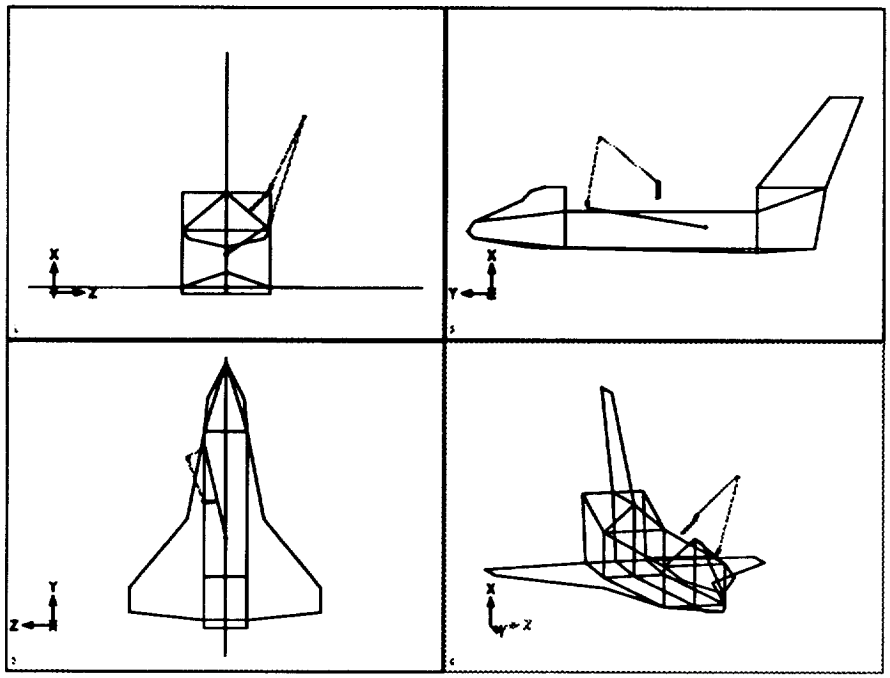

Figure 4-3: Configuration C.

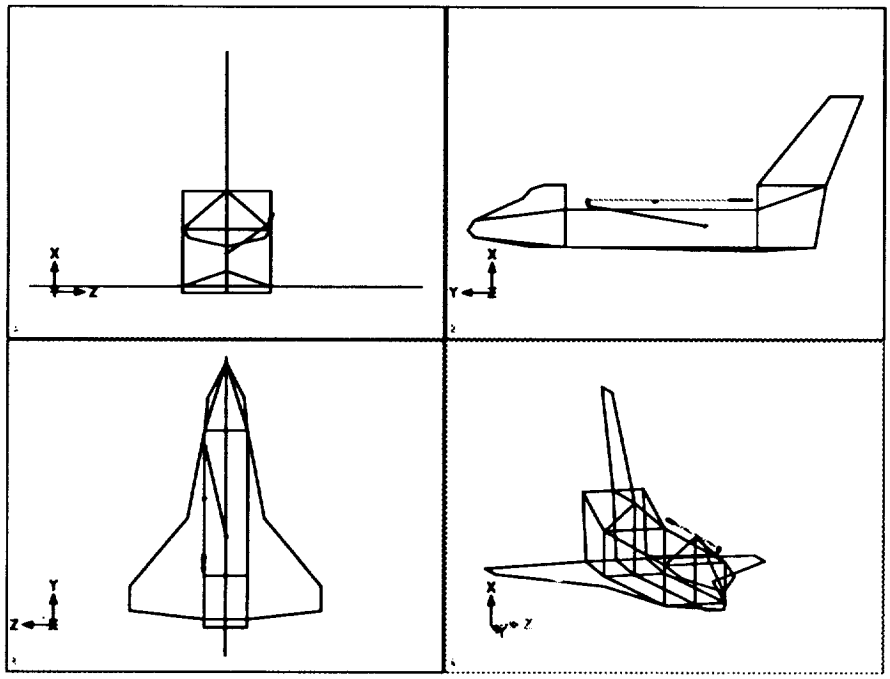

Figure 4-4: Configuration D.

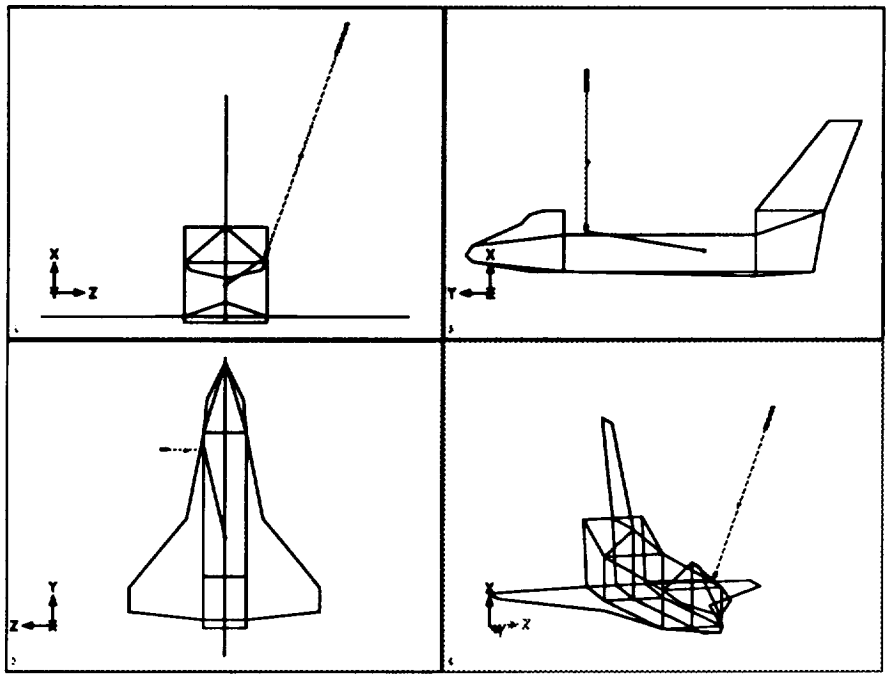

Figure 4-5: Configuration S.

4.2 Existing Finite Element Models

When SPAR Aerospace Limited was designing and fabricating the SRMS, they used a non real-time simulator called ASAD. ASAD is a dynamic analysis simulator (which includes joint nonlinearities, joint servo loops and flight control software) which has the ability of simulating the arm while the joints are in motion. In order to determine that ASAD was yielding accurate vibrational modes of the arm, SPAR created a finite element model using the structural analysis computer code STARDYNE for mode comparisons. The vibrational modes correspond to the configuration of the arm which is fixed spatially with all joint brakes on.

Shortly thereafter, The Charles Stark Draper Laboratory (CSDL) developed two

NASTRAN finite element models, one based on SPAR's STARDYNE model, and the second based on the ASAD dynamic simulator. The CSDL model that was based on STARDYNE will be referred to as the CSDL-STARDYNE model and the one based on ASAD will be referred to as the CSDL-ASAD model. Finally, Alberts *et al.*[25] also developed a NASTRAN finite element model, referred to here as the ODU (Old Dominion University) Model.

4.2.1 CSDL-STARDYNE

Figure 4-6 represents the arm in the stowed configuration with all grid points and CBAR elements labeled. This model consists of the following characteristics:

(a) Sixteen beam elements, $\mathrm{CBAR}_i \left(i = 1, \ldots, 7, 12, 13, 18, \ldots, 24\right)$ are used to represent the flexibility of the joints and their housings by providing bending and torsional stiffnesses.

(b) The flexibility of the upper and lower arm booms (ARM1 and ARM2), $\mathrm{CBAR}_i \left(i = 8, \ldots, 11, 14, \ldots, 17\right)$, are represented by four CBAR elements each.

(c) The Orbiter is assumed to be a rigid body and fixed in space.

(d) Concentrated masses (CONM2 cards) are used to place mass in the arm at grid points $3, \ldots, 25$.

(e) The stiffness of the orbiter port longeron is included in CBAR_1 and CBAR_2.

(f) A rigid homogeneous right circular cylinder is used as a payload.

(g) Elbow offset is included.

The geometrical and material properties of the CBAR elements may be found in [24].

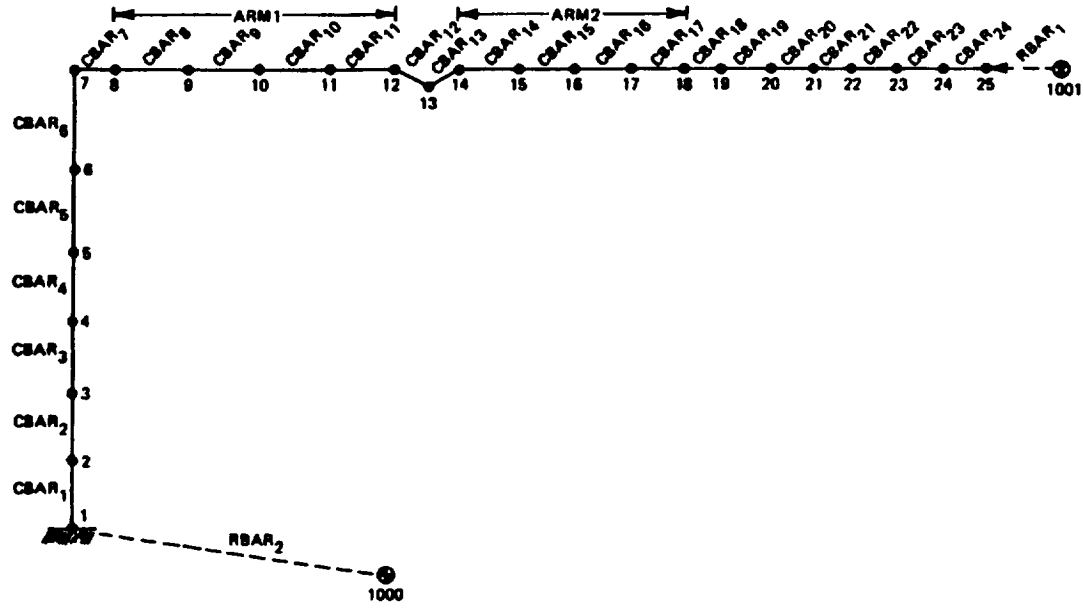

Figure 4-6: SRMS, in Stowed Configuration, as Modeled by the CSDL-STARDYNE Finite Element Model.[24]

4.2.2 CSDL-ASAD

Figure 4-7 represents the arm in the stowed configuration with all CBAR elements labeled. This model consists of the following characteristics:

(a) Seven beam elements, $\mathrm{CBAR}_i \ (i = 1, \ldots, 7)$, are used to represent the flexibility of the links (one CBAR element per link).

(b) 3-D inboard and outboard torsional springs (CELAS2 elements) are used to represent the flexibility of the joints. The joint stiffness about each primary drive axis is rigid.

(c) Non-structural masses in the PBAR cards are used to place mass in the arm.

(d) Orbiter port longeron stiffness included in torsional spring at node 1.

(e) SRMS attachment point (node 1) is fixed in space.

(f) Links are modeled as circular beam cross-sections.

(g) A rigid homogeneous right circular cylinder is used as a payload.

(h) Elbow offset is not included.

The geometrical and material properties of the CBAR elements may be found in [24].

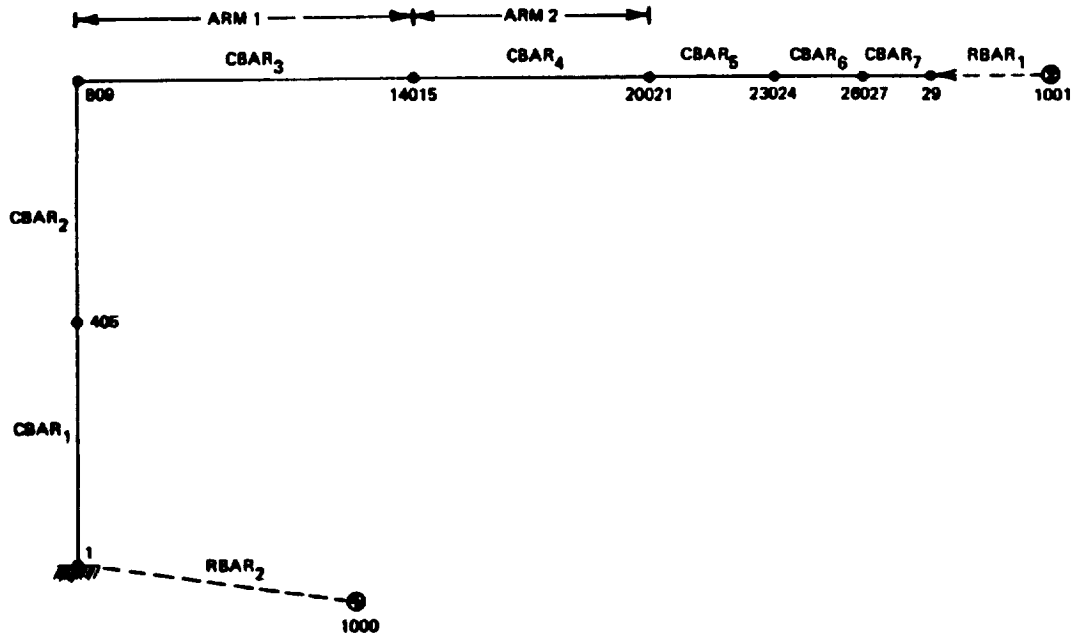

Figure 4-7: SRMS, in Stowed Configuration, as Modeled by the CSDL-ASAD Finite Element Model.[24]

4.2.3 ODU

The ODU model consists of the following characteristics:

(a) Sixteen elastic massless CBAR elements are used to represent the flexibility of the orbiter port longeron, end-effector, and the seven joints (a pair of inboard and outboard CBAR elements for each joint).

(b) The upper and lower arm booms and their stiffening rings are modeled by 720 quadrilateral shell elements (CQUAD4 elements) with uniformly distributed mass and stiffness. These stiffening rings are internal stabilization rings in the booms that maintain ovalization frequencies above 180 Hz and resist local shell buckling. The geometric parameters and mass densities of the booms and the stiffness rings are listed in Table 4-3.

(c) The mass of the joints are represented by 14 concentrated mass points.

(d) The masses of both booms are represented as structural mass (uniformly distributed) in the MAT1 card.

(e) A rigid homogeneous right circular cylinder is used as a payload.

(f) Eighteen local coordinate systems are used to describe the position and motion of the joints, booms, and end-effector.

(g) The SRMS attachment point is fixed in space.

(h) Elbow offset is included.

Table 4-3: ODU Model Boom and Stiffness Ring Geometric and Mass Properties.

	Length (in.)	Diameter (in.)	Thickness (in.)	Mass Density ($lb\text{-}sec^2/in^4$)
Upper Boom	197.084	13.0104	0.0752	1.568×10^{-4}
Stiffness Rings	5.000	12.9600	1.0265	2.536×10^{-4}
Lower Boom	225.984	12.9634	0.0517	1.568×10^{-4}
Stiffness Rings	5.000	12.9600	0.7100	2.536×10^{-4}

The ODU model is based on the CSDL-STARDYNE model with the only primary difference between the them is the use of CQUAD4 elements to model the two booms and their stiffening rings. Hence, the geometric and material properties are the same as

the CSDL-STARDYNE model. This finite element model was written with the intent of evaluating the effectiveness of constrained viscoelastic layer damping treatments for passive vibration control; hence the reason for modeling the booms using the CQUAD4 elements.

All four models used in this comparison use the same type payload: a rigid, homogeneous, right circular cylinder with a radius of 90.0 inches, height of 720.0 inches, and a weight of 32,000 lbs. A CONM2 card defines the mass and mass moments of inertia about the center of mass. The payload center of mass is rigidly attached to the end-effector grapple point with a rigid element (RBAR or RBE2, depending on which model is considered). The mass moments of inertia of the payload are

$$\left(I_{cm}\right)_{payload} = \begin{bmatrix} 37.45 & 0 & 0 \\ 0 & 3.345 & 0 \\ 0 & 0 & 37.45 \end{bmatrix} x\ 10^5 \qquad slinch - inch^2$$

There are three primary differences between all four finite element models: flexibility of the two booms, joints (using beam or 3-D torsional spring elements), and whether or not the elbow offset is included. Table 4-4 lists these differences.

Table 4-4: Summary of the Primary Differences in all Four Finite Element Models.

Model	Both Upper and Lower Arm Booms	Joints	Elbow offset
CSDL-STARDYNE	8 CBAR beam elements	16 CBAR beam elements	yes
CSDL-ASAD	2 CBAR beam elements	3-D torsional springs using CELAS2 spring elements with rigid joint drive stiffnesses	no
ODU	720 CQUAD4 shell elements (includes the stiffening rings)	16 CBAR beam elements	yes
GWU	18 CBAR beam elements	3-D torsional springs using GENEL elements, except for the orbiter port longeron stiffness which is modeled using a 6-D spring (3 translations & 3 rotations)	yes

4.3 Normal Modes Analysis

Ten natural frequencies of Configurations A, B, C, D, and S have been computed by MSC/NASTRAN from the GWU model for comparison with the other three models. These frequencies correspond to the desired arm configuration fixed spatially with all joint brakes on. The results of the analyses are presented in Tables 4-5 through 4-9 for each configuration with a 32,000 lb. cylindrical payload and in Table 4-11 for Configurations A, C and S without a payload. The only model that provided frequencies for the no payload case was ODU, and it only provided them for Configurations A, C, and S, which is why Table 4-11 has only three configurations listed. Percent frequency difference comparisons are made with and without a payload and are shown in Tables 4-10 and 4-12, respectively; a positive percent difference

indicates that the GWU model overestimated the comparison frequency and a negative sign underestimated it. Percent frequency comparisons were not made from the ODU, or CSDL-ASAD models for two reasons. The first reason is that the ODU model obtained SRMS properties from the CSDL-STARDYNE model, and an independent validation of the frequencies would not be possible. The second is of the approximation of the two arm booms using only one CBAR beam element each in the CSDL-ASAD model. The majority of this chapter compares natural frequencies between all the finite element models. Comparison of mode shapes, however, were also looked at, whenever data was available. The first ten mode shapes corresponding to Configuration S (with the 32000 lb. payload) of the CSDL-STARDYNE model are compared to the GWU model.

Table 4-5: Natural Frequencies for Configuration A with a 32,000 lb. Payload.

Mode	Configuration A Frequencies (Hz)			
	GWU	CSDL-STARDYNE	ODU	CSDL-ASAD
1	0.0284	0.0322	0.033	0.0430
2	0.0379	0.0380	0.039	0.0491
3	0.0517	0.0553	0.056	0.0656
4	0.0955	0.1127	0.114	0.1443
5	0.1611	0.1826	0.199	0.2395
6	0.3072	0.3425	0.362	0.4327
7	1.8835	1.5368	1.563	2.4632
8	6.2325	6.2980	6.437	8.8521
9	9.0939	9.2980	9.449	10.6896
10	14.0403 #	18.7895	23.31 #	19.1387
NOTE: # ≡ Boom Bending Mode; otherwise Joint Vibration Mode				

Table 4-6: Natural Frequencies for Configuration B with a 32,000 lb. Payload.

Mode	Configuration B Frequencies (Hz)		
	GWU	CSDL-STARDYNE	CSDL-ASAD
1	0.0371	0.0393	0.0475
2	0.0454	0.0479	0.0605
3	0.0626	0.0719	0.0830
4	0.0694	0.0758	0.1057
5	0.1419	0.1386	0.1867
6	0.3045	0.3390	0.4241
7	1.5405	1.4727	2.3608
8	6.3606	6.3227	8.5511
9	8.6577	9.2931	10.5515
10	14.8751	18.6882	20.8907

Table 4-7: Natural Frequencies for Configuration C with a 32,000 lb. Payload.

Mode	Configuration C Frequencies (Hz)			
	GWU	CSDL-STARDYNE	ODU	CSDL-ASAD
1	0.0375	0.0404	0.042	0.0480
2	0.0421	0.0446	0.048	0.0551
3	0.0549	0.0641	0.065	0.0725
4	0.1050	0.1084	0.111	0.1460
5	0.2085	0.2000	0.218	0.2680
6	0.2540	0.2787	0.287	0.3635
7	1.2154	1.2617	1.276	2.1277
8	6.4826	6.6033	6.828	8.4814
9	8.7889	9.7605	10.118	11.0978
10	15.0892 #	18.3194	22.18 #	23.6765
NOTE: # ≡ Boom Bending Mode; otherwise Joint Vibration Mode.				

Table 4-8: Natural Frequencies for Configuration D with a 32,000 lb. Payload.

Mode	Configuration D Frequencies (Hz)		
	GWU	CSDL-STARDYNE	CSDL-ASAD
1	0.0299	0.0278	0.0373
2	0.0352	0.0323	0.0428
3	0.0426	0.0491	0.0580
4	0.0961	0.1025	0.1280
5	0.2582	0.3083	0.3698
6	1.9932	1.5369	2.8766
7	3.1738	3.3716	3.9711
8	3.8756	3.8630	5.5383
9	9.6282	11.5056	12.6125
10	10.9059	11.5329	15.0551

Table 4-9: Natural Frequencies for Configuration S with a 32,000 lb. Payload.

Mode	Configuration S Frequencies (Hz)			
	GWU	CSDL-STARDYNE	ODU	CSDL-ASAD
1	0.0224	0.0264	0.027	0.0337
2	0.0348	0.0317	0.034	0.0424
3	0.0456	0.0496	0.049	0.0594
4	0.0847	0.0989	0.100	0.1206
5	0.2563	0.3056	0.312	0.3677
6	2.5183 #	2.9949	3.38 #	3.5164
7	2.7965 #	3.1509	3.83 #	4.1033
8	3.3496 #	3.7399	4.21 #	12.2208
9	10.3327	11.3379	11.894	13.4454
10	10.5217	11.5510	12.226	13.8032
NOTE: # ≡ Boom Bending Mode; otherwise Joint Vibration Mode.				

Table 4-10: Percent Frequency Difference between GWU and CSDL-STARDYNE Models for Configurations A, B, C, D, and S.

Mode	Configuration % Frequency Difference				
	A	B	C	D	S
1	-13.4	-5.9	-7.7	+7.0	-17.9
2	-0.3	-5.5	-5.9	+8.2	+8.9
3	-7.0	-14.9	-16.8	-15.3	-8.8
4	-18.0	-9.2	-3.2	-6.7	-16.8
5	-13.3	+2.3	+4.1	-19.4	-19.2
6	-11.5	-11.3	-9.7	+22.9	-18.9
7	+18.4	+4.4	-3.8	-6.2	-12.7
8	-1.1	+0.6	-1.9	+0.3	-11.7
9	-2.2	-7.3	-11.1	-19.5	-9.7
10	-33.8	-25.6	-21.4	-5.7	-9.8

Table 4-11: Comparison of Natural Frequencies between ODU and GWU Finite Element Models for Configurations A, C and S with No Payload.

Mode	Configuration A (Hz)		Configuration C (Hz)		Configuration S (Hz)	
	ODU	GWU	ODU	GWU	ODU	GWU
1	0.492	0.445	0.664	0.651	0.361	0.306
2	0.545	0.587	0.753	0.868	0.424	0.494
3	1.425	1.599	1.084	1.066	3.57 #	2.84 #
4	1.967	1.871	1.580	1.479	3.99 #	3.38 #
5	6.296	6.479	6.952	6.708	9.562	9.089
6	6.874	6.632	7.414	6.967	9.957	9.144
7	23.31 #	14.05 #	22.12 #	14.42 #	23.82 #	15.24 #
8	24.54 #	15.98 #	24.12 #	16.88 #	25.49 #	17.76 #
9	56.24 #	18.07 #	50.35 #	19.67 #	35.38 #	17.85 #
10	58.94 #	22.66 #	54.16 #	20.70 #	37.04 #	19.24 #
NOTE: # ≡ Boom Bending Mode; otherwise Joint Vibration Mode.						

Table 4-12: Percent Frequency Differences between GWU and ODU Models for Configurations A, C and S for No Payload.

Mode	Configuration % Frequency Difference		
	A	C	S
1	-10.6	-2.0	-18.0
2	+7.2	+13.2	+14.2
3	+10.9	-1.7	-25.7
4	-5.1	-6.8	-18.0
5	+2.8	-3.6	-5.2
6	-3.6	-6.4	-8.9
7	-65.9	-53.4	-56.3
8	-53.6	-42.9	-43.5
9	-211.2	-156.0	-98.2
10	-160.1	-161.6	-92.5

Alberts[25] sites several observations from frequency and mode shape information (not shown), which Tables 4-12 through 4-16 support

1. The vibrational characteristics of the SRMS can be categorized in two forms, one results principally from joint flexibility and the other from boom flexibility. The joint modes generally have lower frequencies, while the boom modes typically have higher frequencies. From Tables 4-5 and 4-7, joint flexibility encompasses modes 1 through 9, and boom flexibility in mode 10.

2. The mass of the payload greatly influences the dynamic behavior of the SRMS. As can be seen in Tables 4-5 through 4-9, and 4-11, the first few frequencies with the payload are typically lower than without it. It can also be seen that adding a payload to the SRMS, configurations A, C and S, has the effect of pushing boom bending to higher modes (i.e. from mode 7 to mode 10 in configurations A and C and from mode 3 to mode 6 in configuration S).

3. The SRMS exhibits different vibrational behavior for different configurations. Configurations A and C both have fundamental boom bending at mode 10 (Tables 4-5 and 4-7). Changing the configuration to S produces a fundamental boom bending at mode 6 (Table 4-9). A similar result is produced without a payload (Table 4-11).

4.4 Summary

From Tables 4-5 through 4-9 we see that the CSDL-ASAD model generally yielded higher frequencies for all configurations. CSDL-STARDYNE yielded slightly lower frequencies than CSDL-ASAD. The ODU model matches the frequencies of CSDL-STARDYNE to within an average of approximately 5% for configurations A, C, and S. Since the ODU model is based on the CSDL-STARDYNE model, we expect similar results. Finally, the GWU model generally produced the lowest frequencies. From Table 4-10, the GWU model compares to within an average of approximately 10% of the CSDL-STARDYNE model. However, considering the modeling uncertainties (i.e. variation in modeling techniques, SRMS geometric and material properties not from a common data base), the CSDL-STARDYNE, ODU, and GWU models basically yield good agreement. Also, a dynamic model (GWU model) which produces a slightly lower frequency spectrum (i.e., a conservative model) will generally yield a more robust system when considering disturbance compensation control of the dynamic interaction between manipulators in space and their carrying vehicles.

A possible explanation as to why the ODU model produces the highest boom bending frequencies may be obtained by looking at the method of modeling the booms; mode 10 of Configurations A and C with the 32000 lb. payload (Tables 4-5

and 4-7), and modes 7 through 10 of Configurations A, C, and S without the payload, (Table 4-11). This may also explain the large percent frequency differences for mode 10, exceeding 20% in Table 4-10, and for modes 7 through 10, exceeding 40% in Table 4-12. The ODU finite element model uses CQUAD4 quadrilateral shell elements to model the booms, whereas the other models, including GWU, use CBAR beam elements. The ODU model also includes the boom stiffening rings in the CQUAD4 shell elements. Thus the variations in elements used to model the booms (i.e., CBAR vs. CQUAD4 elements), and the inclusion of the stiffening rings may make the booms stiffer than in the other models, thus resulting in large boom bending frequency variations. This appears to indicate that the modeling process of the booms is an important issue.

The first ten mode shapes of Configuration S (with the payload) between CSDL-STARDYNE and GWU agree very well, and are provided in Appendix D. Since no actual numbers of the mode shapes was available, a qualitative comparison was made of the mode shapes (i.e., only the shape of the modes were compared). Modes 1 and 2 (Figures D-1 and D-2) resemble the first mode shape of a cantilever beam. Mode 3 (Figure D-3) shows a *V-shape* at the elbow joint, and both models yield a similar phenomenon. Both models yield a single *arc-shape* for modes 4 through 8 (Figures D-4 through D-8). A sinusoidal shape is evident from both models in modes 9 and 10 (Figures D-9 and D-10). Overall, mode shapes 1 through 4 produce substantial end-effector motions, while mode shapes 5 through 10 produce essentially no end-effector displacements.

V. SRMS ADMITTANCE MODEL

As stated in section 3.3, the admittance model for the SRMS end-effector will be represented in mode space. The following chapter provides the system natural frequencies and undamped mode shapes of the SRMS end-effector for each of the four brakes locked configurations. Table 5-1 lists 30 natural frequencies for each of the four configurations. Tables 5-2 through 5-9 (sections 5.1 through 5.4) contain 30 SRMS end-effector mode shapes for the Unberth, Low Hover, Deploy, and Capture Configurations, respectively. These mode shapes represent local modes as discussed at the end of section 2.2.1.

The A, B, C, and D state-space matrices given in section 3.3 (equations (3-5) through (3-9)) can be formed based on the data provided in this chapter. Table 5-1 contains the values of ω_i, and Tables 5-2 through 5-9 provide the values required to form the mode shape matrix, Φ^*,

$$\Phi^* = \left[\phi_1^* \;\; \phi_2^* \;\; \cdots \;\; \phi_i^* \right]$$

where each column corresponds to a (6 x 1) eigenvector, three translational and three rotational mode shapes per mode number *i*.

Table 5-1: Admittance Model Natural Frequencies (Hz).

Modes	Configuration			
	Unberth	Low Hover	Deploy	Capture
1	0.6182	0.4921	0.4939	0.3490
2	0.8127	0.7026	0.5845	0.4816
3	1.0843	1.3411	1.3804	2.4456
4	1.5069	1.6965	1.6803	2.5855
5	6.7145	6.2797	7.9893	6.5254
6	6.8671	6.5509	8.3489	6.7986
7	14.4133	14.2605	13.5313	14.5025
8	16.9330	16.2946	17.8877	16.6671
9	20.0820	19.5126	18.8072	18.9332
10	21.2830	21.7611	21.8308	24.6346
11	25.7533	26.6577	23.7091	27.0170
12	27.8345	30.0844	24.6546	31.0854
13	32.1478	32.7095	37.4553	32.9264
14	36.4636	34.7627	39.6217	34.3537
15	42.1060	39.9968	41.7089	37.6423
16	47.9396	47.8694	46.5139	47.2664
17	54.7098	55.9411	55.9033	53.3627
18	60.3445	61.9398	61.8005	57.3731
19	62.1445	64.0790	68.7739	66.2802
20	74.2893	73.3208	71.8406	72.1388
21	76.5157	75.9884	76.2997	78.9213
22	81.8802	83.5739	82.6870	84.2167
23	87.3861	87.3628	91.8621	90.8803
24	98.5659	98.7153	94.1059	95.8865
25	101.3382	102.1677	107.2063	107.1869
26	113.9292	114.5231	110.7147	114.0042
27	119.7751	119.9892	123.2170	119.7116
28	126.5014	126.4623	126.9747	124.6444
29	129.1457	130.9622	131.4500	129.3707
30	147.0188	143.4657	151.4364	143.3232

5.1 Unberth Configuration

Table 5-2: Admittance Model SRMS End-Effector Local Translational Mode Shapes for Configuration Unberth.

Mode	Local Translational Mode Shapes		
	x	y	z
1	-3.6595e-02	9.2002e-01	-5.1284e-01
2	1.0209e+00	3.54040e-01	2.3915e-01
3	1.6868e-01	-5.9444e-01	5.7792e-01
4	-8.7179e-02	-6.1153e-01	-9.4652e-01
5	1.2524e-01	1.0931e+00	-1.4136e+00
6	-2.9917e-01	1.4096e+00	1.2008e+00
7	3.7854e-02	-6.6447e-01	4.5187e-01
8	-1.1815e-01	5.6066e-01	8.7638e-01
9	-2.3965e-01	-3.5045e-01	8.6296e-01
10	-2.7116e-01	9.0189e-01	5.8983e-02
11	6.8829e-02	-3.7574e-01	-1.8520e-01
12	-2.5210e-02	-5.9847e-01	7.9744e-01
13	-2.2353e-03	-7.3901e-01	1.7677e-01
14	2.5187e-01	8.0507e-01	2.1077e+00
15	-1.5147e-02	-1.7893e+00	4.7853e-01
16	-1.5162e-01	-2.7410e-01	1.4525e-01
17	-8.5703e-02	3.8321e-01	-2.6808e-01
18	-1.6365e-01	-4.1020e-01	-8.1132e-02
19	-2.4347e-01	-2.4465e-01	-4.2576e-01
20	2.4219e-02	6.8387e-01	-5.5187e-01
21	2.3317e-02	7.6238e-01	-2.6634e-01
22	-6.1971e-03	1.7977e-01	3.1454e-01
23	3.2197e-02	-1.3067e-01	-1.5803e-01
24	1.6035e-01	-4.1211e-01	-6.5889e-01
25	6.9301e-02	-2.0154e-01	-2.4886e-01
26	-1.6554e-02	-3.3829e-01	1.1397e-01
27	1.7412e-01	-1.5665e-02	-2.6800e-01
28	-2.0674e-01	2.7582e-01	5.1749e-02
29	-1.8483e-01	-5.3121e-02	8.1350e-02
30	4.5154e-03	-1.7697e-01	9.8069e-02

Table 5-3: Admittance Model SRMS End-Effector Local Rotational Mode Shapes for Configuration Unberth.

Mode	Local Rotational Mode Shapes		
	θ_x	θ_y	θ_z
1	3.0003e-03	1.9819e-04	-5.4978e-05
2	5.1562e-04	-3.1221e-03	3.1972e-03
3	-2.2689e-03	-4.5384e-03	-5.9539e-03
4	-4.4506e-05	3.0597e-03	-2.9564e-03
5	-1.7811e-02	3.7900e-02	3.1713e-02
6	-6.5840e-03	-2.7951e-02	3.5377e-02
7	1.2660e-02	-1.9371e-02	-2.6668e-02
8	3.3310e-03	-4.0655e-02	2.4650e-02
9	4.7300e-02	-4.3183e-02	-1.8390e-02
10	-5.8131e-02	-1.4180e-03	4.4886e-02
11	-1.2472e-01	1.1572e-02	-1.8789e-02
12	-1.6065e-01	-4.6087e-02	-3.2172e-02
13	-5.2889e-02	-1.0868e-02	-4.4313e-02
14	8.3523e-03	-1.4256e-01	5.2594e-02
15	4.0865e-02	-3.3335e-02	-1.2061e-01
16	2.2250e-02	-1.0475e-02	-1.9635e-02
17	-6.2809e-02	2.1097e-02	2.8256e-02
18	2.9746e-02	7.2413e-03	-3.2431e-02
19	-8.9126e-03	3.6181e-02	-2.0045e-02
20	-4.4072e-02	4.9239e-02	5.8457e-02
21	7.2804e-02	2.4113e-02	6.6369e-02
22	-6.6195e-02	-2.9236e-02	1.5909e-02
23	-1.4539e-01	1.4909e-02	-1.1809e-02
24	2.6561e-02	6.4206e-02	-3.8903e-02
25	-1.9916e-02	2.4486e-02	-1.9040e-02
26	-5.5025e-03	-1.1374e-02	-3.3004e-02
27	-5.4630e-04	2.7243e-02	-1.5499e-03
28	-3.7134e-03	-5.3253e-03	2.7593e-02
29	3.6590e-03	-8.3608e-03	-5.4026e-03
30	8.4079e-03	-1.0348e-02	-1.8296e-02

5.2 Low Hover Configuration

Table 5-4: Admittance Model SRMS End-Effector Local Translational Mode Shapes for Configuration Low Hover.

Mode	Local Translational Mode Shapes		
	x	y	z
1	-1.7370e-01	7.9517e-01	-4.9274e-01
2	-9.4593e-01	-9.3114e-02	3.8006e-01
3	2.4993e-01	-5.3839e-01	6.9157e-01
4	-5.9458e-01	-7.4823e-01	-6.9670e-01
5	4.1195e-02	1.1470e+00	-1.4922e+00
6	-1.3713e-01	1.5316e+00	1.2730e+00
7	1.6091e-02	4.3935e-01	-6.1434e-01
8	-3.1743e-01	6.4065e-01	5.0454e-01
9	-1.8978e-01	-4.4679e-01	5.7004e-01
10	-2.2391e-01	4.8523e-01	-3.1603e-01
11	-1.1982e-01	8.5326e-02	3.9078e-01
12	2.0109e-02	1.9426e-01	-4.8056e-01
13	-1.6652e-03	-7.6649e-01	9.3185e-02
14	7.7700e-02	9.8978e-01	2.2152e+00
15	-9.4942e-03	1.9764e+00	-7.4307e-01
16	-9.3941e-02	-1.6782e-01	1.6105e-01
17	-1.0998e-01	1.7183e-01	-2.3821e-01
18	2.1977e-01	5.5388e-01	8.6638e-02
19	9.3323e-02	-2.0927e-01	4.2871e-01
20	2.1813e-02	-1.6137e-01	3.3190e-01
21	2.9936e-02	7.7299e-01	-5.1609e-01
22	3.3046e-02	1.2625e-01	2.9134e-01
23	-3.7460e-03	-2.7047e-01	-3.2028e-02
24	2.4217e-02	-5.7374e-01	-6.2508e-01
25	2.5855e-02	-2.4331e-01	-3.0491e-01
26	-2.0701e-02	-3.5335e-01	2.2093e-01
27	-1.3790e-01	1.0380e-01	2.4132e-01
28	-9.4620e-02	2.5954e-01	-5.9698e-02
29	-1.0839e-01	-7.1340e-02	9.7136e-02
30	-4.1222e-03	1.7645e-01	-1.3840e-01

Table 5-5: Admittance Model SRMS End-Effector Local Rotational Mode Shapes for Configuration Low Hover.

Mode	Local Rotational Mode Shapes		
	θ_x	θ_y	θ_z
1	2.0205e-03	-4.1887e-04	-1.5804e-03
2	-1.1434e-03	2.2890e-03	-2.3420e-03
3	-5.6736e-03	-5.5003e-03	-4.9047e-03
4	-1.1864e-03	3.0706e-03	-5.1858e-03
5	-6.3975e-03	4.0174e-02	3.3476e-02
6	-1.6029e-03	-2.7715e-02	3.5909e-02
7	-1.7439e-02	2.6713e-02	1.8352e-02
8	-4.1041e-03	-2.1404e-02	2.6687e-02
9	4.1755e-02	-2.8059e-02	-2.3653e-02
10	-4.8979e-02	1.8971e-02	2.4077e-02
11	6.2740e-02	-2.2804e-02	3.8395e-03
12	1.9378e-01	2.8984e-02	1.0790e-02
13	-9.9836e-02	-5.6153e-03	-4.6924e-02
14	-5.3314e-03	-1.4636e-01	6.3740e-02
15	-1.8794e-02	5.0149e-02	1.2981e-01
16	1.7612e-02	-1.1528e-02	-1.1888e-02
17	-3.3557e-02	1.8929e-02	1.2288e-02
18	-2.2164e-02	-7.9975e-03	4.4500e-02
19	2.6852e-02	-3.6370e-02	-1.6550e-02
20	4.9049e-02	-2.9355e-02	-1.3433e-02
21	-1.6949e-02	4.6546e-02	6.7117e-02
22	-4.9434e-02	-2.7260e-02	1.1214e-02
23	-1.6279e-01	3.0692e-03	-2.4523e-02
24	2.3800e-02	6.0899e-02	-5.4230e-02
25	-1.2636e-02	3.0072e-02	-2.3056e-02
26	-5.8202e-03	-2.2150e-02	-3.4551e-02
27	-1.8607e-03	-2.4518e-02	1.0277e-02
28	-7.5431e-04	6.1205e-03	2.5975e-02
29	2.2759e-03	-1.0021e-02	-7.2620e-03
30	-5.7564e-03	1.4559e-02	1.8186e-02

5.3 Deploy Configuration

Table 5-6: Admittance Model SRMS End-Effector Local Translational Mode Shapes for Configuration Deploy.

Mode	Local Translational Mode Shapes		
	x	y	z
1	8.6877e-01	5.8987e-01	-2.1477e-01
2	-4.5808e-04	-4.2251e-01	-1.1588e+00
3	2.1769e-01	-1.1371e+00	4.1762e-01
4	-1.4667e-03	2.2896e-01	6.1831e-01
5	-2.4252e-01	1.6242e+00	-6.8788e-01
6	1.0896e-02	-6.6088e-01	-1.6161e+00
7	1.8843e-01	-3.7328e-02	-9.5296e-03
8	5.4181e-04	2.5733e-01	1.1751e+00
9	-3.1672e-02	-1.2154e+00	3.2389e-01
10	5.2030e-03	1.8042e-01	6.3383e-01
11	2.6372e-01	-9.0677e-01	5.0679e-01
12	4.7636e-02	-5.2067e-01	-1.1044e+00
13	-5.6116e-02	-3.3618e-01	-8.5112e-01
14	1.3258e-01	3.9558e-01	-1.2545e+00
15	-1.3360e-01	-1.8449e+00	2.9891e-01
16	3.6320e-02	5.6150e-01	1.0441e+00
17	-3.1568e-01	-4.5035e-01	2.3108e-01
18	3.7709e-02	2.8249e-01	4.8334e-01
19	-1.8141e-01	-8.4512e-01	3.7735e-01
20	-2.6803e-02	-4.1912e-01	-8.3608e-01
21	-8.9261e-03	-2.1446e-01	-4.2676e-01
22	-3.6467e-03	-1.1204e-01	-2.2764e-01
23	-1.0616e-02	5.2544e-02	4.4721e-02
24	-2.7204e-01	5.1280e-01	-1.6462e-01
25	1.8757e-01	-5.1085e-01	1.8699e-01
26	-1.8173e-02	1.5594e-01	2.6940e-01
27	-2.2847e-02	-6.4949e-02	-1.9727e-01
28	-5.8841e-01	1.4690e-01	-4.2207e-02
29	7.2638e-03	-2.3840e-02	-5.4931e-02
30	-1.3250e-03	7.0128e-02	1.3531e-01

Table 5-7: Admittance Model SRMS End-Effector Local Rotational Mode Shapes for Configuration Deploy.

Mode	Local Rotational Mode Shapes		
	θ_x	θ_y	θ_z
1	2.1109e-06	1.1031e-03	3.0397e-03
2	2.4165e-03	2.4786e-03	-9.0039e-04
3	5.9729e-06	-1.7192e-03	-4.5680e-03
4	2.9827e-03	-7.9919e-03	2.9078e-03
5	-8.2996e-04	1.9750e-02	4.5315e-02
6	-1.9063e-02	4.8106e-02	-1.9111e-02
7	1.1053e-04	6.1920e-04	-7.2224e-04
8	-1.1014e-02	-5.4490e-02	1.1214e-02
9	1.1726e-03	-1.6059e-02	-5.7125e-02
10	1.6530e-01	-3.4727e-02	9.6181e-03
11	-2.5005e-02	-2.7355e-02	-4.7164e-02
12	1.3434e-01	6.0133e-02	-2.7091e-02
13	1.3440e-02	5.7514e-02	-2.1700e-02
14	-2.2314e-03	8.7203e-02	2.6701e-02
15	5.1828e-03	-2.1667e-02	-1.2564e-01
16	4.9282e-02	-7.7458e-02	3.9810e-02
17	8.9668e-03	-1.8752e-02	-3.5112e-02
18	8.8294e-02	-4.0082e-02	2.2536e-02
19	-3.4101e-03	-3.3084e-02	-7.1108e-02
20	8.8722e-02	7.3948e-02	-3.5645e-02
21	-4.0730e-03	3.8411e-02	-1.8596e-02
22	-1.2729e-01	2.0951e-02	-9.9558e-03
23	-1.0046e-01	-4.1930e-03	4.8348e-03
24	3.6041e-03	1.5876e-02	4.7811e-02
25	-1.1596e-03	-1.8617e-02	-4.9431e-02
26	-1.0342e-02	-2.6817e-02	1.5138e-02
27	-4.2579e-03	2.0115e-02	-6.4624e-03
28	1.2009e-04	4.3302e-03	1.4710e-02
29	-4.8154e-04	5.6667e-03	-2.4058e-03
30	9.4927e-03	-1.4306e-02	7.2870e-03

5.4 Capture Configuration

Table 5-8: Admittance Model SRMS End-Effector Local Translational Mode Shapes for Configuration Capture.

Mode	Local Translational Mode Shapes		
	x	y	z
1	1.0457e+00	1.1821e-01	3.7313e-02
2	-8.6221e-02	9.8983e-01	-4.9139e-01
3	-3.9570e-01	-8.7571e-01	-7.2548e-01
4	7.4608e-02	-5.6126e-01	1.0088e+00
5	-2.7702e-01	1.1833e+00	1.4596e+00
6	6.9630e-02	1.3112e+00	-1.1290e+00
7	2.6454e-01	-4.6744e-01	-5.3198e-01
8	3.8442e-03	-6.5628e-01	6.0476e-01
9	3.2207e-01	-4.1126e-02	3.7721e-02
10	7.1887e-02	-4.2329e-01	1.7541e-01
11	-1.1254e-01	5.3657e-01	8.8733e-01
12	-8.1829e-02	-8.0135e-01	2.0782e-01
13	-1.8112e-01	2.4579e-01	-7.1454e-01
14	-7.8403e-02	-4.2742e-01	-2.1787e+00
15	-2.8422e-02	1.9032e+00	-1.2405e-01
16	-2.7189e-02	-1.6737e-01	1.1114e-01
17	-2.2170e-02	9.7629e-01	-4.0954e-01
18	2.1418e-01	4.6611e-01	1.0291e-01
19	2.4001e-02	-4.7390e-01	5.0206e-01
20	-1.5527e-01	-5.1684e-01	-2.5338e-01
21	3.8619e-02	5.6301e-01	-4.9570e-01
22	3.3530e-02	-3.0353e-01	-3.1735e-01
23	4.7552e-03	-2.5062e-01	7.8471e-02
24	4.7704e-02	-4.2944e-01	-6.6715e-01
25	-1.4542e-01	-8.1276e-02	3.4719e-01
26	-5.6670e-03	-4.1967e-01	-1.0650e-02
27	5.8276e-02	-1.2625e-01	-9.3003e-02
28	1.2043e-01	3.1970e-02	1.0031e-01
29	3.4947e-02	1.3786e-01	-1.6058e-01
30	-1.7098e-02	-2.3150e-01	6.6471e-02

Table 5-9: Admittance Model SRMS End-Effector Local Rotational Mode Shapes for Configuration Capture.

Mode	Local Rotational Mode Shapes		
	θ_x	θ_y	θ_z
1	1.9435e-04	-1.9908e-03	3.9894e-04
2	2.4836e-03	4.3590e-04	4.4973e-04
3	-7.2396e-04	5.3982e-03	-1.1529e-02
4	-3.6068e-03	-1.1324e-02	-1.0339e-02
5	-1.3378e-03	-3.0493e-02	2.6515e-02
6	-1.1583e-02	3.2972e-02	4.0630e-02
7	-1.3501e-03	2.1452e-02	-1.7658e-02
8	3.9700e-02	-2.9674e-02	-3.0782e-02
9	-3.2471e-03	-4.2550e-03	6.1139e-04
10	9.1107e-02	-1.1416e-02	-2.3816e-02
11	7.6265e-02	-5.2792e-02	2.9528e-02
12	-1.8159e-01	-1.1552e-02	-4.7797e-02
13	5.2670e-02	4.6435e-02	1.3536e-02
14	3.9737e-02	1.4292e-01	-2.8728e-02
15	-5.2890e-02	6.5851e-03	1.2080e-01
16	-3.2669e-02	-8.7055e-03	-1.2880e-02
17	-8.8366e-03	3.2284e-02	7.3393e-02
18	-5.6754e-03	-8.9544e-03	3.6587e-02
19	6.4304e-02	-4.2811e-02	-3.8263e-02
20	-5.1688e-03	2.2727e-02	-4.4118e-02
21	-1.9157e-02	4.5323e-02	4.9567e-02
22	-1.3836e-01	2.9432e-02	-2.7223e-02
23	-8.6922e-02	-7.4258e-03	-2.2804e-02
24	5.2889e-02	6.4579e-02	-4.0064e-02
25	-1.2666e-02	-3.4435e-02	-7.8764e-03
26	6.7096e-03	1.0935e-03	-4.1054e-02
27	-4.1528e-03	9.5163e-03	-1.2373e-02
28	-3.3694e-03	-1.0329e-02	3.2998e-03
29	1.6920e-03	1.6565e-02	1.3848e-02
30	6.9391e-03	-7.0231e-03	-2.3837e-02

VI. ADMITTANCE MODEL APPLICATION USING LOAD CELL SIMULATION

6.1 Introduction

This chapter presents an application of the admittance model by simulating the load cell output. The Load Cell Simulation (LCS) wrench will be referred to as the admittance wrench because it is the input to the admittance model, and is discussed in section 6.3. The LCS will be determined, in part, from two types of SRMS payloads, and are discussed in section 6.2. Section 6.4 provides results obtained from transient analyses conducted on the compound and admittance models. Finally, the SRMS end-effector residual motions from the admittance wrench are presented in section 6.5.

6.2 Compound Model

Section 6.2.1 provides a description of the two types of SRMS payloads analyzed in this study, and section 6.2.2 lists the system natural frequencies obtained from a normal modes analysis using MSC/NASTRAN.

6.2.1 Description

To evaluate SRMS end-effector response with different robotic manipulators attached to it, two types of rigid SRMS payloads are analyzed. The first is the DOSS manipulator, and the second is the DOSS manipulator carrying a 1000 lb. rigid,

C-2

homogeneous, right circular cylinder. The reason for adding the 1000 lb. DOSS payload was to explore the increase in the number of modes required in the admittance model to represent the SRMS end-effector motion. The DOSS manipulator is capable of maneuvering a 3000 lb. object in space, so the one used is well within its weight capacity. For the results presented in sections 6.4 and 6.5, the case of *no DOSS payload* refers to the DOSS arm itself as the SRMS payload. Similarly, the case of *with the 1000 lb. DOSS payload* refers to the DOSS arm with the 1000 lb. cylinder as the SRMS payload. For a description of the DOSS manipulator the reader is referred to Appendix E.

The DOSS arm is a seven degree-of-freedom, seven-link, redundant manipulator. It consists of shoulder roll, yaw, and pitch joints, an elbow pitch joint, and wrist pitch, yaw, and roll joints. Figure 6-1 shows the joint angular limits of the DOSS manipulator.

The configuration of the DOSS arm when attached to the end-effector of the SRMS is shown in Figures 6-2 and 6-3 without and with the 1000 lb. DOSS payload, respectively, and the configuration joint angles are listed in Table 6-1. This arbitrary configuration is representative of an operational configuration. The base coordinate frame of the DOSS in Figures 6-2 and 6-3 is initially parallel to the wrist roll frame of the SRMS (see Figure 2-5, or 2-6).

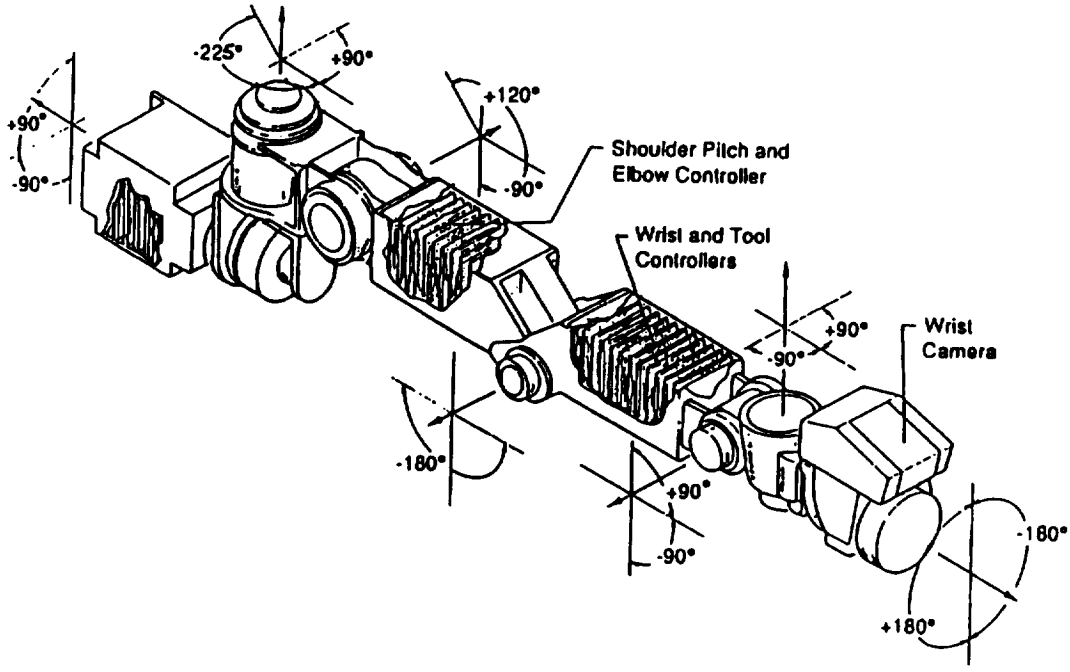

Figure 6-1: DOSS Manipulator Showing Joint Angular Limits.[26]

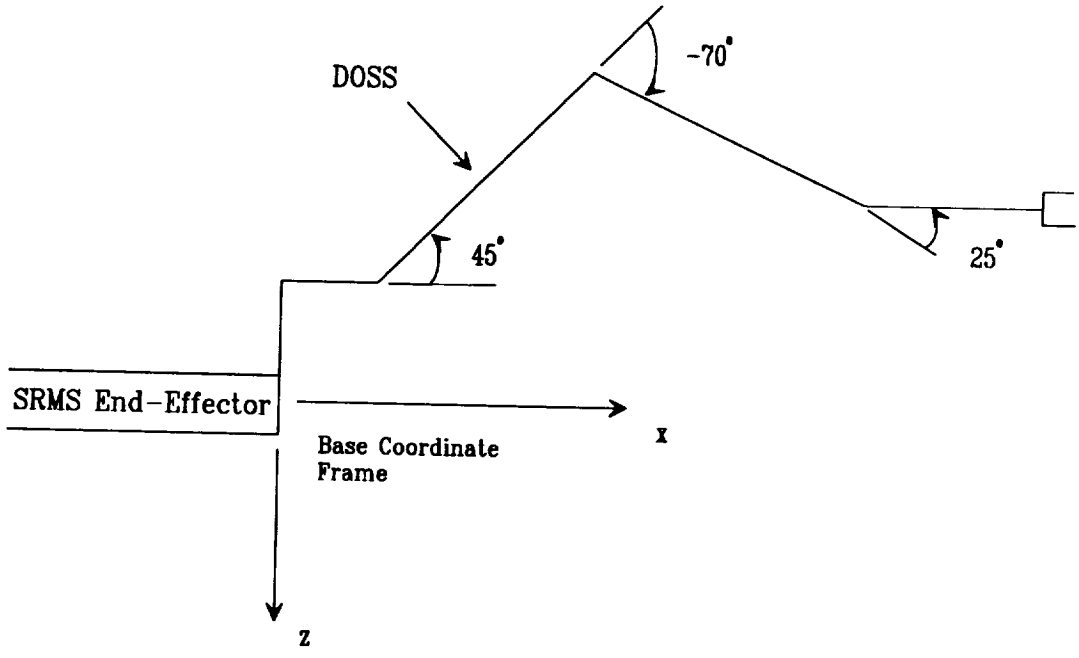

Figure 6-2: DOSS Manipulator Operational Configuration with No DOSS Payload.

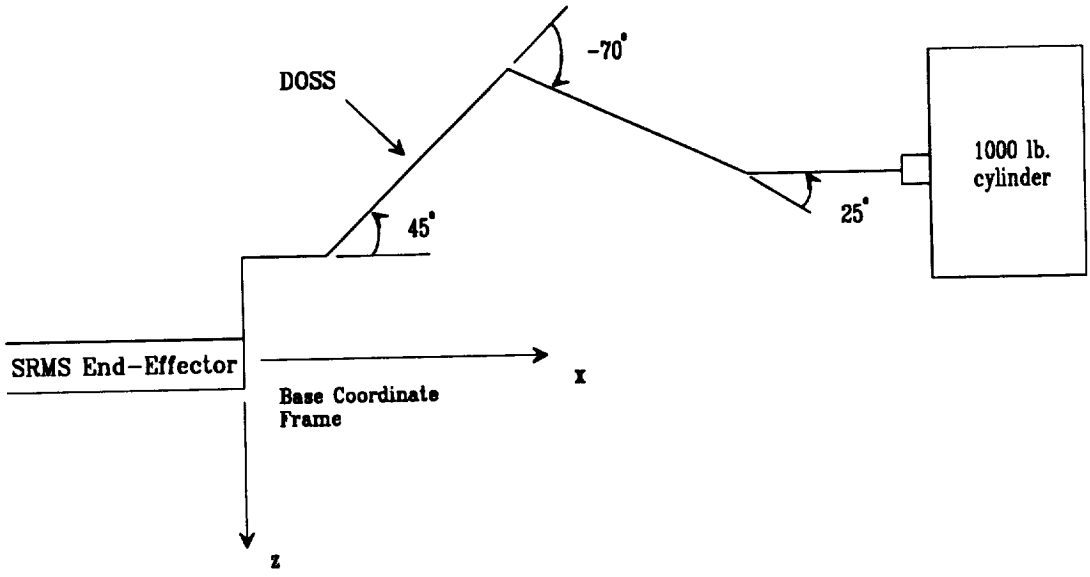

Figure 6-3: DOSS Manipulator Operational Configuration with the 1000 lb. Cylinder.

Table 6-1: Joint Angles of the DOSS Arm Operational Configuration shown in Figures 6-2 and 6-3.

Joint Angles (degrees)						
SHR	SHY	SHP	ELP	WRP	WRY	WRR
0.0	0.0	45.0	-70.0	25.0	0.0	0.0

Based on available data, the system center of mass location and mass moment of inertia about the center mass were calculated for the operational configurations shown in Figures 6-2 and 6-3. The inertias are based on the positive integral formulation (i.e.,

not the tensor form of the inertia), and the location of the system center of mass is measured from the origin of the base coordinate frame. The calculations for the mass moment of inertia were based on the following assumptions:

a. The upper and lower arm links are assumed to be rigid rectangular parallelopipeds with a cross-sectional size of 6 x 7 inches.

b. The connections between other joint actuators (excluding those in (a)) are assumed to be rigid, homogeneous, right circular cylinders with 6 inch diameters and uniformly distributed mass with the mass properties listed in Table E-1.

c. The presence of the mounting block (i.e., the first cubical-shaped segment of the DOSS manipulator on the left hand side in Figure 6-1) was not taken into account during the calculations of the mass moment of inertia. Hence the total mass of the arm (no payload) was calculated to be 196.05 lbs. (see Table E-1). The reason for this assumption was that no data were available concerning this piece of the DOSS arm.

d. The 1000 lb. payload is assumed to be a rigid, homogeneous, right circular cylinder of radius 18 inches and a height of 48 inches (assumed to be grappled by the DOSS end-effector at the midpoint height). With this payload, the total weight of the arm becomes 1196.05 lbs.

The location of the center of mass carrying no DOSS payload is

$$\left(\vec{r}_{cm}\right)_{no\ payload} = \left(31.39, 0.0360, -14.62\right) \quad inches$$

and the mass moment of inertia at the center of mass about axes initially parallel to the base coordinate frame is

$$\left[\left(I_{DOSS}\right)_{cm}\right]_{no\ payload} = \begin{bmatrix} 192.2 & 0.030 & -288.4 \\ 0.030 & 3025.1 & -0.152 \\ -288.4 & -0.152 & 2869.8 \end{bmatrix} \quad slug - inch^2$$

The location of the center of mass carrying the 1000 lb. DOSS payload is

$$\left(\vec{r}_{cm}\right)_{payload} = \left(72.06, 5.9x10^{-3}, -14.48\right) \quad inches$$

and the mass moment of inertia at the center of mass about axes initially parallel to the base coordinate frame is

$$\left[\left(I_{DOSS}\right)_{cm}\right]_{payload} = \begin{bmatrix} 8669.4 & 5.0x10^{-3} & -419.2 \\ 5.0x10^{-3} & 23571.7 & -0.025 \\ -419.2 & -0.025 & 20015.2 \end{bmatrix} \quad slug-inch^2$$

The mass moment of inertia about the shoulder yaw joint with no DOSS payload is

$$\left[\left(I_{DOSS}\right)_{yaw}\right]_{no\ payload} = \begin{bmatrix} 439.3 & 6.9 & -1505.8 \\ 6.9 & 9271.5 & -1.5 \\ -1505.8 & -1.5 & 8869.1 \end{bmatrix} \quad slug-inch^2$$

Likewise, for the shoulder pitch joint

$$\left[\left(I_{DOSS}\right)_{pitch}\right]_{no\ payload} = \begin{bmatrix} 439.3 & 4.9 & -1156.8 \\ 4.9 & 6323.7 & -1.5 \\ -1156.8 & -1.5 & 5922.1 \end{bmatrix} \quad slug-inch^2$$

The slew axes for the shoulder yaw and pitch joints are in the z and y directions at the joint, respectively. With the 1000 lb. DOSS payload, the shoulder yaw joint inertia is

$$\left[\left(I_{DOSS}\right)_{yaw}\right]_{payload} = \begin{bmatrix} 10111.1 & 15.8 & -17094.7 \\ 15.8 & 217892.1 & -1.4 \\ -17094.7 & -1.4 & 212893.9 \end{bmatrix} \quad slug-inch^2$$

Likewise, for the shoulder pitch joint

$$\left[(I_{DOSS})_{pitch}\right]_{payload} = \begin{bmatrix} 10111.1 & 13.8 & -15012.0 \\ 13.8 & 172716.1 & -1.4 \\ -15012.0 & -1.4 & 167723.1 \end{bmatrix} \quad slug-inch^2$$

These four DOSS joint mass moment of inertias are also based on the positive integral formulation.

The finite element model discussed in section 2.2 is modified to include the DOSS and DOSS plus 1000 lb. cylinder as SRMS payloads. Each of these two finite element models will be referred herein as the *compound model.* The motivation for using this compound model is given in section 6.3. This SRMS payload is included in the finite element model as a rigid body by specifying the mass and inertia at the center of mass (at a single grid point using the CONM2 element). The center of mass grid point is then rigidly attached to the SRMS end-effector using the RBE2 element. Compound finite element models were developed for each of the four brakes locked SRMS configurations.

6.2.2 Normal Modes Analysis

The first 30 system natural frequencies from a normal modes analysis on the compound finite element models without and with the 1000 lb. DOSS are presented in Tables 6-2 and 6-3, respectively. The first 30 SRMS end-effector compound model mode shapes are presented in Appendix F for both types of SRMS payloads in all four configurations. Comparing the admittance model natural frequencies listed in Chapter 5 to those of the compound, we see that, as expected, adding a payload to the SRMS results in lowering the natural frequencies. The heavier the payload, the lower the frequencies become.

Table 6-2: Compound Model Natural Frequencies for the Four SRMS Configurations with no DOSS Payload.

Mode	Natural Frequency (Hz) (No DOSS Payload)			
	Unberth	Low Hover	Deploy	Capture
1	0.4687	0.4034	0.3832	0.2753
2	0.6055	0.5625	0.4223	0.3675
3	0.9275	1.0350	0.9814	1.4232
4	1.1271	1.1777	1.4778	1.7187
5	3.0835	2.8324	3.4918	3.6355
6	3.2761	3.0094	3.6114	3.9643
7	11.3466	11.7747	12.3463	11.3829
8	11.5741	12.6114	12.9052	13.0335
9	15.7575	16.2922	13.4578	15.7347
10	17.8536	17.5598	16.7893	17.5140
11	19.2348	18.9759	20.2079	18.8841
12	21.6411	20.7563	21.5748	21.9894
13	26.1289	25.7949	29.0374	27.7041
14	29.4296	28.3341	30.5155	29.6279
15	33.5305	32.9541	38.3522	32.9880
16	47.5552	47.6595	43.1819	46.8579
17	53.0600	55.0814	54.3439	49.4826
18	58.8446	59.8732	58.1132	56.2832
19	60.8465	62.2742	63.7356	62.5215
20	67.4150	70.3644	64.7843	69.3558
21	71.4322	72.5465	75.0927	75.9336
22	78.9142	78.1499	77.8888	76.5196
23	82.8382	82.3949	89.3720	88.0262
24	92.4441	91.5158	89.9529	90.4305
25	100.8791	101.6226	104.1891	105.9611
26	112.6119	112.6036	109.7062	112.2919
27	118.7229	119.1556	121.2892	119.4651
28	125.0537	125.5411	122.8167	124.2297
29	128.6209	130.6451	131.4052	128.8197
30	146.3752	142.7389	150.9998	142.4955

Table 6-3: Compound Model Natural Frequencies for the Four SRMS Configurations with the 1000 lb. DOSS Payload.

Mode	Natural Frequency (Hz) (1000 lb. DOSS Payload)			
	Unberth	Low Hover	Deploy	Capture
1	0.2269	0.2267	0.1988	0.1581
2	0.2875	0.3265	0.2016	0.1914
3	0.5664	0.4402	0.4842	0.4821
4	0.7948	0.7379	1.1424	0.9889
5	1.9000	1.8267	2.1888	2.9233
6	2.0508	2.0276	2.4006	3.1867
7	4.0082	4.3612	3.7196	4.4194
8	9.7386	10.2012	11.4872	9.4616
9	10.9141	11.2355	11.7907	11.8402
10	15.8804	15.7673	13.3422	14.9942
11	18.6068	17.0636	19.8023	18.5115
12	20.4962	20.2146	21.0660	19.7182
13	25.2589	24.4108	27.0812	26.7760
14	28.1686	27.5478	29.4489	28.7788
15	32.6951	32.6703	38.2093	32.8569
16	47.2882	47.5381	42.6062	46.7127
17	52.2044	54.6020	53.2171	48.8490
18	58.2539	59.1044	55.7805	55.8894
19	60.6282	61.7875	61.4297	60.8942
20	65.6588	69.4959	64.1898	68.6699
21	69.0896	71.0229	74.3411	73.9300
22	77.8930	75.8904	76.9363	75.4809
23	81.9665	81.8138	85.9376	86.4861
24	90.7021	90.2612	89.5670	90.0591
25	100.8177	101.5715	103.3409	105.5228
26	112.3749	112.2413	109.5237	112.0018
27	117.9952	118.7363	117.1007	119.3875
28	124.3466	125.3178	122.6365	124.0178
29	128.3014	130.4401	131.3966	128.7018
30	146.2457	142.6067	150.9077	142.3352

6.3 Load Cell Simulation (LCS)

This section describes the procedure to calculate the admittance wrench. The calculation of this wrench is a two-step process, and is known as the Load Cell Simulation (LCS). The first step is to obtain the compound wrench, section 6.3.1, and the second step is to calculate the feedback wrench, section 6.3.2. Before developing the compound and feedback wrenches, the LCS is discussed in more detail.

There are seven computational steps to the LCS:

1. Develop a finite element model of the SRMS, with a robotic manipulator as a rigid payload. The manipulator's mass and inertia properties are included in the finite element model. For this study, the DOSS manipulator will be used in the configuration shown in Figures 6-2 and 6-3, unloaded and carrying a 1000 lb. cylinder, respectively. This will represent the *compound model.*

2. Based on a hypothetical manipulator motion, calculate the wrench generated at the manipulator's base by assuming that the SRMS end-effector is fixed throughout the maneuver. The reaction wrench, the negative of the wrench generated at the base, will be referred to as the *compound wrench.*

3. Apply the compound wrench to the compound model, and obtain the translational and rotational accelerations of the SRMS end-effector.

4. Using rigid body kinematic equations and accelerations of the SRMS end-effector (from item 3), calculate the translational and rotational accelerations of the manipulator center of mass.

5. Using the accelerations of the manipulator center of mass (from item 4), apply the Newton-Euler equations at the manipulator center of mass and obtain the wrench required to cause the same manipulator center of mass motions as in item 4.

6. Because of the rigid body assumption, the wrench calculated at the center of mass in item 5 can be moved to the base, bearing in mind to modify the moment terms by adding the cross product of the distance from the center of mass to the manipulator base and the force. The negative of this wrench will be referred to as the *feedback wrench.*

7. The summation of the compound (from item 2) and feedback (from item 6) wrenches will be called the *admittance wrench.* The admittance wrench will now be the input to the admittance model.

In a hardware simulation of the Stewart Platform, the wrench measured by the load cell should be identical to the one obtained from the LCS (except for the non-linear terms to be discussed later). Also, the response of the SRMS end-effector from the admittance model should be identical to the compound model response. Any differences will be attributed to model reduction in one or both models.

6.3.1 Input Wrench to Compound Model

This section presents step 2 of the LCS. Initially, this study analyzed three types of DOSS slewing maneuvers: rotating the shoulder roll, yaw, and pitch joints 30° in 5 and 10 seconds, respectively. Only one of these joints was slewed at any given time (i.e., no coordinated moves of the DOSS arm were analyzed). It was found that the maneuvers pertaining to the shoulder yaw and pitch joints produced the largest SRMS end-effector residual motions, and therefore, only these two particular joints will be analyzed further.

Two basic assumptions were made in calculating the compound wrench. First, the DOSS is assumed to be a rigid manipulator, and second, the SRMS end-effector is assumed to be fixed throughout the slew maneuver. In the compound finite element model, the DOSS is not moving, but is fixed in the configuration shown in section 6.2.1. Hence the reason why the compound wrench is hypothetical.

The general angular equations of motion of a rigid body in vector form are given as

$$\vec{M} = \dot{\vec{h}}_{xyz} + \vec{\omega} \times \vec{h} \tag{6-1}$$

where $\vec{M}$ denotes the externally applied moment vector, $\vec{\omega}$ is the angular velocity vector, and $\vec{h}$ is the angular momentum vector. Since only one joint of the DOSS arm is slewed at any given time, only one term of the angular velocity vector is non-zero; ω_z and ω_y for the shoulder yaw and pitch joints, respectively. Therefore, for the shoulder yaw joint, the moment equations are

$$\begin{aligned} M_x &= -I_{xz}\dot{\omega}_z + I_{yz}\omega_z^2 \\ M_y &= -I_{yz}\dot{\omega}_z - I_{xz}\omega_z^2 \\ M_z &= I_{zz}\dot{\omega}_z \end{aligned} \tag{6-2}$$

Likewise, for the shoulder pitch joint

$$\begin{aligned} M_x &= -I_{xy}\dot{\omega}_y - I_{yz}\omega_y^2 \\ M_y &= I_{yy}\dot{\omega}_y \\ M_z &= -I_{yz}\dot{\omega}_y + I_{xy}\omega_y^2 \end{aligned} \tag{6-3}$$

These are the moments generated at the joint of interest from the hypothetical slew maneuver. The inertias are in tensor form (i.e., negative signs are added to the products of inertia, or off-diagonal terms of the inertia matrix). The values for these inertias were provided in section 6.2.1.

The form of the torque profile, in the primary drive axis of the joint, was assumed to be rectangular and is shown in Figure 6-4. The variables a and b, shown in the figure, indicate the time of constant torque application, and drift, or coast time (i.e., joint produces no torque during this time), respectively.

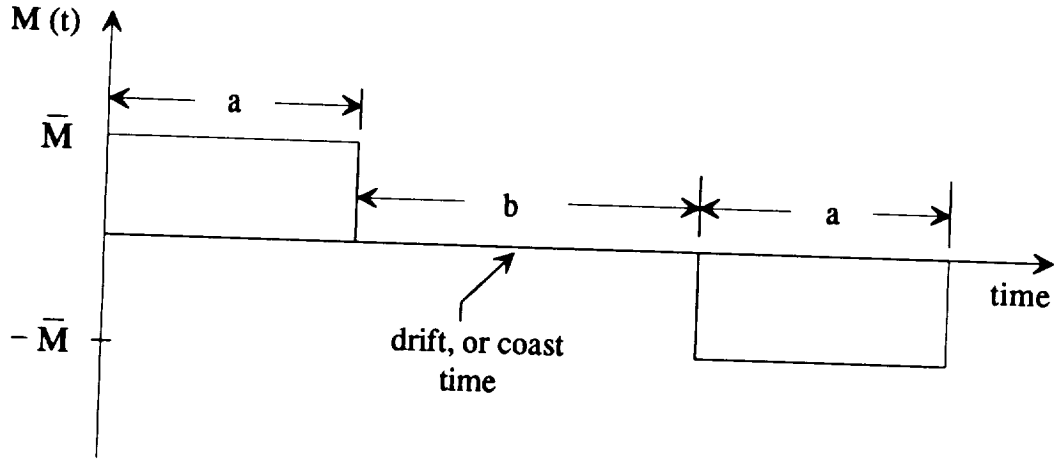

Figure 6-4: Drive Axis Joint Torque Profile used in the DOSS Shoulder Yaw and Pitch Slew Maneuvers.

The inertial forces are computed from Newton's Law. Consider the general situation of Figure 6-5 in which the motion of point p is to be described with respect to the moving xyz reference frame. The XYZ is assumed to be inertial where

$\vec{R}_o$ is the position vector of the origin of the moving xyz frame,

$\vec{r}$ is the position vector of point p expressed in the moving xyz frame, and

$\vec{R}$ is the position vector of point p expressed in the inertial XYZ frame.

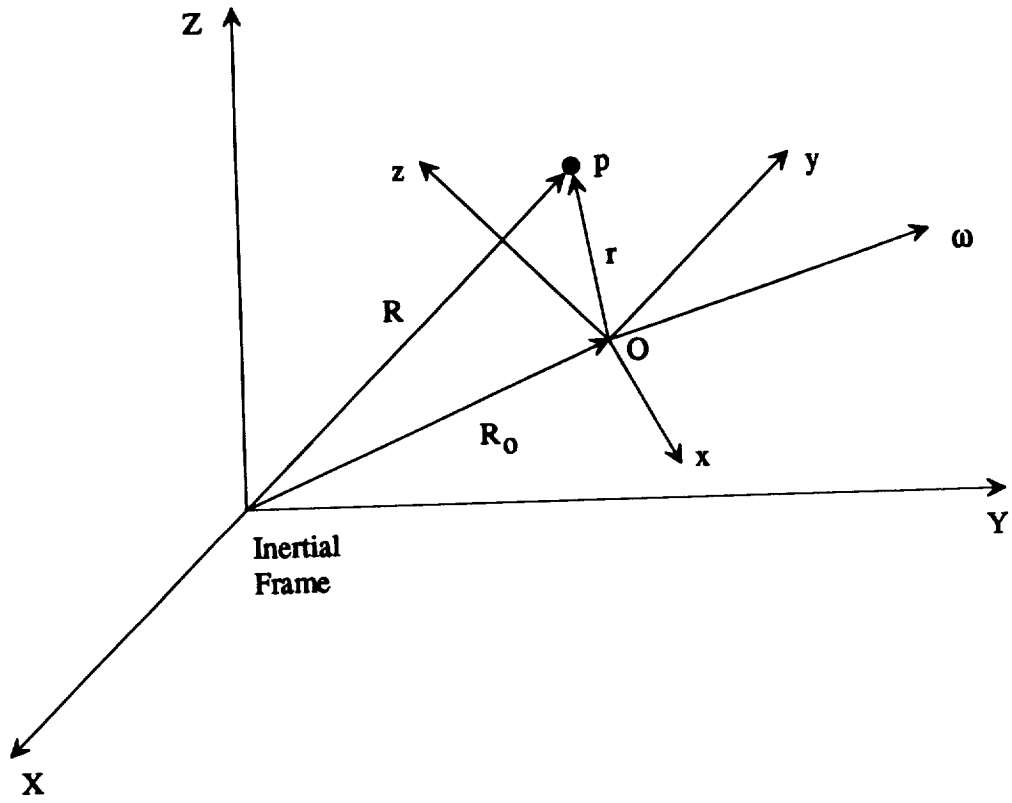

Figure 6-5: Point p given with respect to a Moving xyz Frame and an Inertial XYZ Frame.

The inertial forces are computed from Newton's Second Law

$$\vec{F} = m\left(\ddot{\vec{R}}_o + \ddot{\vec{r}} + 2\,\vec{\omega} \times \dot{\vec{r}} + \dot{\vec{\omega}} \times \vec{r} + \vec{\omega} \times \vec{\omega} \times \vec{r} \right) \tag{6-4}$$

where each term on the right-hand side can be identified on a physical basis

$\ddot{\vec{R}}_o$ is the acceleration of the origin of the moving frame,

$\ddot{\vec{r}}$ is the acceleration of point p in the moving frame,

$2\vec{\omega} x \dot{\vec{r}}$ is the Coriolis acceleration due to motion in the moving frame,

$\dot{\vec{\omega}} x \vec{r}$ is the acceleration because $\vec{\omega}$ is changing (Euler acceleration),

$\vec{\omega} x \vec{\omega} x \vec{r}$ is the centrifugal acceleration due to the angle between $\vec{\omega}$ and $\vec{r}$.

Point p is chosen to be the center of mass of the SRMS payload, and the $\vec{\omega}$ vector represents the angular velocity of the center of mass. The position vector $\vec{r}$ corresponds to the distance from the joint of interest to the center of mass of the payload and is provided in Table 6-4. Since the end-effector of the SRMS is assumed to be fixed, it will represent the inertial frame. The origin of the moving frame is not accelerating with respect to the inertial frame, therefore, $\ddot{\vec{R}}_o = \vec{0}$. The center of mass in the moving frame does not have a velocity, nor is it accelerating, therefore, $\dot{\vec{r}} = \ddot{\vec{r}} = \vec{0}$. Thus, equation (6-4) simplifies to:

$$\vec{F} = m\left(\dot{\vec{\omega}} x \vec{r} + \vec{\omega} x \vec{\omega} x \vec{r}\right) \qquad (6\text{-}5)$$

Table 6-4: Values of the Position Vector $\vec{r}$ used in Calculating the Inertial Forces in Equation (6-5).

	Joint	$\vec{r}$ (x,y,z) inches
No DOSS payload	Shoulder Yaw	(31.39 , 0.036 , -6.37)
	Shoulder Pitch	(22.39 , 0.036 , -6.37)
1000 lb. DOSS payload	Shoulder Yaw	(72.06 , 5.9×10^{-3} , -6.23)
	Shoulder Pitch	(63.06 , 5.9×10^{-3} , -6.23)

By assuming the form of the torque profile (M_z and M_y for the shoulder yaw and pitch joints, respectively), the angular acceleration about the drive axis of the joint of interest can be determined from the last equation of (6-2), or the middle equation of (6-3) for the shoulder yaw and pitch joints, respectively. Performing a double integration on the torque profile given in Figure 6-4, and combining terms, results in an equation that determines the value for $\bar{M}$

$$\bar{M} = \frac{\theta\, I_o}{12\left(a^2 + a\,b\right)} \tag{6-6}$$

where θ is the desired angular displacement, and I_o is the inertia about the joint slew axis. Table 6-5(a) provides a listing of the mass moment of inertia about the slew axis of the shoulder roll, yaw, and pitch joints of the DOSS. Performing 30° slew maneuvers in 5 and 10 seconds, the required joint torque $\bar{M}$ can be obtained from equation (6-6) and is tabulated in Table 6-5(b) together with the maximum flight arm joint torque. The

value for a was taken to be 1.5 seconds for both slewing times, and the value for b was 2.0 and 7.0 seconds, for the 5 and 10 second slew times, respectively. As expected, performing the slew maneuver more slowly requires less joint torque (approximately two and one half times less for all the torques).

Table 6-5(a): Shoulder Joint Slew Axis Mass Moment of Inertia.

	Joint	Slew Axis Mass Moment of Inertia (slug - in^2)
No DOSS payload	Shoulder Roll	1493.6
	Shoulder Yaw	8869.1
	Shoulder Pitch	6323.7
1000 lb. DOSS payload	Shoulder Roll	16457.5
	Shoulder Yaw	212893.9
	Shoulder Pitch	172716.1

Table 6-5(b): Primary Joint Drive Axis Torque $(\bar{M})$ for both Slew Maneuvers and Durations.

	Joint	Maximum Joint Torque (lb - in)	$\bar{M}$ (lb - in) 30°	
			5 sec.	10 sec.
No DOSS payload	Shoulder Roll	1416	12.4	5.1
	Shoulder Yaw		73.7	30.4
	Shoulder Pitch		52.6	21.6
1000 lb. DOSS payload	Shoulder Roll		136.8	56.3
	Shoulder Yaw		1769.4	728.6
	Shoulder Pitch		1435.5	591.1

Comparing the maximum joint torque that each actuator can provide and the joint torque required to produce the maneuver, we see that slewing the shoulder yaw and pitch joints 30° in 5 seconds for the 1000 lb. payload exceeds the capabilities of the joints (a maximum of 1416 lb-in compared to 1769.4 and 1435.5 lb-in, respectively). Therefore, two of the slewing scenarios with the 1000 lb. payload are not physically realizable, but nevertheless will be included in the results. Slewing the 1000 lb. payload in 10 seconds produces no torque violations. Also, notice that slewing the shoulder yaw joint requires the greatest torque and slewing the shoulder roll joint requires the least. This is expected since the yaw axis has more inertia to slew, whereas the roll axis has the least.

Equation (6-2) for the shoulder yaw, or (6-3) for the shoulder pitch joint, $\left(\vec{M}_{joint}\right)$, together with equation (6-5), $\left(\vec{F}_{joint}\right)$, represent the wrench generated from the hypothetical DOSS slew maneuver. The subscript *joint* indicates where the load is generated (i.e., at the joint). The wrench at the DOSS base is then given by

$$\vec{W}_{base} = \begin{Bmatrix} \vec{F}_{base} \\ \vec{M}_{base} \end{Bmatrix} = \begin{Bmatrix} \vec{F}_{joint} \\ \vec{M}_{joint} + \vec{r}^{\bullet} \times \vec{F}_{joint} \end{Bmatrix} \tag{6-7}$$

where $\vec{r}^{\bullet}$ is the position vector from DOSS base to the joint of interest and is tabulated in Table 6-6.

Table 6-6: Values of the Position Vector $\vec{r}^{\bullet}$ used in Equation (6-7).

Joint	$\vec{r}^{\bullet}$ (x,y,z) inches
Shoulder Roll	(0.0 , 0.0 , 0.0)
Shoulder Yaw	(0.0 , 0.0 , -8.25)
Shoulder Pitch	(9.0 , 0.0 , -8.25)

The compound wrench is the negative of equation (6-7). The compound wrench for the DOSS shoulder yaw joint is

$$\left(\vec{W}_{compound}\right)_{yaw} = \begin{bmatrix} -\vec{F}_{base} \\ -8.25F_y + I_{xz}\dot{\omega}_z - I_{yz}\omega_z^2 \\ 8.25F_x + I_{yz}\dot{\omega}_z + I_{xz}\omega_z^2 \\ -I_{zz}\dot{\omega}_z \end{bmatrix} \tag{6-8}$$

and, likewise, for the DOSS shoulder pitch joint

$$\left(\vec{W}_{compound}\right)_{pitch} = \begin{bmatrix} -\vec{F}_{base} \\ I_{xy}\dot{\omega}_y + I_{yz}\omega_y^2 \\ 8.25F_x + 9.0F_z - I_{yy}\dot{\omega}_y \\ I_{yz}\dot{\omega}_y - I_{xy}\omega_y^2 \end{bmatrix} \tag{6-9}$$

where $\vec{F}_{base} = \{F_x \;\; F_y \;\; F_z\}^T$, and ^{T} denotes transpose. Performing the algebra on equation (6-5), the component of force in the z and y directions at the base of the DOSS

manipulator for the shoulder yaw and pitch joints, respectively, is zero. This completes the discussion of item 2 of the LCS.

6.3.2 Input Wrench to Admittance Model

Next items 3 through 7 of the LCS will be calculated. The SRMS end-effector translational and rotational accelerations are obtained from the transient analysis of the compound model using the compound wrench. The accelerations of the DOSS center of mass can be obtained from the following equation because of the rigid body assumption

$$\ddot{\vec{y}}_{c.m.} = \ddot{\vec{y}}_{E.E.} + \dot{\vec{\omega}}_{c.m.} x \ \vec{r}_{c.m.} + \vec{\omega}_{c.m.} x \ \vec{\omega}_{c.m.} x \ \vec{r}_{c.m.} \qquad (6\text{-}10)$$

where the first term on the right hand side represents the translational acceleration of the SRMS end-effector, and the other two terms are the relative motion of the DOSS center of mass with respect to the SRMS end-effector. Equation (6-10) is identical to the acceleration of equation (6-4) dropping the relative and Coriolis terms. Since the DOSS manipulator is assumed to be rigid, the angular position, velocity, and acceleration of the DOSS center of mass are identical to those of the SRMS end-effector. The values of $\vec{r}_{c.m.}$ describe the location of the DOSS center of mass from the base coordinate frame given in Figures 6-2 and 6-3, and were provided in section 6.2.1. However, since NASTRAN is performing a linear analysis, any nonlinear term (e.g., centrifugal terms) that appear in equation (6-10) must be excluded, otherwise, inconsistent analyses will be made. Hence,

eliminating the last term on the right hand side of equation (6-10) reduces to

$$\ddot{\vec{y}}_{c.m.} = \ddot{\vec{y}}_{E.E.} + \dot{\vec{\omega}}_{c.m.} x \vec{r}_{c.m.} \tag{6-11}$$

Now that the full motion of the DOSS center of mass is known (equation (6-11), $\dot{\vec{\omega}}_{c.m.}$ and $\vec{\omega}_{c.m.}$) the feedback wrench can be calculated. The force generated at the DOSS center of mass can be obtained by multiplying equation (6-11) by its mass

$$\vec{F}_{c.m.} = m_{DOSS} \ddot{\vec{y}}_{c.m.} \tag{6-12}$$

The moments at the DOSS center of mass can be calculated from equation (6-1). Eliminating the second term on the right hand side of equation (6-1) because of the linear assumption in NASTRAN, and combining the moment with the force given by equation (6-12) produces the wrench at the center of mass

$$\vec{W}_{c.m.} = \begin{Bmatrix} \vec{F}_{c.m.} \\ \vec{M}_{c.m.} \end{Bmatrix} = \begin{Bmatrix} m_{DOSS}\left(\ddot{\vec{y}}_{E.E.} + \dot{\vec{\omega}}_{c.m.} x \vec{r}_{c.m.}\right) \\ I_{c.m.} \dot{\vec{\omega}}_{c.m.} \end{Bmatrix} \tag{6-13}$$

where $I_{c.m.}$ is the mass moment of inertia tensor about the SRMS payload center of mass,

given in section 6.2.1. The feedback wrench, $\vec{W}_{feedback}$, is the negative of equation (6-13), first accounting for the moment due to moving the force to the DOSS base.

$$\vec{W}_{feedback} = \begin{Bmatrix} -\vec{F}_{c.m.} \\ -\vec{M}_{c.m.} \end{Bmatrix} = \begin{Bmatrix} -m_{DOSS}\left(\ddot{\vec{y}}_{E.E.} + \dot{\vec{\omega}}_{c.m.} x \vec{r}_{c.m.}\right) \\ -I_{c.m.}\dot{\vec{\omega}}_{c.m.} - \vec{r}_{c.m.} x \vec{F}_{c.m.} \end{Bmatrix} \quad (6\text{-}14)$$

Adding the compound wrench from equation (6-8), or (6-9), $\vec{W}_{compound}$, with the feedback wrench, $\vec{W}_{feedback}$, from equation (6-14), results in the admittance wrench that is applied to the admittance model of the SRMS

$$\vec{W}_{admittance} = \vec{W}_{compound} + \vec{W}_{feedback} \quad (6\text{-}14)$$

6.4 Dynamic Fidelity vs. Admittance Model Order

The transient analyses conducted on the compound and admittance models was performed using MATLAB, a matrix manipulation package. MATLAB has a built in function routine called *lsim*. The zero-order hold option of lsim solved equation (3-5). Zero-order hold means that the force is held constant over the sampling interval. For the present analysis, no damping of the SRMS is considered in either the compound, or admittance models; therefore the second term on the left hand side of equation (3-4) is zero. The simulations were performed for 30 seconds using a sampling interval of 0.001 seconds.

For verification, the admittance model simulations will be compared to the compound model simulations. The simulations of the compound model will represent the *exact* response of the SRMS end-effector, and all error comparisons will be made with this model. Prior to the comparisons, the number of compound modes required to accurately simulate the SRMS end-effector response must be determined. Comparison of 10 and 20 compound modes of the compound model resulted in a maximum displacement Root Sum Square (RSS) error of $2.2 x 10^{-6}$ inches and $1.4 x 10^{-5}$ degrees for the Capture configuration, DOSS shoulder pitch 30° in 5 seconds, with no DOSS payload. Performing the same error analysis with the 1000 lb. DOSS payload, results in RSS errors of $3.5 x 10^{-5}$ inches and $2.8 x 10^{-5}$ degrees. Thus a 20 mode compound model is expected to have even smaller errors. Therefore, for the present analysis, the compound model using 20 compound modes will represent the *exact* response, which will be used to compare with the admittance responses.

The response from the compound model (using the compound wrench), and the admittance model (using the admittance wrench) is shown as a function of the number of modes in the admittance model. Figures 6-6 (a) through (f) show the 20 mode compound model response (solid line) compared to 1 (dotted), 3 (dash-dot), and 5 (dashed) modes of the admittance model. The response presented is for the SRMS in the Capture configuration with no DOSS payload, and the shoulder pitch is rotating 30° in 5 seconds. Figures 6-6 (a) through (c) show the x, y, and z translations of the SRMS end-effector, respectively, and Figures 6-6 (d) through (f) show the θ_x , θ_y , and , θ_z

rotations, respectively. All translations and rotations are reported in inches and degrees, respectively. As expected, increasing the number of admittance modes better approximates the compound response. Admittance modes 3 and 5 in Figures 6-6 (a) through (d) are barely noticeable because they are superimposed onto the exact response; it is not until Figures 6-6 (e) and (f) that these modes become noticeable. The curves shown in Figure 6-7 represent the input wrenches to the compound and admittance models for the above case. The compound wrench is represented by the solid curve, and the admittance wrench by the dashed curve. The forces and moments are reported in pounds and lb-in, respectively.

Figures 6-8 (a) through (f) provide the same information as Figures 6-6 (a) through (f) with the same legend, except now the DOSS is slewing the 1000 lb. cylinder. A similar trend is seen, however, more admittance modes need to be included because of the larger payload. Using one admittance mode for the no DOSS payload case resulted in a maximum displacement difference of 0.24", and with the 1000 lb. payload resulted in approximately 4". By the fifth admittance mode, the maximum displacement difference reduced to 0.005" for no DOSS payload, and with the 1000 DOSS lb. payload to approximately 0.2". Figure 6-9 show the compound (solid) and admittance (dashed) wrenches for the aforementioned maneuver with the 1000 lb. DOSS payload. As expected, the wrench with the 1000 lb. DOSS payload is much greater than without it. Similar comparisons hold for the other three configurations, regardless of SRMS payload, type and duration of slewing maneuver.

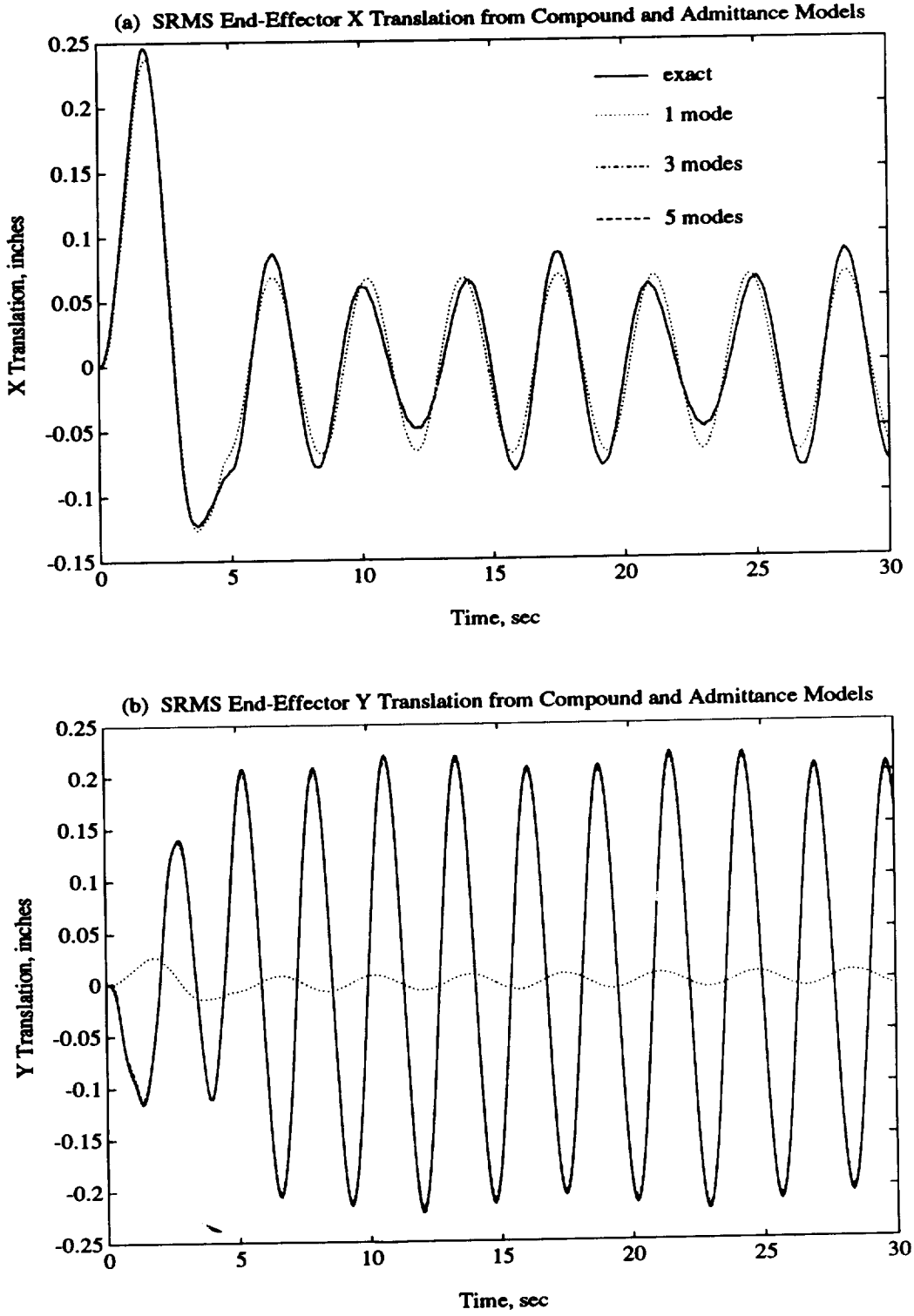

Figure 6-6: Capture Configuration, Shoulder Pitch 30° in 5 seconds, No DOSS Payload, SRMS End-Effector (a) X Translation (b) Y Translation.

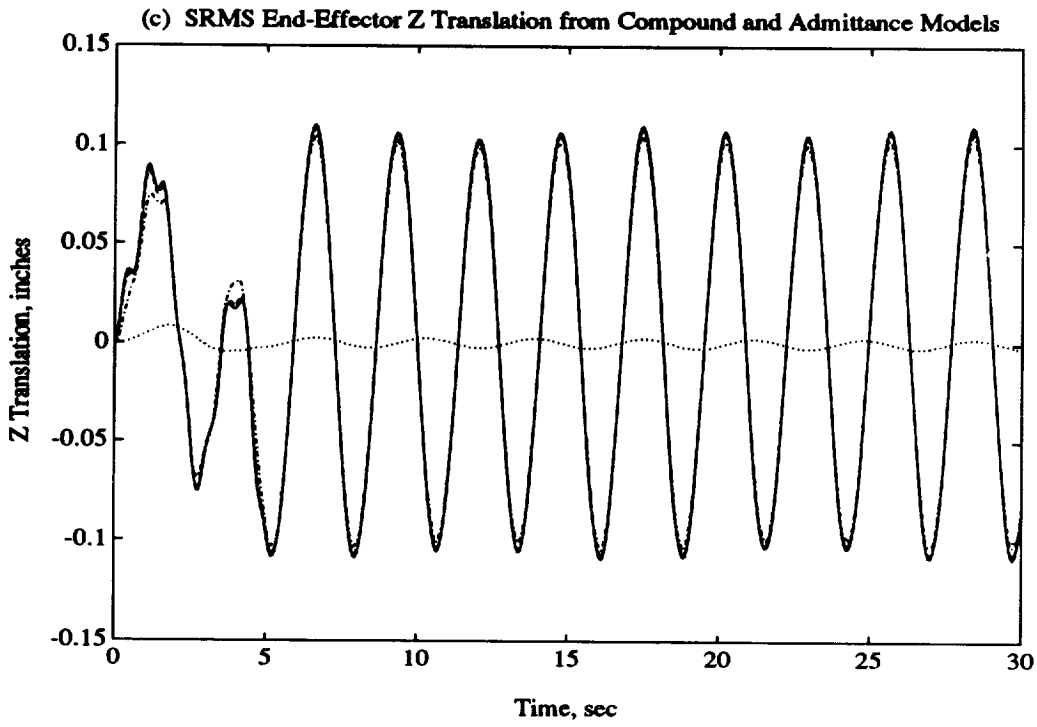

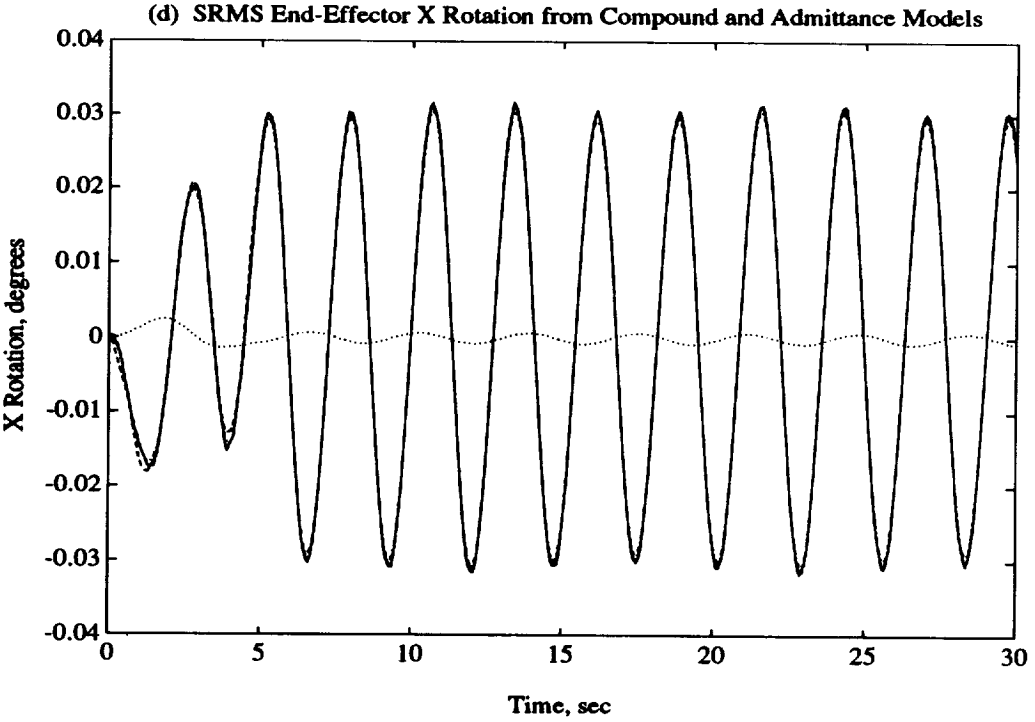

Figure 6-6: Capture Configuration, Shoulder Pitch 30° in 5 seconds, No DOSS Payload, SRMS End-Effector (c) Z Translation, and (d) X Rotation.

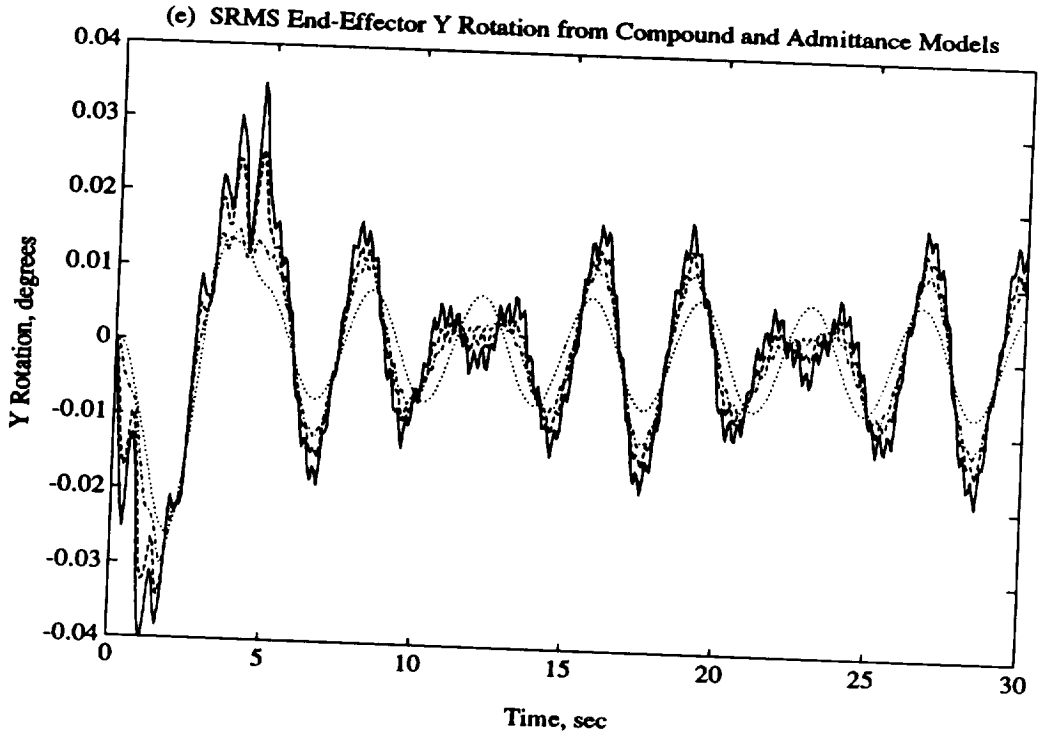

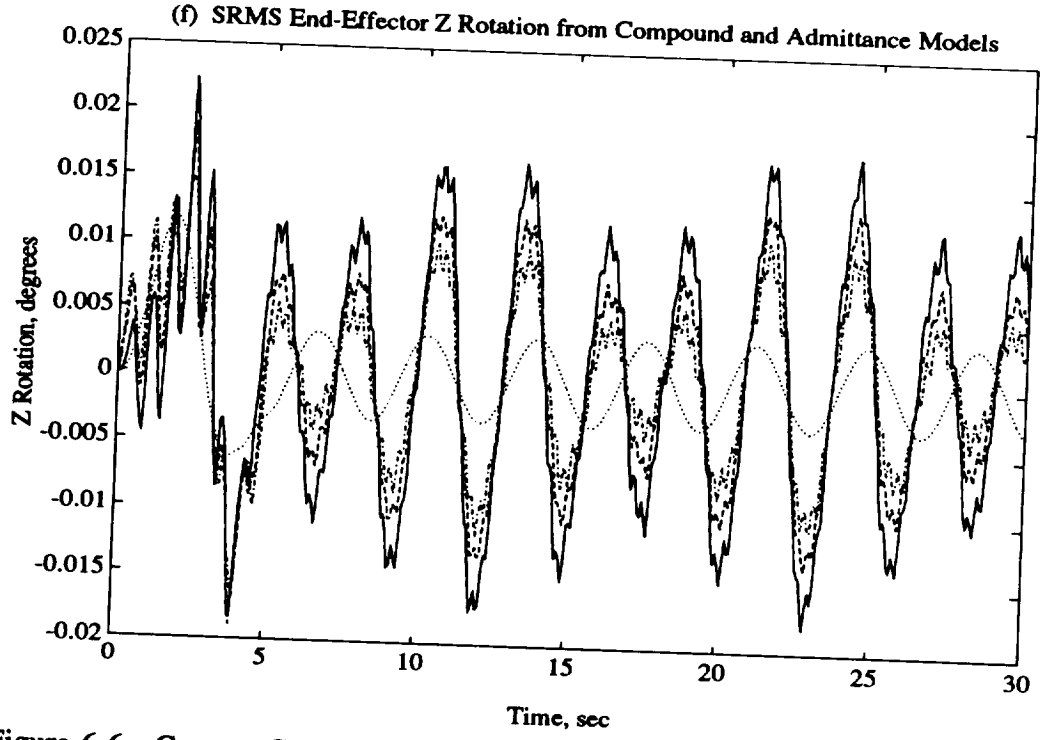

Figure 6-6: Capture Configuration, Shoulder Pitch 30° in 5 seconds, No DOSS Payload, SRMS End-Effector (e) Y Rotation, and (f) Z Rotation.

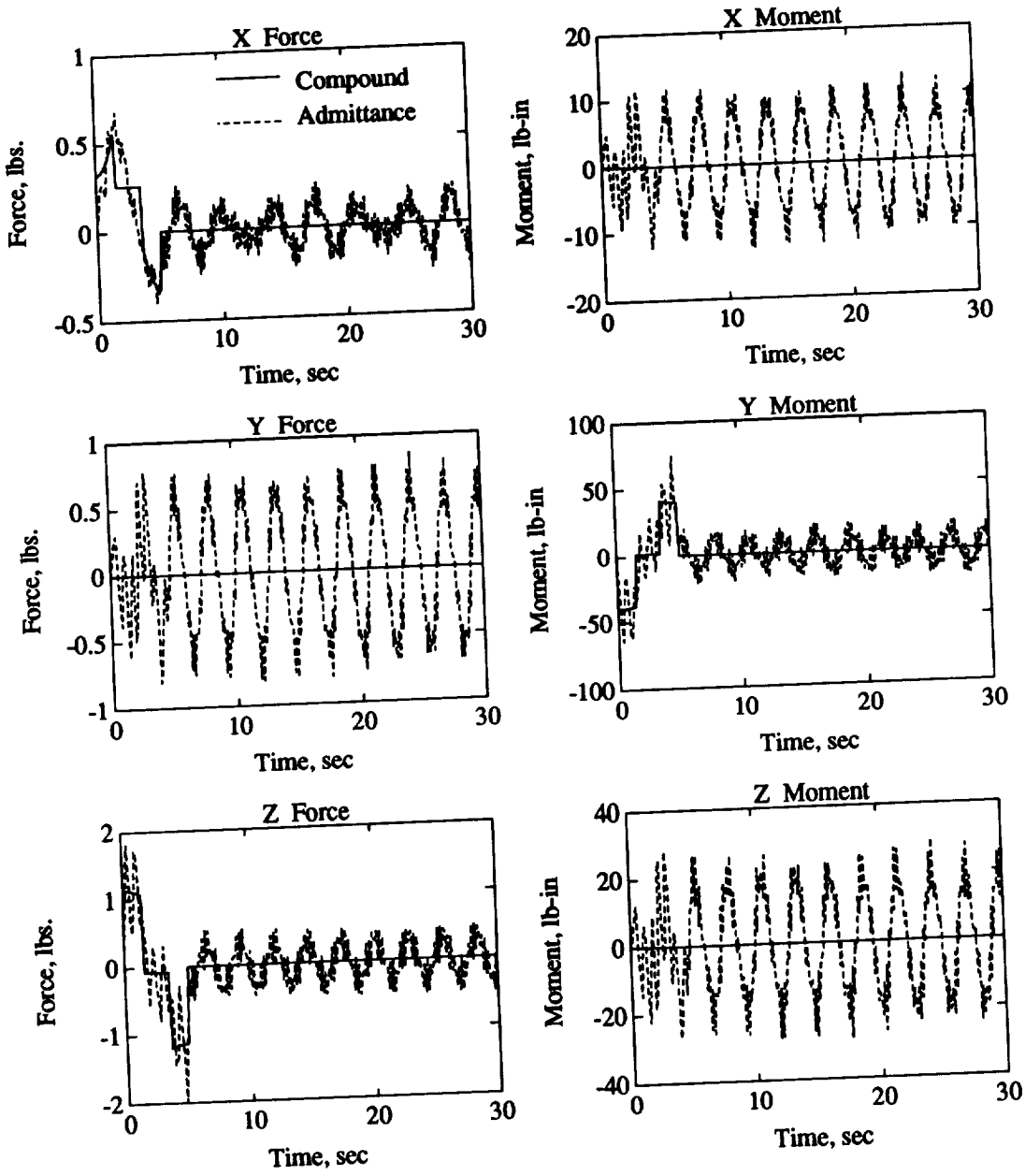

Figure 6-7: Capture Configuration, Shoulder Pitch 30° in 5 seconds, No DOSS Payload, Compound (solid) vs. Admittance (dashed) Wrenches.

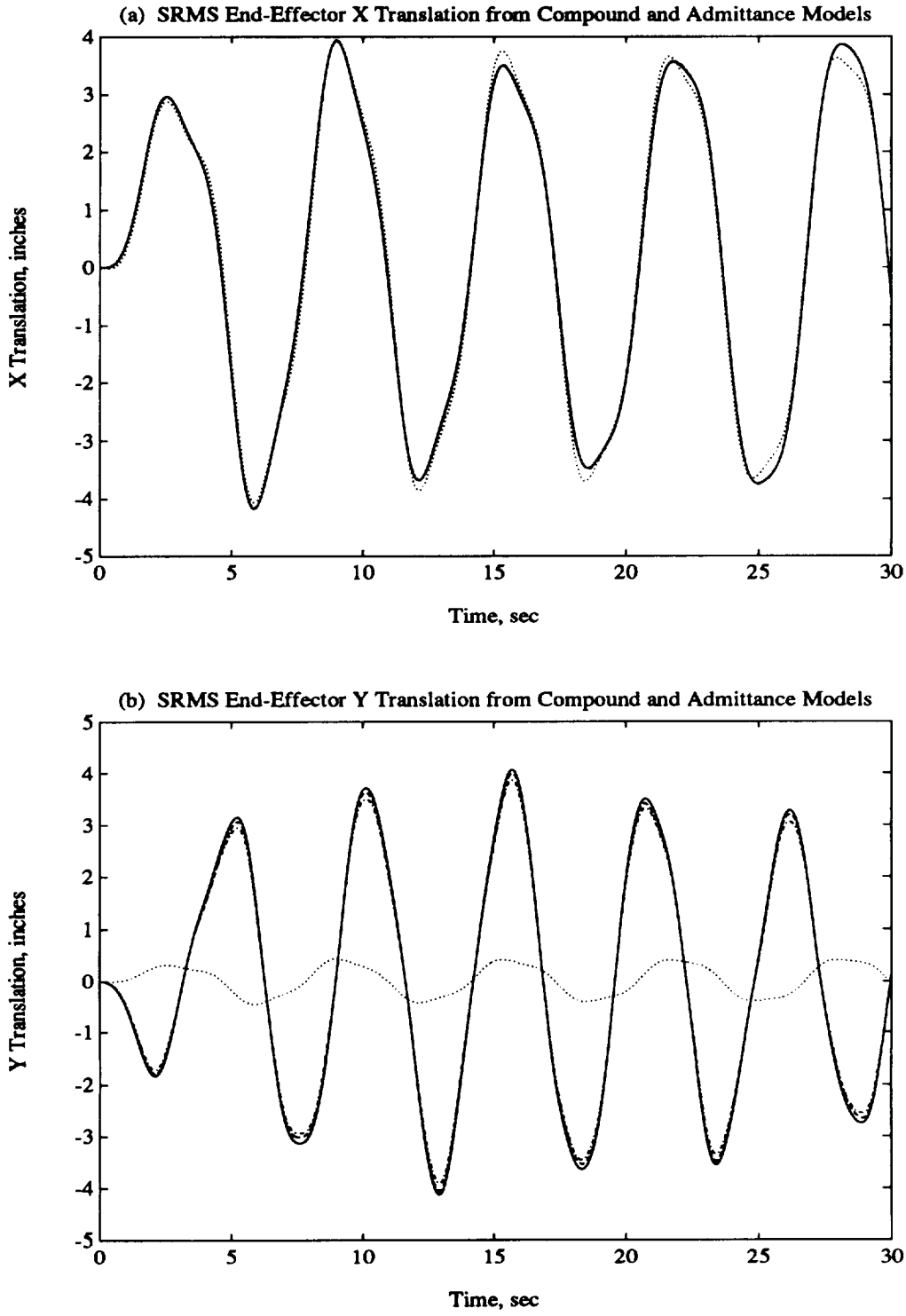

Figure 6-8: Capture Configuration, Shoulder Pitch 30° in 5 seconds, with the 1000 lb. DOSS Payload, SRMS End-Effector (a) X Translation, and (b) Y Translation.

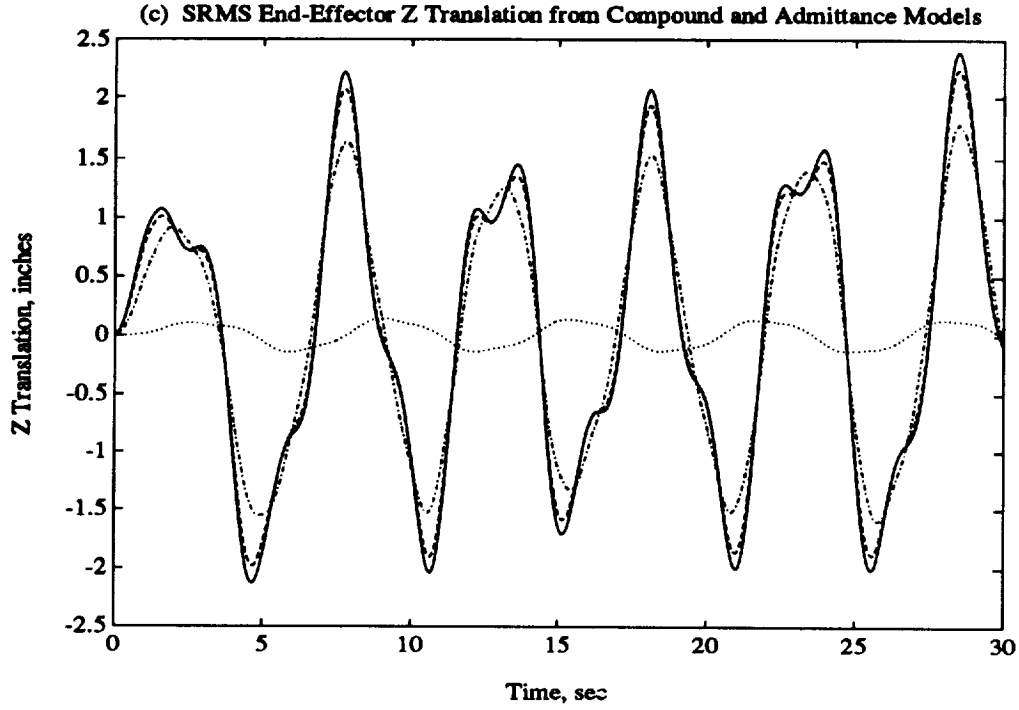

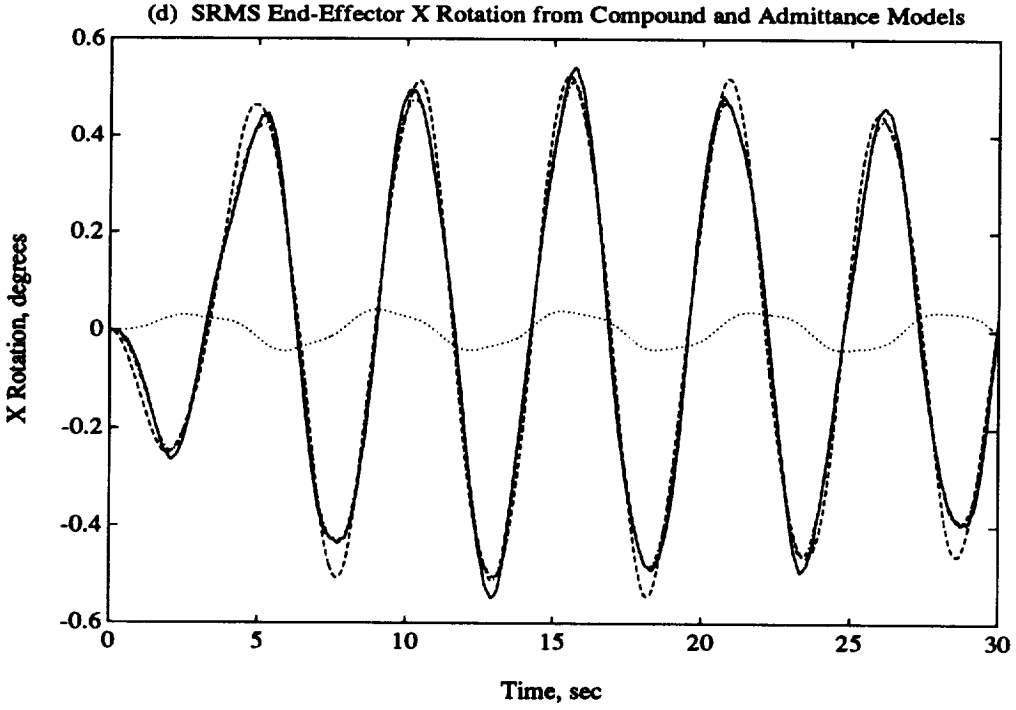

Figure 6-8: Capture Configuration, Shoulder Pitch 30° in 5 seconds, with the 1000 lb. DOSS Payload, SRMS End-Effector (c) Z Translation, and (d) X Rotation.

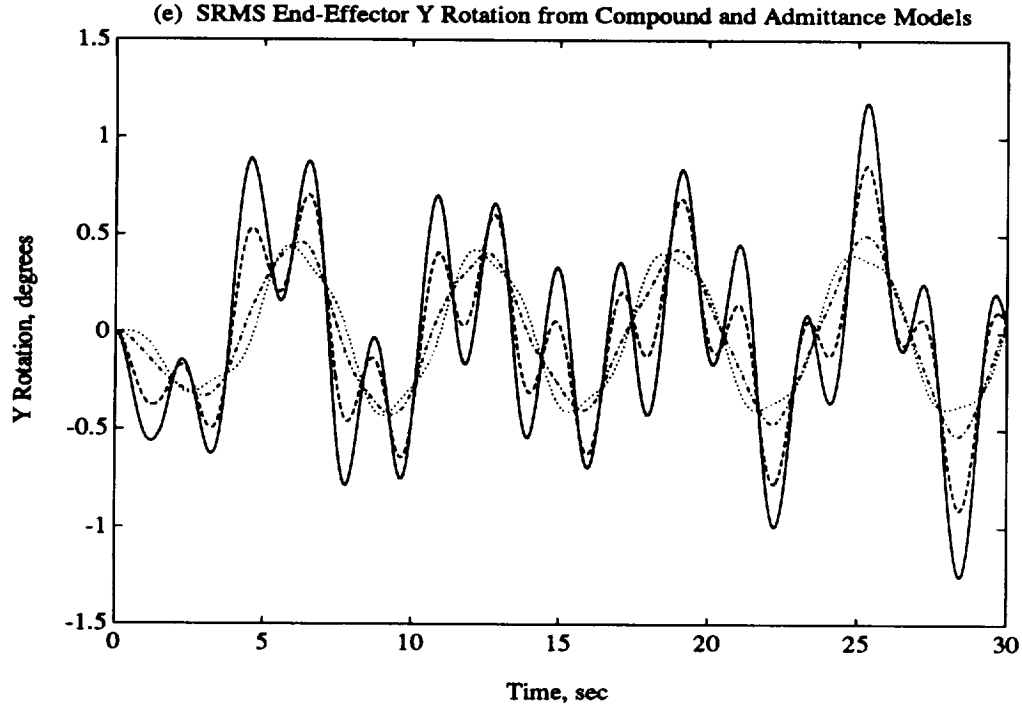

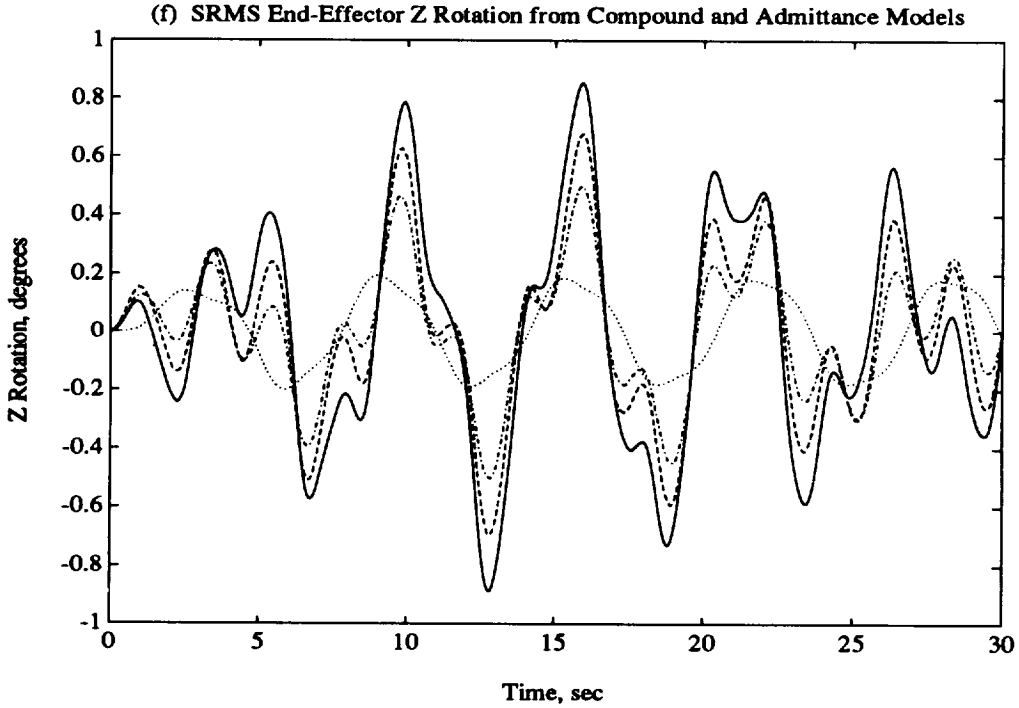

Figure 6-8: Capture Configuration, Shoulder Pitch 30° in 5 seconds, with the 1000 lb. DOSS Payload, SRMS End-Effector (e) Y Rotation, and (f) Z Rotation.

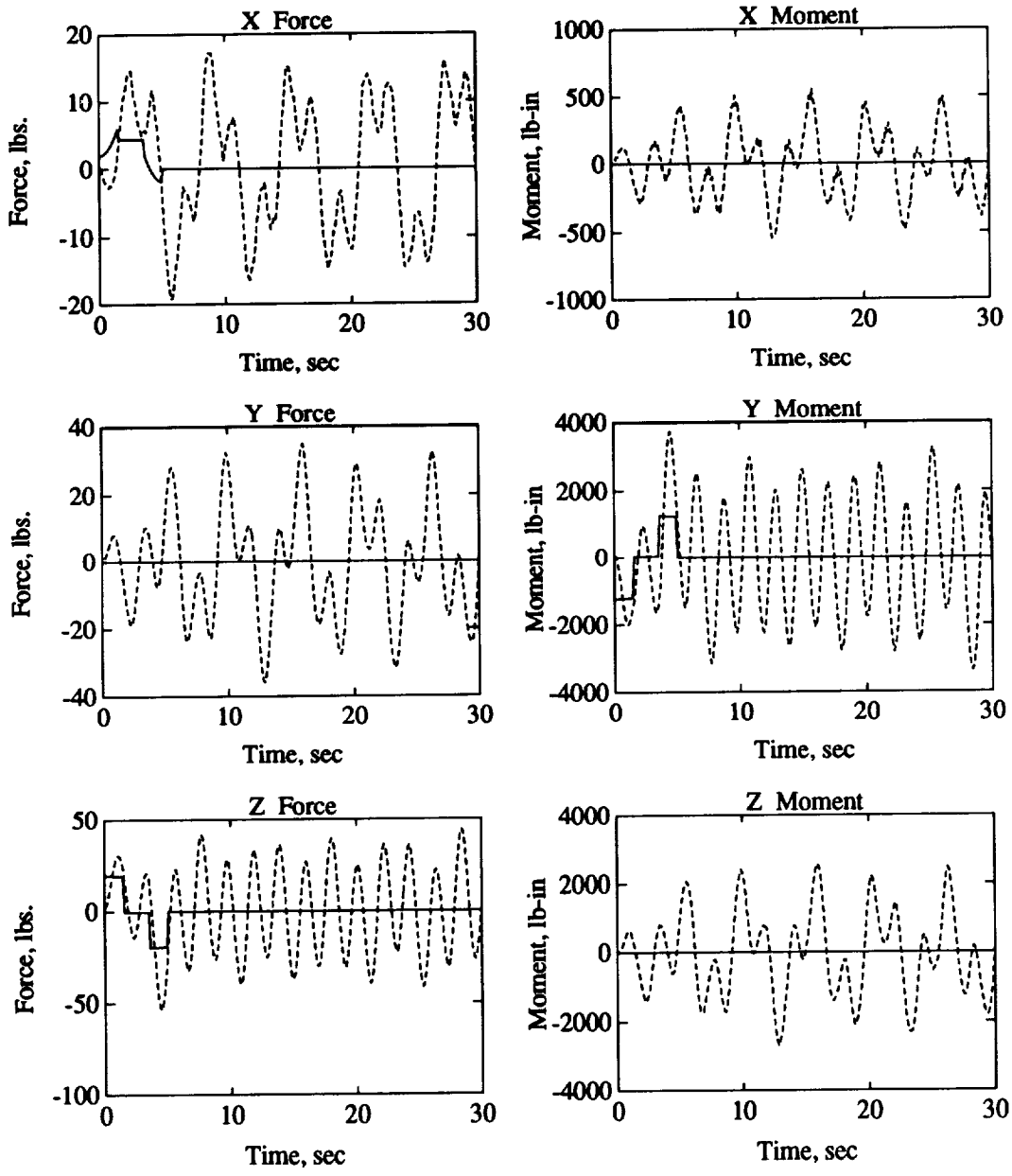

Figure 6-9: Capture Configuration, Shoulder Pitch 30° in 5 seconds, with the 1000 lb. DOSS Payload, Compound (solid) vs. Admittance (dashed) Wrenches.

Comparison of various numbers of modes of the admittance model for each configuration of the SRMS with the two payload types were analyzed to determine how many modes must be kept in order to maintain a certain level of fidelity. These comparisons are presented in Figures 6-10 and 6-11 for the 5 and 10 second shoulder pitch maneuver, respectively, and similarly in Figures 6-12 and 6-13 for the shoulder yaw maneuvers. Plotted are the maximum displacement (in inches in the top graph) and orientation (in degrees in the bottom graph) differences associated with inclusion of various numbers of admittance modes (i.e., the first 10, followed by 15, and 20) as compared to the *exact* response. The error numbers were obtained from the following equations:

$$(disp)_{max} = \max\left(\sqrt{(x_{comp}(t) - x_{adm}(t))^2 + (y_{comp}(t) - y_{adm}(t))^2 + (z_{comp}(t) - z_{adm}(t))^2}\right)$$

$$(orien)_{max} = \max\left(\sqrt{(\theta_x(t)_{comp} - \theta_x(t)_{adm})^2 + (\theta_y(t)_{comp} - \theta_y(t)_{adm})^2 + (\theta_z(t)_{comp} - \theta_z(t)_{adm})^2}\right)$$

both equations apply during: $0 < t < 30$ sec *at* 0.001sec

where the subscripts *comp* and *adm* refer to compound and admittance, respectively.

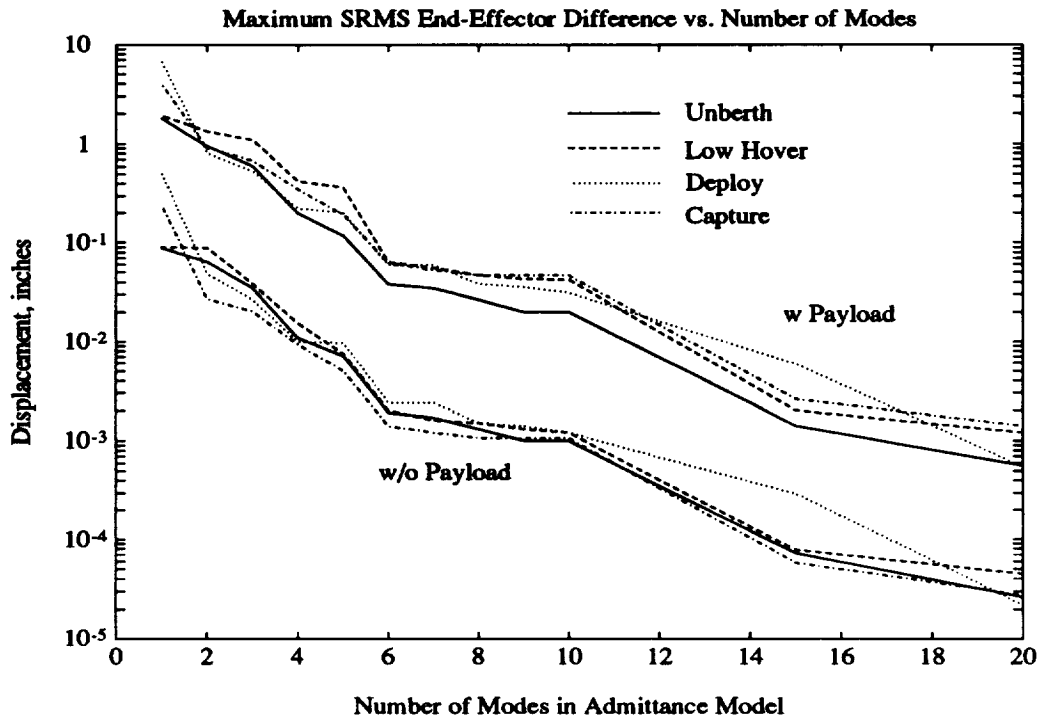

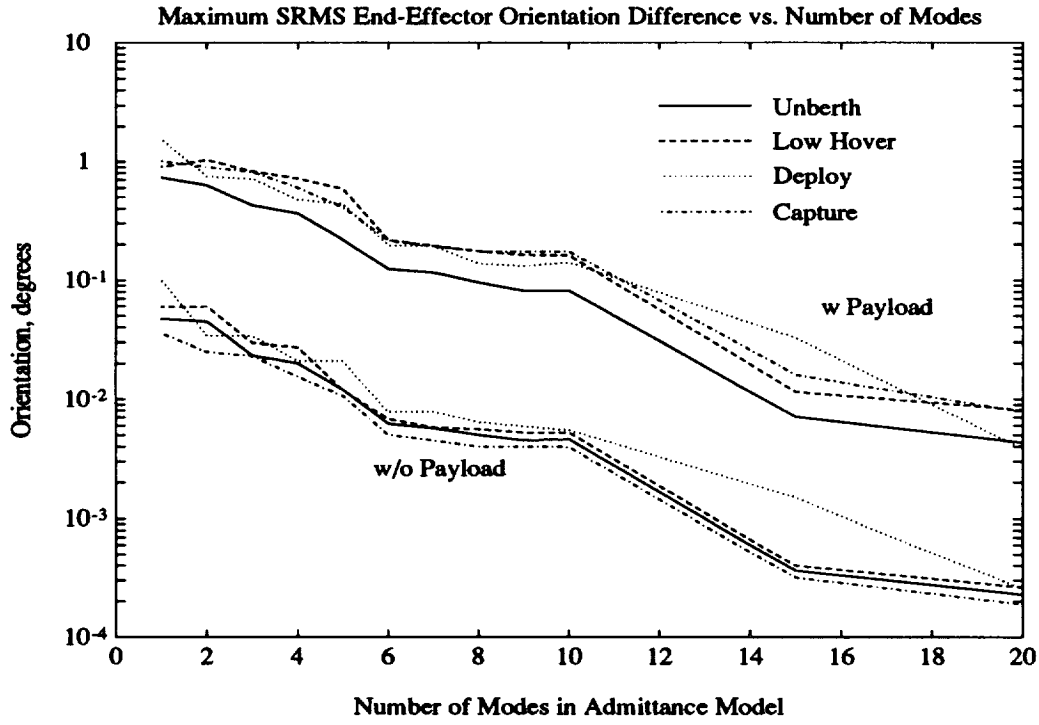

Figure 6-10: SRMS End-Effector Fidelity Curves for the Shoulder Pitch 30° in 5 seconds.

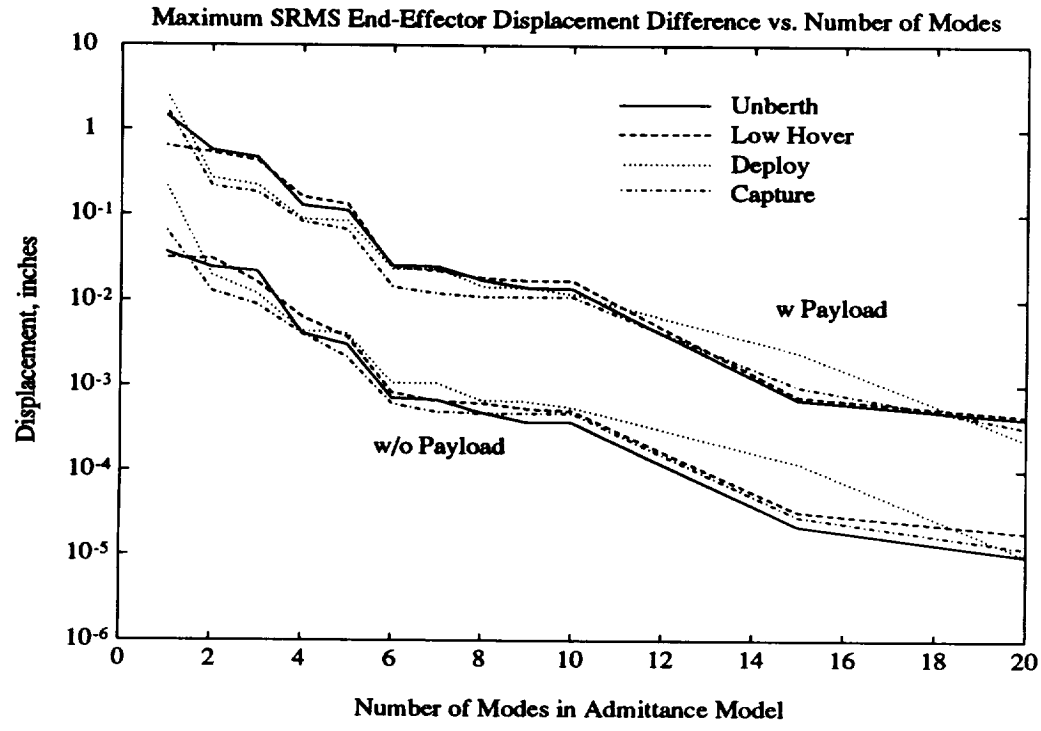

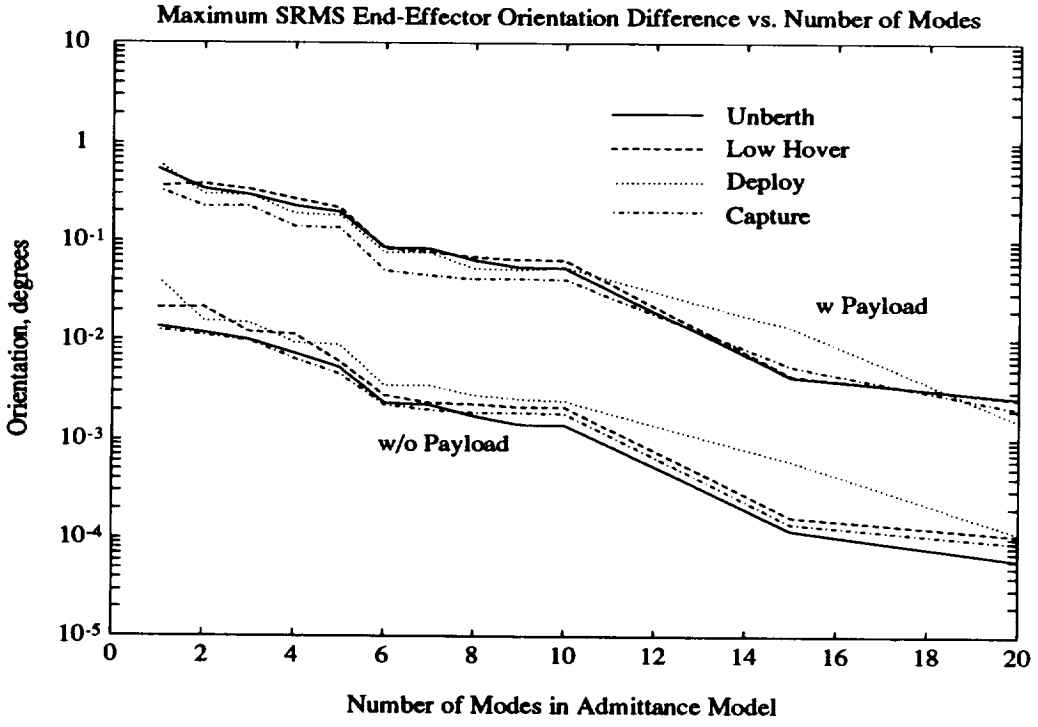

Figure 6-11: SRMS End-Effector Fidelity Curves for the Shoulder Pitch 30° in 10 seconds.

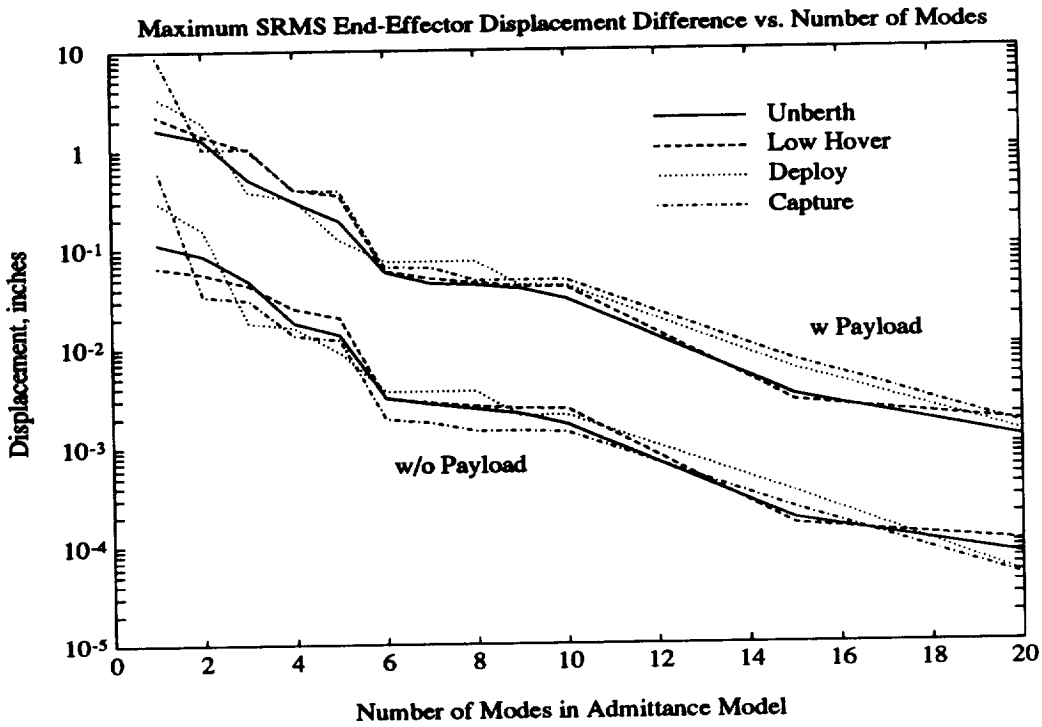

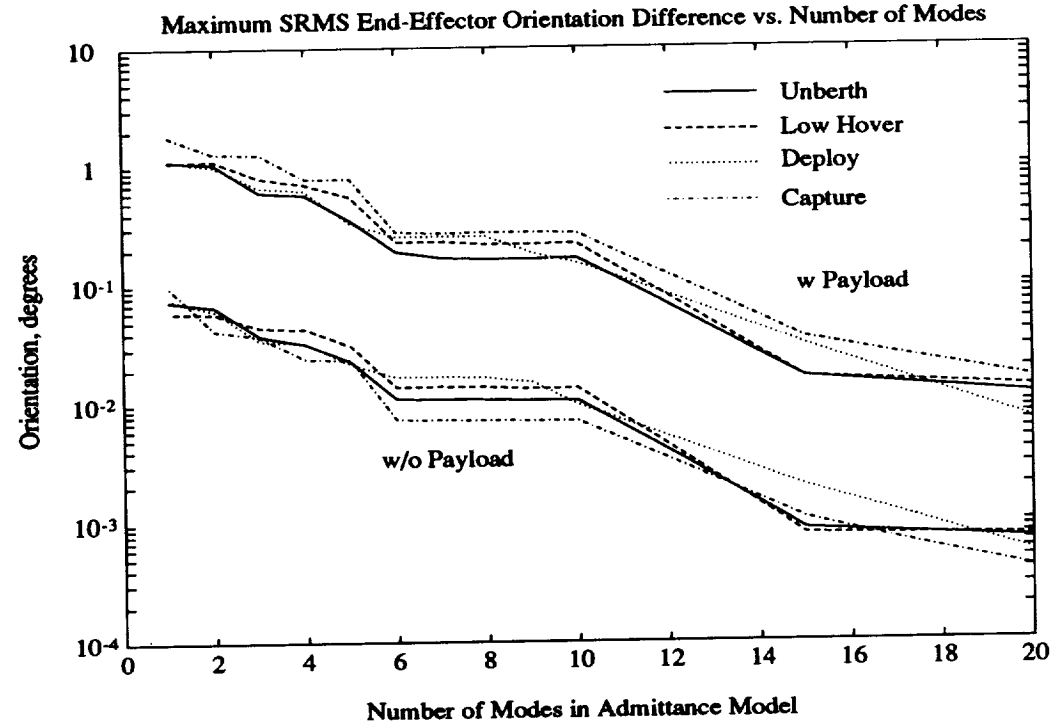

Figure 6-12: SRMS End-Effector Fidelity Curves for the Shoulder Yaw 30° in 5 seconds.

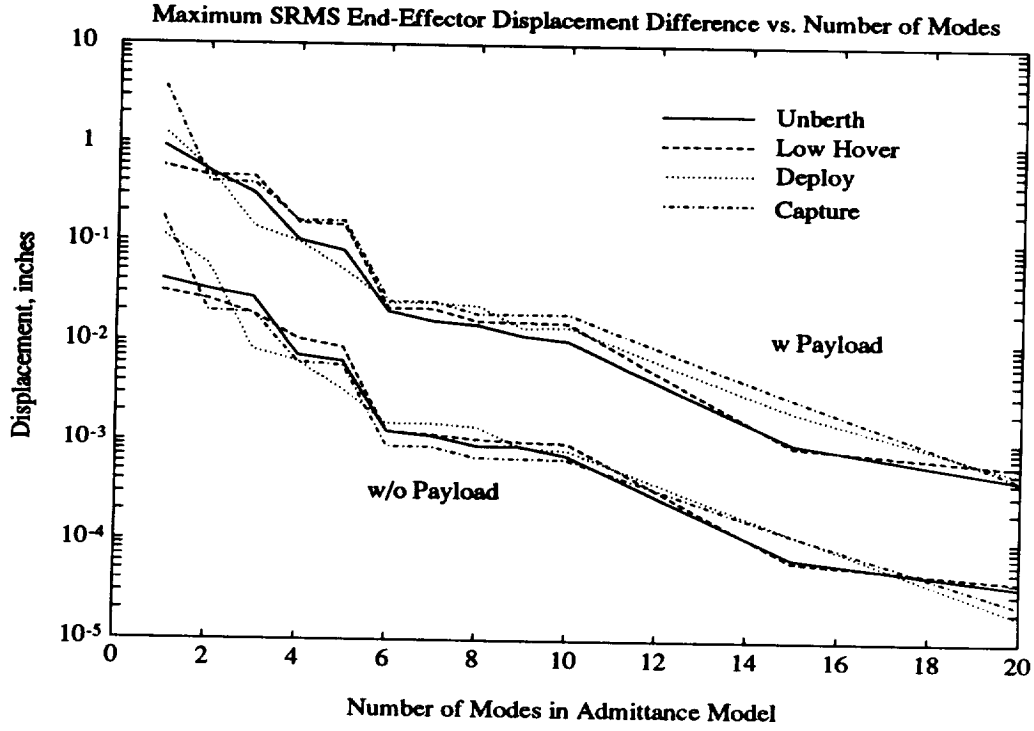

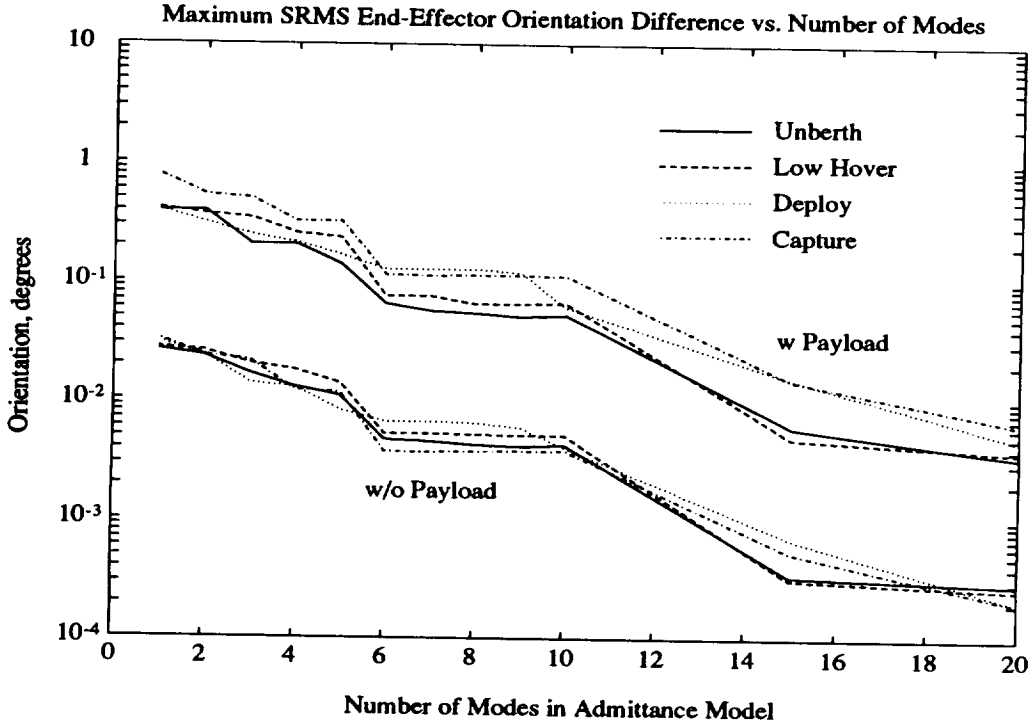

Figure 6-13: SRMS End-Effector Fidelity Curves for the Shoulder Yaw 30° in 10 seconds.

Upon examination of Figures 6-10 through 6-13, several observation can be made

1. As expected, the higher order admittance model generally yields less displacement and orientation differences than a lower order model (i.e., typically, *monotonic convergence* is observed). For example, consider the Unberth configuration with no DOSS payload, shoulder pitch slewing 30° in 5 seconds, 2 modes yield displacement and orientation differences of approximately 0.064" and 0.045°, respectively, while 10 modes yield 0.001" and 0.0046°, respectively (Figure 6-10).

2. The effect of adding the 1000 lb. cylindrical payload at the end-effector of the DOSS can clearly be seen. The displacement and orientation differences are approximately an order of magnitude larger than without the 1000 lb. payload. For instance, 1 mode of the Deploy configuration with the 1000 lb. DOSS payload (shoulder pitch 30° in 5 seconds) yields differences of approximately 6.7" and 1.5°. Removing the 1000 lb. payload reduces them to approximately 0.51" and 0.1° (Figure 6-10). This suggests that as the size of the SRMS payload becomes larger, more admittance modes will be required in order to adequately represent the motion of the SRMS end-effector.

3. Notice how all four configurations yield similar displacement and orientation differences (i.e., closely spaced admittance model fidelity difference curves). Even performing the maneuver slower, or with the 1000 lb. DOSS payload does not alter the pattern. This suggests that choosing configurations similar in geometry to the four configurations examined here, will yield similar fidelity curves. If this is the case, then the order of the admittance model based on Figures 6-10 through 6-13 should also be valid for those other configurations.

4. Taking twice as long to perform the DOSS slew maneuver has the effect of reducing the displacement and orientation differences by at least half an order of magnitude, thereby allowing less modes to be included in the admittance model. For instance, 1 mode of the Unberth and Low Hover configurations for the shoulder pitch joint slewing 30° in 5 seconds with no DOSS payload, yields RSS errors of approximately 0.09" and 0.055°, and 0.036" and 0.015° for the 10 second slew, respectively (Figures 6-10 and 6-11). Thereby allowing a lower order admittance model to be used in the Stewart Platform, which has the benefit of reducing computations for real-time simulations. This appears to be valid without the DOSS payload, but not with the 1000 lb. DOSS payload, as will be shown shortly.

5. Following along the lines of item 4, performing the DOSS slew maneuvers twice as long yields displacement differences of slightly less than 0.05" for the Unberth and Low Hover configurations using one admittance mode (Figures 6-11 and 6-13). If a tenth of an inch is the tolerance criteria for model fidelity, then the SRMS can essentially be modeled with 0 modes as a rigid structure. Therefore, for these two configurations, the Stewart Platform can be held fixed during DOSS maneuvers.

6. Admittance modes 7 through 10 for all four configurations in Figures 6-10 through 6-13 all show slight plateaus in the fidelity curves. This indicates that inclusion of these modes do not significantly increase accuracy of the response, therefore, they can be left out from the admittance model (i.e., these four modes can be skipped from the admittance model). Furthermore, these modes are boom bending modes, which do not play as important a role as joint modes (see chapter 4).

Figures 6-10 through 6-13 can be used in conjunction with the information contained in chapter 5 to determine the order of the admittance model. After deciding on a tolerance criteria, the number of admittance modes required to produce that tolerance can be obtained from the four figures mentioned above. Once the number of modes is chosen, those number of modes and frequencies can be entered into the Stewart Platform.

Arbitrarily choosing tolerance criteria of 0.01" translation and 0.01° rotation differences, the number of modes required in the admittance model are tabulated in Tables 6-7 and 6-8, without and with the 1000 lb. DOSS payload, respectively. These two tables exhibit the behaviors described in items 2 and 4. Tables 6-7 and 6-8 indicate that the 1000 lb. DOSS payload requires approximately three or four times more modes than without it (item 2). Also, generally, when the slew maneuver is performed twice as long (item 4), 4 modes rather than 6 modes are required, without the DOSS payload in both displacement and orientation (Table 6-7). However, with the 1000 lb. DOSS

payload, the number of modes remain at 15 (Table 6-8). Curiously, the Unberth, Low Hover, and Deploy configurations (shoulder pitch 30° in 5 seconds, without the 1000 lb. DOSS payload), require substantially more modes (approximately twice as many) than the 10 second shoulder pitch slew, or the two yaw maneuvers; greater than 20 admittance modes is indicated for these configurations because by the 20th mode, the rotation errors are greater than the tolerance criteria.

Table 6-7: Number of Admittance Modes Required to Maintain Fidelity of 0.01" Translations and 0.01° Rotations without the DOSS Payload.

Type	30° Slew Maneuver	Slew Duration (sec)	SRMS Configuration	Number of Admittance Modes	
				0.01" disp.	0.01° orien.
No DOSS Payload	Shoulder Yaw Joint	5	Unberth	6	15
			Low Hover	6	15
			Deploy	5	10
			Capture	6	6
		10	Unberth	4	6
			Low Hover	5	6
			Deploy	3	5
			Capture	4	6
	Shoulder Pitch Joint	5	Unberth	5	6
			Low Hover	5	6
			Deploy	4	6
			Capture	4	6
		10	Unberth	4	3
			Low Hover	4	5
			Deploy	4	4
			Capture	3	3

Table 6-8: Number of Admittance Modes Required to Maintain Fidelity of 0.01" Translations and 0.01° Rotations with the 1000 lb. DOSS Payload.

Type	30° Slew Maneuver	Slew Duration (sec)	SRMS Configuration	Number of Admittance Modes	
				0.01" disp.	0.01° orien.
With 1000 lb. DOSS Payload	Shoulder Yaw Joint	5	Unberth	15	> 20
			Low Hover	15	> 20
			Deploy	15	20
			Capture	15	> 20
		10	Unberth	15	15
			Low Hover	15	15
			Deploy	15	20
			Capture	15	20
	Shoulder Pitch Joint	5	Unberth	15	15
			Low Hover	15	20
			Deploy	15	20
			Capture	15	20
		10	Unberth	15	15
			Low Hover	15	15
			Deploy	15	15
			Capture	15	15

6.5 Summary of SRMS End-Effector Response

Maximum SRMS end-effector displacements and orientations for both yaw and pitch slew maneuvers of 5 and 10 second duration are presented as bar graphs in Figures 6-14

and 6-15 for no DOSS payload, and in Figures 6-16 and 6-17 with the 1000 lb. DOSS payload, respectively. Upon examination of these four figures, three observations can be made. The first observation is that as the size of the payload becomes larger, the response of the SRMS end-effector becomes greater. For example, approximately 0.65" and 0.1° for no DOSS payload to a little over 9.5" and about 1.75° with the 1000 lb. DOSS payload for the Capture configuration, shoulder yaw slew 30° in 5 seconds (Figures 6-14 through 6-17). The second observation regards the effect of the duration of the slew maneuver on the SRMS end-effector oscillations. If the slew maneuver is performed in twice the time, the maximum oscillations decrease by more than a factor of two, from approximately 5" for the Unberth and Low Hover configurations to just short of 2", for the shoulder yaw maneuver with the 1000 lb. payload (Figure 6-16). This suggests that performing maneuvers in space slowly will result in less oscillations of the supporting structure. Of course, the draw back is that more flight time will be required which becomes very costly. Finally, the shoulder yaw maneuver generally produced the greatest response of the SRMS end-effector, which is not surprising since the shoulder yaw axis has the greatest inertia to slew (Table 6-5(a)), and therefore would produce the greatest reaction torque.

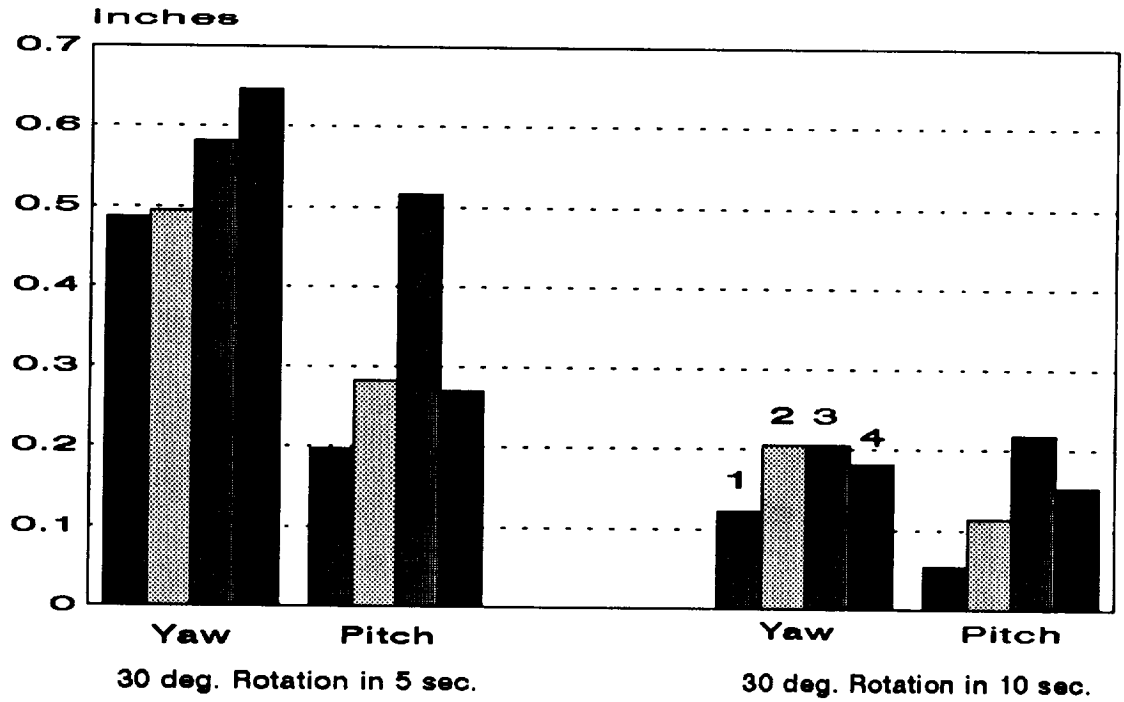

Figure 6-14: SRMS End-Effector Maximum Displacement for Configurations Unberth (1), Low Hover (2), Deploy (3), and Capture (4) with no DOSS payload.

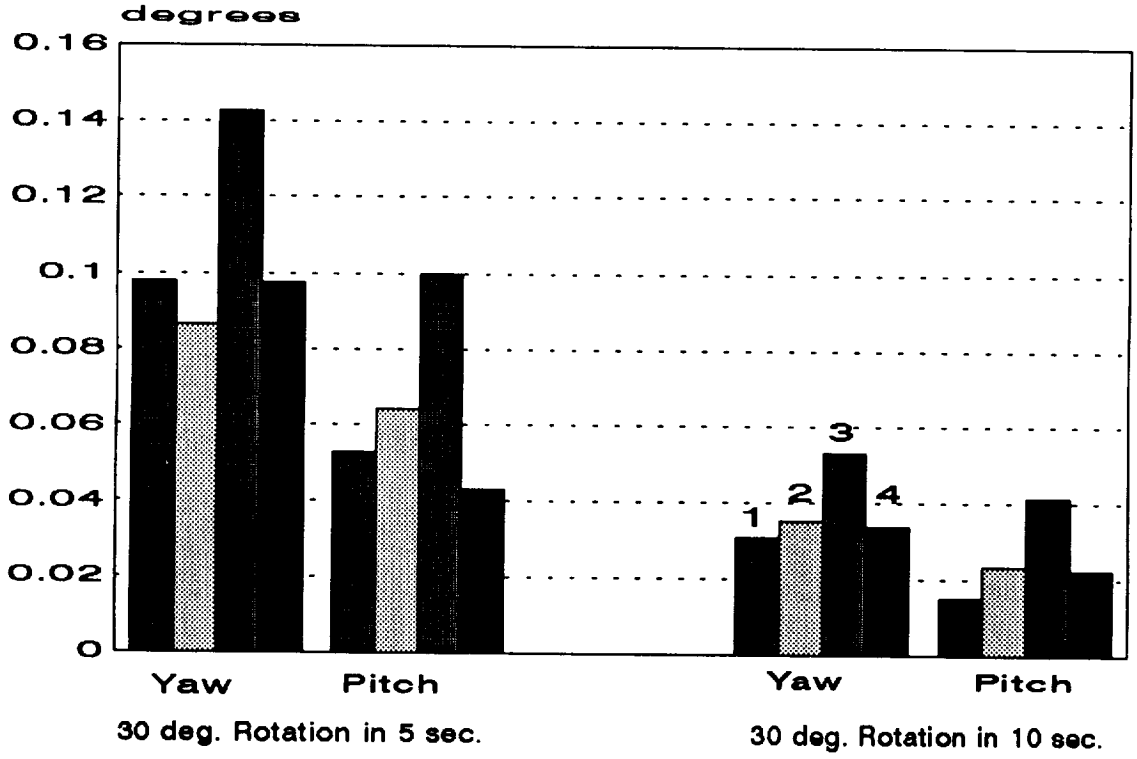

Figure 6-15: SRMS End-Effector Maximum Orientation for Configurations Unberth (1), Low Hover (2), Deploy (3), and Capture (4) with no DOSS payload.

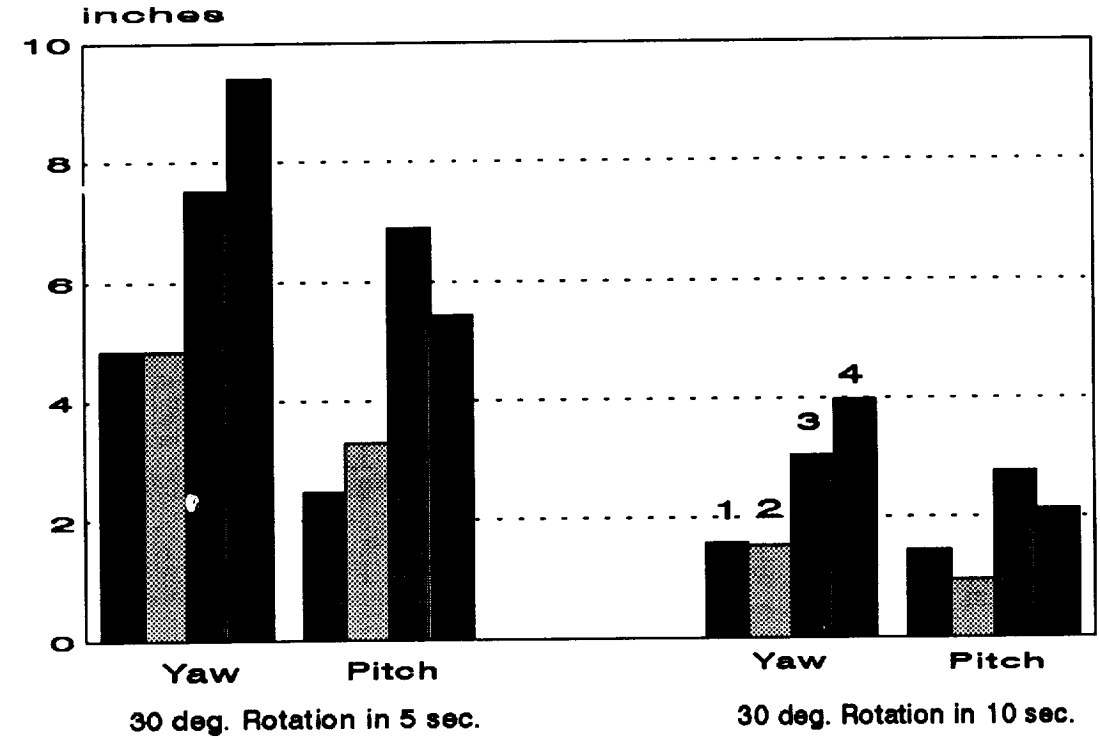

Figure 6-16: SRMS End-Effector Maximum Displacement for Configurations Unberth (1), Low Hover (2), Deploy (3), and Capture (4) with 1000 lb. DOSS payload.

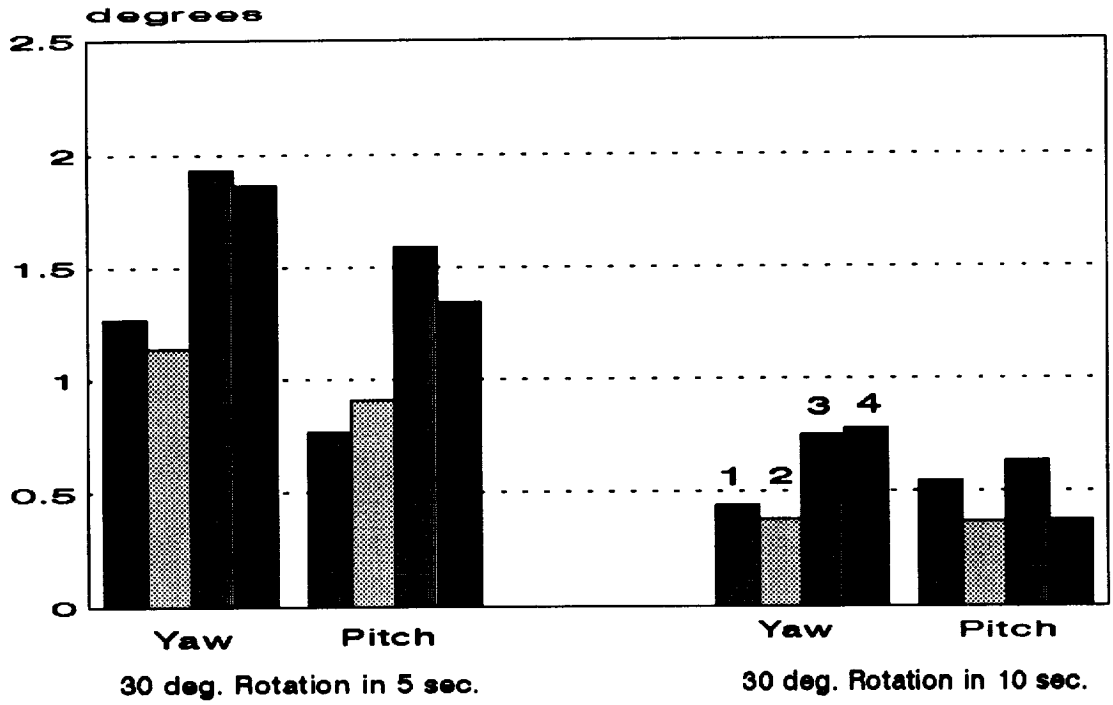

Figure 6-17: SRMS End-Effector Maximum Orientation for Configurations Unberth (1), Low Hover (2), Deploy (3), and Capture (4) with a 1000 lb. DOSS payload.

Three caveats must be presented concerning the results in Figures 6-10 through 6-17. These are

1. Figures 6-10 through 6-13 are applicable only to the DOSS, or DOSS plus 1000 lb. cylinder, as SRMS payloads, and should only be used as a guideline for other type payloads attached to the SRMS.

2. The calculated displacements of the SRMS end-effector in Figures 6-14 through 6-17 are only approximate because the compound wrench was based on a hypothetical motion of the DOSS manipulator assuming the SRMS end-effector was fixed during that motion.

3. The centrifugal $\vec{\omega} \times \vec{\omega} \times \vec{r}$, and $\vec{\omega} \times \vec{h}$ terms in the force and moment of the feedback wrench, respectively, are omitted in the dynamic simulations (i.e., load cell simulation) because of the linearity assumption in NASTRAN.

VII. CONCLUDING REMARKS

The primary objective of this study was to determine an admittance model of the SRMS in four brakes locked configurations: Unberth, Low Hover, Deploy, and Capture. This objective was accomplished by performing a modal analysis on a finite element model of the SRMS using MSC/NASTRAN. The finite element model of the SRMS was compared to other existing finite element models, where the natural frequencies agreed to within $\pm 10\%$, and whenever available, mode shape comparisons were also made (i.e., in a qualitative sense, since no actual numbers for the mode shapes were available from the other models) and was found to agree extremely well.

An application of the admittance model was presented by simulating the load cell output using two types of SRMS payloads (e.g., DOSS and DOSS plus 1000 lb. cylinder). This simulated load cell output was the input wrench to the admittance model, and was obtained from the Newton-Euler equations (omitting any nonlinear terms) applied to the SRMS payload center of mass. A 20 mode compound model (i.e., SRMS end-effector dynamics with a payload attached to it), was assessed to yield an *exact* response of the SRMS end-effector motions. Comparisons made with the exact response from the compound model determined that an admittance model with between 5 and 15 modes was sufficient to obtain an accurate response of the end-effector. It has been shown that the LCS is an effective procedure for calculating the load cell output prior to

conducting hardware simulations of the Stewart Platform. In conclusion, the dynamic interaction problem between manipulator and support structure in space related tasks can be studied with aid of a Stewart Platform.

REFERENCES

1. Stelman, N. M., "Design and Control of a Six-Degree-of-Freedom Platform with Variable Admittance", Master of Science Thesis, Department of Mechanical Engineering, M.I.T., Cambridge, MA, May 1988.

2. Müller, U., B., "Design of a Second Generation Experimental System for Studying Mobile Manipulator Control", Master of Science Thesis, Department of Mechanical Engineering, M.I.T., Cambridge, MA, June 1992.

3. Stovman, J. A., Wagner-Bartak, C. G., and Doetsch, K. H., "A Real-Time Simulation Facility for the Development of Manipulator Systems with Man-In-The-Loop", 10th Space Simulation Conference, Bethesda, Md, October 16-18, 1978 (AIAA 1978), pp. 19-29.

4. Carr, R., Nguyen, P., Ravindran, R., Trudel, C., "ASAD - A Non-Real Time Simulation Program for the Shuttle Remote Manipulator System", Proceedings of the 1981 Summer Computer Simulation Conference, Washington, D. C., July 15-17, 1981, pp. 255-260.

5. Gray, C., Koenig, M., Metzinger, R., Reasor, G., and Turnbull, J., "Validation of the Draper RMS Simulation (DRS) Against Flight Data", CSDL-R-1755, Volume 1-2, The Charles Stark Draper Laboratory, Cambridge, Massachusetts, April 1985.

6. Yang, Y., and Kuo, Y., "A Real-Time Simulator for the Shuttle Manipulator System in the System Engineering Laboratory", Simulation, Volume 57, Number 1, July 1991, pp. 48-55.

7. "Systems Engineering Simulator Remote Manipulator Flight-to-Simulation Validation Report", LESC-30028, Lockheed Engineering and Sciences Company, Houston, Texas, May 1992.

8. Baker, J. E., "Gravity Compensation for Experiments in Space Robotics", Master of Science Thesis, Department of Mechanical Engineering, M.I.T., Cambridge, MA, September 1992.

9. Cooper, P. A., Wu, Shih-Chin, Stockwell, A. E., Demeo, M. E., Garrison, J. L., and Montgomery, R. C., "Simulation of the Assembly Dynamics and Control of Space Station Freedom", Proceeding of the AIAA Guidance Navigation and Control Conference, Monterey CA, August 9-11, 1993.

10. Hunter, J. A., Ussher, T. H., and Gossain, D. M., "Structural Dynamic Design Considerations of the Shuttle Remote Manipulator System", presented at the AIAA/ASME/ASCE 23rd Structures, Structural Dynamics & Materials Conference, Part 1, New Orleans, Louisiana, May 10-12, 1982, pp. 499-505.

11. Ussher, T. H., and Doetsch, K. H., "An Overview of the Shuttle Remote Manipulator System", NASA CP-2342, Part 2, Space Shuttle Technical Conference, Houston, Tx, June 28-30, 1983, pp. 892-904.

12. Kumar, P., Truss, P., and Wagner-Bartak, C. G., "System Design Features of the Space Shuttle Remote Manipulator", Proceedings of the Fifth World Congress on Theory of Machines and Mechanisms, Montreal, Canada, July 8-13, 1979, pp. 839-842.

13. Doetsch, K. H., "The Remote Manipulator System for the Space Shuttle Orbiter", presented at the Jahrestagung 1977 of the Deutsche Gesellschaft fur Luft-und Raumfahrt eV, Berlin, W. Germany, September 13-15, 1977.

14. Dunbar, D., and Robertson, A., "Graphite/Epoxy Booms for the Space Shuttle Remote Manipulator", Aerospace Applications of Advanced Composite Materials, ICCM/2, April 16-20, 1978, Toronto, Canada.

15. Nguyen, P. K., Ravindran, R., Carr, R., Gossain, D. M., and Doetsch, K. H., "Structural Flexibility of the Shuttle Remote Manipulator System Mechanical Arm", AIAA Guidance and Control Conference, San Diego, CA, August 9-11, 1982, pp.246-256.

16. Payload Deployment and Retrieval System Simulation Database, Version 1.0, Flight Support Equipment, RMS Operations, NASA JSC-25134, July 1, 1991.

17. Staff, SRMS MASTER PARAMETERS LIST, SPAR-R.775, Issue H, February 1983.

18. Cooper, P. A., Garrison, J. L., Montgomery, R. C., Wu, Shih-Chin, Stockwell, A. E., Demeo, M. E., "Simulation of the Assembly Dynamics and Control of Space Station Freedom", AIAA Guidance, Navigation and Control Conference, August 1993, AIAA-93-3712.

19. Abelow, A. V., Dynamic Equation Set for a Simplified Simulation of the Space Shuttle Remote Manipulator System, Charles Stark Draper Laboratory, Report R-1258, May 1979 (Revised February 1980).

20. Systems Design Group, Space Shuttle Remote Manipulator System Design Definition Report, SPAR-R.776, Issue E, March 1980.

21. Blevins, R. D., Formulas for Natural Frequency and Mode Shape, Krieger Publishing Company, 1979, pp. 108 and 193.

22. Scott, M. A., Gilbert, M. G., and Demeo, M. E., "Active Vibration Damping of the Space Shuttle Remote Manipulator System", NASA TM-104149, NASA-Langley Research Center, Hampton, VA, August 1991.

23. Idris, H. R., "Real-Time Control of a Six Degree-of-Freedom Vehicle Emulation System", Master of Science Thesis, Department of Mechanical Engineering, M.I.T., Cambridge, MA, April 1992.

24. Abelow, A. V., Comparisons of Remote Manipulator System Finite Element Models, Charles Stark Draper Laboratory, Report R-1210, November 1978.

25. Alberts, T. E., Xia, H., and Chen, Y., "Dynamic Analysis to Evaluate Viscoelastic Passive Damping Augmentation for the Space Shuttle Remote Manipulator System", ASME Journal of Dynamics Systems, Measurement and Control, Volume 114, Number 3, pp. 468-475, September 1992.

26. Western Space and Marine, Inc., *Design Review Data Package*, WSM Document E91/004, Revised March 1, 1991, prepared for Critical Design Review (CDR) March 12-13, 1991.

27. Ugural, A. C. and Fenster, S. K., Advanced Strength and Applied Elasticity, Elsevier Science Publishing Co., 1975, pp. 139-140.

APPENDIX A. SHUTTLE REMOTE MANIPULATOR SYSTEM PROPERTIES

This Appendix contains geometric, mass, and structural properties of the SRMS given in section A.1 through A.3, respectively.

A.1 Geometric Properties

Each link of the SRMS is composed of several sections or segments. Links 1 and 7 are composed of two sections, while links 2, 3, 4, 5, and 6 of three. Table A-1 provides a description and length of each section, and Figure A-1 shows the arm in the stowed configuration labeling all these sections.

The distance between the swing-out joint and the port longeron of the cargo bay is 2.25 inches in the positive Z direction of the swing-out joint frame. The elbow pitch joint is offset from the shoulder pitch joint by 6.0 inches in the positive Z direction of the shoulder pitch joint coordinate system, as seen in Figure 2-5. The purpose of the elbow offset is to permit the elbow joint to have -160° of travel (Figure 2-2).

Table A-1: Description and Length of each SRMS Link.[16]

Link	Segment	Length (inches)	Description
1	L_{01}	11.489	Structure between the swing-out joint and the Rockwell/SPAR Interface Point
	L_{12}	11.000	Rockwell/SPAR Interface transition piece Inner Shoulder Yaw sleeve One-half of the Shoulder Yaw bearing
2	$L_{2'3}$	1.850	Outer Shoulder Yaw sleeve One-half of the Shoulder Yaw bearing
	L_{23}	3.500	Shoulder Yaw transition piece
	$L_{23'}$	6.650	Shoulder Pitch center toroid One-half of the Shoulder Pitch bearing
3	$L_{3'4}$	28.466	One-half of the Shoulder Pitch bearing Outer toroids Shoulder Pitch transition piece Electronics housing
	L_{34}	197.084	Upper Arm Boom
	$L_{34'}$	25.500	Elbow electronics compartment Elbow transition piece Elbow Pitch lug One-half of the Elbow Pitch bearing
4	$L_{4'5}$	12.500	One-half of the Elbow Pitch bearing Inner toroid Transition piece
	L_{45}	225.984	Lower Arm Boom
	$L_{45'}$	39.466	Wrist electronics compartment Wrist Pitch transition piece Wrist Pitch lugs
5	$L_{5'6}$	6.000	One-half of the Wrist Pitch bearing Wrist Pitch inner toroid
	L_{56}	6.000	Wrist Pitch to Wrist Yaw transition piece
	$L_{56'}$	6.000	Wrist Yaw inner toroid One-half of the Wrist Yaw bearing

Table A-1: Continued.

6	$L_{6'7}$	9.966	Wrist Yaw outer toroid Wrist Yaw transition piece
	L_{67}	10.140	Aft Wrist electronics compartment
	$L_{67'}$	9.894	Wrist Roll inner sleeve One-half of the Wrist Roll bearing
7	$L_{7'8}$	4.500	One-half of the Wrist Roll bearing Wrist Roll outer sleeve
	L_{78}	21.500	End-Effector

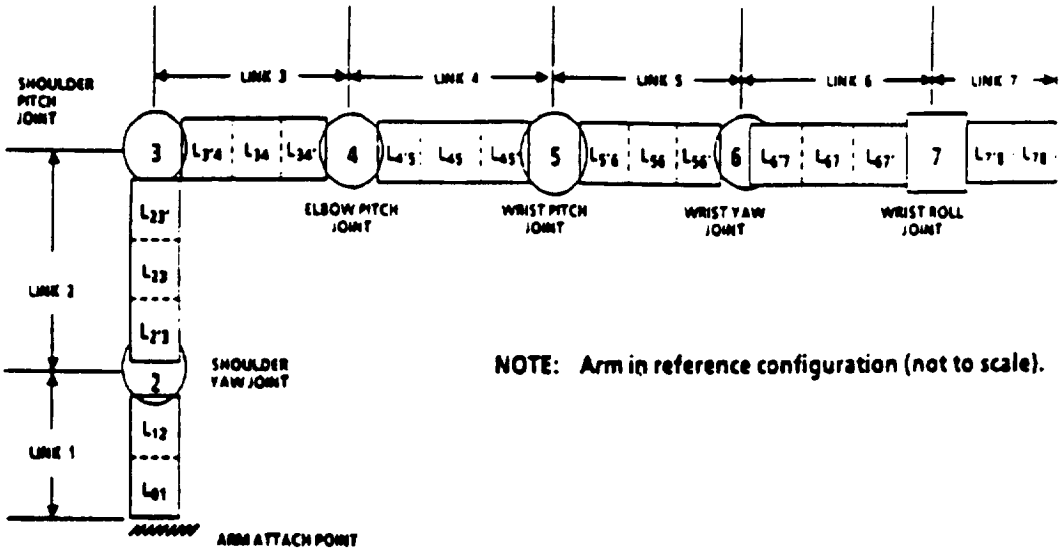

Figure A-1: SRMS, in Stowed Configuration, Labeling All Sections of a Link.[16]

A.2 Mass Properties

The mass and weight of each link is listed in Table A-2. The mass value in parenthesis for link 4 in Table A-2 is to be used when the SRMS is equipped with an

elbow CCTV camera. The mass moment of inertia of each link (with respect to the link center of mass) of the SRMS as used in SPAR's non-real time dynamic simulator, ASAD is presented in Table A-3. The * symbol for link 4 in Table A-3 denotes properties of the link when SRMS is equipped with an elbow CCTV camera. The inertias were based on modeling each link as a thin-walled circular beam with a 13 inch diameter and uniform mass distribution.[16]

Table A-2: Mass of each Link of the SRMS. [16]

Mass	Link						
	1	2	3	4	5	6	7
slugs	4.3333	2.2010	9.5485	5.9901 (6.860)	0.5809	3.1479	3.0980
lbs.	139.5	70.9	307.5	192.9 (220.9)	18.7	101.4	99.8

Table A-3: Mass Moment of Inertia about the Center of Mass for all Seven Links of the SRMS as used in the ASAD model.[16]

Link	Mass Moment of Inertia (slug-ft^2)					
	I_{xx}	I_{xy}	I_{xz}	I_{yy}	I_{yz}	I_{zz}
1	1.2672	0.0	0.0	1.2672	0.0	1.272
2	0.1833	0.0	0.0	0.1833	0.0	0.6463
3	2.8025	0.0	0.0	347.955	0.0	347.955
4	1.7596	0.0	0.0	267.8036	0.0	267.8036
4*	2.0152	0.0	0.0	306.7	0.0	306.7
5	0.1704	0.0	0.0	0.1088	0.0	0.1088
6	0.9254	0.0	0.0	1.6406	0.0	1.6406
7	0.9107	0.0	0.0	1.212	0.0	1.212

A.3 Structural Properties

The link bending and torsional stiffnesses, EI and GJ, respectively, are listed for each link section in Table A-4. The # symbol for section L_{78} in Table A-4 denotes SRMS end-effector bending moments exceeding 350 lb-ft. The flexibility of the Orbiter port longeron, swing-out joint, and section L_{01} of link 1, can be modeled by an equivalent 6-D spring (3 translations and 3 rotations)[16]. The spring stiffness will be referred to as the arm/Orbiter Interface Stiffness (given in OSR coordinates, see Figure 2-4), and is listed in Table A-5, which applies to a deployed arm moment M_z < 13,680 lb-in. If the deployed arm moment M_z > 13,680 lb-in then reference 16 provides another Arm/Orbiter Interface Stiffness value. The bending and torsional stiffnesses of section L_{01} for link 1 are not listed in Table A-4 because they are included in the arm/Orbiter Interface Stiffness.

Table A-4: Bending and Torsional Stiffnesses for each Link of the SRMS.[16]

Link	Section	Bending Stiffness (lb-in^2)			Torsional Stiffness, GJ (lb-in^2) $x\ 10^8$
		EI_{xx} (y-z plane) $x\ 10^8$	EI_{yy} (x-z plane) $x\ 10^8$	EI_{zz} (x-y plane) $x\ 10^8$	
1	L_{12}	5.49	4.58	---	6.94
2	$L_{2'3}$	1.53	1.27	---	11.6
	L_{23}	7.18	12.1	---	4.80
	$L_{23'}$	5.26	76.8	---	3.05

Table A-4: Continued.

3	$L_{3'4}$	---	8.13	7.50	3.75
	L_{34}	---	14.7	14.7	7.39
	$L_{34'}$	---	5.44	4.50	2.65
4	$L_{4'5}$	---	4.92	3.51	2.80
	L_{45}	---	9.83	9.83	5.17
	$L_{45'}$	---	2.07	1.76	1.03
5	$L_{5'6}$	---	0.972	1.04	1.04
	L_{56}	---	0.722	0.722	0.432
	$L_{56'}$	---	0.972	0.662	0.972
6	$L_{6'7}$	---	0.501	0.728	0.926
	L_{67}	---	1.72	1.72	1.45
	$L_{67'}$	---	0.371	0.364	0.678
7	$L_{7'8}$	---	0.445	0.437	0.820
	L_{78}	---	0.97	0.97	1.86
	$L_{78}^{\#}$	---	0.098	0.098	1.86

Table A-5: Arm/Orbiter Interface Stiffness for a Deployed Port Arm Moment $M_x < 13{,}680$ lb-in given in OSR Coordinates.[16]

Translational Stiffness (lb/in)			Rotational Stiffness (lb-in)/rad		
K_x	K_y	K_z	K_{θ_x}	K_{θ_y}	K_{θ_z}
112420.0	-3649.1	-18611.00	-16674.0	-459880.0	15300.0
	14702.0	-924.72	89457.0	13496.0	-11482.0
		47188.00	1397.5	67750.0	5854.5
			2372200.0	61373.0	-49036.0
Symmetric				11362000.0	-63043.0
					8359000.0

APPENDIX B. FINITE ELEMENT PROGRAMS FOR EACH OF THE FOUR CONFIGURATIONS

The entire NASTRAN GWU Finite Element Program is provided for the Unberth Configuration in section B.1. The finite element programs for the other configurations (Low Hover, Deploy, and Capture) are the same as the one presented, except the coordinate definition cards change. Readers not familiar with MSC/NASTRAN bulk data cards are referred to the Nomenclature for definitions. Therefore, coordinate definition cards (CORD2R) for Low Hover, Deploy, and Capture are presented in sections B.2 through B.4, respectively. See section 2.2 for a description of the GWU finite element model. Also, presented are the grid point, and mass and inertia specification of the center of mass of the two types of SRMS payload analyzed (i.e., DOSS manipulator, section B.5, and DOSS plus 1000 lb. cylinder, section B.6). This rigid payload is rigidly attached to the SRMS end-effector. To obtain the admittance finite element model comment out (or remove) bulk data deck cards: GRID 921777, RBE2 950703, and CONM2 950751, from the finite element model. Leaving these three cards in the finite element model will yield one of the compound finite element models. See section 6.2 for a description of the two types of SRMS payloads.

B.1 Unberth Configuration Finite Element Model

```
ID LOUKAS,ORBITER AND SRMS MODEL
$
$  WRITTEN BY ALAN E. STOCKWELL (LOCKHEED CONTRACTOR AT NASA-LANGLEY) AND CHRISTOPHER D.
$  SONTAG (GWU GRADUATE STUDENT)
$  DATE: APRIL 1992
$
$
$  MODIFIED BY:  LOUKAS PAPADOPOULOS (GWU GRADUATE STUDENT)
$  DATE: APRIL 1993
$
$
$  THE FOLLOWING FILE CONTAINS THE ORBITER AS A RIGID BODY (LUMPED MASS AT ITS C.M.) FIXED IN
$  SPACE.  THE SRMS IS MODELED AS A FLEXIBLE MANIPULATOR WITH THE FOLLOWING CHARACTERISTICS:
$
$        1.  THE UPPER AND LOWER ARM BOOMS ARE FLEXIBLE
$        2.  EVERY OTHER LINK, EXCEPT THE UPPER AND LOWER ARM
$            BOOMS ARE
$            MODELLED AS RIGID BODIES, AND
$        3.  EACH JOINT HAS TORSIONAL STIFFNESS AND IS CONSTRAINED $                IN TRANSLATION.
$
$  THE TORSIONAL SPRINGS AT EACH JOINT SIMULATE THE BRAKES LOCKED MODE OF THE SRMS.
$
$  EACH JOINT CONTAINS ROTATIONAL STIFFNESS WHICH WAS OBTAINED FROM ABELOW'S PAPER (CSDL
$  R-1258).
$
$  THE DOSS (Dextrous Orbital Servicing System) MANIPULATOR ARM IS ATTACHED TO THE END-EFFECTOR AS A
$  PAYLOAD.  THE DOSS ARM ITSELF IS ALSO CARRYING A 1000 LB. PAYLOAD., WHICH IS A RIGID
$  HOMOGENEOUS RIGHT CIRCULAR CYLINDER OF RADIUS 18 INCHES AND HEIGHT 48 INCHES.
$
$*****************************************************************************
$
$         SRMS CONFIGURATION:   UNBERTH
$         ---------------------
$
$     UNBERTH IS AN ACTUAL CONFIGURATION USED DURING THE DEPLOYMENT OF THE SPAS SATELLITE ON
$     THE STS-07 SHUTTLE MISSION.  SPAS IS THE Shuttle PAllet Satellite FREE-FLYER SPACECRAFT.  IT IS
$     REPRESENTATIVE OF A TYPICAL SSF ASSEMBLY MODULE.  THIS CONFIGURATION REPRESENTS THE
$     POSITION OF THE ARM AND PAYLOAD JUST AFTER RELEASE FROM THE CARGO BAY ATTACHMENTS.
$
$  RELATIVE JOINT ANGLES IN DEGREES:
$
$  Swing-out      :   19.48
$  Shoulder Yaw   :   -8.96
$  Shoulder Pitch :   73.90
$  Elbow Pitch    : -112.64
$  Wrist Pitch    :  -51.96
$  Wrist Yaw      :    4.43
$  Wrist Roll     :   28.99
$
$  THESE JOINT ANGLES ARE DEFINED WITH RESPECT TO THE LOCAL JOINT COORDINATE SYSTEMS FOUND
$  IN THE GWU FINITE ELEMENT MODEL, SECTION 2.1, FIGURE 2-5; ARM IN THE STOWED CONFIGURATION.
$
$*****************************************************************************
$
$  PLEASE NOTE THAT ALL THE VALUES IN THIS MODEL ARE BASED ON THE ENGLISH SYSTEM OF UNITS.
$

$  FOR EXAMPLE:
```

```
$
$       UNIT OF LENGTH  :  INCH    (in.)
$       UNIT OF MASS    :  SLINCH  ( 1 SLINCH = 12 SLUGS)
$       UNIT OF TIME    :  SECOND  (sec.)
$       UNIT OF FORCE   :  POUND   (lb.)
$
$*****************************************************************************************
$
SOL 103
TIME 5
$
$ This is what you put in the case control deck if you want to see what the mass and stiffness matrices look like.
$
$ Put this stuff right before the cend of the case control deck.
$
$*****************************************************************************************
$
$ DMAP TO PRINT OUT THE MASS and STIFFNESS MATRIX
$
$COMPILE PHASE1 SOUIN=MSCSOU, NOREF, NOLIST
$ALTER 49
$   MATGPR GPLS,USET,SILS,MJJ//'G'/'G'//1.-2$
$   MATGPR GPLS,USET,SILS,KJJ//'G'/'G'//1.-2$
$
$ The J Set is before any constraints are applied yet to the Mass and Stiffness Matrices.
$
$ENDALTER $  NOTE - ONLY NECESSARY IF THERE'S STUFF BETWEEN HERE AND CEND
$
$ (END DMAP) <--  Not a DMAP COMMAND
$
$
$*****************************************************************************************
$
CEND
TITLE = ORBITER AND SRMS MODEL - MSC/NASTRAN
METHOD = 1
SPC = 1
DISP(PLOT) = ALL
PARAM POST 0
$
$
BEGIN BULK
$
$
$ THIS IS PARAM COUPMASS IS PLACED HERE TO GET A BIT MORE ACCURATE RESULTS, THAN IF WE JUST
$ LEAVE IT OFF.  IT PUTS IN THE OFF DIAGONAL TERMS IN THE MASS MATRIX, RATHER THAN JUST THE MAIN
$ DIAGONAL TERMS.
$
PARAM,COUPMASS,1
$
$
$
$ THE MODIFIED GIVENS METHOD IS USED AS THE EIGENVALUE AND EIGENVECTOR EXTRACTION METHOD.
$
EIGR,1,MGIV,,,,10
$
$
$ THIS SECTION CONTAINS ALL DEFINED COORDINATE SYSTEMS
$
```

```
$ CS FOR ORBITER VISUAL AID ONLY - ONLY USED BY GRID POINTS 925001t925039
CORD2R  920600  204000  -58.842 1.847   -342.78 -58.842 1.847   -341.78 +
        -57.842 1.847   -342.78
$ PDA - FRAME
CORD2R  200000  0       -261.48 -132.82 190.95  -260.48 -132.82 190.95  +
        -261.48 -133.82 190.95
$ OSR (used for displ of support strt and slide beam)
CORD2R  200110  0       -789.48 503.18  200.95  -788.48 503.18  200.95  +
        -789.48 502.18  200.95
$ OSR (ORBITER STRUCTURAL REFERENCE FRAME)
CORD2R  204000  0       -789.48 503.18  200.95  -788.48 503.18  200.95  +
        -789.48 502.18  200.95
$ SSF FRAME - COINCIDENT WITH BASIC
CORD2R  250010  0       0.0     0.0     0.0     0.0     0.0     1.      +
        1.      0.0     0.0
$ STARBOARD ALPHA JOINT
CORD2R  250011  0       0.0     0.0     0.0     -.7879880.0     .615691 +
        .615691 0.0     .787988
$ SAME AS 250010
CORD2R  299999  0       0.0     0.0     0.0     0.0     0.0     1.      +
        1.      0.0     0.0
$ ORBITER PROPERTY REFERENCE FRAME
CORD2R  920402  0       -342.77758.842  -1.847  -341.77758.842  -1.847  +
        -342.77757.842  -1.847
$ ROCKWELL/SPAR INTERFACE POINT
CORD2R  920500  0       -709.177-117.478299.433-708.234-117.478299.766+
        -709.177-118.478299.433
$ SHOULDER YAW AXIS
CORD2R  920502  0       -698.805-117.478303.096-699.748-117.478302.763+
        -698.753-118.466302.949
$ SHOULDER PITCH AXIS
CORD2R  920503  0       -687.49 -117.478307.092-687.701-118.427306.858+
        -686.569-117.752307.371
$ ELBOW PITCH AXIS
CORD2R  920504  0       -457.651-191.823375.714-458.419-191.205375.547+
        -458.200-192.594375.391
$ WRIST PITCH AXIS
CORD2R  920505  0       -605.817-409.657286.904-605.857-408.67 287.055 +
        -606.761-409.645286.573
$ WRIST YAW AXIS
CORD2R  920506  0       -622.802-409.434280.95  -622.842-408.447281.101+
        -623.768-409.434280.692
$ WRIST ROLL AXIS
CORD2R  920507  0       -651.786-409.425273.210-651.698-408.485272.88  +
        -652.753-409.424272.952
$
$
$ ORBITER CONCENTRATED MASS
$23456781234567812345678123456781234567812345678
GRID    920402  200110  1057.1583.44701 8.56     200110
$ ROCKWELL-SPAR INTERFACE POINT (START OF LINK 1)
GRID    920999  200110  620.658 -98.483 80.3     200110
$ END OF LINK 1
GRID    921102  920500  0.0     0.0     11.     920500
$ LINK 2
GRID    921201  920502  0.0     0.0     0.0     920502
GRID    921202  920502  0.0     0.0     -6.     920502
GRID    921203  920502  0.0     0.0     -12.    920502
$ UPPER ARM - LINK 3
GRID    921301  920503  0.0     0.0     0.0     920503
GRID    921302  920503  28.4664 0.0     0.0     920503
```

```
GRID    921303 920503 56.6208 0.0     0.0     920503
GRID    921304 920503 84.7764 0.0     0.0     920503
GRID    921305 920503 112.931 0.0     0.0     920503
GRID    921306 920503 141.085 0.0     0.0     920503
GRID    921307 920503 169.24  0.0     0.0     920503
GRID    921308 920503 197.395 0.0     0.0     920503
GRID    921309 920503 225.55  0.0     0.0     920503
GRID    921310 920503 251.05  0.0     6.0     920503
$ LOWER ARM - LINK 4
GRID    921401 920504 0.0     0.0     0.0     920504
GRID    921402 920504 12.4998 0.0     -6.0    920504
GRID    921403 920504 44.7838 0.0     -6.0    920504
GRID    921404 920504 77.0675 0.0     -6.0    920504
GRID    921405 920504 109.351 0.0     -6.0    920504
GRID    921406 920504 141.633 0.0     -6.0    920504
GRID    921407 920504 173.917 0.0     -6.0    920504
GRID    921408 920504 206.201 0.0     -6.0    920504
GRID    921409 920504 238.484 0.0     -6.0    920504
GRID    921410 920504 277.95  0.0     -6.0    920504
$ LINK 5
GRID    921501 920505 0.0     0.0     0.0     920505
GRID    921502 920505 9.0     0.0     0.0     920505
GRID    921503 920505 18.0    0.0     0.0     920505
$ LINK 6
GRID    921601 920506 0.0     0.0     0.0     920506
GRID    921602 920506 15.0    0.0     0.0     920506
GRID    921603 920506 30.0    0.0     0.0     920506
$ LINK 7
GRID    921701 920507 0.0     0.0     0.0     920507
GRID    921702 920507 13.0    0.0     0.0     920507
GRID    921703 920507 26.0    0.0     0.0     920507
$ 921703 IS TIP OF END EFFECTOR
$
$
$ THE FOLLOWING GRID POINT IS AT THE C.M. OF THE PAYLOAD
GRID    921777 920507 98.06   5.9-3   -14.48  920507
$
$
$ FLEXIBLE UPPER ARM BOOM
CBAR    950301 999320 921301 921302 0.0     0.0     1.
CBAR    950302 999310 921302 921303 0.0     0.0     1.
CBAR    950303 999310 921303 921304 0.0     0.0     1.
CBAR    950304 999310 921304 921305 0.0     0.0     1.
CBAR    950305 999310 921305 921306 0.0     0.0     1.
CBAR    950306 999310 921306 921307 0.0     0.0     1.
CBAR    950307 999310 921307 921308 0.0     0.0     1.
CBAR    950308 999310 921308 921309 0.0     0.0     1.
CBAR    950309 999330 921309 921310 0.0     0.0     1.
$ FLEXIBLE LOWER ARM BOOM
CBAR    950401 999420 921401 921402 0.0     0.0     1.
CBAR    950402 999410 921402 921403 0.0     0.0     1.
CBAR    950403 999410 921403 921404 0.0     0.0     1.
CBAR    950404 999410 921404 921405 0.0     0.0     1.
CBAR    950405 999410 921405 921406 0.0     0.0     1.
CBAR    950406 999410 921406 921407 0.0     0.0     1.
CBAR    950407 999410 921407 921408 0.0     0.0     1.
CBAR    950408 999410 921408 921409 0.0     0.0     1.
CBAR    950409 999430 921409 921410 0.0     0.0     1.
$
$
$
```

```
$ THE FOLLOWING DEFINES RIGID BODY ELEMENTS FOR LINKS 1, 2, 5, 6, AND 7 OF THE SRMS.
$
$ LINK 1
RBE2   950000 920999 123456 921102
$ LINK 2
RBE2   950201 921201 123456 921202
RBE2   950202 921202 123456 921203
$ LINK 5
RBE2   950501 921501 123456 921502
RBE2   950502 921502 123456 921503
$ LINK 6
RBE2   950601 921601 123456 921602
RBE2   950602 921602 123456 921603
$ LINK 7
RBE2   950701 921701 123456 921702
RBE2   950702 921702 123456 921703
$ 921703 = END EFFECTOR
$
$ THE FOLLOWING RBE2 CARD RIGIDLY ATTACHES THE PAYLOAD C.M. (GRID POINT 921777) TO THE
$ END-EFFECTOR (GRID POINT 921703) OF THE SRMS.
RBE2   950703 921703 123456 921777
$
$
$
$ THE FOLLOWING RBE2 CARDS CORRESPOND TO EACH JOINT OF THE SRMS. THEY RIGIDLY FIX ALL THE 6
$ D.O.F AT EACH JOINT. THIS SIMULATES THE JOINTS LOCKED CASE.
$
$ ********************************************************************************
$ THESE ARE COMMENTED OUT IN LIEU OF ROTATIONAL STIFFNESSES PLACED AT EACH JOINT.
$ ********************************************************************************
$
$ SHOULDER YAW JOINT (DOF 6)
$RBE2   950001 921102 123456 921201
$ SHOULDER PITCH JOINT (DOF 5)
$RBE2   950203 921203 123456 921301
$ ELBOW PITCH JOINT (DOF 5)
$RBE2   950310 921310 123456 921401
$ WRIST PITCH JOINT (DOF 5)
$RBE2   950410 921410 123456 921501
$ WRIST YAW JOINT (DOF 6)
$RBE2   950503 921503 123456 921601
$ WRIST ROLL JOINT (DOF 4)
$RBE2   950603 921603 123456 921701
$
$
$
$ THE FOLLOWING RBE2 CARDS CORRESPOND TO EACH JOINT OF THE SRMS. THEY RIGIDLY FIX THE
$ TRANSLATIONAL D.O.F. (D.O.F. 1, 2, AND 3) OF EACH JOINT. HENCE, ONLY ROTATIONAL D.O.F. ARE
$ ALLOWED TO TAKE PLACE AT THESE JOINTS (i.e. BALL JOINT).
$
$
$ SHOULDER YAW JOINT (DOF 6)
RBE2   950001 921102 123    921201
$ SHOULDER PITCH JOINT (DOF 5)
RBE2   950203 921203 123    921301
$ ELBOW PITCH JOINT (DOF 5)
RBE2   950310 921310 123    921401
$ WRIST PITCH JOINT (DOF 5)
RBE2   950410 921410 123    921501
$ WRIST YAW JOINT (DOF 6)
RBE2   950503 921503 123    921601
```

```
$ WRIST ROLL JOINT (DOF 4)
RBE2    950603 921603 123     921701
$
$
$ THE FOLLOWING GENEL REPRESENTS THE ARM/ORBITER INTERFACE STIFFNESS GIVEN IN TABLE 1.5-3 (CASE
$ 1A.) OF THE PDRS DATABASE [19], FOR DEPLOYED PORT ARM MOMENT Mz < 13680 in-lb. THE 16 FIELD DATA
$ ENTRY CARD IS BEING UTILIZED.
$
$ HENCE, THIS GENEL REPRESENTS ALL THE FLEXIBILITY BETWEEN THE ROCKWELL/SPAR INTERFACE POINT
$ (START OF LINK 1; LOCATED AT GRID POINT 920999) AND THE ORBITER (LOCATED AT GRID POINT 920402),
$ WHICH IS WHY IT IS CALLED THE ARM/ORBITER INTERFACE STIFFNESS.
$
$ NOTE: STIFFNESS MATRIX, K, IS IN ORBITER STRUCTURAL REFERENCE (OSR) FRAME.
$ ********************************************************************
$
$     THEREFORE, OUTPUT COORDINATE SYSTEMS FOR GRID POINTS 920999 AND 920402 HAS BEEN CHANGED
$     TO 200110 (ORBITER STRUCTURAL REFERENCE FRAME)
$
$
$ ARM/ORBITER INTERFACE STIFFNESS
GENEL   1             920999 1      920999 2      920999 3      +C101
+C101   920999 4      920999 5      920999 6                    +C102
+C102   ud            920402 1      920402 2      920402 3      +C103
+C103   920402 4      920402 5      920402 6                    *C104
*C104   K             112420.00     -3649.10      -18611.00     *C105
*C105   -16674.00     -459880.00    15300.00      14702.00      *C106
*C106   -924.72       89457.00      13496.00      -11482.00     *C107
*C107   47188.00      1397.50       67750.00      5854.50       *C108
*C108   2372200.00    61373.00      -49036.00     11362000.00   *C109
*C109   -63043.00     8359000.00
$
$
$
$ THE FOLLOWING GENEL CARDS DEFINE THE TORSIONAL SPRING CONSTANTS THAT EACH JOINT CONTAINS.
$ THE 16 FIELD DATA ENTRY CARDS ARE BEING UTILIZED. THESE ROTATIONAL STIFFNESS VALUES WERE
$ OBTAINED FROM ABELOW'S PAPER (CSDL R-1258). THE VALUES OF STIFFNESSES OBTAINED FROM ABELOW'S
$ PAPER ARE ENTERED INTO THE GENEL BY INPUTTING EITHER THE LOWER TRIANGULAR, OR UPPER
$ TRIANGULAR PART OF EACH MATRIX AT EACH JOINT (SINCE THE MATRIX IS SYMMETRIC, IT DOESN'T
$ MATTER WHICH PORTION YOU ENTER: THE LOWER OR UPPER PART OF THE MATRIX).
$
$
$ SHOULDER YAW JOINT (DOF 6)
GENEL   2             921201 4      921201 5      921201 6      +C201
+C201   ud            921102 4      921102 5      921102 6      *C202
*C202   K             19118480.637  304098.759    0.0           *C203
*C203   16019581.646  0.0           30034680.091
$
$
$ SHOULDER PITCH JOINT (DOF 5)
GENEL   3             921301 4      921301 5      921301 6      +C301
+C301   ud            921203 4      921203 5      921203 6      *C302
*C302   K             12014634.361  0.0           -1150703.385  *C303
*C303   54569137.946  0.0           9837743.822
$
$
$ ELBOW PITCH JOINT (DOF 5)
GENEL   4             921401 4      921401 5      921401 6      +C401
+C401   ud            921310 4      921310 5      921310 6      *C402
*C402   K             7514584.216   0.0           -240905.560   *C403
*C403   13836000.0    0.0           10008992.250
$
$
```

```
$ WRIST PITCH JOINT (DOF 5)
GENEL  5          921501 4     921501 5     921501 6     +C501
+C501  ud         921410 4     921410 5     921410 6     *C502
*C502  K          2263802.529  0.0          0.0          *C503
*C503  3960000.0  0.0          12476025.596
$
$
$ WRIST YAW JOINT (DOF 6)
GENEL  6          921601 4     921601 5     921601 6     +C601
+C601  ud         921503 4     921503 5     921503 6     *C602
*C602  K          2336888.177  -15212.328   0.0          *C603
*C603  2141709.006  0.0        2085744.476
$
$
$ WRIST ROLL JOINT (DOF 4)
GENEL  7          921701 4     921701 5     921701 6     +C701
+C701  ud         921603 4     921603 5     921603 6     *C702
*C702  K          1428113.409  0.0          0.0          *C703
*C703  825348.902  20231.384    1056830.987
$
$
$ CONCENTRATED MASS ELEMENTS PLACED ON EACH LINK OF THE SRMS.  THESE CARDS SERVE DIFFERENT
$ PURPOSES, DEPENDING ON WHAT LINK, ONE IS CONSIDERING.
$
$ THE ORBITER (CONM2 920407) IS USED TO PLACE MASS AT THE GRID POINT.  THE INERTIAS ARE NOT HERE,
$ SINCE THE ORBITER IS FIXED; ACTUALLY THE MASS DOESN'T HAVE TO BE HERE ALSO BECAUSE THE ORBITER
$ IS FIXED.
$
$ THE CONM2 CORRESPONDING TO LINKS 1, 2, 5, 6, AND 7 ARE USED TO PLACE MASS AND MASS MOMENT OF
$ INERTIA AT THE GEOMETRIC CENTER OF EACH LINK.
$
$ THE CONM2 CORRESPONDING TO THE UPPER AND LOWER ARM BOOMS ARE USED TO PLACE AXIAL MASS
$ MOMENT OF INERTIA ALONG THE BOOMS.  IN THIS CASE, SINCE EACH BOOM HAS LOCAL X-AXES RUNNING
$ ALONG AXIALLY, THESE CONM2 SERVE THE PURPOSE OF PLACING Ixx MASS MOMENT OF INERTIA, WHICH
$ THE CBAR CANNOT HANDLE.
$
$
$ MASS OF ORBITER ELEMENT
CONM2  920407 920402 920402 638.55
$ LINK 1
CONM2  950150 920999 920500 0.36111                    +
       15.2064       15.2064       15.264
$ LINK 2
CONM2  950250 921202 920502 0.18342                    +
       2.1996        2.1996        7.7556
$ UPPER ARM (TO ACCOUNT FOR IXX NOT FOUND IN CBAR ELEMENTS)
CONM2  950351 921301 920503 0.0                        +
       3.22176
CONM2  950352 921302 920503 0.0                        +
       3.22176
CONM2  950353 921303 920503 0.0                        +
       3.22176
CONM2  950354 921304 920503 0.0                        +
       3.22176
CONM2  950355 921305 920503 0.0                        +
       3.22176
CONM2  950356 921306 920503 0.0                        +
       3.22176
CONM2  950357 921307 920503 0.0                        +
       3.22176
CONM2  950358 921308 920503 0.0                        +
       3.22176
```

```
CONM2   950359 921309 920503 0.0                        +
        3.22176
CONM2   950360 921310 920503 0.0                        +
        3.22176
$ LOWER ARM (TO ACCOUNT FOR DXX NOT FOUND IN CBAR ELEMENTS)
CONM2   950451 921401 920504 0.0                        +
        2.06784
CONM2   950452 921402 920504 0.0                        +
        2.06784
CONM2   950453 921403 920504 0.0                        +
        2.06784
CONM2   950454 921404 920504 0.0                        +
        2.06784
CONM2   950455 921405 920504 0.0                        +
        2.06784
CONM2   950456 921406 920504 0.0                        +
        2.06784
CONM2   950457 921407 920504 0.0                        +
        2.06784
CONM2   950458 921408 920504 0.0                        +
        2.06784
CONM2   950459 921409 920504 0.0                        +
        2.06784
CONM2   950460 921410 920504 0.0                        +
        2.06784
$ LINK 5
CONM2   950550 921502 920505 0.048408                     +
        2.0448          1.3056              1.3056
$ LINK 6
CONM2   950650 921602 920506 0.262325                     +
        11.1048         19.6872             19.6872
$ LINK 7
CONM2   950750 921702 920507 0.258167                     +
        10.9284         14.544              14.544
$
$
$ PAYLOAD ENTRY
$
$ THE FOLLOWING CONM2 IS FOR THE PAYLOAD, WHICH IS THE DOSS (DEXTROUS ORBITAL SERVICING SYSTEM)
$ MANIPULATOR ARM (A 1000 LB. PAYLOAD IS ALSO ATTACHED TO THE END OF THE DOSS ARM, WITH A
$ RADIUS OF 18 INCHES AND HEIGHT OF 48 INCHES). THE DOSS ARM IS ATTACHED TO THE END-EFFECTOR OF
$ THE SRMS.  THESE INERTIAS CORRESPOND TO AN AXIS PARALLEL TO THE WRIST ROLL JOINT LOCATED AT
$ THE PAYLOAD C.M.
CONM2   950751 921777 920507 3.095  0.0    0.0    0.0          +
        722.45  4.167-4 1957.96 -34.933 -2.08-3 1667.933
$
$
$
PLOTEL  999991 920402 920999
$
$
$ BULK DATA FOR ORBITER PLOT ELEMENTS
$
$
GRID    925001 920600 236.   0.0    335.
GRID    925002 920600 260.   0.0    310.
GRID    925003 920600 260.   0.0    370.
GRID    925004 920600 438.   0.0    450.
GRID    925005 920600 438.   0.0    280.
GRID    925006 920600 470.   0.0    485.
GRID    925007 920600 470.   0.0    275.
GRID    925008 920600 520.   0.0    500.
```

```
GRID    925009 920600 520.   0.0    274.
GRID    925010 920600 1307.  0.0    500.
GRID    925011 920600 1307.  0.0    258.
GRID    925012 920600 1574.  0.0    830.
GRID    925013 920600 1694.  0.0    830.
GRID    925014 920600 1560.  0.0    500.
GRID    925015 920600 1520.  0.0    273.
GRID    925016 920600 598.   0.0    500.
GRID    925017 920600 598.   0.0    274.
GRID    925018 920600 438.   -90.   390.
GRID    925019 920600 438.   90.    390.
GRID    925020 920600 598.   105.   274.
GRID    925021 920600 598.   -105.  274.
GRID    925022 920600 598.   -105.  410.
GRID    925023 920600 598.   105.   410.
GRID    925026 920600 1307.  -105.  410.
GRID    925027 920600 1307.  -105.  258.
GRID    925028 920600 1307.  105.   258.
GRID    925029 920600 1307.  105.   410.
GRID    925030 920600 1560.  105.   500.
GRID    925031 920600 1520.  105.   273.
GRID    925032 920600 1520.  -105.  273.
GRID    925033 920600 1560.  -105.  500.
GRID    925034 920600 1480.  -468.  273.
GRID    925035 920600 1360.  -468.  273.
GRID    925036 920600 1024.  -188.  273.
GRID    925037 920600 1480.  468.   273.
GRID    925038 920600 1360.  468.   273.
GRID    925039 920600 1024.  188.   273.
$
$
$
$ THE FOLLOWING PLOTEL CARDS ARE USED TO PLOT AN OUTLINE PICTURE OF THE ORBITER WHILE USING
$ MSC/XL (THIS IS USED AS A VISUAL AID ONLY).
$
$
PLOTEL  990001 925001 925002
PLOTEL  990002 925001 925003
PLOTEL  990003 925003 925004
PLOTEL  990004 925006 925004
PLOTEL  990005 925006 925008
PLOTEL  990006 925016 925008
PLOTEL  990007 925010 925012
PLOTEL  990008 925013 925012
PLOTEL  990009 925013 925014
PLOTEL  990010 925015 925014
PLOTEL  990011 925015 925011
PLOTEL  990012 925009 925017
PLOTEL  990013 925009 925007
PLOTEL  990014 925005 925007
PLOTEL  990015 925005 925002
PLOTEL  990016 925016 925017
PLOTEL  990017 925010 925011
PLOTEL  990018 925026 925010
PLOTEL  990019 925026 925027
PLOTEL  990020 925011 925027
PLOTEL  990021 925011 925028
PLOTEL  990022 925029 925028
PLOTEL  990023 925029 925010
PLOTEL  990024 925029 925023
PLOTEL  990025 925016 925023
PLOTEL  990026 925016 925022
```

```
PLOTEL  990027  925021  925022
PLOTEL  990028  925021  925017
PLOTEL  990029  925020  925017
PLOTEL  990030  925020  925023
PLOTEL  990031  925020  925028
PLOTEL  990032  925021  925027
PLOTEL  990033  925022  925026
PLOTEL  990034  925011  925017
PLOTEL  990035  925022  925023
PLOTEL  990036  925029  925026
PLOTEL  990037  925010  925014
PLOTEL  990038  925014  925030
PLOTEL  990039  925031  925030
PLOTEL  990040  925031  925015
PLOTEL  990041  925032  925015
PLOTEL  990042  925032  925033
PLOTEL  990043  925014  925033
PLOTEL  990044  925033  925026
PLOTEL  990045  925032  925027
PLOTEL  990046  925031  925028
PLOTEL  990047  925030  925029
PLOTEL  990048  925032  925034
PLOTEL  990049  925035  925034
PLOTEL  990050  925035  925036
PLOTEL  990051  925021  925036
PLOTEL  990052  925031  925037
PLOTEL  990053  925038  925037
PLOTEL  990054  925038  925039
PLOTEL  990055  925020  925039
PLOTEL  990056  925023  925019
PLOTEL  990057  925003  925019
PLOTEL  990058  925022  925018
PLOTEL  990059  925003  925018
PLOTEL  990060  925021  925002
PLOTEL  990061  925020  925002
$
$
$2345678*2345678*2345678*2345678*2345678*2345678*2345678*2345678*2345678*2345678
RBE2    950800  920402  123456  925001  925002  925003  925004  925005  OR1
+R1     925006  925007  925008  925009  925010  925011  925012  925013  OR2
+R2     925014  925015  925016  925017  925018  925019  925020  925021  OR3
+R3     925022  925023  925026  925027  925028  925029  925030  925031  OR4
+R4     925032  925033  925034  925035  925036  925037  925038  925039
$
$
$
$ THE FOLLOWING SPC CORRESPONDS TO THE ORBITER (GRID POINT 920402) ONLY.  THE C.M. OF THE ORBITER
$ IS FIXED IN SPACE.
$
SPC     1       920402  123456  0.0
$
$
$ THIS SECTION CONTAINS THE PROPERTY AND MATERIAL BULK DATA CARDS
$
$2345678*2345678*2345678*2345678*2345678*2345678*2345678*2345678*2345678*2345678
PBAR    999310  999310  3.2472+06.3919+16.3919+11.2783+23.1608-3
PBAR    999320  999320  2.1216+04.6712+14.3091+15.6010+13.1608-3
PBAR    999330  999320  2.1216+03.1255+12.5856+13.9585+13.1608-3
PBAR    999410  999410  2.2368+04.3699+14.3699+18.7303+11.7871-3
PBAR    999420  999420  1.1535+02.8269+12.0167+14.1829+11.7871-3
PBAR    999430  999420  5.2546-11.1893+11.0112+11.5388+11.7871-3
$
```

```
MAT1    999310 2.3003+75.7798+6
MAT1    999320 1.7405+76.6935+6
MAT1    999410 2.2495+75.9103+6
MAT1    999420 1.7405+76.6935+6
ENDDATA
```

B.2 Low Hover Configuration Coordinate Definition

```
$*****************************************************************************************
$
$          SRMS CONFIGURATION:   LOW HOVER
$          ---------------------------
$
$      LOW HOVER IS AN ACTUAL CONFIGURATION USED DURING THE DEPLOYMENT OF THE SPAS SATELLITE
$      ON THE STS-07 SHUTTLE MISSION.  SPAS IS THE Shuttle PAllet Satellite FREE-FLYER SPACECRAFT.  IT IS
$      REPRESENTATIVE OF A TYPICAL SSF ASSEMBLY MODULE.  THIS CONFIGURATION REPRESENTS THE
$      POSITION OF THE ARM AND PAYLOAD AFTER BEING LIFTED FROM THE UNBERTH CONFIGURATION TO A
$      POINT WHICH COMPLETELY CLEARS THE SIDES OF THE CARGO BAY.
$
$   RELATIVE JOINT ANGLES IN DEGREES:
$
$    Swing-out      :   19.48
$    Shoulder Yaw   :  -18.91
$    Shoulder Pitch :   83.95
$    Elbow Pitch    :  -90.55
$    Wrist Pitch    :  -84.85
$    Wrist Yaw      :    4.24
$    Wrist Roll     :   38.97
$
$   THESE JOINT ANGLES ARE DEFINED WITH RESPECT TO THE LOCAL JOINT COORDINATE SYSTEMS FOUND
$   IN THE GWU FINITE ELEMENT MODEL, SECTION 2.1, FIGURE 2-5; ARM IN THE STOWED CONFIGURATION.
$
$*****************************************************************************************
$
$ THIS SECTION CONTAINS ALL DEFINED COORDINATE SYSTEMS
$
$  CS FOR ORBITER VISUAL AID ONLY - ONLY USED BY GRID POINTS 925001t925039
CORD2R  920600  204000 -58.842 1.847  -342.78 -58.842 1.847  -341.78 +
        -57.842 1.847  -342.78
$  PDA - FRAME
CORD2R  200000  0      -261.48 -132.82 190.95  -260.48 -132.82 190.95  +
        -261.48 -133.82 190.95
$  OSR (used for displ of support strt and slide beam)
CORD2R  200110  0      -789.48 503.18  200.95  -788.48 503.18  200.95  +
        -789.48 502.18  200.95
$  OSR (ORBITER STRUCTURAL REFERENCE FRAME)
CORD2R  204000  0      -789.48 503.18  200.95  -788.48 503.18  200.95  +
        -789.48 502.18  200.95
$  SSF FRAME - COINCIDENT WITH BASIC
CORD2R  250010  0      0.0     0.0     0.0     0.0     0.0     1.      +
        1.      0.0     0.0
$  STARBOARD ALPHA JOINT
CORD2R  250011  0      0.0     0.0     0.0     -.7879880.0     .615691 +
        .615691 0.0     .787988
$  SAME AS 250010
CORD2R  299999  0      0.0     0.0     0.0     0.0     0.0     1.      +
        1.      0.0     0.0
```

```
$ ORBITER PROPERTY REFERENCE FRAME
CORD2R 920402 0      -342.77758.842 -1.847 -341.77758.842 -1.847 +
      -342.77757.842 -1.847
$ ROCKWELL/SPAR INTERFACE POINT
CORD2R 920500 0      -709.177-117.478299.433-708.234-117.478299.766+
      -709.177-118.478299.433
$ SHOULDER YAW AXIS
CORD2R 920502 0      -698.805-117.478303.096-699.748-117.478302.763+
      -698.697-118.424302.790
$ SHOULDER PITCH AXIS
CORD2R 920503 0      -687.49 -117.478307.092-687.482-118.419306.752+
      -686.541-117.578307.391
$ ELBOW PITCH AXIS
CORD2R 920504 0      -449.196-148.218380.12 -450.145-148.109379.824+
      -449.197-149.158379.777
$ WRIST PITCH AXIS
CORD2R 920505 0      -443.776-409.982286.62 -443.86 -409.037286.935 +
      -444.721-409.958286.294
$ WRIST YAW AXIS
CORD2R 920506 0      -460.788-409.539280.755-460.872-408.594281.070+
      -461.754-409.539280.496
$ WRIST ROLL AXIS
CORD2R 920507 0      -489.766-409.526272.99 -489.677-408.586272.661+
      -490.732-409.526272.731
```

B.3 Deploy Configuration Coordinate Definition

```
$*****************************************************************************************
$
$         SRMS CONFIGURATION:  DEPLOY
$         ---------------------
$
$      DEPLOY IS AN ACTUAL CONFIGURATION USED DURING THE DEPLOYMENT OF THE SPAS SATELLITE ON
$      THE STS-07 SHUTTLE MISSION.  SPAS IS THE Shuttle PAllet Satellite FREE-FLYER SPACECRAFT.  IT IS
$      REPRESENTATIVE OF A TYPICAL SSF ASSEMBLY MODULE.  THIS CONFIGURATION REPRESENTS THE
$      ACTUAL DEPLOYMENT POSITIONING AT THE TIME OF THE SPAS RELEASE.
$
$   RELATIVE JOINT ANGLES IN DEGREES:
$
$   Swing-out      :   19.48
$   Shoulder Yaw   :  -89.96
$   Shoulder Pitch :  125.30
$   Elbow Pitch    : -108.61
$   Wrist Pitch    :  -21.17
$   Wrist Yaw      :   -0.04
$   Wrist Roll     :  110.00
$
$   THESE JOINT ANGLES ARE DEFINED WITH RESPECT TO THE LOCAL JOINT COORDINATE SYSTEMS FOUND
$   IN THE GWU FINITE ELEMENT MODEL, SECTION 2.1, FIGURE 2-5; ARM IN THE STOWED CONFIGURATION.
$
$*****************************************************************************************
$
$ THIS SECTION CONTAINS ALL DEFINED COORDINATE SYSTEMS
$
$  CS FOR ORBITER VISUAL AID ONLY - ONLY USED BY GRID POINTS 925001t925039
CORD2R 920600 204000 -58.842 1.847  -342.78 -58.842 1.847  -341.78 +
      -57.842 1.847  -342.78
```

```
$ PDA - FRAME
CORD2R 200000 0      -261.48 -132.82 190.95 -260.48 -132.82 190.95 +
      -261.48 -133.82 190.95
$ OSR (used for displ of support strt and slide beam)
CORD2R 200110 0      -789.48 503.18 200.95 -788.48 503.18 200.95 +
      -789.48 502.18 200.95
$ OSR (ORBITER STRUCTURAL REFERENCE FRAME)
CORD2R 204000 0      -789.48 503.18 200.95 -788.48 503.18 200.95 +
      -789.48 502.18 200.95
$ SSF FRAME - COINCIDENT WITH BASIC
CORD2R 250010 0      0.0    0.0    0.0    0.0    0.0    1.     +
      1.     0.0    0.0
$ STARBOARD ALPHA JOINT
CORD2R 250011 0      0.0    0.0    0.0    -.7879880.0    .615691 +
      .615691 0.0    .787988
$ SAME AS 250010
CORD2R 299999 0      0.0    0.0    0.0    0.0    0.0    1.     +
      1.     0.0    0.0
$ ORBITER PROPERTY REFERENCE FRAME
CORD2R 920402 0      -342.77758.842 -1.847 -341.77758.842 -1.847 +
      -342.77757.842 -1.847
$ ROCKWELL/SPAR INTERFACE POINT
CORD2R 920500 0      -709.177-117.478299.433-708.234-117.478299.766+
      -709.177-118.478299.433
$ SHOULDER YAW AXIS
CORD2R 920502 0      -698.805-117.478303.096-699.748-117.478302.763+
      -698.472-117.479302.153
$ SHOULDER PITCH AXIS
CORD2R 920503 0      -687.49 -117.478307.092-686.673-117.479306.515+
      -686.913-117.477307.908
$ ELBOW PITCH AXIS
CORD2R 920504 0      -537.763-117.233508.695-538.571-117.233508.105+
      -537.173-117.234507.888
$ WRIST PITCH AXIS
CORD2R 920505 0      -369.006-117.511287.758-369.972-117.511287.5  +
      -368.748-117.512286.792
$ WRIST YAW AXIS
CORD2R 920506 0      -364.361-117.529270.368-365.327-117.529270.11 +
      -364.103-117.529269.401
$ WRIST ROLL AXIS
CORD2R 920507 0      -356.62 -117.529241.384-356.289-116.589241.472+
      -356.362-117.529240.418
```

B.4 Capture Configuration Coordinate Definition

```
$*****************************************************************************************
$
$     SRMS CONFIGURATION:   CAPTURE
$     ----------------------
$
$     ON THE SIXTH SSF ASSEMBLY FLIGHT, THE ORBITER CARRIES THE U.S. LABORATORY MODULE TO THE
$     STAGE 5 STATION SPACE STATION.  THIS IS THE CONFIGURATION JUST WHEN THE END-EFFECTOR HAS
$     GRAPPLED THE STAGE 5 STATION.
$
$
$     RELATIVE JOINT ANGLES IN DEGREES:
$
```

```
$   Swing-out      :   19.48
$   Shoulder Yaw   : -109.24
$   Shoulder Pitch :   90.60
$   Elbow Pitch    :  -30.35
$   Wrist Pitch    :  -80.79
$   Wrist Yaw      :   18.10
$   Wrist Roll     :   26.12
$
$   THESE JOINT ANGLES ARE DEFINED WITH RESPECT TO THE LOCAL JOINT COORDINATE SYSTEMS FOUND
$   IN THE GWU FINITE ELEMENT MODEL, SECTION 2.1, FIGURE 2-5; ARM IN THE STOWED CONFIGURATION.
$
$*****************************************************************************************
$
$ THIS SECTION CONTAINS ALL DEFINED COORDINATE SYSTEMS
$
$ CS FOR ORBITER VISUAL AID ONLY - ONLY USED BY GRID POINTS 925001t925039
CORD2R  920600  204000  -58.842 1.847   -342.78 -58.842 1.847   -341.78 +
        -57.842 1.847   -342.78
$ PDA - FRAME
CORD2R  200000  0       -261.48 -132.82 190.95  -260.48 -132.82 190.95  +
        -261.48 -133.82 190.95
$ OSR (used for displ of support strt and slide beam)
CORD2R  200110  0       -789.48 503.18  200.95  -788.48 503.18  200.95  +
        -789.48 502.18  200.95
$ OSR (ORBITER STRUCTURAL REFERENCE FRAME)
CORD2R  204000  0       -789.48 503.18  200.95  -788.48 503.18  200.95  +
        -789.48 502.18  200.95
$ SSF FRAME - COINCIDENT WITH BASIC
CORD2R  250010  0       0.0     0.0     0.0     0.0     0.0     1.      +
        1.      0.0     0.0
$ STARBOARD ALPHA JOINT
CORD2R  250011  0       0.0     0.0     0.0     -.7879880.0     .615691 +
        .615691 0.0     .787988
$ SAME AS 250010
CORD2R  299999  0       0.0     0.0     0.0     0.0     0.0     1.      +
        1.      0.0     0.0
$ ORBITER PROPERTY REFERENCE FRAME
CORD2R  920402  0       -342.77758.842  -1.847  -341.77758.842  -1.847  +
        -342.77757.842  -1.847
$ ROCKWELL/SPAR INTERFACE POINT
CORD2R  920500  0       -709.177-117.478299.433-708.234-117.478299.766+
        -709.177-118.478299.433
$ SHOULDER YAW AXIS
CORD2R  920502  0       -698.805-117.478303.096-699.748-117.478302.763+
        -698.490-117.148302.205
$ SHOULDER PITCH AXIS
CORD2R  920503  0       -687.49 -117.478307.092-687.166-117.148306.205+
        -686.550-117.481307.434
$ ELBOW PITCH AXIS
CORD2R  920504  0       -449.645-116.269387.654-449.84 -115.983386.716+
        -448.670-116.105387.501
$ WRIST PITCH AXIS
CORD2R  920505  0       -177.584-72.446 350.853 -178.577-72.5619350.853+
        -177.620-72.1374349.902
$ WRIST YAW AXIS
CORD2R  920506  0       -178.232-66.8938333.743-179.225-67.0098333.743+
        -178.232-66.894 332.743
$ WRIST ROLL AXIS
CORD2R  920507  0       -178.231-66.8997303.743-179.174-66.5666303.743+
        -178.231-66.8999302.743
```

B.5 NASTRAN Bulk Data Cards for No DOSS Payload Specification

The Following corresponds to the grid point of the Payload Center of Mass. This is for the DOSS carrying no object.

```
$
$ THE FOLLOWING GRID POINT IS AT THE C.M. OF THE PAYLOAD
GRID    921777  920507  57.39   0.0360  -14.62  920507
$
$
$ THE FOLLOWING RBE2 CARD RIGIDLY ATTACHES THE PAYLOAD C.M. (GRID POINT 921777) TO THE
$ END-EFFECTOR (GRID POINT 921703) OF THE SRMS.
RBE2    950703  921703  123456  921777
$
$
$ PAYLOAD ENTRY
$
$ THE FOLLOWING CONM2 IS FOR THE PAYLOAD, WHICH IS THE DOSS (DEXTROUS ORBITAL
$ SERVICING SYSTEM) MANIPULATOR ARM (NO PAYLOAD IS ATTACHED TO THE END OF THE DOSS
$ ARM). THE DOSS ARM IS ATTACHED TO THE END-EFFECTOR OF THE SRMS. THESE INERTIAS
$ CORRESPOND TO AN AXIS PARALLEL TO THE WRIST ROLL JOINT LOCATED AT THE PAYLOAD
$ C.M.
CONM2   950751  921777  920507  0.50738 0.0     0.0     0.0             +
      16.0167 2.5-3   241.917 -24.033 -.01267 239.15
```

B.6 NASTRAN Bulk Data Cards for with the 1000 lb. DOSS Payload Specification

The Following corresponds to the grid point of the Payload Center of Mass. This is for the DOSS carrying the 1000 lb. object.

```
$
$ THE FOLLOWING GRID POINT IS AT THE C.M. OF THE PAYLOAD
GRID    921777  920507  98.06   5.9-3   -14.48  920507
$
$
$ THE FOLLOWING RBE2 CARD RIGIDLY ATTACHES THE PAYLOAD C.M. (GRID POINT 921777) TO THE
$ END-EFFECTOR (GRID POINT 921703) OF THE SRMS.
RBE2    950703  921703  123456  921777
$
$
$ PAYLOAD ENTRY
$
$ THE FOLLOWING CONM2 IS FOR THE PAYLOAD, WHICH IS THE DOSS (DEXTROUS ORBITAL
$ SERVICING SYSTEM) MANIPULATOR ARM (A 1000 LB. PAYLOAD IS ALSO ATTACHED TO THE END
$ OF THE DOSS ARM, WITH A RADIUS OF 18 INCHES AND HEIGHT OF 48 INCHES). THE DOSS ARM
$ IS ATTACHED TO THE END-EFFECTOR OF THE SRMS. THESE INERTIAS CORRESPOND TO AN AXIS
$ PARALLEL TO THE WRIST ROLL JOINT LOCATED AT THE PAYLOAD C.M.
CONM2   950751  921777  920507  3.095   0.0     0.0     0.0             +
      722.45  4.167-4 1957.96 -34.933 -2.08-3 1667.933
```

APPENDIX C. DERIVATION OF JOINT STIFFNESS IN THE FINITE ELEMENT MODEL

This Appendix contains the development, as given by [19], for determining the stiffness of an SRMS joint that is used in the GWU finite element model to simulate the brakes locked mode of the SRMS (section C.1). Also discussed, is the development for lumping link flexibility with joint flexibility, section C.2. Section C.3 contains the values of the joint stiffnesses for each of the four SRMS configurations studied, as used in the GWU finite element model using the GENEL bulk data card.

C.1 Joint Flexibility

To derive the stiffness matrix for a joint consider the potential energy for a system of torsional springs

$$U_r = \frac{1}{2} G_r^T F_{rr} G_r \tag{C-1}$$

where,

U_r = joint r potential energy,
G_r = vector of joint r torques, and
F_{rr} = joint r flexibility matrix

and the inverse of F_{rr} yields the stiffness matrix of joint r $\left(F_{rr}^{-1} = K_{rr}\right)$. Since the joint stiffness is composed of an inboard and an outboard stiffness, equation (C-1) can be written in two parts as

$$U_r = \left(\frac{1}{2} G_r^T \bar{F}_{rr}^T G_r\right)_{outboard} + \left(\frac{1}{2} G_r^T \bar{F}_{rr}^T G_r\right)_{inboard} \qquad \text{(C-2)}$$

where, $\bar{F}_{rr}$ is the flexibility matrix at a point due to the joint only. Expanding the inboard and outboard terms in equation (C-2) obtains

$$\begin{aligned} U_r = & \frac{1}{2}\left\{G_u^r \;\; G_v^{ro} \;\; G_w^{ro}\right\} diag\left[0 \;\; , \frac{1}{K_v^{ro}} \;\; , \frac{1}{K_w^{ro}}\right]\begin{Bmatrix} G_u^r \\ G_v^{ro} \\ G_w^{ro} \end{Bmatrix} \\ & + \frac{1}{2}\left\{G_u^r \;\; G_v^{ri} \;\; G_w^{ri}\right\} diag\left[\frac{1}{K_u^r} \;\; , \frac{1}{K_v^{ri}} \;\; , \frac{1}{K_w^{ri}}\right]\begin{Bmatrix} G_u^r \\ G_v^{ri} \\ G_w^{ri} \end{Bmatrix} \end{aligned} \qquad \text{(C-3)}$$

where G_u^r is the primary joint r drive axis torque, and G_v^{ro}, G_w^{ro}, G_v^{ri}, G_w^{ri} are the outboard and inboard joint r torques along the two freeplay axes (subscripts *u* and *v*), respectively. The superscripts *o* and *i* denote outboard and inboard, respectively. The (1,1) element of the outboard flexibility matrix is zero because the K_u^r drive stiffness is considered part of the inboard portion of the joint, thus producing no contribution to the outboard matrix.

The torsional springs of a joint can be seen in Figure C-1 (or in Figure 2-8), where the spring K_u^r is normal to the plane of the page.

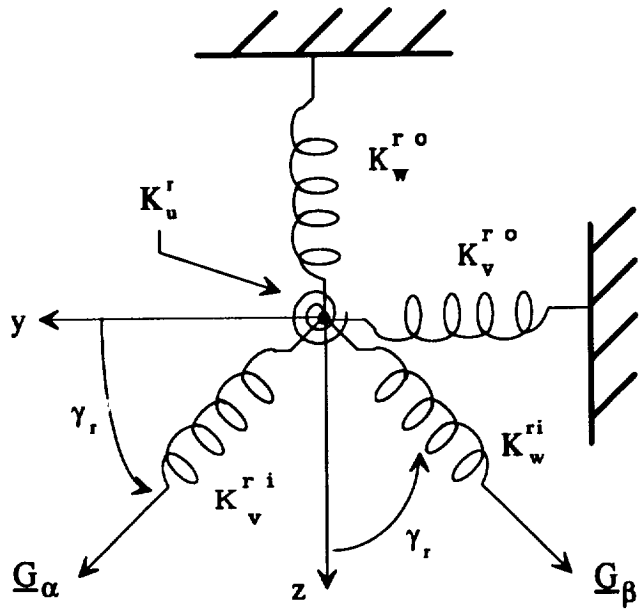

Figure C-1: Torsional Spring Representation of Joint r.[19]

From Figure C-1 the joint r outboard torque vector can be written as

$$\begin{Bmatrix} G_u^r \\ G_v^{ro} \\ G_w^{ro} \end{Bmatrix} = \left[R^{r-1,r}\right] \begin{Bmatrix} G_\gamma^r \\ G_\alpha^r \\ G_\beta^r \end{Bmatrix} = \begin{bmatrix} 1 & 0 & 0 \\ 0 & \cos\gamma_r & -\sin\gamma_r \\ 0 & \sin\gamma_r & \cos\gamma_r \end{bmatrix} \begin{Bmatrix} G_\gamma^r \\ G_\alpha^r \\ G_\beta^r \end{Bmatrix} \tag{C-4}$$

where, $\left[R^{r-1,r}\right]$ is the transformation from body r to body r - 1 coordinates and were given in equations (2-1) through (2-3). Also, the joint r inboard torque vector can be written as

$$\left\{G_u^r \;\; G_v^{ri} \;\; G_w^{ri}\right\}^T = \left\{G_\gamma^r \;\; G_\alpha^r \;\; G_\beta^r\right\}^T \tag{C-5}$$

where, G_γ^r, G_α^r, and G_β^r are the joint r torques along the primary drive axis, and freeplay axes, respectively. Now, substituting equations (C-4) and (C-5) into (C-3) yields

$$\begin{aligned} U_r = \frac{1}{2}\left\{G_\gamma^r \;\; G_\alpha^r \;\; G_\beta^r\right\}\left[R^{r-1,r}\right]^T diag\left[0 \;\; , \frac{1}{K_v^{ro}} \;\; , \frac{1}{K_w^{ro}}\right]\left[R^{r-1,r}\right]\begin{Bmatrix} G_\gamma^r \\ G_\alpha^r \\ G_\beta^r \end{Bmatrix} \\ + \;\; \frac{1}{2}\left\{G_\gamma^r \;\; G_\alpha^r \;\; G_\beta^r\right\} diag\left[\frac{1}{K_u^r} \;\; , \frac{1}{K_v^{ri}} \;\; , \frac{1}{K_w^{ri}}\right]\begin{Bmatrix} G_\gamma^r \\ G_\alpha^r \\ G_\beta^r \end{Bmatrix} \end{aligned} \tag{C-6}$$

Combining terms, equation (C-6) may be rewritten as

$$U_r = \frac{1}{2}\left\{G_\gamma^r \;\; G_\alpha^r \;\; G_\beta^r\right\} \bar{F}_{rr} \begin{Bmatrix} G_\gamma^r \\ G_\alpha^r \\ G_\beta^r \end{Bmatrix}$$

where $\bar{F}_{rr}$ is defined as

$$\begin{aligned} \bar{F}_{rr} = \left[R^{r-1,r}\right]^T diag\left[0 \;\; , \frac{1}{K_v^{ro}} \;\; , \frac{1}{K_w^{ro}}\right]\left[R^{r-1,r}\right] \\ + \;\; diag\left[\frac{1}{K_u^r} \;\; , \frac{1}{K_v^{ri}} \;\; , \frac{1}{K_w^{ri}}\right] \end{aligned} \tag{C-7}$$

Equation (C-7) represents the flexibility of a joint. As stated in section 2.2.2.2, because a link is modeled as rigid, its flexibility should be included in the surrounding joint (discussed in the next section).

C.2 Link Flexibility

To lump link flexibility at the joint, consider a simple cantilever beam shown in Figure C-2. The following procedure parallels that of Abelow [19].

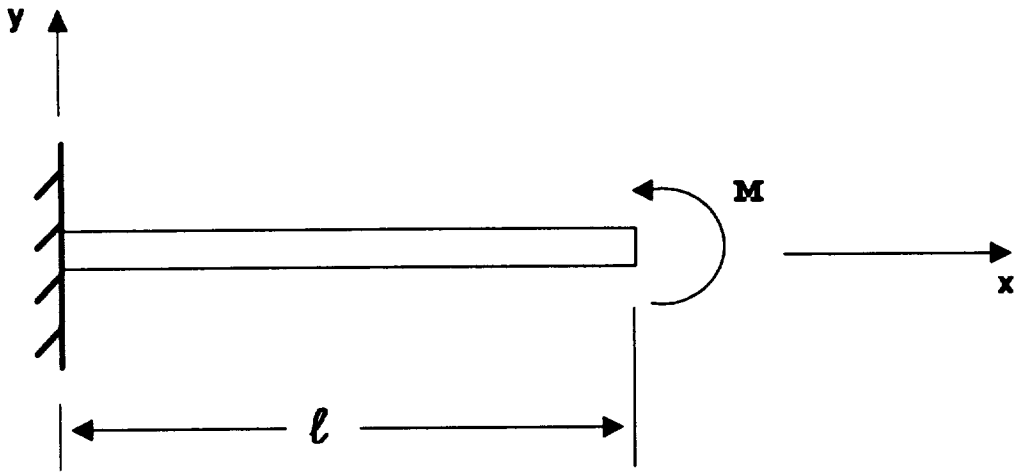

Figure C-2: A Simple Cantilever Beam.

From Euler-Bernoulli beam theory[27], we know that

$$M = EI\frac{d\theta}{dx} \tag{C-8}$$

where M is the applied bending moment, EI is the bending stiffness of beam, and θ is the angular displacement. Assuming M and EI are constant, integrating equation (C-8) results in

$$Mx = EI\,\theta(x) \tag{C-9}$$

Desiring the angular displacement at the end of the beam, $x = l$, and comparing equation (C-9) to $T = K_{bend}\,\theta$, produces

$$K_{bend} = \frac{EI}{l}$$

and the link flexibility due to bending, f_{bend}, whose inverse yields the stiffness constant, K_{bend}, is

$$f_{bend} = \frac{1}{K_{bend}} = \frac{l}{EI} \tag{C-10}$$

Similarly, the link flexibility due to torsion is

$$K_{tor} = \frac{T}{\theta} = \frac{GJ}{l}$$

$$f_{tor} = \frac{1}{K_{tor}} = \frac{l}{GJ} \tag{C-11}$$

Equations (C-10) and (C-11) represent the bending and torsional flexibility of the link connected to the joint, respectively.

The above discussion pertains to a single beam. The links of the SRMS, however, are composed of three sections each, except links 1 and 7, which are

composed of one and two sections, respectively. Generalizing equations (C-10) and (C-11) for a link of N sections, produces

$$f_{bend} = \left(\frac{l}{EI}\right)_{section1} + \left(\frac{l}{EI}\right)_{section2} + \cdots + \left(\frac{l}{EI}\right)_{sectionN}$$

$$f_{tor} = \left(\frac{l}{GJ}\right)_{section1} + \left(\frac{l}{GJ}\right)_{section2} + \cdots + \left(\frac{l}{GJ}\right)_{sectionN}$$

Setting the appropriate value for N, we obtain the following link section flexibility matrices.

Link's 1 (N = 1, j = 1) and 2 (N = 3, j = 2):

$$f_{j,j+1} = diag\left[\frac{l}{EI}, \frac{l}{EI}, \frac{l}{GJ}\right]_{j,j+1} \tag{C-12}$$

Link's 5 (N = 3, j = 5), 6 (N = 3, j = 6), and 7 (N = 2, j = 7):

$$f_{j,j+1} = diag\left[\frac{l}{GJ}, \frac{l}{EI}, \frac{l}{EI}\right]_{j,j+1} \tag{C-13}$$

Links 1 and 2 have their torsion axes in the local z-axis, hence the (3,3) term in equation (C-12). Likewise, links 5, 6, and 7 have torsion in the local x-axis, hence the (1,1) term in equation (C-13). With the use of equations (C-12) and (C-13), the total flexibility matrix for all the links are

$$f_{link1} = f_{12} \tag{C-14}$$

$$f_{link\,j} = f_{j',j+1} + f_{j,j+1} + f_{j,(j+1)'} \qquad j = 2,5,6 \qquad \text{(C-15)}$$

C.3 Joint Stiffness Values for the Four Configurations

Joint stiffnesses simulating the brakes locked mode of the SRMS are given for the Unberth, Low Hover, Deploy, and Capture Configurations. These stiffnesses are given with respect to the GWU finite element model joint coordinate axes, Figure 2-5. These values correspond to the GENEL cards for the joint in the finite element model. They were obtained from using of equations (2-10) through (2-13), and transforming to the aforementioned coordinates by use of equation (2-14).

C.3.1 Unberth Configuration

Local Joint Torsional Stiffnesses of the SRMS in the joint coordinate systems of the GWU Finite Element Model, Section 2.1, Figure 2-5 Units of (lb-in)/rad

Shoulder Yaw Joint

K22 =

1.911848063678970e+07	3.040987591877203e+05	0
3.040987591877204e+05	1.601958164585835e+07	0
0	0	3.003468009095823e+07

Shoulder Pitch Joint

K33 =

1.201463436096261e+07	0	-1.150703385052052e+06
0	5.456913794621721e+07	0
-1.150703385052052e+06	0	9.837743822018737e+06

Elbow Pitch Joint

K44 =

7.514584215769522e+06	0	-2.409055603550879e+05
0	1.383600000000000e+07	0
-2.409055603550879e+05	0	1.000899225035918e+07

Wrist Pitch Joint

K55 =

2.263802528597231e+06	0	3.933258134456233e-11
0	3.960000000000000e+06	0
-3.933258134456233e-11	0	1.247602559627690e+07

Wrist Yaw Joint

K66 =

2.336888177391539e+06	-1.521232779706134e+04	0
-1.521232779706137e+04	2.141709006274836e+06	0
0	0	2.085744476236710e+06

Wrist Roll Joint

K77 =

1.428113408568125e+06	0	0
0	8.253489020983370e+05	2.023138402665436e+04
0	2.023138402665431e+04	1.056830987321372e+06

C.3.2 Low Hover Configuration

Local Joint Torsional Stiffnesses of the SRMS in the joint coordinate systems of the GWU Finite Element Model, Section 2.1, Figure 2-5 Units of (lb-in)/rad

Shoulder Yaw Joint

K22 =

1.894678423231506e+07	6.056437091913476e+05	0
6.056437091913471e+05	1.616897208998024e+07	0
0	0	3.003468009095823e+07

Shoulder Pitch Joint

K33 =

1.225476415482335e+07	0	-4.510339435809759e+05
0	5.456913794621721e+07	0
-4.510339435809758e+05	0	9.519384851766601e+06

Elbow Pitch Joint

K44 =

7.584884689494650e+06	0	-6.482944968619466e+03
0	1.383600000000000e+07	0
-6.482944968619466e+03	0	9.869394279886385e+06

Wrist Pitch Joint

K55 =

2.263802528597231e+06	0	2.270064874584660e-12
0	3.960000000000000e+06	0
-2.270064874584660e-12	0	1.247602559627691e+07

Wrist Yaw Joint

K66 =

2.336986922313783e+06	-1.456475933100725e+04	0
-1.456475933100724e+04	2.141610261352593e+06	0
0	0	2.085744476236710e+06

Wrist Roll Joint

K77 =

1.428113408568125e+06	0	0
0	8.315076621523750e+05	2.329274695014474e+04
0	2.329274695014474e+04	1.047266096688970e+06

C.3.3 Deploy Configuration

Local Joint Torsional Stiffnesses of the SRMS in the joint coordinate systems of the GWU Finite Element Model, Section 2.1, Figure 2-5 Units of (lb-in)/rad

Shoulder Yaw Joint

K22 =

1.705886428473695e+07	1.369463376501180e+03	0
1.369463376501182e+03	1.781162267604373e+07	0
0	0	3.003468009095823e+07

Shoulder Pitch Joint

K33 =

1.105984212563868e+07	0	2.065805731816524e+06
0	5.456913794621721e+07	0
2.065805731816524e+06	0	1.110358704769834e+07

Elbow Pitch Joint

K44 =

7.536642007002129e+06	0	-2.048225414292739e+05
0	1.383600000000000e+07	0
-2.048225414292739e+05	0	9.965191366438763e+06

Wrist Pitch Joint

K55 =

2.263802528597231e+06	0	-2.591752459827310e-11
0	3.960000000000000e+06	0
2.591752459827310e-11	0	1.247602559627691e+07

Wrist Yaw Joint

K66 =

2.338066618584342e+06	1.379062706189077e+02	0
1.379062706189077e+02	2.140530565082034e+06	0
0	0	2.085744476236710e+06

Wrist Roll Joint

K77 =

1.428113408568125e+06	0	0
0	8.500618153239778e+05	-1.522657424524190e+04
0	-1.522657424524190e+04	1.018450483756157e+06

C.3.4 Capture Configuration

Local Joint Torsional Stiffnesses of the SRMS in the joint coordinate systems of the GWU Finite Element Model, Section 2.1, Figure 2-5 Units of (lb-in)/rad

Shoulder Yaw Joint

K22 =

1.728651883611892e+07	-6.108158795757880e+05	0
-6.108158795757880e+05	1.761354389482881e+07	0
0	0	3.003468009095823e+07

Shoulder Pitch Joint

K33 =

1.229473817841796e+07	0	4.503462282386083e+04
0	5.456913794621721e+07	0
4.503462282386085e+04	0	9.466388142013069e+06

Elbow Pitch Joint

K44 =

7.225659302489298e+06	0	3.004709084071611e+05
0	1.383600000000000e+07	0
3.004709084071612e+05	0	1.058271998469349e+07

Wrist Pitch Joint

K55 =

2.263802528597231e+06	0	1.330098313450107e-11
0	3.960000000000000e+06	0
-1.330098313450107e-11	0	1.247602559627690e+07

Wrist Yaw Joint

K66 =

2.319000547221646e+06	-5.833301324046495e+04	0
-5.833301324046506e+04	2.159596636444729e+06	0
0	0	2.085744476236710e+06

Wrist Roll Joint

K77 =

1.428113408568125e+06	0	0
0	8.237707341465051e+05	1.887333001311111e+04
0	1.887333001311112e+04	1.059281968318584e+06

APPENDIX D. MODE SHAPES OF CONFIGURATION S WITH A 32000 LB. PAYLOAD FROM CSDL-STARDYNE AND GWU FINITE ELEMENT MODELS

This Appendix contains 10 mode shapes of the Shuttle Remote Manipulator System in configuration S with brakes locked. Configuration S is when the arm is straight up; the distance from the arm attachment point to the end-effector is maximum. The joint angles for this configuration may be found in Table 4-2, and a picture of the configuration in Figure 4-5. The gray, or lightly colored curve corresponds to the undeformed configuration, and the darker curve is the mode shape. A 32000 lb. homogeneous, right circular cylinder is used as a payload (see section 4.2). Comparison is made between the GWU (top graph) and CSDL-STARDYNE (bottom graph) finite element models. Both finite element models yield mode shapes, which in a qualitative sense (since no actual numbers of the mode shapes were available), yield very good agreement. Mode shapes 1 through 4 produce substantial end-effector motions, while mode shapes 5 through 10 produce essentially no end-effector displacements.

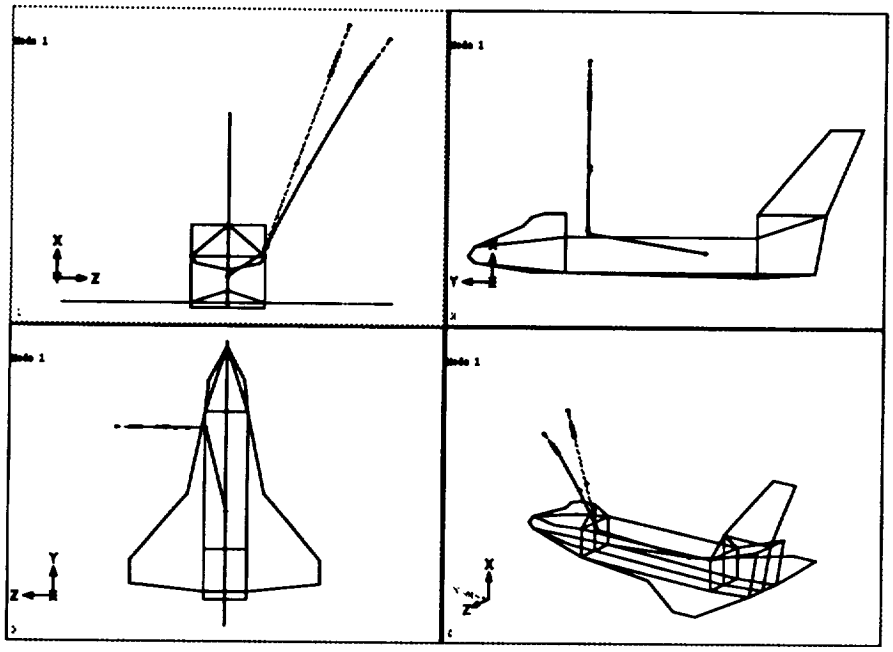

(a) GWU Mode 1.

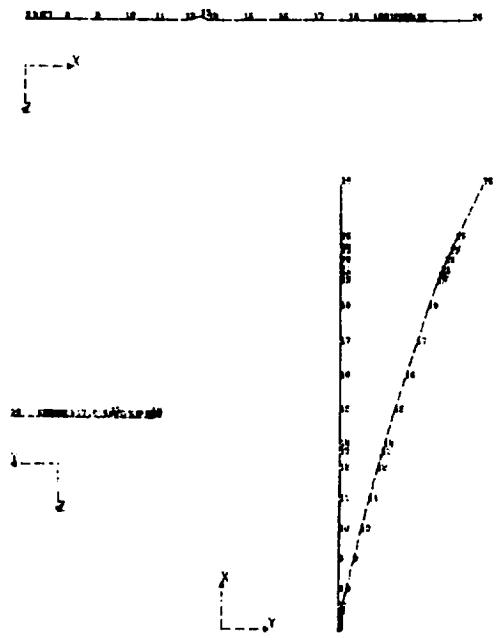

(b) CSDL-STARDYNE Mode 1.

Figure D-1: Comparison of Configuration S Mode Shape 1 from (a) GWU and (b) CSDL-STARDYNE Finite Element Models.

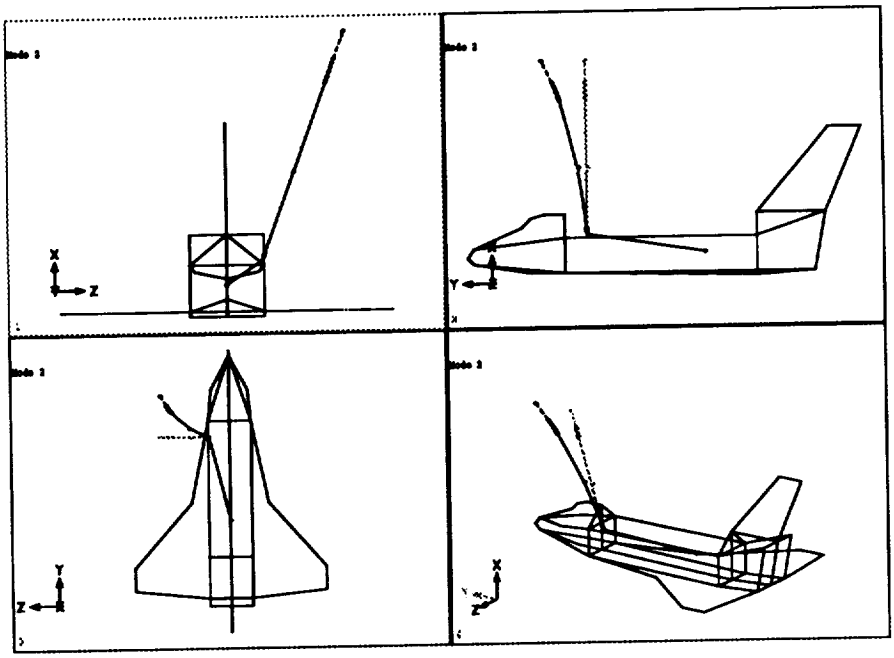

(a) GWU Mode 2.

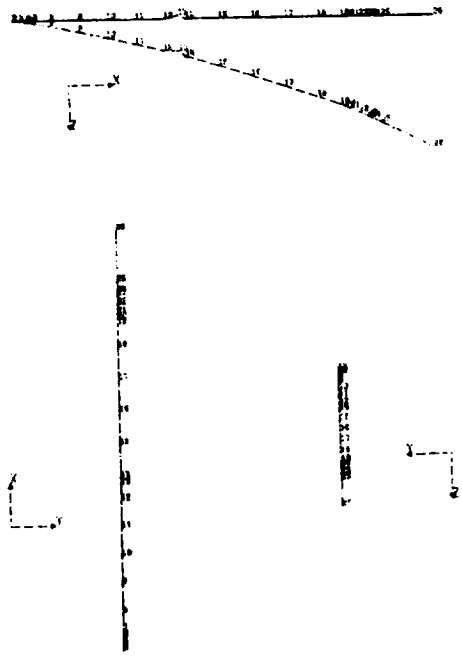

(b) CSDL-STARDYNE Mode 2.

Figure D-2: Comparison of Configuration S Mode Shape 2 from (a) GWU and (b) CSDL-STARDYNE Finite Element Models.

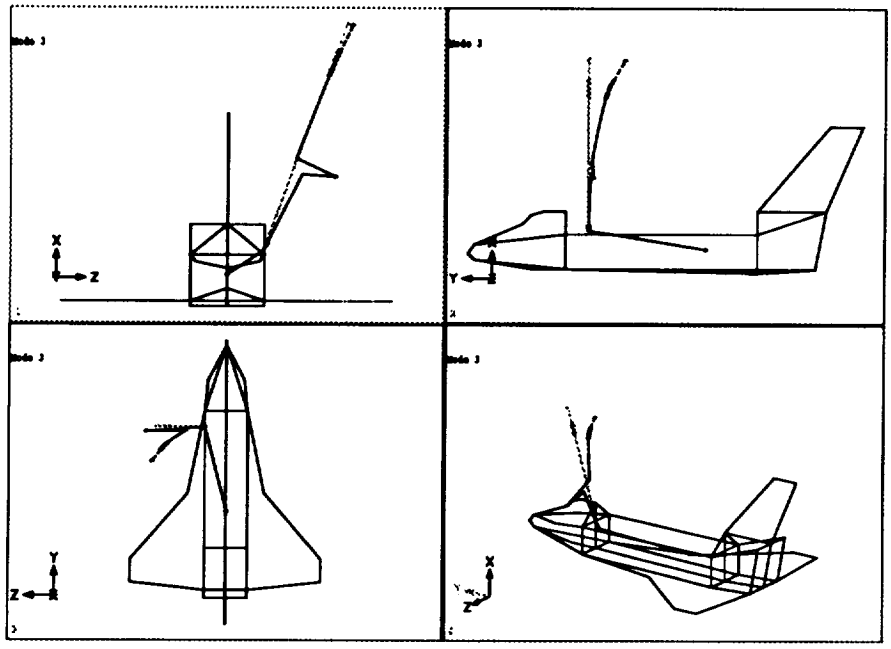

(a) GWU Mode 3.

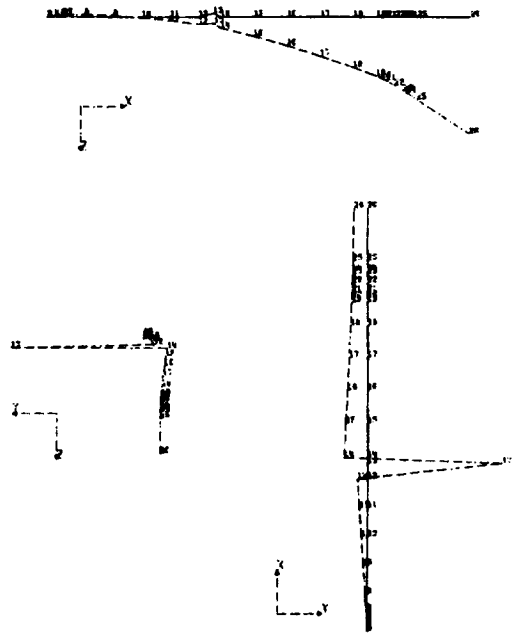

(b) CSDL-STARDYNE Mode 3.

Figure D-3: Comparison of Configuration S Mode Shape 3 from (a) GWU and (b) CSDL-STARDYNE Finite Element Models.

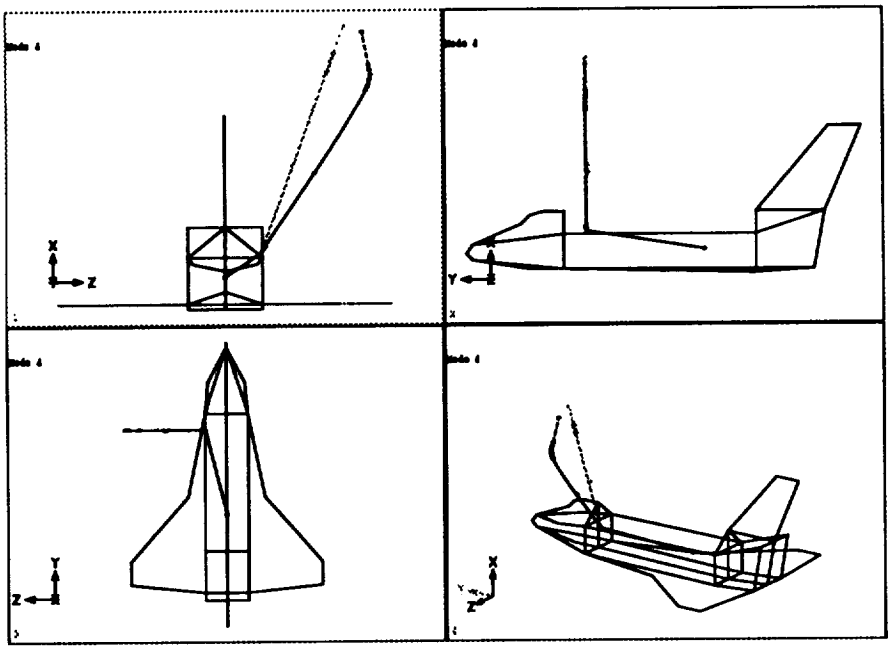

(a) GWU Mode 4.

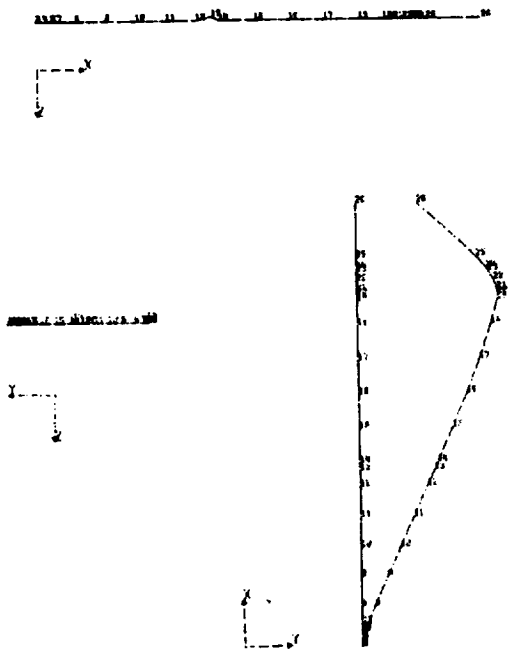

(b) CSDL-STARDYNE Mode 4.

Figure D-4: Comparison of Configuration S Mode Shape 4 from (a) GWU and (b) CSDL-STARDYNE Finite Element Models.

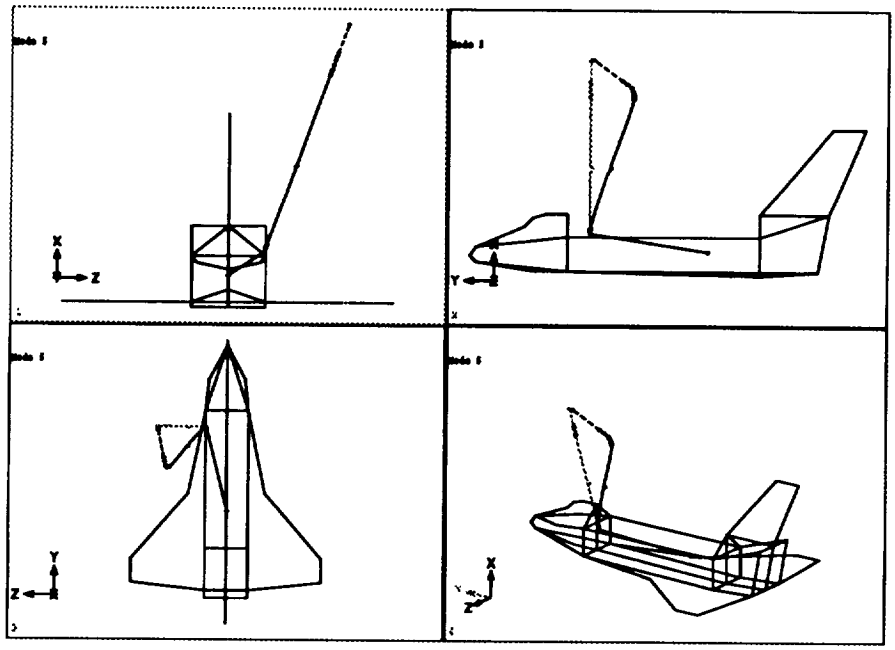

(a) GWU Mode 5.

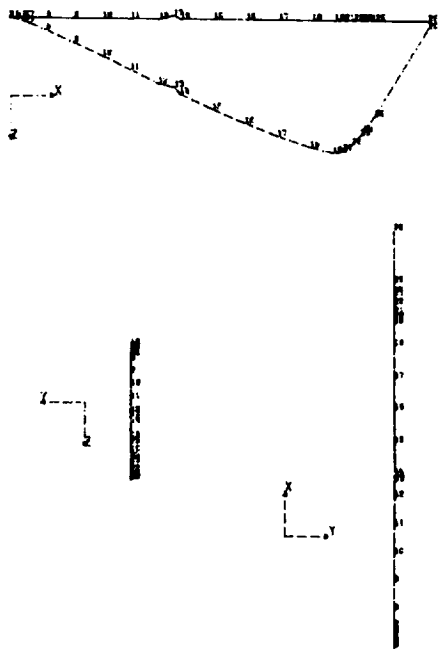

(b) CSDL-STARDYNE Mode 5.

Figure D-5: Comparison of Configuration S Mode Shape 5 from (a) GWU and (b) CSDL-STARDYNE Finite Element Models.

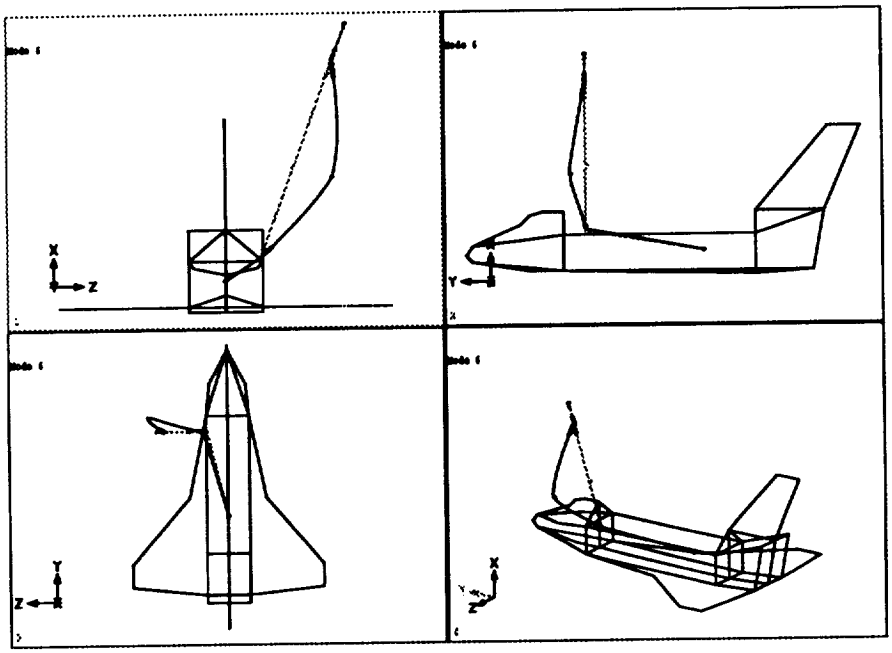

(a) GWU Mode 6.

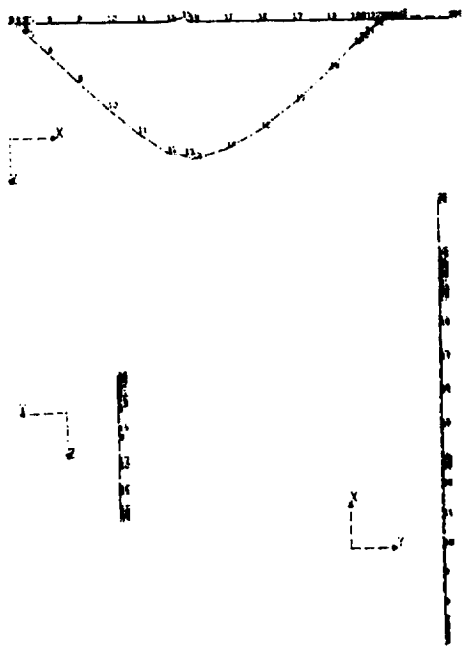

(b) CSDL-STARDYNE Mode 6.

Figure D-6: Comparison of Configuration S Mode Shape 6 from (a) GWU and (b) CSDL-STARDYNE Finite Element Models.

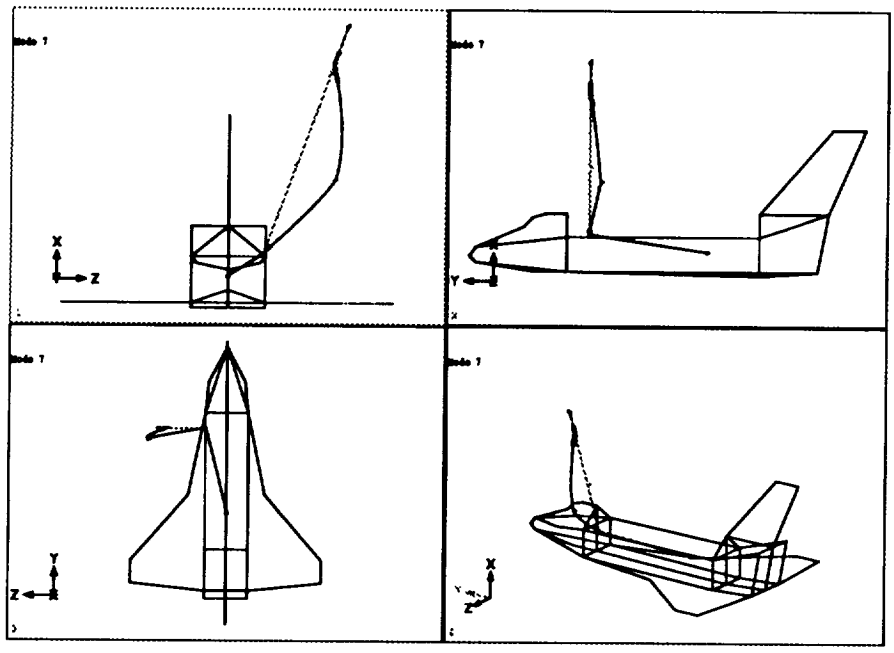

(a) GWU Mode 7.

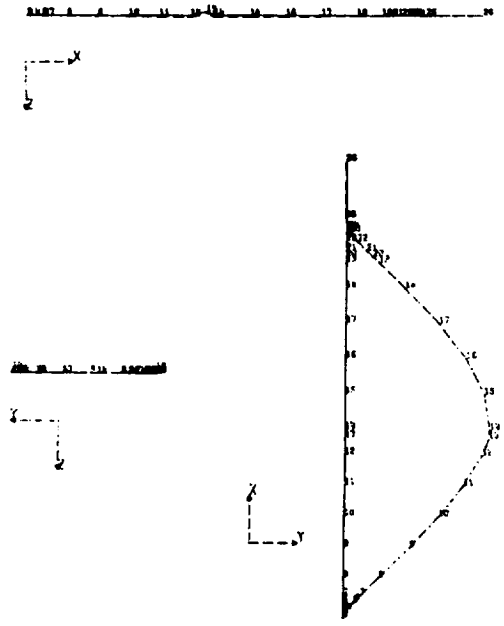

(b) CSDL-STARDYNE Mode 7.

Figure D-7: Comparison of Configuration S Mode Shape 7 from (a) GWU and (b) CSDL-STARDYNE Finite Element Models.

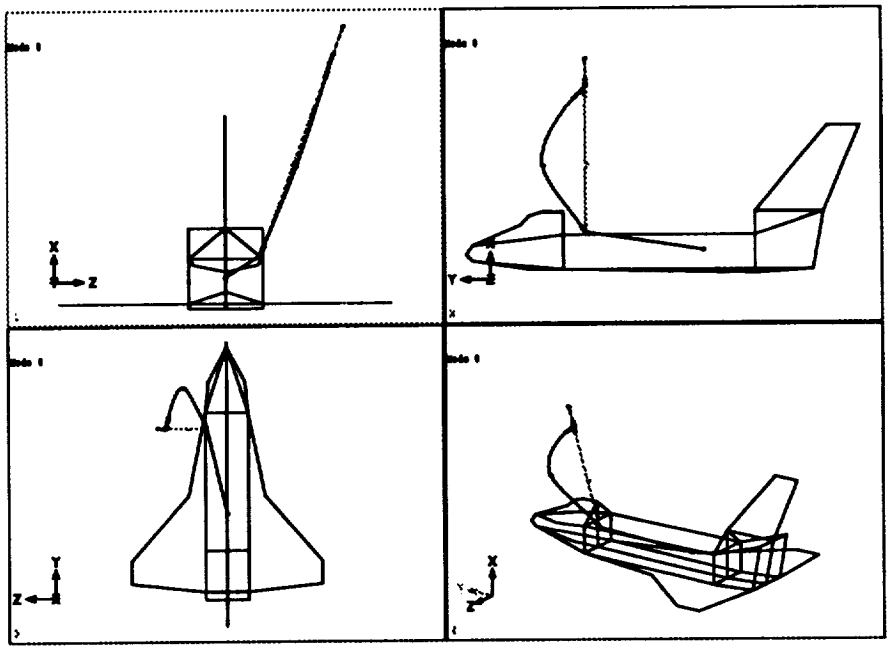

(a) GWU Mode 8.

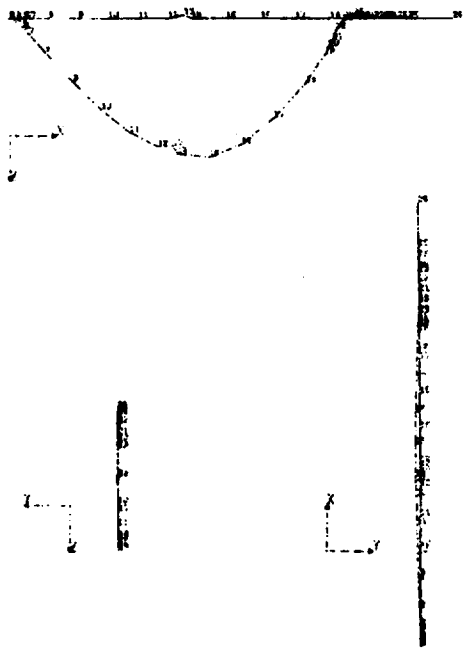

(b) CSDL-STARDYNE Mode 8.

Figure D-8: Comparison of Configuration S Mode Shape 8 from (a) GWU and (b) CSDL-STARDYNE Finite Element Models.

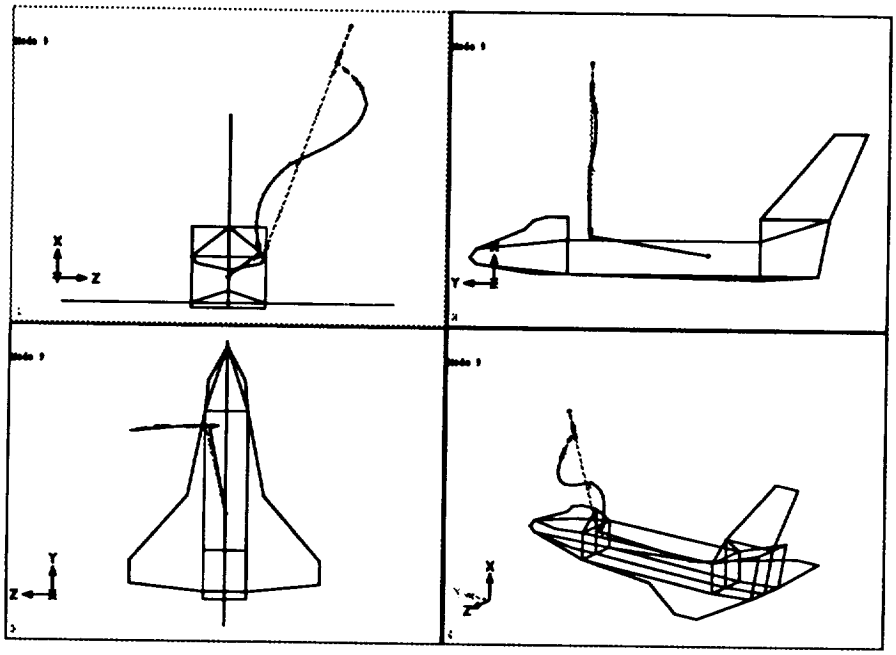

(a) GWU Mode 9.

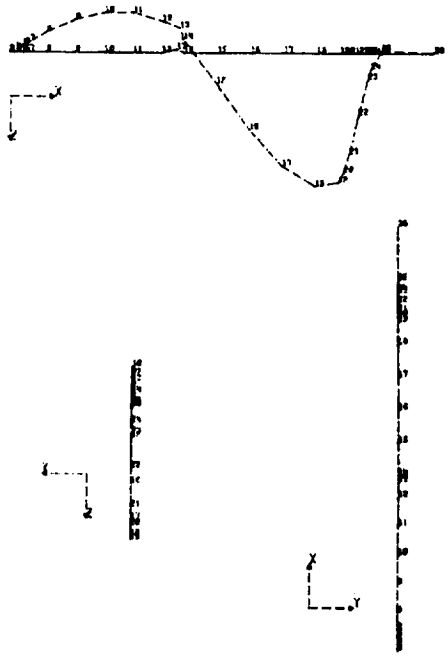

(b) CSDL-STARDYNE Mode 9.

Figure D-9: Comparison of Configuration S Mode Shape 9 from (a) GWU and (b) CSDL-STARDYNE Finite Element Models.

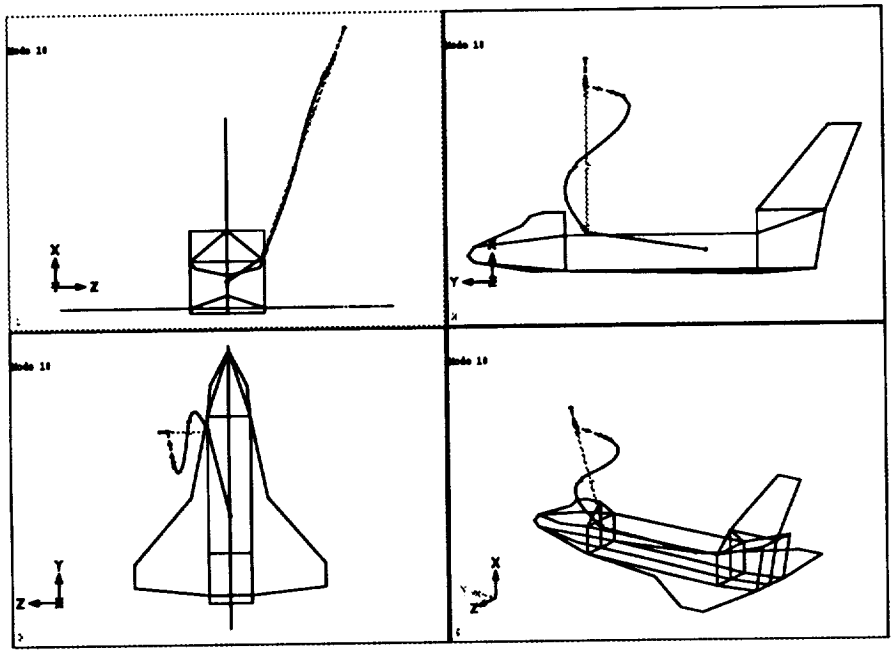

(a) GWU Mode 10.

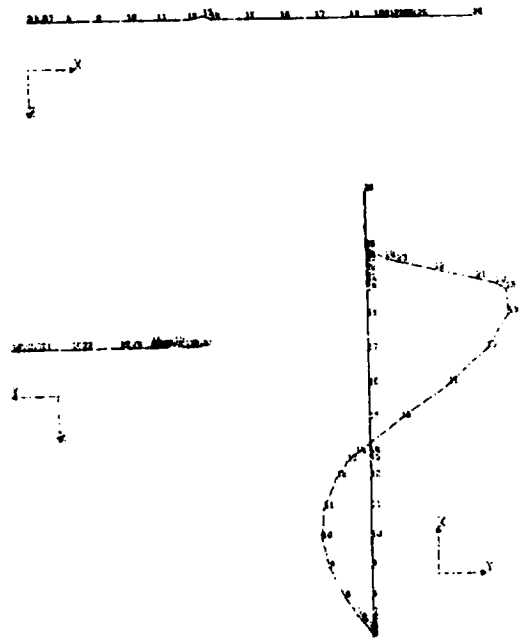

(b) CSDL-STARDYNE Mode 10.

Figure D-10: Comparison of Configuration S Mode Shape 10 from (a) GWU and (b) CSDL-STARDYNE Finite Element Models.

APPENDIX E. THE DEXTROUS ORBITAL SERVICING SYSTEM (DOSS) MANIPULATOR

The DOSS arm is a seven degree-of-freedom, seven-link, redundant manipulator. It consists of shoulder roll, yaw, and pitch joints, an elbow pitch joint, and wrist pitch, yaw, and roll joints. The manipulator is redundant because it has one more degree-of-freedom than general 3-D tasks require (i.e., six degree-of-freedom manipulator). Figure E.1 shows a photograph of the DOSS manipulator, and Figure E.2 illustrates the link dimensions and center of mass locations. The arm weighs approximately 250 lbs. and is 6.72 feet when fully extended (from shoulder yaw joint to end-effector tip). Table E-1 lists the weights of each section of the DOSS manipulator. Table E-2 lists the design torque capabilities of the space based, electrically driven manipulator.

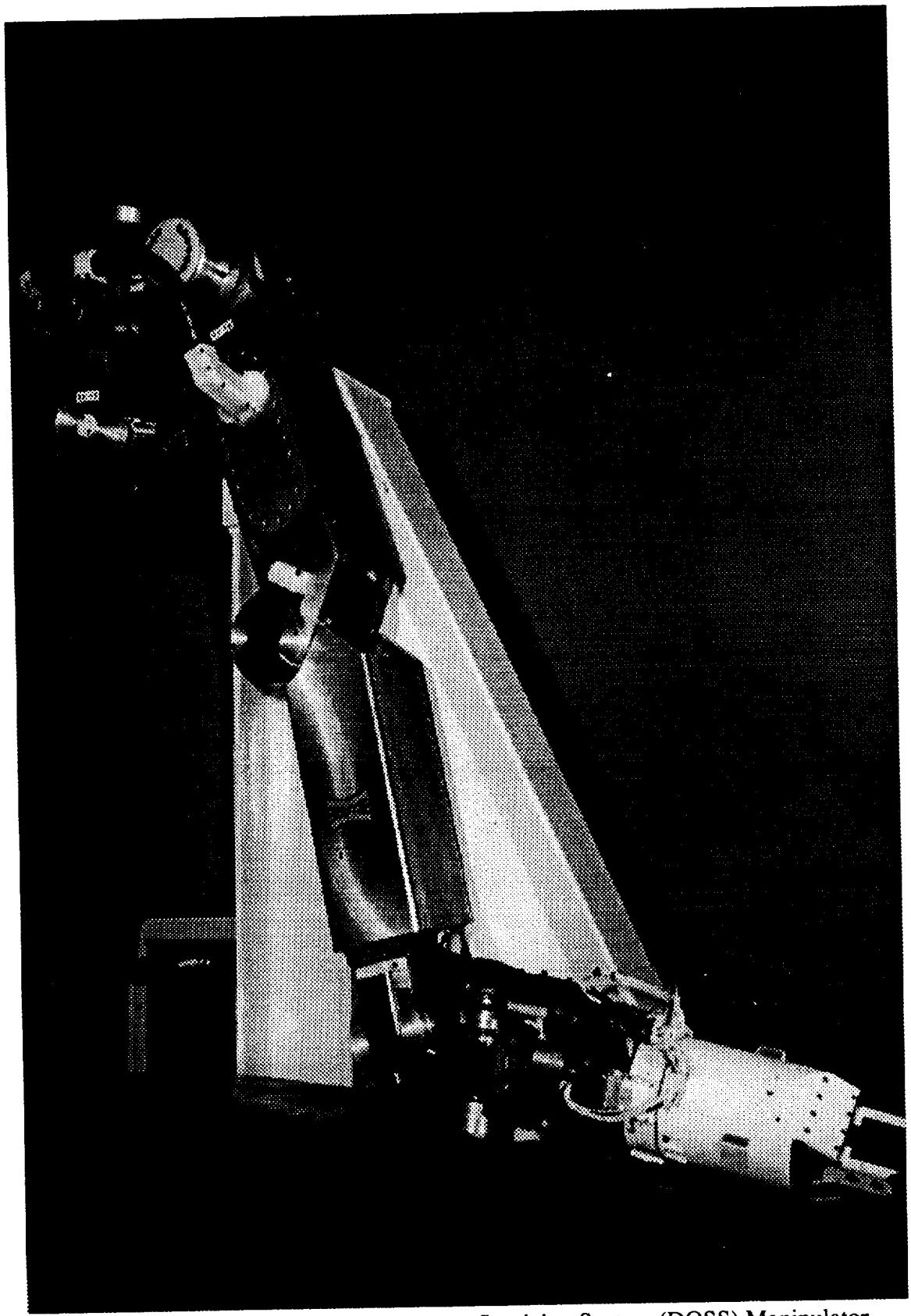

Figure E-1: Photograph of the Dextrous Servicing System (DOSS) Manipulator.

C-3

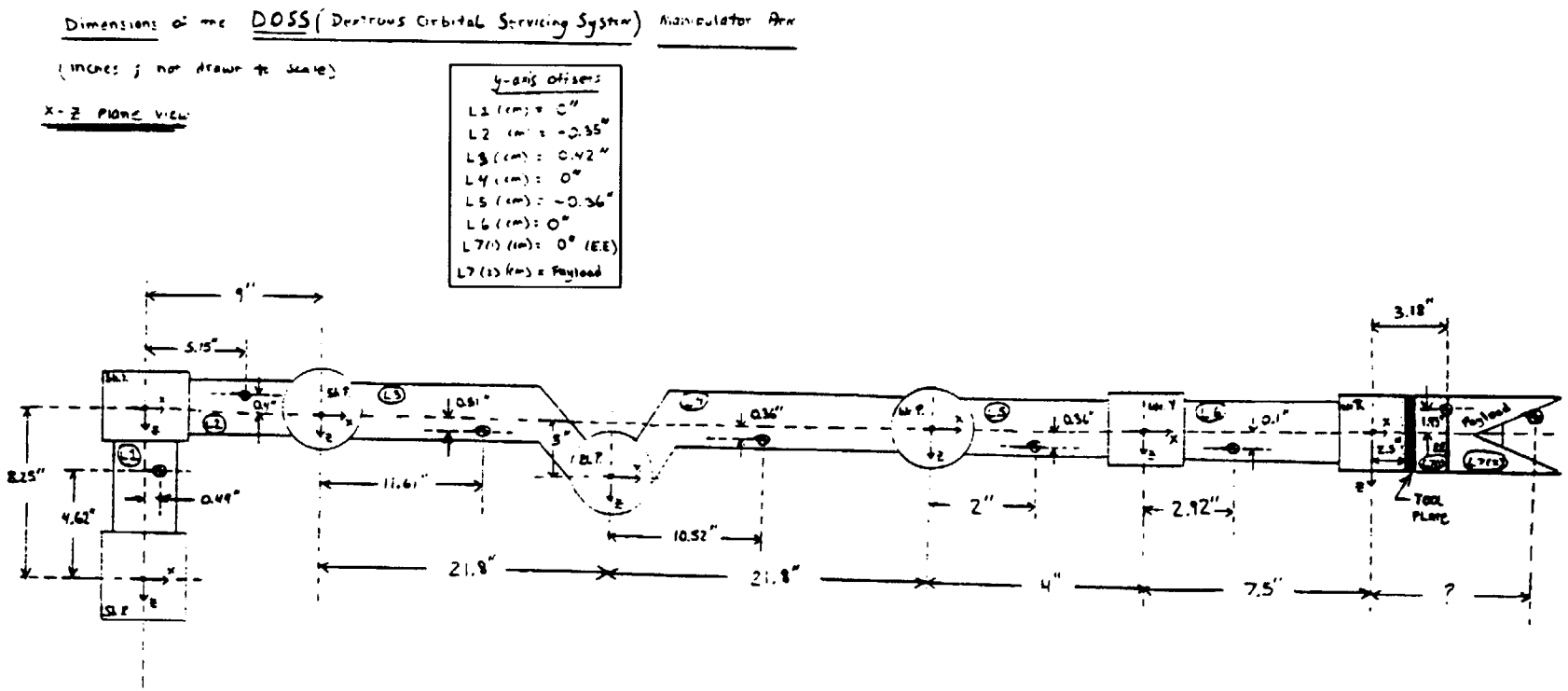

Figure E-2: DOSS Manipulator Showing Link Dimensions and Center of Mass Locations.

Table E-1: DOSS Manipulator Masses and Weights of Indicated Sections.[27]

Description	Mass (slugs)	Weight (lbs.)
Shoulder Roll to Shoulder Yaw	0.6577	21.18
Shoulder Yaw to Shoulder Pitch	0.6126	19.73
Shoulder Pitch to Elbow Pitch	1.4367	46.26
Elbow Pitch to Wrist Pitch	1.1308	36.41
Wrist Pitch to Wrist Yaw	0.4725	15.21
Wrist Yaw to Wrist Roll	0.2521	8.12
Wrist Roll to End-Effector (No Load)	1.5262	49.14

Table E-2: Space-based DOSS Manipulator Maximum Joint Torque and Sensor Output.[29]

Joint Actuator	Maximum Torque Output (lb-in)	Maximum Output Torque Sensor can Measure (lb-in)
Shoulder Roll	1416	1608
Shoulder Yaw	1416	1596
Shoulder Pitch	1416	1584
Elbow Pitch	732	828
Wrist Roll	288	324
Wrist Yaw	288	324
Wrist Roll	288	324

APPENDIX F. COMPOUND MODEL SRMS END-EFFECTOR MODE SHAPES

Sections F.1.1 through F.1.4 list the first 30 local mode shapes of the SRMS end-effector for each of the four brakes locked configurations with the DOSS manipulator as an SRMS payload. Sections F.2.1 through F.2.4 list the first 30 local mode shapes of the SRMS end-effector for each of the four brakes locked configurations with the DOSS manipulator and a 1000 lb. cylinder as an SRMS payload.

F.1 DOSS Manipulator as an SRMS Payload

F.1.1 Unberth Configuration

Table F-1: Compound Model SRMS End-Effector Local Translational Mode Shapes for Configuration Unberth.

Mode	Local Translational Mode Shapes		
	x	y	z
1	-1.8534e-02	-7.7113e-01	4.2235e-01
2	-7.5224e-01	-1.9289e-01	-3.3949e-01
3	-3.0869e-02	-7.7420e-02	3.1334e-01
4	-2.5294e-01	3.9123e-01	6.1175e-01
5	-3.6224e-01	-1.4325e-02	3.0801e-02
6	1.3222e-01	-5.1542e-02	-5.3809e-02
7	-3.7069e-02	1.8499e-01	-4.8681e-01
8	-6.8571e-03	-6.8680e-01	-2.4518e-01
9	-5.4026e-02	6.8876e-01	-1.7453e-01
10	1.6156e-02	5.9893e-01	1.0918e-01
11	7.0641e-02	-1.5627e-01	1.6709e-01
12	2.1548e-01	-1.2792e-01	-3.1081e-01
13	-1.2157e-01	8.3729e-02	2.3059e-02
14	-1.8860e-03	-6.6148e-03	-1.5921e-01
15	-3.3551e-02	-1.7841e-02	-7.7450e-02
16	-9.7694e-02	-3.0426e-02	-3.1918e-02
17	-3.8363e-02	1.0618e-01	5.3710e-02
18	-1.1784e-01	7.6062e-02	5.9505e-02
19	-3.8531e-02	5.9307e-02	9.2715e-02
20	-4.1196e-02	3.8119e-01	-1.6240e-01
21	3.6473e-02	2.9536e-01	5.9434e-02
22	-6.0171e-02	6.0131e-02	-1.1774e-01
23	-7.6338e-02	-1.9088e-01	-1.2134e-01
24	-1.7266e-01	-9.1572e-02	-2.3286e-01
25	2.3204e-02	5.4829e-02	2.6293e-02
26	-1.7517e-02	1.1038e-01	-4.6343e-02
27	1.2490e-01	9.6187e-03	9.1376e-02
28	1.1902e-01	7.1742e-02	2.0551e-02
29	9.1076e-02	-2.0320e-02	3.0893e-02
30	-4.8220e-03	4.6648e-02	-3.6719e-02

Table F-2: Compound Model SRMS End-Effector Local Rotational Mode Shapes for Configuration Unberth.

Mode	Local Rotational Mode Shapes		
	θ_x	θ_y	θ_z
1	-2.4268e-03	-7.2256e-04	-1.3315e-03
2	-8.8409e-05	3.3674e-03	-2.3000e-03
3	-3.6162e-04	-4.4150e-03	-5.5930e-03
4	3.6525e-04	-2.6804e-03	3.7655e-03
5	5.5632e-03	-2.2307e-02	-1.4597e-03
6	3.8221e-03	-1.2822e-03	-2.3226e-02
7	-1.5475e-02	-1.8772e-02	-1.1840e-03
8	3.9540e-02	-8.5629e-03	1.0305e-02
9	-7.6334e-02	-6.6083e-03	8.9462e-03
10	-1.0598e-01	3.4758e-03	2.6419e-02
11	5.4508e-02	6.0068e-03	-1.9202e-02
12	-1.9482e-03	-8.3991e-03	5.2713e-03
13	2.4212e-02	-5.5482e-05	-1.3536e-02
14	4.0410e-02	-4.7668e-03	-1.7446e-02
15	3.8887e-02	-2.4822e-03	-1.6196e-02
16	1.0250e-02	-1.4857e-03	-3.3276e-03
17	-2.8474e-02	1.2539e-03	8.5619e-03
18	7.4398e-03	9.3327e-04	-5.4103e-03
19	-8.4181e-03	2.3072e-03	1.6592e-03
20	-2.0454e-02	-4.6763e-03	-3.1958e-03
21	-4.7509e-02	1.7939e-03	1.0512e-02
22	-2.5739e-02	-3.5555e-03	8.6936e-03
23	2.3284e-02	-3.6941e-03	-3.7507e-03
24	-7.6522e-03	-7.2648e-03	5.8397e-03
25	-4.8554e-03	8.3282e-04	3.3600e-04
26	-2.8219e-04	-1.3363e-03	-3.1507e-03
27	-2.4948e-04	3.1655e-03	-1.8328e-04
28	1.5598e-03	1.2535e-03	-2.7427e-03
29	-1.3260e-03	1.3575e-03	1.1323e-03
30	2.7442e-03	-9.9400e-04	-2.4718e-03

F.1.2 Low Hover Configuration

Table F-3: Compound Model SRMS End-Effector Local Translational Mode Shapes for Configuration Low Hover.

Mode	Translational Mode Shapes		
	x	y	z
1	1.1095e-01	-6.8289e-01	4.4667e-01
2	-7.8519e-01	-3.3368e-02	2.3906e-01
3	2.0009e-01	5.0910e-02	5.6742e-01
4	1.5407e-01	5.2940e-01	4.1102e-01
5	3.1666e-01	-1.0738e-02	-6.4474e-02
6	2.0845e-01	-8.0668e-02	-9.6762e-02
7	1.4470e-01	9.1650e-02	4.9956e-01
8	1.0789e-01	6.2940e-01	1.5354e-01
9	7.1801e-02	-4.1278e-01	3.3181e-01
10	-1.1674e-01	8.0311e-01	1.6615e-01
11	8.7389e-02	4.4162e-01	-2.6086e-01
12	1.2801e-01	-1.9737e-01	2.7059e-03
13	-9.9869e-02	-5.0101e-02	-8.1697e-02
14	-9.9036e-03	1.1270e-01	1.4492e-01
15	-1.6020e-02	-4.3047e-02	-3.7045e-02
16	-6.1358e-02	-2.3531e-02	-2.9487e-02
17	-4.8074e-02	6.3717e-02	7.0879e-02
18	1.1814e-01	-9.1740e-02	4.2186e-05
19	2.5504e-02	-2.4698e-02	-1.4794e-01
20	3.5632e-02	-4.4537e-02	1.4225e-01
21	1.3422e-02	-3.1069e-01	3.2110e-02
22	-1.4788e-03	3.1222e-01	-5.6345e-02
23	-3.4763e-02	-1.6750e-01	-1.4681e-01
24	-8.3528e-02	-1.3529e-01	-2.1585e-01
25	2.0847e-02	3.9337e-02	3.9937e-02
26	2.6329e-02	-1.1993e-01	8.4548e-02
27	9.4733e-02	2.6026e-02	7.6703e-02
28	-4.6311e-02	-7.2652e-02	1.8607e-02
29	6.6476e-02	-1.8392e-02	3.8296e-02
30	-6.2280e-03	4.8295e-02	-4.8739e-02

Table F-4: Compound Model SRMS End-Effector Local Rotational Mode Shapes for Configuration Low Hover.

Mode	Rotational Mode Shapes		
	θ_x	θ_y	θ_z
1	-1.9561e-03	-6.7810e-05	5.8559e-04
2	-7.7602e-04	1.8844e-03	-2.2286e-03
3	-2.6558e-03	-7.3226e-03	-3.4036e-03
4	2.4367e-03	-1.2443e-03	7.7339e-03
5	-5.1447e-03	2.0864e-02	5.8801e-03
6	1.4744e-03	2.2508e-03	-2.0464e-02
7	-1.0412e-02	1.9533e-02	2.1505e-03
8	-2.3516e-02	5.7523e-03	-1.5171e-02
9	3.4549e-02	1.1925e-02	8.1867e-05
10	-8.5399e-02	4.3540e-03	9.3749e-03
11	-9.7644e-02	-8.0085e-03	2.8018e-02
12	4.9884e-02	1.0477e-03	-1.5638e-02
13	4.7064e-02	-3.2007e-03	-1.9094e-02
14	-4.7020e-02	4.3659e-03	1.6893e-02
15	2.4991e-02	-1.2306e-03	-9.4248e-03
16	7.9164e-03	-1.2102e-03	-2.5717e-03
17	-1.8106e-02	1.6729e-03	5.5665e-03
18	-1.2668e-02	7.0319e-04	8.0415e-03
19	1.2619e-02	-3.8870e-03	-4.4428e-03
20	-1.6422e-02	4.0556e-03	8.0700e-03
21	2.8092e-02	9.6145e-04	-2.1095e-03
22	-4.9657e-02	-1.5746e-03	1.0864e-02
23	7.1698e-03	-4.1484e-03	2.1155e-03
24	-8.0794e-03	-6.2867e-03	7.3198e-03
25	-3.4364e-03	1.1824e-03	2.1941e-04
26	3.1042e-04	2.4036e-03	3.4206e-03
27	5.0204e-04	2.5985e-03	-9.7128e-04
28	-8.8219e-04	2.1592e-04	2.4955e-03
29	-8.4533e-04	1.4072e-03	8.8040e-04
30	1.9786e-03	-1.3203e-03	-2.2120e-03

F.1.3 Deploy Configuration

Table F-5: Compound Model SRMS End-Effector Local Translational Mode Shapes for Configuration Deploy.

Mode	Local Translational Mode Shapes		
	x	y	z
1	-6.6215e-01	-4.9867e-01	1.5926e-01
2	-1.6459e-02	2.9511e-01	8.6085e-01
3	-3.5292e-01	7.0269e-01	-2.3690e-01
4	-4.1191e-02	2.6449e-02	1.7028e-01
5	7.1177e-02	6.3028e-02	-6.0669e-02
6	1.2681e-01	1.1908e-01	5.8752e-02
7	-1.4917e-01	6.0963e-01	-3.3151e-01
8	8.7494e-03	-4.2178e-01	-2.9219e-01
9	-1.4059e-01	7.9680e-03	-3.8834e-02
10	2.4996e-02	7.8777e-01	6.5519e-02
11	1.8832e-02	-1.0280e-01	2.3858e-01
12	-1.0329e-01	-4.0531e-02	4.3960e-03
13	-2.4118e-01	3.1980e-01	-1.1430e-01
14	-7.1482e-02	-1.7897e-01	-3.7787e-01
15	5.6982e-02	1.0380e-01	7.0823e-02
16	9.0675e-03	-1.7514e-01	-1.2761e-01
17	-2.0908e-01	6.5776e-02	-6.8337e-02
18	-4.7123e-03	3.0550e-01	7.5601e-02
19	2.9954e-02	-1.8967e-01	2.5170e-01
20	3.3746e-02	-1.6256e-01	6.2404e-02
21	1.4571e-02	1.5909e-01	9.0112e-02
22	7.1306e-03	2.1545e-01	4.4532e-02
23	-2.5462e-01	-1.7005e-01	2.9172e-02
24	3.1136e-02	1.2127e-01	-2.3061e-02
25	-1.1360e-01	-1.2612e-01	3.4095e-02
26	1.9798e-02	2.9474e-02	8.9927e-02
27	-3.1132e-01	-1.1391e-02	-1.5805e-02
28	-9.9451e-02	-3.4991e-02	-7.0377e-02
29	7.4798e-03	8.4430e-03	1.8784e-02
30	-1.1378e-02	-4.3457e-02	-5.1275e-02

Table F-6: Compound Model SRMS End-Effector Local Rotational Mode Shapes for Configuration Deploy.

Mode	Rotational Mode Shapes		
	θ_x	θ_y	θ_z
1	-5.3049e-05	-8.3892e-04	-2.6644e-03
2	-1.5158e-03	-2.4125e-03	7.5688e-04
3	5.6740e-04	1.6533e-03	4.2067e-03
4	4.2470e-03	-8.4064e-03	2.8029e-03
5	-4.0408e-03	-1.5059e-02	-1.7727e-02
6	-1.0324e-02	1.8180e-02	-1.3489e-02
7	-4.7263e-02	-1.3444e-02	-1.9553e-03
8	1.4288e-02	-1.0704e-02	1.0604e-02
9	-1.0733e-03	-2.2051e-03	4.0409e-04
10	-1.4071e-01	1.8954e-03	3.6042e-02
11	2.3545e-02	7.8225e-03	-6.9544e-03
12	-2.8096e-02	-5.1125e-04	1.4248e-02
13	1.6670e-02	-4.7839e-03	-1.8078e-02
14	1.4038e-02	-1.1669e-02	-4.1056e-05
15	-8.7082e-03	2.3732e-03	3.1472e-04
16	2.3471e-02	-3.5657e-03	-4.2742e-03
17	6.1267e-03	-3.1145e-03	-4.5629e-03
18	-4.2742e-02	2.0323e-03	8.2281e-03
19	4.3624e-02	7.0952e-03	-1.2141e-02
20	-9.9216e-03	1.8913e-03	9.0323e-03
21	-2.0706e-02	2.5072e-03	3.6580e-03
22	-3.3909e-02	1.2134e-03	7.3525e-03
23	-4.3479e-03	-7.3116e-04	6.8442e-03
24	-1.8024e-02	-4.5321e-04	3.7069e-03
25	-7.5547e-04	2.3308e-04	4.0422e-03
26	2.6226e-03	2.5140e-03	-1.9343e-03
27	-5.6528e-04	-2.2658e-03	5.6248e-04
28	1.1175e-03	-2.4549e-03	5.7970e-04
29	-1.2558e-04	5.4150e-04	-1.9770e-04
30	2.7515e-03	-1.4175e-03	1.6489e-04

F.1.4 Capture Configuration

Table F-7: Compound Model SRMS End-Effector Local Translational Mode Shapes for Configuration Capture.

Mode	Local Translational Mode Shapes		
	x	y	z
1	8.2562e-01	9.8483e-02	3.4182e-02
2	-6.7297e-02	7.6922e-01	-3.8385e-01
3	2.6692e-02	-3.3620e-01	-7.2963e-01
4	9.5644e-02	2.3811e-01	-1.1848e-01
5	3.7420e-01	-4.1687e-03	-1.9870e-02
6	7.0791e-02	-5.0474e-02	1.4266e-01
7	1.1497e-01	4.1747e-01	5.4817e-01
8	-2.0943e-02	-4.7584e-01	2.7982e-01
9	-1.2101e-01	6.0948e-01	2.4259e-01
10	-4.2416e-02	-7.0895e-01	2.5786e-01
11	-1.8235e-01	2.2767e-01	-1.4134e-01
12	6.7813e-03	-2.6169e-01	-7.4124e-02
13	-8.4091e-02	-2.2076e-02	3.9628e-02
14	-4.4522e-02	1.6668e-01	9.1198e-02
15	8.7421e-02	2.9352e-02	3.7314e-02
16	3.3656e-02	-1.3662e-01	3.8852e-02
17	4.5523e-02	-1.3490e-01	1.0101e-01
18	-1.1454e-01	8.3116e-02	4.7758e-02
19	3.3295e-02	1.3577e-01	1.6879e-01
20	-3.9226e-02	2.4245e-01	9.7224e-02
21	5.9451e-02	-7.7812e-02	1.5468e-01
22	4.7145e-02	3.7735e-01	2.5126e-02
23	-8.3087e-02	5.8956e-02	-2.0526e-01
24	-5.8289e-02	-1.0047e-01	-1.2703e-01
25	-9.7148e-02	5.2407e-02	-9.9786e-02
26	-4.1298e-03	-1.1440e-01	1.8453e-03
27	3.7026e-02	3.6306e-02	3.0068e-02
28	-6.2828e-02	1.4506e-03	2.4381e-02
29	2.9101e-02	-4.6812e-02	5.5703e-02
30	8.9776e-03	-6.7694e-02	2.2528e-02

Table F-8: Compound Model SRMS End-Effector Local Rotational Mode Shapes for Configuration Capture.

Mode	Rotational Mode Shapes		
	θ_x	θ_y	θ_z
1	1.6535e-04	-1.6497e-03	7.5762e-04
2	1.9307e-03	6.0517e-04	8.3847e-04
3	-4.5840e-04	1.0310e-02	-4.4489e-03
4	6.3312e-04	7.1363e-03	1.4737e-02
5	-2.8445e-03	1.2585e-02	-8.9729e-03
6	-6.4148e-03	1.1836e-02	1.5397e-02
7	-2.1039e-02	2.0528e-02	-7.0123e-03
8	1.9013e-02	1.0223e-02	1.1533e-02
9	-4.4179e-02	6.9168e-03	-2.6791e-03
10	1.0604e-01	8.5881e-03	-2.1736e-02
11	-3.2219e-02	-6.0310e-03	6.4748e-03
12	8.3558e-02	-2.2488e-03	-2.8378e-02
13	3.7138e-02	6.2737e-04	-1.5589e-02
14	-5.1594e-02	2.4997e-03	1.7076e-02
15	-1.0362e-02	1.6716e-03	3.4817e-03
16	9.4449e-03	1.2724e-03	2.9183e-04
17	-1.2699e-02	3.0776e-03	9.5096e-03
18	-1.5500e-04	6.2946e-04	-2.4888e-03
19	-3.3921e-02	4.8068e-03	9.8258e-03
20	-1.0728e-02	2.4053e-03	-2.9645e-03
21	-4.5045e-03	4.5230e-03	4.1690e-03
22	-4.7993e-02	9.2494e-04	8.2163e-03
23	-2.3291e-02	-6.0226e-03	7.7115e-03
24	-3.7633e-03	-3.7522e-03	4.5393e-03
25	-1.5139e-03	-3.2349e-03	-9.3721e-04
26	-2.7037e-03	2.0091e-05	4.4756e-03
27	-1.0619e-03	1.0151e-03	-6.4575e-04
28	8.1389e-04	2.7276e-04	-3.6922e-04
29	-6.5970e-06	1.6465e-03	1.3804e-03
30	-2.3953e-03	6.4368e-04	2.9495e-03

F.2 DOSS with 1000 lb. Cylinder as an SRMS Payload

F.2.1 Unberth Configuration

Table F-9: Compound Model SRMS End-Effector Local Translational Mode Shapes for Configuration Unberth.

Mode	Local Translational Mode Shapes		
	x	y	z
1	-1.8951e-02	-3.6283e-01	1.9938e-01
2	3.0659e-01	1.0578e-01	2.0959e-01
3	-3.8321e-01	1.2939e-01	1.6927e-01
4	-2.0187e-02	-2.7863e-01	1.6861e-01
5	1.4524e-01	-2.0489e-01	5.2845e-01
6	-1.2257e-01	-4.7369e-01	-2.7011e-01
7	-2.0197e-02	3.5305e-01	-1.1145e-01
8	-5.3507e-02	-2.4511e-01	-6.7076e-01
9	1.5410e-02	-5.3828e-01	7.0103e-02
10	-3.0631e-02	2.8216e-01	-1.6066e-01
11	-2.1786e-02	-1.9135e-01	-1.9165e-01
12	6.2116e-02	-1.2328e-01	-2.0800e-01
13	4.2473e-02	-2.7299e-01	7.4320e-02
14	-8.7661e-03	1.9445e-01	-1.4972e-01
15	1.2548e-02	-1.2936e-01	4.5062e-02
16	-3.5351e-02	1.9355e-02	-4.0894e-02
17	-1.0457e-02	-3.4635e-02	3.4339e-02
18	3.3344e-02	-1.0581e-01	-4.0609e-02
19	2.2523e-03	-1.3496e-02	-7.0446e-02
20	2.1549e-02	-2.4681e-01	1.3342e-01
21	2.1616e-02	-4.0513e-02	8.4897e-02
22	-3.5525e-02	-9.5483e-02	-1.2446e-01
23	-4.0006e-02	-6.5566e-02	-1.2854e-01
24	7.2042e-02	1.2157e-01	2.0602e-01
25	-8.2350e-03	-2.2829e-02	-2.0319e-02
26	-9.6576e-03	9.9367e-02	-4.1900e-02
27	4.8043e-02	1.1617e-02	8.3625e-02
28	3.5096e-02	6.7251e-02	1.7718e-02
29	2.4177e-02	-3.2986e-02	2.5565e-02
30	-4.2556e-03	5.6162e-02	-3.1126e-02

Table F-10: Compound Model SRMS End-Effector Local Rotational Mode Shapes for Configuration Unberth.

Mode	Local Rotational Mode Shapes		
	θ_x	θ_y	θ_z
1	-1.0195e-03	-7.3157e-04	-1.3776e-03
2	7.4559e-05	-2.2510e-03	1.1514e-03
3	3.2239e-04	-1.9886e-03	4.1971e-04
4	-1.4604e-03	2.4289e-03	5.5291e-03
5	-6.7537e-03	8.3458e-03	4.9037e-03
6	-3.2016e-03	-4.2012e-03	8.3030e-03
7	-3.5427e-02	-1.6376e-03	1.8773e-03
8	7.0743e-04	-8.8688e-03	3.1747e-03
9	-1.1965e-03	9.6585e-04	7.5898e-03
10	8.0686e-05	-2.1338e-03	-3.8176e-03
11	2.7076e-04	-2.5040e-03	2.5132e-03
12	4.6195e-04	-2.5538e-03	1.5481e-03
13	-2.2034e-04	1.0290e-03	3.6775e-03
14	7.4179e-04	-1.9278e-03	-2.7304e-03
15	-6.6518e-04	5.9796e-04	1.8437e-03
16	4.2776e-04	-5.8200e-04	-3.3605e-04
17	-1.2261e-03	4.1610e-04	6.8992e-04
18	2.2559e-05	-4.5210e-04	1.3858e-03
19	4.9267e-04	-8.8513e-04	8.3740e-05
20	2.2382e-03	1.7215e-03	2.8164e-03
21	-1.5893e-03	1.1097e-03	8.3181e-04
22	-5.0757e-04	-1.6325e-03	1.3475e-03
23	8.8117e-04	-1.6912e-03	6.9348e-04
24	-9.0995e-05	2.7241e-03	-1.5751e-03
25	2.4511e-04	-2.7050e-04	2.5280e-04
26	-3.0714e-04	-5.4459e-04	-1.2423e-03
27	-4.3834e-05	1.1390e-03	-1.4378e-04
28	-1.4508e-04	2.8673e-04	-8.5229e-04
29	3.9922e-05	3.6544e-04	4.2379e-04
30	-5.6252e-05	-3.9884e-04	-7.2353e-04

F.2.2 Low Hover Configuration

Table F-11: Compound Model SRMS End-Effector Local Translational Mode Shapes for Configuration Low Hover.

Mode	Local Translational Mode Shapes		
	x	y	z
1	2.4259e-02	-3.6746e-01	2.6156e-01
2	-4.5749e-01	-1.6496e-03	2.6264e-02
3	-1.4410e-01	2.1579e-01	2.4668e-01
4	-3.7868e-03	-2.8978e-01	2.2448e-01
5	1.8702e-01	-6.8628e-02	5.1439e-01
6	1.1542e-01	4.3814e-01	1.1761e-01
7	-1.6673e-02	2.9868e-01	-9.0347e-02
8	1.1278e-01	2.4453e-01	7.0461e-01
9	5.8867e-03	6.3148e-01	-2.6848e-02
10	3.2787e-02	-1.7093e-01	2.7731e-01
11	-4.0137e-02	3.3442e-01	1.7004e-01
12	-3.2886e-02	-1.1542e-01	5.3576e-02
13	-4.5606e-02	2.4206e-01	-1.5088e-01
14	-1.3987e-03	-8.2361e-02	1.0162e-01
15	-6.2788e-03	7.0525e-02	-2.3196e-02
16	-2.2087e-02	2.0444e-02	-3.2940e-02
17	8.0238e-03	3.9733e-02	-6.3474e-02
18	3.6823e-02	-1.5486e-01	1.4853e-02
19	3.6601e-03	-3.1733e-02	1.2700e-01
20	-1.6881e-02	6.7150e-02	-9.2708e-02
21	-1.3915e-02	1.8368e-01	-7.9391e-02
22	-7.1558e-03	-1.2626e-03	-5.9443e-02
23	-2.6972e-02	-1.2966e-01	-1.4611e-01
24	4.2284e-02	1.6001e-01	1.8225e-01
25	-9.1119e-03	-1.5388e-02	-3.2923e-02
26	-1.5030e-02	1.0820e-01	-7.4917e-02
27	-3.4980e-02	-2.7545e-02	-6.9177e-02
28	-1.2039e-02	-6.8211e-02	1.3609e-02
29	-2.2124e-02	2.2584e-02	-3.5728e-02
30	5.5110e-03	-5.3357e-02	4.0959e-02

Table F-12: Compound Model SRMS End-Effector Local Rotational Mode Shapes for Configuration Low Hover.

Mode	Local Rotational Mode Shapes		
	θ_x	θ_y	θ_z
1	-1.1901e-03	-5.8864e-04	-5.6806e-04
2	-2.3625e-04	1.7635e-03	-1.6214e-03
3	7.4168e-05	-2.7144e-03	8.7368e-04
4	2.2905e-04	3.6866e-03	6.3611e-03
5	-6.4706e-03	8.2104e-03	2.5041e-03
6	4.7262e-03	1.9355e-03	-8.0141e-03
7	-3.5369e-02	-1.2805e-03	2.7415e-03
8	2.4351e-04	9.4050e-03	-3.3311e-03
9	-1.1395e-03	-3.7517e-04	-8.3944e-03
10	-1.0661e-04	3.6473e-03	2.3357e-03
11	-5.9549e-04	2.1070e-03	-4.3620e-03
12	-2.4542e-04	6.2726e-04	1.6058e-03
13	6.5365e-04	-2.0212e-03	-3.3572e-03
14	-6.5649e-04	1.2983e-03	1.2285e-03
15	4.1951e-04	-3.0919e-04	-1.0182e-03
16	2.8598e-04	-4.5775e-04	-3.2360e-04
17	7.6301e-04	-7.8819e-04	-6.6868e-04
18	-1.3298e-04	2.5447e-04	2.0594e-03
19	-4.9272e-04	1.6092e-03	5.0991e-04
20	9.9038e-04	-1.1993e-03	-1.0677e-03
21	-2.0291e-03	-1.0255e-03	-2.0256e-03
22	-1.4640e-03	-7.6237e-04	2.9253e-04
23	5.5527e-04	-1.8890e-03	1.5949e-03
24	-2.1802e-04	2.3711e-03	-2.0546e-03
25	1.7222e-04	-4.3060e-04	1.6921e-04
26	-3.3454e-04	-9.6959e-04	-1.3526e-03
27	6.4874e-05	-9.3356e-04	3.4816e-04
28	1.6963e-04	1.4911e-04	8.6016e-04
29	-3.1967e-05	-4.8942e-04	-2.8921e-04
30	7.8866e-05	5.2469e-04	6.8261e-04

F.2.3 Deploy Configuration

Table F-13: Compound Model SRMS End-Effector Local Translational Mode Shapes for Configuration Deploy.

Mode	Local Translational Mode Shapes		
	x	y	z
1	-3.0328e-01	-3.0625e-01	-2.9675e-02
2	-1.0138e-01	4.6660e-02	4.1281e-01
3	3.5338e-01	-1.8750e-01	3.7178e-02
4	-8.0168e-02	-1.8232e-01	-3.9659e-01
5	-2.0843e-02	6.0279e-01	-3.3102e-01
6	-8.0192e-02	-3.3739e-01	-4.3627e-01
7	-2.3745e-02	9.6555e-02	-1.1723e-01
8	1.0243e-01	-5.1616e-01	3.2747e-01
9	-4.1816e-02	-3.3227e-01	-4.1076e-01
10	5.4345e-02	1.8985e-02	3.0089e-02
11	-2.8444e-02	-6.0737e-02	-2.2691e-01
12	-3.2513e-02	-2.1490e-01	1.8264e-02
13	1.0920e-01	-3.8636e-01	1.5974e-01
14	4.8362e-02	1.2693e-01	3.3723e-01
15	-2.5481e-02	-5.6562e-02	-6.2073e-02
16	1.9077e-03	3.6907e-02	9.3935e-02
17	-8.1366e-02	7.7628e-02	-7.3433e-02
18	-1.3711e-02	3.7412e-02	-1.6169e-02
19	-2.8943e-02	-8.8841e-02	-2.1831e-01
20	-1.4436e-02	1.9397e-01	-8.2673e-02
21	1.2993e-02	4.8655e-02	9.1519e-02
22	-1.6000e-03	-1.2432e-02	-2.0268e-02
23	-9.8603e-02	-2.0176e-01	-2.8582e-03
24	1.3396e-03	2.2620e-03	-1.7285e-02
25	-3.7110e-02	-1.0460e-01	1.0834e-02
26	1.3813e-02	3.8051e-02	7.8589e-02
27	-9.6496e-02	6.8383e-03	-5.6902e-02
28	1.4159e-02	2.1078e-02	5.7391e-02
29	-3.1428e-03	-6.6874e-03	-1.5974e-02
30	-7.1790e-03	-2.5274e-02	-4.3969e-02

Table F-14: Compound Model SRMS End-Effector Local Rotational Mode Shapes for Configuration Deploy.

Mode	Local Rotational Mode Shapes		
	θ_x	θ_y	θ_z
1	8.9355e-05	-5.6591e-05	-1.7238e-03
2	-5.5998e-04	-1.6088e-03	-5.6479e-05
3	-2.7611e-04	-8.8835e-04	-2.0473e-03
4	4.9381e-03	-7.0091e-03	2.1854e-03
5	-2.3965e-03	-5.0553e-03	-8.8760e-03
6	4.2203e-03	-6.8191e-03	4.4272e-03
7	-3.5518e-02	-1.7535e-03	5.7560e-03
8	-5.2956e-05	4.4422e-03	7.0161e-03
9	1.8249e-03	-5.4356e-03	4.1611e-03
10	-2.6173e-05	4.7885e-04	-2.6159e-04
11	-2.2547e-04	-2.9640e-03	8.5435e-04
12	2.7069e-04	1.7980e-04	2.8235e-03
13	7.5978e-04	2.2281e-03	4.9870e-03
14	-1.0229e-03	4.3848e-03	-1.4906e-03
15	6.2670e-04	-8.3345e-04	6.2925e-04
16	-1.2955e-03	1.1951e-03	-2.4188e-04
17	2.6529e-04	-1.0738e-03	-1.0701e-03
18	-2.5513e-03	-2.2794e-04	-9.9380e-06
19	-1.1076e-03	-2.8075e-03	1.3760e-03
20	-4.6699e-04	-1.0690e-03	-2.4582e-03
21	-1.1779e-03	1.1769e-03	-4.1566e-04
22	9.6038e-04	-2.5814e-04	-1.8349e-05
23	5.2242e-04	-2.1467e-04	2.5448e-03
24	-6.1570e-04	-2.1538e-04	8.6625e-05
25	2.9163e-04	6.8849e-05	1.3140e-03
26	-1.9228e-05	1.0137e-03	-4.9433e-04
27	-2.5894e-05	-8.9111e-04	-8.4469e-05
28	-1.1152e-04	7.4734e-04	-2.5469e-04
29	2.5108e-05	-2.0652e-04	8.2719e-05
30	1.8546e-04	-5.6555e-04	2.9540e-04

F.2.4 Capture Configuration

Table F-15: Compound Model SRMS End-Effector Local Translational Mode Shapes for Configuration Capture.

Mode	Local Translational Mode Shapes		
	x	y	z
1	4.7154e-01	6.3473e-02	2.4713e-02
2	-3.8423e-02	3.9065e-01	-1.9736e-01
3	-1.5354e-01	1.1210e-01	2.1920e-01
4	5.5938e-02	-4.2790e-01	2.2275e-01
5	1.7116e-01	2.3714e-01	3.7991e-01
6	3.3233e-02	-2.1490e-01	2.8452e-01
7	-3.0514e-02	3.5081e-01	-1.6780e-01
8	-8.9120e-02	-3.8630e-01	-7.5618e-01
9	1.3886e-02	-5.2484e-01	2.1774e-01
10	-3.1061e-02	2.9925e-01	1.9753e-01
11	6.0096e-02	4.2542e-02	5.8486e-02
12	-2.9480e-02	3.0094e-01	-1.8103e-01
13	-2.3766e-02	1.8025e-01	-1.4300e-02
14	-1.1816e-02	-4.0193e-02	8.4550e-02
15	3.0467e-02	-1.7676e-02	4.1769e-02
16	1.4786e-02	-9.1185e-02	3.9498e-02
17	2.4122e-02	-1.9099e-01	9.7659e-02
18	3.1049e-02	-7.5813e-02	-3.4949e-02
19	2.5198e-02	-1.9608e-02	1.5245e-01
20	-2.7958e-03	1.8335e-01	7.2452e-02
21	1.2901e-02	7.4489e-02	-6.0293e-03
22	3.0217e-02	-9.6024e-02	1.4077e-01
23	-4.9226e-02	-9.7004e-02	-2.0644e-01
24	1.9559e-02	9.5716e-02	7.4726e-02
25	-3.6450e-02	4.2545e-02	-8.7670e-02
26	-1.3712e-03	-1.1724e-01	2.0641e-03
27	-1.3439e-02	-2.6616e-02	-2.6549e-02
28	1.6837e-02	-5.2127e-03	-1.6024e-02
29	1.2641e-02	-4.2384e-02	4.8464e-02
30	4.1867e-03	-7.3198e-02	1.9243e-02

Table F-16: Compound Model SRMS End-Effector Local Rotational Mode Shapes for Configuration Capture.

Mode	Local Rotational Mode Shapes		
	θ_x	θ_y	θ_z
1	1.0815e-04	-1.0421e-03	5.0993e-04
2	9.3831e-04	5.8597e-04	8.9533e-04
3	2.4405e-04	-3.6622e-03	1.5909e-03
4	-1.8013e-03	3.9894e-03	8.4902e-03
5	-2.6873e-03	5.7116e-03	-3.1186e-03
6	-1.3747e-02	3.9747e-03	6.0102e-03
7	-3.3409e-02	-2.3782e-03	1.5683e-03
8	-2.8494e-04	-1.0017e-02	5.2796e-03
9	4.2357e-04	2.8832e-03	7.0950e-03
10	-5.7815e-04	2.4815e-03	-3.9028e-03
11	3.1965e-04	8.6572e-04	-6.4903e-04
12	7.0721e-04	-2.3905e-03	-4.1825e-03
13	6.5125e-04	-2.3182e-04	-2.5294e-03
14	-8.9115e-04	1.0607e-03	7.1492e-04
15	-2.0420e-04	5.8838e-04	2.7220e-04
16	6.7432e-04	5.2499e-04	1.0702e-03
17	3.0922e-05	1.2786e-03	2.5080e-03
18	2.7629e-04	-3.8509e-04	9.4353e-04
19	-1.5731e-03	1.9707e-03	5.5546e-04
20	-1.1321e-03	9.0874e-04	-2.1921e-03
21	-2.0562e-03	-5.2414e-05	-5.8930e-04
22	3.5696e-04	1.8282e-03	1.1908e-03
23	-5.1063e-04	-2.6888e-03	1.3674e-03
24	-2.9627e-04	9.7609e-04	-1.1982e-03
25	-1.7267e-04	-1.1691e-03	-5.2407e-04
26	2.5118e-04	2.3396e-05	1.4867e-03
27	1.2357e-04	-3.5821e-04	3.2506e-04
28	-1.6041e-05	-1.7072e-04	7.1066e-05
29	1.2480e-04	6.3223e-04	5.3077e-04
30	1.2125e-04	2.4937e-04	9.3402e-04

REPORT DOCUMENTATION PAGE

Form Approved
OMB No. 0704-0188

1. AGENCY USE ONLY (Leave blank)	2. REPORT DATE	3. REPORT TYPE AND DATES COVERED
	November 1993	Contractor Report

4. TITLE AND SUBTITLE
Admittance Model for the Shuttle Remote Manipulator System in Four Configurations

5. FUNDING NUMBERS
NCC1-104
586-02-11

6. AUTHOR(S)
Loukas Papadopoulos and Robert H. Tolson

7. PERFORMING ORGANIZATION NAME(S) AND ADDRESS(ES)
Joint Institute for Advancement of Flight Sciences
The George Washington University
Langley Research Center, Hampton, VA 23681-0001

8. PERFORMING ORGANIZATION REPORT NUMBER

9. SPONSORING/MONITORING AGENCY NAME(S) AND ADDRESS(ES)
National Aeronautics and Space Administration
Langley Research Center
Hampton, VA 23681-0001

10. SPONSORING/MONITORING AGENCY REPORT NUMBER
NASA CR-4555

11. SUPPLEMENTARY NOTES
Originally published as Master of Science Thesis by the first author.

12a. DISTRIBUTION/AVAILABILITY STATEMENT
Unclassified - Unlimited
Subject Category 63

12b. DISTRIBUTION CODE

13. ABSTRACT *(Maximum 200 words)*
A scenario for robot task performance in space is to mount two small, dexterous arms to the Shuttle Remote Manipulator System (SRMS). As these small robots perform tasks, the flexibility of the SRMS may cause unsuccessful task executions. In order to simulate the dynamic coupling between the SRMS and the arms, admittance models of the SRMS in four brakes locked configurations have been developed. The admittance model permits calculating the SRMS end-effector response due to end-effector disturbing forces. The model will then be used in conjunction with a Stewart Platform, a vehicle emulation system. An application of the admittance model has been shown by simulating the disturbing forces using two SRMS payloads, the Dextrous Orbital Servicing System (DOSS) manipulator and DOSS carrying a 1000 lb. cylinder. Comparisons were conducted to determine the minimum number of modes required in the admittance model while retaining dynamic fidelity. It was determined that for all four SRMS configurations studied, between 4 and 6 modes of the SRMS structure were sufficient to retain tolerances of 0.01 inches and 0.01°. These tolerances correspond to the DOSS manipulator carrying no object. When the DOSS carries the 1000 lb. cylinder, between 15 and 20 modes were sufficient, approximately three or four times as many modes as for the unloaded case.

14. SUBJECT TERMS
Remote Manipulator, Admittance Model, Disturbance Compensation, Robotics.

15. NUMBER OF PAGES
192

16. PRICE CODE
A09

17. SECURITY CLASSIFICATION OF REPORT	18. SECURITY CLASSIFICATION OF THIS PAGE	19. SECURITY CLASSIFICATION OF ABSTRACT	20. LIMITATION OF ABSTRACT
Unclassified	Unclassified	Unclassified	